

**Fabrication and Characterization of Chalcogenide
nano composite based materials for Photonic
device applications**

Thesis submitted to

Cochin University of Science and Technology

In partial fulfillment of the requirements for the Degree of

Doctor of Philosophy

By

Tintu.R



**International School of Photonics
Cochin University of Science and Technology**

Cochin - 682 022, India

June 2011

Fabrication and Characterization of Chalcogenide nano composite based materials for Photonic device applications

Ph D Thesis in the field of Photonics

Author

Tintu.R

Research Fellow

International School of Photonics,

Cochin University of Science and Technology,

Cochin – 682 022, India.

Email: tintu_tillanivas@yahoo.co.in,tintuisp@gmail.com

Research Advisor

Dr. Sheenu Thomas

Reader,

Centre of Excellence in Lasers and Optoelectronic Sciences,

Cochin University of Science and Technology,

Cochin – 682 022, India.

Email : st@cusat.ac.in

Cover page: *Confocal image of $Ga_5Sb_{10}Ge_{25}Se_{60}$ nano colloid, image of photoluminescence from $Ga_5Sb_{10}Ge_{25}Se_{60}$ nano colloid doped PMMA fiber on excitation with white LED, AFM image of $Ge_{28}Sb_{12}Se_{60}$ /PVA composite film, Z-scan trace for $Ge_{28}Sb_{12}Se_{60}$ nano colloid, Thermal lens signal for $Ga_5Sb_{10}Ge_{25}Se_{60}$ nano colloid, excitation wavelength dependent luminescence from $Ga_5Sb_{10}Ge_{25}Se_{60}$ nano colloid, structure of $Ge_{28}Sb_{12}Se_{60}$ glass.*

International School of Photonics, Cochin University of Science & Technology

Cochin – 682 022, INDIA, www.photonics.cusat.edu

June 2011

ബ്രഹ്മണ്യായ കർമ്മാണി
സംഗം തൃശ്ശൂർ കരോതി യഃ
ലിപ്യതേ ന സ പാപേന
പദ്പത്രമിവാംസോ

ഭവതീതി അദ്ധ്യായം 5,10

എന്റെ മാതാപിതാക്കന്മാർക്ക് സമർപ്പണം

Dr. Sheenu Thomas

Reader,

Centre of Excellence in Lasers and Optoelectronic Sciences

Cochin University of Science and Technology

Cochin – 682 022, India

Email: st@cusat.ac.in

Certificate

*Certified that the research work presented in the thesis entitled “**Fabrication and Characterization of Chalcogenide nano composite based materials for Photonic device applications**” submitted by Ms. **Tintu.R** is an authentic record of research work carried out by her under my guidance and supervision at the International School of Photonics, Cochin University of Science and Technology, Cochin–22, India and the work embodied in this thesis has not been included in any other thesis submitted previously for the award of any degree.*

Cochin 22

Date:

Dr. Sheenu Thomas

(Supervising Guide)

Declaration

Certified that the work presented in the thesis entitled “*Fabrication and Characterization of Chalcogenide nano composite based materials for Photonic device applications*” is based on the original work done by me under the guidance and supervision of Dr. Sheenu Thomas, Assistant Professor, Centre of Excellence in Lasers and Optoelectronic Sciences, Cochin University of Science and Technology, Cochin – 22, India and has not been included in any other thesis submitted previously for the award of any degree.

Cochin 22

Tintu.R

Preface

Presently, great interest has been devoted to the fabrication of new materials suitable for photonics applications. Among these, the amorphous chalcogenide structures are significant due to their effectiveness as excellent materials for optical ultrafast nonlinear devices like demultiplexers, wavelength converters, and optical Kerr shutters. Chalcogenide glasses assure importance in various fields due to their high refractive index, high transparency in the IR region, low phonon energies, large optical nonlinearities, ability to be directly patterned by exposure to near-band gap light and the ability to incorporate relatively high concentrations of rare-earth dopants with minimal clustering. Photosensitivity mechanisms in these materials find potential application in optoelectronics (photoresists, optical memories, optoelectronic circuits etc).

In this context, in search of new materials based on chalcogenide glasses, we have developed a novel technique for fabrication of chalcogenide nano composites which are presented in this thesis. The technique includes the dissolution of bulk chalcogenide glasses in amine solvent. This solution casting method allows to retain the attractive optical properties of chalcogenide glasses enabling new fabrication routes for the realization of large area thick/thin films with less cost. Chalcogenide glass fiber geometry opens new possibilities for a large number of applications in optics, like remote temperature measurements, CO₂ laser power delivery, and optical sensing and single-mode propagation of IR light. We have fabricated new optical polymer fibers doped with chalcogenide glasses which can be used for many optical applications. The present thesis also describes the structural, thermal and optical characterization of certain chalcogenide based materials prepared by different methods and its applications. The thesis is organized into eight chapters.

Chapter 1 gives an overview on the structure, properties and potential applications of chalcogenide glasses (ChG). Recent trends like the fabrication of new hybrid materials based on chalcogenide glass and polymer and their possibility

in the different fields are mentioned. Brief description of structural, electronic, thermal and optical properties of the chalcogenide glasses is given. Different permanent and temporary photoinduced mechanisms like photodarkening and photoluminescence in these materials are described along with well defined models. Photodarkening and photoluminescence are found to be very interesting in ChG due to their band gap structure with the presence of localized states and different defects. Finally, the scope of the work presented in this thesis is also given.

Chapter 2 focuses on the fabrication of materials and the experimental tools and techniques used in the present work. The method used for the preparation of bulk, thin film, nano colloid, nano composite film, stacked films and nano colloid ChG doped polymer fibers are discussed in detail. The characterization tools and experimental techniques along with theory used for the study of absorption spectroscopy, photoinduced darkening, photoluminescence mechanism, thermal diffusivity measurement and z-scan technique used for investigating ChG based samples are also discussed.

Chapter 3 deals with the studies on $\text{Ga}_5\text{Sb}_{10}\text{Ge}_{25}\text{Se}_{60}$ chalcogenide glass. Melt quenched $\text{Ga}_5\text{Sb}_{10}\text{Ge}_{25}\text{Se}_{60}$ bulk glass is found to be amorphous and have a glass transition temperature of 316°C . The kinetics of photoinduced effects on thermally evaporated $\text{Ga}_5\text{Sb}_{10}\text{Ge}_{25}\text{Se}_{60}$ thin film exposed to continuous wave laser radiations are studied as a function of exposure time, laser intensity and laser wavelength (near band gap and above band gap). The transmission and reflection spectra of thin films before and after exposure are investigated. Generalized Miller's rule and linear refractive index are used to find the nonlinear susceptibility and non linear refractive index of thin films. The studies show a red shift in bandgap with increase in exposure time and laser power which is attributed to the photoinduced darkening in the films. Studies show that a low power radiation is sufficient enough to provide a shift in the absorption edge and a change in the refractive index. This mechanism in $\text{Ga}_5\text{Sb}_{10}\text{Ge}_{25}\text{Se}_{60}$ glasses can be used to realize continuous wave laser written waveguide and for fabricating photosensitive optical

components for various applications. Nano colloidal solutions of $\text{Ga}_5\text{Sb}_{10}\text{Ge}_{25}\text{Se}_{60}$ synthesised by chemical method from bulk glass are optically characterized. The optical band gap of the material is found to be tunable depending on the cluster size. The cluster formation and the dependence of the cluster size with concentration are confirmed by the SEM analysis. Photoluminescence studies show that there is an excitation wavelength and cluster size dependent red shift in emission peak. Thermal studies on the nano colloids using thermal lens method show band gap dependent change in thermal diffusivity. Nonlinear optical characteristics of these solutions are studied by the z-scan technique using Nd:YAG laser (532 nm, 7 ns, 10 Hz). The nonlinear studies show that the material is highly nonlinear. Nano composite thin films of $\text{Ga}_5\text{Sb}_{10}\text{Ge}_{25}\text{Se}_{60}$ /PVA prepared from nano colloid solutions are characterized using AFM, transmission and reflection spectroscopy. Non linear optical studies on the composite films show these materials can be used as optical limiters and are potential nanocomposite material for the development of nonlinear optical devices with a relatively small limiting threshold.

Chapter 4 condenses the studies done on $\text{Ge}_{28}\text{Sb}_{12}\text{Se}_{60}$ glass. Structural and optical characterizations are done on bulk $\text{Ge}_{28}\text{Sb}_{12}\text{Se}_{60}$ glass. The optical parameters are calculated from the analysis of the transmission and reflection spectra for the $\text{Ge}_{28}\text{Sb}_{12}\text{Se}_{60}$ thin films and composite films using Swanepoel's method. Photo induced studies on the $\text{Ge}_{28}\text{Sb}_{12}\text{Se}_{60}$ thin films shows that there is a power, wavelength and duration of laser radiation dependent shift in the band gap and refractive index resulting to photodarkening. The linear and non linear optical studies are carried out for the $\text{Ge}_{28}\text{Sb}_{12}\text{Se}_{60}$ nano colloid and $\text{Ge}_{28}\text{Sb}_{12}\text{Se}_{60}$ /PVA composite films. Two-photon induced photoluminescence is observed in nano colloid $\text{Ge}_{28}\text{Sb}_{12}\text{Se}_{60}$ chalcogenide glass solutions on excitation with nano second Nd:YAG laser (532 nm). These strong two photon induced photoluminescence signals can be used to image molecularly targeted colloids for cancer cells in vitro and to image biological samples. Influence of cluster size of nano colloids in the

nonradiative recombination is studied using thermal lens technique. The nonlinear absorption coefficient, limiting property and imaginary part of third order non linear susceptibility are studied using open aperture z-scan technique for nano colloids and composite films.

Chapter 5 presents the study on $\text{Ge}_{28}\text{Se}_{60}\text{Ga}_5$ bulk glass prepared by melt quenching method. Optical characterization of the $\text{Ge}_{28}\text{Se}_{60}\text{Ga}_5$ thin film fabricated by thermal evaporation technique is discussed. Synthesis and Optical properties of $\text{Ge}_{28}\text{Se}_{60}\text{Ga}_5$ nano colloids are also presented in this section. Absorption spectroscopy of the nano colloids are analyzed using a UV visible spectrophotometer. The band gap estimated from the absorption spectra of the nano colloids show cluster size dependent change in band gap. Luminescence mechanism in the colloid solutions are studied using Varian Cary 50 Spectrophotometer. The photoluminescence studies on the nano colloids show the dependence of the bandgap and the defect states in the emission spectra. The non linear optical properties of the nano colloids are studied using an open aperture z-scan technique. $\text{Ge}_{28}\text{Se}_{60}\text{Ga}_5$ /PVA composite films are fabricated from the nano colloid solutions and are optically characterized. The nonlinear optical properties of the thin films studied using open aperture z- scan technique show reverse saturable absorption in the investigated samples.

Chapter 6 reports the studies on of erbium doped $\text{Ge}_{28}\text{Sb}_{12}\text{Se}_{60}$ bulk and thin films. The thermal analyses of the doped and undoped samples are studied using differential scanning calorimeter. The refractive index (n), the optical band gap (E_g) and dielectric properties are analyzed from the transmission and reflection spectra on the basis of Wemple – Di Domenico (WDD) single effective oscillator model. Optical band gap obtained from WDD model is found to increase with increase in erbium concentration and it is in good agreement with the values obtained by Tauc's extrapolation method. The observed results have been interpreted as due to rare earth impurities strongly affecting the network and structurally modifying these glasses. Generalized Miller's rule and linear refractive

index are used to find the nonlinear susceptibility and non linear refractive index of the films.

Chapter 7 is devoted to fabrication and characterization of the passive and active devices using chalcogenide glass and polymers. Films stacked with thermally evaporated $\text{Ga}_5\text{Sb}_{10}\text{Ge}_{25}\text{Se}_{60}$ and spin coated $\text{Ga}_5\text{Sb}_{10}\text{Ge}_{25}\text{Se}_{60}$ /PVA are optical characterized using transmission and reflection spectra. The optical parameters and the band gap studies show that the method of stacking results in the tuning of the optical parameters. Photosensitivity of the stacked film studied using a nano second laser irradiation is also presented in this chapter. Studies show that the flexible thin composite IR transmitting filters can be achieved by suitably stacking the films. $\text{Ga}_5\text{Sb}_{10}\text{Ge}_{25}\text{Se}_{60}$ nano colloid doped polymer fibers are developed using preform method and are optically characterized. The optical studies showed that the size-tunable optical properties can be achieved in the polymer fibers by addition of nano colloids of $\text{Ga}_5\text{Sb}_{10}\text{Ge}_{25}\text{Se}_{60}$ chalcogenide glass. Propagation length dependent luminescence studies show that there exist an optimum length at which the luminescence intensity is maximum. The fabricated fiber also exhibits tunability in luminescence peak in accordance with the cluster size of the dopant.

Chapter 8 deals with the summary of the present work along with a brief report of the future prospects.

Lists of publications

I. Journal Publications

- 1) **R. Tintu**, V.P.N. Nampoori, P. Radhakrishnan, Sheenu Thomas, “*Photoinduced changes in optical properties of Ga–Sb–Ge–Se glasses*”, Optics Communications., 284, 222–225 (2011).
- 2) **R. Tintu**, V. P. N. Nampoori, P. Radhakrishnan, and Sheenu Thomas, “*Nonlinear optical studies on nanocolloidal Ga–Sb–Ge–Se chalcogenide Glass*”, Journal of Applied Physics., 108, 073525 (2010).
- 3) **R. Tintu**, V.P.N. Nampoori, P. Radhakrishnan, Sheenu Thomas, “*Preparation and optical characterization of novel Ge–Se–Sb/PVA composite films for optical limiting application*”, J. Phys. D: Appl. Phys., 44, 025101 (2011).
- 4) **R. Tintu**, K Sulakshna, K Saurav, V P N Nampoori, P Radhakrishnan and Sheenu Thomas, “*Ge₂₈Se₆₀Sb₁₂/PVA Composite Films For Photonic Applications*”, Journal of Non-Oxide Glasses., 2, 167- 174 (2010).
- 5) **R. Tintu** , V.P.N. Nampoori, P. Radhakrishnan, Sheenu Thomas, “*Non linear Optical Characterization of erbium doped Ge- Sb- Se thin films*, Discourse - Science (In press).
- 6) **R. Tintu** , V.P.N. Nampoori, P. Radhakrishnan, Sheenu Thomas “*Nanocomposite thin films of Ga₅Sb₁₀Ge₂₅Se₆₀ chalcogenide glass for optical limiting applications*”, Optical Materials., 33, 1221–1225 (2011).
- 7) **R. Tintu**, V.P.N. Nampoori, P. Radhakrishnan, Sheenu Thomas, “*Reverse saturable absorption in nano colloidal Ge₂₈ Sb₁₂ Se₆₀ chalcogenide glass*”, Journal of Non-Crystalline Solids., doi:10.1016/j.jnoncrysol.2011.03.028.
- 8) **R. Tintu** , V.P.N. Nampoori, P. Radhakrishnan, Sheenu Thomas, “*Cluster size and Excitation wavelength dependent Photoluminescence behaviour of nano colloidal Ge- Se- Sb- Ga chalcogenide glass solution*”, Digest Journal of Nanomaterials and Biostructures (under review).
- 9) **R. Tintu** , V.P.N. Nampoori, P. Radhakrishnan, Sheenu Thomas, “*Two photon induced Photoluminescence from Ge₂₈Se₆₀Sb₁₂ nano colloid*” communicated to J. Phys. D: Appl. Phys.

- 10) **R. Tintu**, V.P.N. Nampoory, P. Radhakrishnan, Sheenu Thomas, “*Size dependent Photoluminescence from $Ge_{28}Se_{60} Sb_{12}$ nano colloid*”, communicated to Chalcogenide Letters.
- 11) **R. Tintu**, K.J Thomas, M. Kailasnath, V.P.N. Nampoory, P. Radhakrishnan and Sheenu Thomas, “*Spectral Characteristics of $Ga_5Sb_{10}Ge_{25}Se_{60}$ nano colloid doped PMMA fiber*”, communicated to Optics express.
- 12) **R. Tintu**, V.P.N. Nampoory, P. Radhakrishnan, Sheenu Thomas, “*Stacked $Ga_5Sb_{10}Ge_{25}Se_{60}$ composite films for photonic applications*”, communicated to Material letters.
- 13) **R. Tintu**, V.P.N. Nampoory, P. Radhakrishnan, Sheenu Thomas “*Spectral and non linear optical characterization of $Ge_{28}Se_{60}Ga_5$ nano colloids*”, communicated to Physica Scripta.
- 14) Nithyaja,V.K Jisha , **R.Tintu** ,A.V Saramma and V. P N. Nampoory, “*Kinetics of bacterial colony growth by laser induced fluorescence*”, Laser Physics B., 19, 468-472 (2009).

II. Conference Publications

- 1) **R.Tintu**, V. P. N. Nampoory, P. Radhakrishnan and Sheenu Thomas, “*Optical properties of optical properties of erbium doped Ge-Sb-Se thin films*”, International Conference On Materials For the Millennium, MATCON 2010, Department of Applied Chemistry, CUSAT, Jan 11-13, 2010.
- 2) **R.Tintu**, V P N Nampoory, P Radhakrishnan and Sheenu Thomas, “*Spectral and optical Characterization of Ga-Sb-Ge-Se and polyvinyl alcohol amorphous composite*”, International conference on Advances in Polymer Technology (APT-2010), EOP 04 .JJ Murphy Research Centre, Rubber Park [P] Ltd, Feb 26-27, 2010.
- 3) B Nithyaja, V.K Jisha, **R.Tintu**, A.V Saramma and V P N Nampoory, “*Laser Bacterial Interaction By using Laser Induced Fluorescence Technique*”, Photonics 2008,International Conference on Fiber Optics and Photonics.,IIT Delhi, Dec 13-17, 2008.
- 4) **R.Tintu**, K Sulakshna ,K Saurav, V P N Nampoory, P Radhakrishnan and Sheenu Thomas, “*Amorphous composite chalcogenide glass films for nonlinear optical applications*”, The International Conference on Fiber Optics and Photonics–

PHOTONICS-2010, Indian Institute of Technology Guwahati (IIT Guwahati), Dec 11-15, 2010.

- 5) **R.Tintu**, V. P. N Nampoori, P. Radhakrishnan and Sheenu Thomas “*Fabrication of Ga-Sb-Ge-Se /PVA composite films with strong optical limiting*”, International Conference on Recent Trends in Materials Science and Technology(ICMST), IIST, Thiruvananthapuram, Kerala, Thiruvananthapuram, Oct 29-31, 2010.
- 6) **R.Tintu**, V. P. N. Nampoori, P. Radhakrishnan and Sheenu Thomas, “*Laser induced Photo-darkening in Ga-Sb-Ge-Se thin film*”, National laser Symposium (NLS-09), BARC, INDIA, Jan 13-16, 2010.
- 7) **R.Tintu**, V. P. N. Nampoori, P. Radhakrishnan and Sheenu Thomas, “*Optical Characterization of Ga-Sb-Ge-Se and polyvinyl alcohol amorphous composite*”, National Seminar on Nano Structured materials and Nano photonics, Department of Physics, ST.Teresa’s college, Kerala, Feb 4-5, 2010.
- 8) **R.Tintu**, V. P. N. Nampoori, P. Radhakrishnan and Sheenu Thomas, “*Laser induced photodarkening in chalcogenide thin films*”, Kerala Women’s Science Congress 2010, St. Teresa’s College, Emakulam, Aug 10- 12, 2010.
- 9) **R.Tintu**, V. P. N. Nampoori, P. Radhakrishnan and Sheenu Thomas, “*Optical limiting properties of nano colloid Ge-Se-Sb-Ga chalcogenide glass*”, DAE-BRNS National Laser Symposium, RRCAT, Indore, Dec.1-4, 2010.
- 10) **R.Tintu**, K. Sulakshna ,K. Saurav, V. P. N. Nampoori, P. Radhakrishnan and Sheenu Thomas, “*Third-Order Optical Nonlinearity of nano composite $Ge_{28}Se_{60}Sb_{12}$ /PVA films*”, icmf 2011, Second International Conference on materials for the future, Government Engineering College, Thrissur, Feb 23-25, 2011.

Acknowledgements

*I express my sincere and revered gratitude to my supervising guide **Dr. Sheenu Thomas** for accepting me as research student and offering an opportunity to work in the area of chalcogenide glasses. Gratefully I acknowledge her for the constant support, availability and freedom of work extended to me throughout the period. Her inspiring and friendly nature has been of great value for me.*

*I am very much thankful to **Prof. V P N Nampoori** for his constructive suggestions and constant support he rendered in my work throughout the period. At all stages of my work, his valuable suggestions and critical comments lead me through the right way. I would like to thank **Prof. P Radhakrishnan, Prof C P Girjavallabhan, Prof Nandakumaran and Mr. Kailasnath** for the timely help and encouragement.*

*The utmost care and time set apart by **Dr. Sheenu Thomas, Prof. V P N Nampoori and Prof. P Radhakrishnan** for the final formation of the thesis is really commendable.*

*I am also grateful to **Dr. Johney Issac**, Dept. of Instrumentation, CUSAT, who devoted his precious time whenever I need a help in instrumentation part of the experiments. I am thankful to **Dr. C.S Paulose**, Biotechnology, CUSAT for allowing me to record the Confocal microscope images of the samples. I extend my sincere thanks to the non-teaching staff of ISP and CELOS for all the help and assistance.*

The financial assistance from UGC through CELOS Project is greatly acknowledged. At this moment, let me express my indebtedness towards all my teachers who opened the door of knowledge to me.

I am very much indebted to Cimi and Vidya for proof reading this thesis patiently and providing valuable feedback. I am grateful to Nithyaja for all the support and affection she had given to me. The days spent with Sithara has left warm

memories in my heart. She used to send me journal papers which are not available here within seconds. Only because of those collections of journal papers I was able to get the awareness of advances in the area of my research. With pleasure I acknowledge Sreelekha for her inspiring words. I would like to express my heart-felt thanks to all the friends of the photonics family, Dr. Lyjo, Dr. Geetha, Dr. Sheeba, Dr. Parvathy, Dr. Litty, Dr. Manu, Dr. Rajesh, Dr. Saritha, Dr. Santhi, Thomas Chettan, Jayasree teacher Murali, Mathew, Sony, Linesh, Sudeesh, Mishra, Rose Leena, Divya, Susmitha, Rajeena, Sreeja.S, Bejoy, Jinesh, Retheesh, Reetha teacher, Annie teacher, Libeesh mashi, Bobbey Sir, Pradeep. I am thankful to Indu for accompanying me to lab whenever I have to do experiments in night. I am fortunate to have loving and caring Cimi, Vidya, Nimmy as my friends. They were with me in all my circumstance in my CUSAT life. I also acknowledge my friends Jojo, Lajna, Asha, Abraham for their constant love and support.

I am blessed with my loving family, the greatest gift that God had given me on this earth. There are no words to express gratitude to my **Acha** and **Amma** who have always guided me, believed in me and strived for my achievements. It is only because of them, who I am now. I am deeply and forever indebted to **Sree** for his encouragement and great source of strength that he gave me. His presence has rendered a lot to make my dream come true. My sister, **Kunju** was there for me always and I value it more in my life.

I would like to thank everybody who was important to the successful realization of thesis, as well as expressing my apology that I could not mention personally one by one.

Last, but most important of all, I thank **God** for the wisdom and perseverance that he has been bestowed upon me throughout my life.

Tintu.R

Contents

Chapter 1 Chalcogenide glass: Structure, properties and applications.....	1
1.1. Chalcogens	2
1.2. Amorphous Selenium.....	2
1.3. Chalcogenide glasses	4
1.4. Recent trends in Chalcogenide glasses	7
1.4.1. Chalcogenide glass as nano material.	8
1.4.2. Chalcogenide /Polymer nano composite films.....	11
1.4.3. Chalcogenide glasses fibers.	12
1.4.4. Nano composite chalcogenide glass fiber.....	13
1.5. Properties of Chalcogenide glasses.	13
1.5.1. Structural Property.....	14
1.5.2. Electrical properties and Electronic band structure.	16
1.5.3. Thermal properties.	19
1.5.4. Optical Properties.	20
1.5.4.1. Absorption Spectroscopy.....	21
1.5.4.2. Photoinduced properties.....	22
1.5.5. Optical Non linearity	31
1.6. Applications of ChG.....	34
1.7. Scope of the thesis.....	37
1.8. Conclusions.	38
1.9. Reference.	38
Chapter 2. Materials and Methods.....	49
2.1. Section 1. Preparation techniques	50
2.1.1. Chalcogenide bulk glass preparation.....	50
2.1.2. Thin film preparation.....	52
2.1.2 a) Thermal evaporation technique.	52
2.1.2 b) Spin coating and drop casting	54

2.1.3. Chalcogenide Nano colloid preparation.	55
2.1.4. Composite film preparation.....	57
2.1.5. Multilayers of chalcogenide glass.....	57
2.1.6. Fiber fabrication.	58
2.1.6.1. Continuous extrusion method.....	58
2.1.6.2. Vapor phase oxidation.....	59
2.2. Section 2. Experimental tool and techniques used for characterization of ChG.	63
2.2.1. Structural Characterization.	63
2.2.1 a) X-Ray diffraction (XRD).	63
2.2.1 b) Scanning electron microscopy (SEM)	64
2.2.1 c) Atomic force microscopy (AFM).....	64
2.2.1 d) Bruker Avance III 400MHz NMR spectrometer	65
2.2.1 e) Confocal microscope.....	65
2.2.2. Thermal Characterization.....	66
2.2.3. Thickness measurement	67
2.2.4. Optical characterization.....	67
2.2.4 a) Absorption , reflection and transmission measurements.	67
2.2.4 b) Optical absorption spectroscopy of amorphous semiconductors.....	68
2.2.4 c) Analysis of Transmission Spectra of thin films using Swanepoels method.	70
2.2.4 d) Refractive index of films without interference fringes.....	73
2.2.4 e) Dispersive analysis of the refractive index using Wemple– Di Domenico model.	74
2.2.4 f) Calculation of Nonlinear susceptibility and refractive index using Generalized Millers rule and WDD model	75
2.2.4 g) Absorption coefficient, extinction coefficient, dielectric constants and optical conductivity.....	76
2.2.4 h) Photodarkening experiment.....	77
2.2.4 i) Photoluminescence spectroscopy.	78
2.2.5. Thermal lens technique for diffusivity measurement.	81

2.2.6 .Z-scan technique for the analysis of nonlinear optical properties of the samples investigated	86
2.2.6.1 Open aperture Z Scan.....	88
2.2.7. Two Photon absorption.....	91
2.2.8. Optical limiting studies.	92
2.3. Conclusions.	93
2.4. References	93
Chapter 3. Studies on Ga₅Sb₁₀Ge₂₅Se₆₀ Chalcogenide glass	99
3.1. Section1. Studies on Bulk and thin film Ga₅Sb₁₀Ge₂₅Se₆₀ ChG.	100
3.1.1. Introduction.....	100
3.1.2. Preparation and characterization of Ga ₅ Sb ₁₀ Ge ₂₅ Se ₆₀ bulk glass.	103
3.1.3. Fabrication and Optical characterisation of Ga ₅ Sb ₁₀ Ge ₂₅ Se ₆₀ thin film.	106
3.2. Section 2. Photoinduced darkening in thermally evaporated Ga₅Sb₁₀Ge₂₅Se₆₀ films.....	110
3.2.1. Introduction.....	110
3.2.2. Experimental.....	113
3.2.3. Results and Discussion	114
3.3. Section 3. Studies on Nano colloid Ga₅Sb₁₀Ge₂₅Se₆₀ chalcogenide glass.....	122
3.3.1. Introduction.....	122
3.3.2. Synthesis of Ga ₅ Sb ₁₀ Ge ₂₅ Se ₆₀ nano colloids.....	123
3.3.3. Structural Characterization and absorption spectroscopy.....	124
3.3.4. Photoluminescence from nano colloid Ga ₅ Sb ₁₀ Ge ₂₅ Se ₆₀ ChG.....	128
3.3.5 Thermal diffusivity of Ga ₅ Sb ₁₀ Ge ₂₅ Se ₆₀ nano colloid	134
3.3.6. Nonlinear optical studies on Ga ₅ Sb ₁₀ Ge ₂₅ Se ₆₀ nano colloid.	136
3.3.7. Optical limiting.....	139
3.4 .Section 4. Optical Characterization on nano composite Ga₅Sb₁₀Ge₂₅Se₆₀ /PVA films.....	141
3.4.1. Introduction.....	141

3.4.2. Fabrication of $Ga_5Sb_{10}Ge_{25}Se_{60}$ /PVA composite films.	141
3.4.3. Determination of the optical parameters.	142
3.4.3 a) Refractive index and dispersion analysis of refractive index.....	145
3.4.4. NLO studies on $Ga_5Sb_{10}Ge_{25}Se_{60}$ /PVA composite films.....	146
3.5. Conclusions	150
3.6 .References	152
Chapter 4. Studies on $Ge_{28} Sb_{12}Se_{60}$ Chalcogenide glass	159
4.1. Introduction	160
4.1 Section 1. Studies on bulk and thin films of $Ge_{28}Se_{60}Sb_{12}$	162
4.1.1. Preparation and characterization of $Ge_{28}Se_{60}Sb_{12}$ bulk glass.....	162
4.1.2. Fabrication and Optical characterisation of $Ge_{28}Se_{60} Sb_{12}$ thin films.....	165
4.2. Section 2. Photoinduced darkening in $Ge_{28}Se_{60}Sb_{12}$ films	168
4.2.1. Introduction.	168
4.2.2. Experimental.....	169
4.2.3. Results and discussion	169
4.3 Section 3. Studies on Nano colloid $Ge_{28} Sb_{12}Se_{60}$ chalcogenide glass	172
4.3.1. Introduction.....	172
4.3.2. Synthesis of $Ge_{28}Se_{60}Sb_{12}$ nano colloids.....	173
4.3.3. Results and discussion	173
4.3.3.1. Structural Characterization and absorption spectroscopy.....	173
4.3.3.2 Photoluminescence from nano colloid $Ge_{28}Se_{60}Sb_{12}$ ChG.....	176
4.3.3.3. Thermal diffusivity of $Ge_{28}Se_{60}Sb_{12}$ ChG nano colloids.....	184
4.3.3.4 Non Linear Optical studies on $Ge_{28}Se_{60} Sb_{12}$ nano colloids.	185
4.4. Section 4: $Ge_{28}Se_{60}Sb_{12}$ /PVA nano composite films for photonic applications	190
4.4.1. Introduction.....	190
4.4.2. Experimental.....	190

4.4. 3. Results and Discussion	191
4.4.3.1. Optical parameters.....	191
4.4.3.2. NLO studies on $Ge_{28}Se_{60}Sb_{12}/PVA$ composite films.....	196
4.5. Conclusions.	200
4.6. References.	201
Chapter 5. Studies on $Ge_{28}Ga_5Se_{60}$ Chalcogenide glass.....	205
5.1. Introduction.....	206
5.2. Studies on bulk and thin film $Ge_{28}Ga_5Se_{60}$ glass.	207
5.2.1. Preparation and characterization of bulk $Ge_{28}Ga_5Se_{60}$ ChG.....	207
5.2.2. Optical characterization of $Ge_{28}Se_{60}Ga_5$ thin films prepared by thermal evaporation.....	208
5.3. Studies on Nano colloids of $Ge_{28}Se_{60}Ga_5$ chalcogenide glass.	211
5.3.1. Synthesis, structural analysis and absorption spectroscopy of $Ge_{28}Se_{60}Ga_5$ nano colloids.	211
5.3.2. Excitation wavelength and cluster size dependent change in photoluminescence spectra of $Ge_{28}Se_{60}Ga_5$ nano colloids.	213
5.3.3. Nonlinear optical studies on $Ge_{28}Se_{60}Ga_5$ nano colloids	216
5.4 Fabrication and characterization of $Ge_{28}Se_{60}Ga_5/PVA$ nano composite films	219
5.4.1. Preparation and optical parameters of $Ge_{28}Se_{60}Ga_5/PVA$ nano composite films	219
5.4.2. Nonlinear optical properties of $Ge_{28}Se_{60}Ga_5/PVA$ nano composite films.	221
5.5. Conclusions.....	222
5.6. References	223
Chapter 6. Fabrication and characterization of erbium doped $Ge_{28}Sb_{12}Se_{60}$ ChG.....	225
6.1. Introduction.....	226

6.2. Experimental.....	227
6.3. Structural, thermal and optical characterization of bulk glasses.	228
6.3.2. Structural and thermal analysis	228
6.3.3. Absorption spectroscopy of erbium doped bulk glasses.....	230
6.4. Optical characterization of erbium doped thin films.	231
6.4.1. Dispersion analysis of the refractive index	235
6.5. Conclusions.	238
6.6. References.....	239
Chapter 7. Chalcogenide Nano Composites for active and passive photonic devices.....	241
7.1. Section 1. Double-layered chalcogenide nano composites.....	242
7.1.1. Introduction.....	242
7.1.2. Fabrication of stacked layers.....	245
7.1.3. Optical studies on double layered films.	246
7.2. Section 2. Fabrication and characterization of nano colloid $Ga_5Sb_{10}Ge_{25}Se_{60}$ doped polymer optical fibers.....	252
7.2.1. Introduction.....	252
7.2.2. Fabrication of nano colloid doped polymer optical fibers.	255
7.2.3. Optical characterization.....	261
7.2.4. Luminescence studies on $Ga_5Sb_{10}Ge_{25}Se_{60}$ nano colloid doped PMMA fiber.....	262
7.2.4.1. Luminescence studies on excitation with DPSS laser.....	263
7.2.4.2. Luminescence from the fiber on excitation with white LED.....	271
7.3. Conclusions.....	274
7.4. References.....	275
Chapter 8. Conclusions and future prospects.....	281
8.1. Conclusions.....	282
8.2. Scope for future work.....	287
Curriculum Vita	

Chapter 1

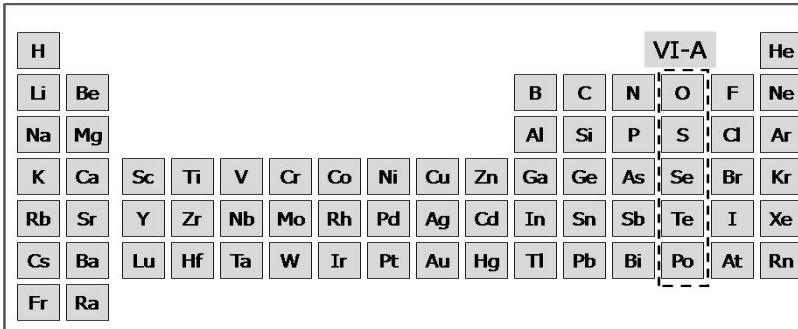
CHALCOGENIDE GLASS: STRUCTURE, PROPERTIES AND APPLICATIONS

- 1.1. Chalcogens
- 1.2. Amorphous Selenium
- 1.3. Chalcogenide glasses (ChG)
- 1.4. Recent trends in Chalcogenide glasses
- 1.5. Properties of Chalcogenide glasses
- 1.6. Applications of ChG
- 1.7. Scope of the thesis
- 1.8. Conclusions
- 1.9. Reference

This chapter gives an overview on the structure, properties and potential applications of chalcogenide glasses. Recent trends like the fabrication of new hybrid materials based on chalcogenide glass and polymer and their possibility in the different fields are mentioned. Brief description of structural, electronic, thermal and optical properties of the chalcogenide glasses is given. Different permanent and temporary photoinduced mechanisms like photodarkening and photoluminescence in these materials are described along with well defined models. Finally, the scope of the work presented in this thesis is also given.

1.1. Chalcogens

Chalcogens are elements in group 16 (or VI) in the Periodic Table. The group consists of the elements: oxygen, sulfur, selenium, tellurium, and polonium as shown in Figure 1.1. The name of the group was proposed by Wilhelm Blitz and colleague Werner Fischer of the Institute of Inorganic Chemistry at the University of Hannover, Germany in 1932¹. The term "chalcogens" was derived from the Greek word *chalcos*, meaning "ore formers," since they all are found as copper ores¹. Their compounds are referred to as "chalcogenides." The members of this group show increasing metal character as the atomic number increases. Both oxygen (O) and sulfur (S) are nonmetals, while selenium (Se) and tellurium (Te) are metalloids (both are semiconductors) and polonium (Po) is a metal.



H																			VI-A	He
Li	Be										B	C	N	O	F	Ne				
Na	Mg										Al	Si	P	S	Cl	Ar				
K	Ca	Sc	Ti	V	Cr	Co	Ni	Cu	Zn	Ga	Ge	As	Se	Br	Kr					
Rb	Sr	Y	Zr	Nb	Mo	Rh	Pd	Ag	Cd	In	Sn	Sb	Te	I	Xe					
Cs	Ba	Lu	Hf	Ta	W	Ir	Pt	Au	Hg	Tl	Pb	Bi	Po	At	Rn					
Fr	Ra																			

Figure 1.1: Periodic table.

1.2. Amorphous Selenium

The chalcogen used in the present work is selenium. Amorphous selenium has wide commercial applications. The

material is known to be composed of entangled chains and or ring molecules as given in Figure 1.2. The structure of amorphous selenium consist of random mixture of rings and helical chains accompanied by coordination defects. In the stable condensed phase, chalcogenide elements form covalent bonds with two nearest neighbours in accordance with 8-N rule². The atoms have six electrons in the outermost shell with a configuration of s^2p^4 . Electrons in s state do not participate in bonding since these states have energies well below those of p states. Two covalent bonds are formed between chalcogen atoms by p electrons, but the other electron pair called lone pair (LP) remains unbonded.

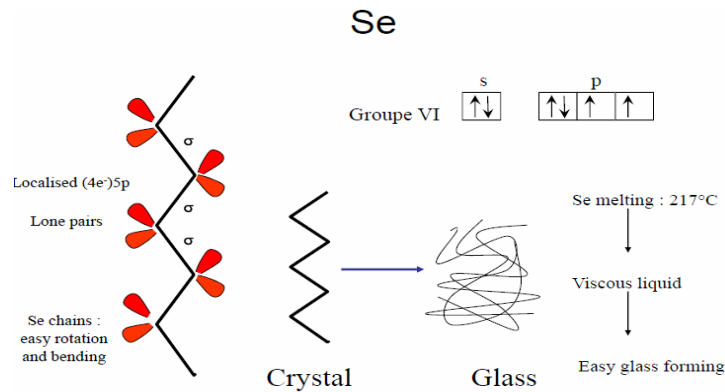


Figure 1.2: Structure of crystalline and amorphous Selenium along with the electronic configuration.

Such structures are typical of organic polymers such as polyethylene and because of this resemblance, amorphous selenium can be referred to as an “*inorganic polymer*”¹³. Its applications in devices like rectifiers, photocells, xerography, switching, memory etc. made it very attractive in the field of instrumentation⁴⁻⁶. Because of

the large atomic radius compared with oxygen in oxide glasses and sulfur in sulfide glasses, selenium plays an important role in the non-linear optical properties in selenide glasses. But working with Se causes some problems like the ageing effect and low sensitivity⁷. Hence in order to produce changes in the properties of selenium glass, it is worth adding more than one component into the selenium matrix to get rid of these problems. To overcome these problems, certain additives (Ge, Bi, As, etc) are added to make binary alloys with selenium, which in turn give high sensitivity, a high crystallization temperature and smaller ageing effects. The addition of the network formers (Group IV and V) such as silicon (Si), germanium (Ge), tin (Sn), phosphorus (P), arsenic (As), and antimony (Sb) establishes cross-linking between the tetrahedral and pyramidal units which facilitates stable glass formation. The addition of Ge with 4-fold bond coordination compared with As (3-fold) and S, Se (2-fold) produces a more 3-D glass network which increases glass transition temperature (T_g). It is also well established that substituting Se for S moves the band-gap from the visible to IR allowing the nonlinearity to be resonantly enhanced in the 1550 nm telecommunications band⁸.

1.3. Chalcogenide glasses

Chalcogenide glasses (ChG) belong to an important class of amorphous solids which contain at least one chalcogen element (sulphur, selenium and tellurium) as a major constituent¹. An amorphous solid is defined as any solid that shows a short range order molecular structure or medium range order but does not show

any long range order¹. Glass, an amorphous solid is defined in American Society for Testing and Materials as ‘an inorganic product of fusion which has been cooled to a rigid condition without crystallization’⁹. Glass formation is possible in a system of any composition provided that it contains sufficient ‘network modifier’⁹. Network modifiers produce three dimensional random network of strong bonds in a system. Glass is an isotropic material, where as crystalline materials are generally anisotropic. Like all glasses ChG’s exhibit a glass transition temperature, a fact which becomes very important for the processing of bulk glasses into thin film and fiber form as required for most applications.

Chalcogenide glasses have certain unique properties that make them of interest compared to other materials for optoelectronic applications¹⁰⁻¹³. Their good infrared transparency (as shown in Figure 1.3), high refractive index, photosensitivity, amenability to doping and alloying, low phonon energy and compatibility with low temperature processing make them smart materials for optical integration. Moreover, due to their amorphous nature, chalcogenide glasses do not need to be grown on single crystalline substrates and can potentially be incorporated within the interconnect levels of a CMOS chip⁹. This back-end compatibility minimizes the need for dedicated processing facilities, which reduces fabrication costs and leverages the existing and well-developed semiconductor technologies. Many of the unique properties of ChG are a direct result of low phonon energy associated with this material resulting from the heaviness of the chalcogen nuclei ¹².ChG

with heavier nuclei and weaker bonding have lower vibrational frequency and thus lower phonon energies.

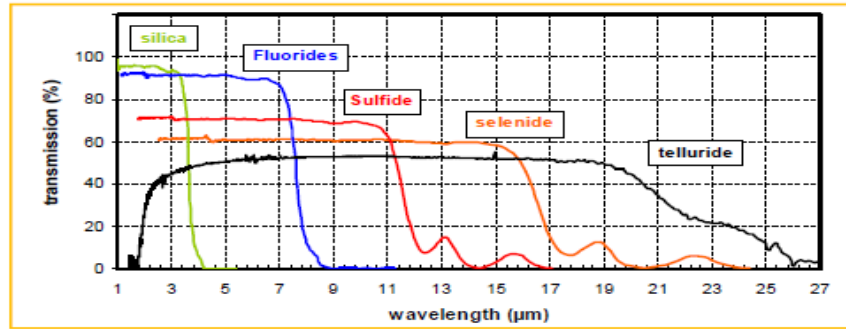


Figure 1.3: Optical transmission of the three families of chalcogenide glass, compared to silica and fluoride glasses.

Semiconducting and glassy nature of ChG in comparison to other materials is schematically represented in Figure 1.4.

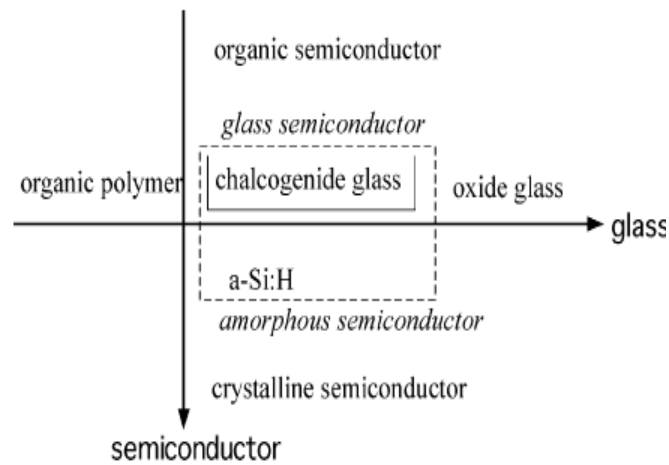


Figure 1.4: Characterization of chalcogenide glasses as glasses and Semiconductors in comparison with other materials.

The historical development of ChG as optical materials in infrared systems began with the rediscovery of arsenic trisulfide glass

by R. Frerichs¹⁴ in 1950. Development of the glass as a practical optical material was continued by W. A. Fraser and J. Jerger¹⁵ in 1953 at Servo Corporation. Jerger, Billian, and Sherwood¹⁵ extended their investigation of arsenic glasses containing selenium and tellurium, and later adding germanium as a third constituent. Research in this fascinating area of chalcogenides glasses gained its momentum in with the discovery that ChG's behave like intrinsic semiconductors by Kolomiets¹⁵. Later on Eaton, Ovshinsky and Pearson¹⁶ observed their semiconductor properties and switching phenomenon. The discovery of switching and memory effects in ChG was a turning point which attracted many researches to the world of amorphous chalcogenide semiconductors.

1.4. Recent trends in Chalcogenide glasses

Device applications using ChG usually require the glass to be processed into either fiber or thin film form. Conventionally, chalcogenide films are deposited using physical vapour deposition (PVD) techniques such as thermal evaporation, pulsed laser deposition or sputtering from the bulk melt quenched ChG¹⁷⁻²¹. These methods suffer from several shortcomings which intermittently confine their use. They are in general limited to largely two-dimensional surfaces and require high-vacuum processing and sometimes difficult target preparation in the case of laser deposition and sputtering. Another impediment, particularly for thermal evaporation, is the observation that the resulting film often has a different composition (stoichiometry) from that of the parent glass

target, or is inhomogeneous in thickness, owing to differential volatility in multi-component materials. A common solution to this problem is solution-based coating methods²². Solution-based coating methods offer a prospective pathway to overcome these limitations by controlling the chemical composition of the solution phase and hence the chemistry of the film with high accuracy. Solution casting method offers higher production rate, simpler processing and opportunity to incorporate other materials like metals, semiconductors, nano particles, polymers etc.

1.4.1. Chalcogenide glass as nano material

Nano colloids of chalcogenide glass have gained a lot of interest in the research field recently²³⁻²⁷. Understanding the chemical stability of the glasses, and finding the suitable solvent for making solutions is very important in nano colloid preparations. Laser ablation method was employed for the preparation of aqueous As_2S_3 colloidal solution by R A Ganeev et al.²⁸. Their investigation of nonlinear-optical parameters on the prepared nano colloids showed the non linear refractive index to be $-7.5 \times 10^{-18} \text{ m}^2\text{W}^{-1}$ and nonlinear absorption coefficient to be 1 cmGW^{-1} . Eventhough the samples showed good optical non linearity the ageing occurs in the solution due to spontaneous nanoparticles clusterization. So in order to avoid this ageing, stabilizer have to be added.

Another method for the preparation of chalcogenide nano colloid was by reorganisation of dissolution of As_2S_3 in liquid ammonia by Berzelius and Bineau²⁹. Then onwards a lot of structural

and optical studies were carried out on chalcogenide nano colloid prepared by dissolution in different solvents like ethylenediamine, n-butylamine, n-propylamine, diethylamine, triethylamine and other organic solvents³⁰⁻⁴². Even though attempts to understand the mechanism of dissolution of chalcogenides in amines and the existence of chalcogenide clusters with dimensions of several nanometres were reported earlier, factors such as the use of suitable solvent for bulk glass dissolution solubility and solution viscosity have only been studied recently by Song et al.³⁵. G.C. Chern and I. Lauks³⁶⁻³⁸ had made important contribution in the area of nano colloid chalcogenide glass like As_2S_2 , As_2Se_3 , As_2Te_3 and Ge-Se. The proposed dissolution product of As_2S_3 and $Ge_{23}Sb_7S_{70}$ in amine solvent is as given³⁹ in Figure 1.5.

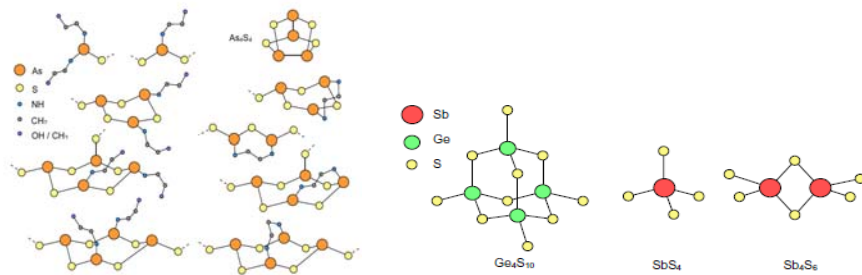


Figure 1.5: Structure of dissolution product of a) As_2S_3 b) $Ge_{23}Sb_7S_{70}$ in amine solvent.

Thin films prepared from nano colloid $Ge_{23}Sb_7S_{70}$ ChG are reported to be of promising optical properties. Shanshan Song et al.⁴⁰ have shown that photo-responsive nano colloid ChG can be used for tuning quantum cascade (QC) lasers. The photosensitivity of the cladded chalcogenide layer is utilized for tuning of over 30 nm, by

deep-etched distributed Bragg gratings in cladding layer. ChG based QC lasers offers high power and room temperature operation making them a promising choice for trace-gas detection in the mid-infrared where the spectroscopic fingerprints of majority atmospheric trace gas are found. Recently in 2010 Chalcogenide opal and inverse opal photonic crystals were successfully fabricated from nano colloid $As_{30}S_{70}$ chalcogenide glass by Tomas Kohoutek et al.⁴¹. The fabricated photonic structures from nano colloid $As_{30}S_{70}$ and silica as shown in Figure 1.6, are proposed for designing novel flexible colloidal crystal laser devices, photonic waveguides and chemical sensors.

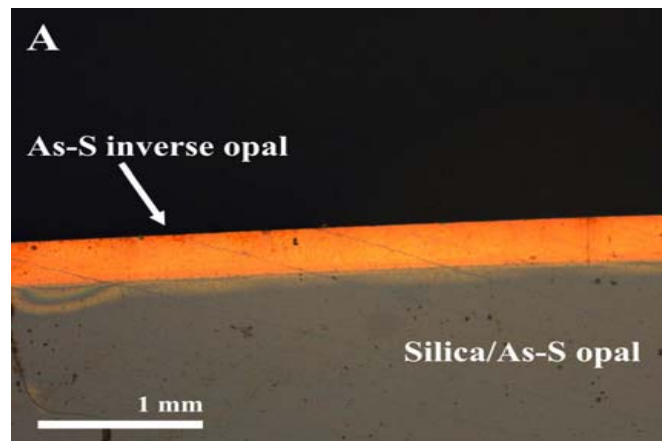


Figure 1.6: Photonic structures from nano colloid $As_{30}S_{70}$ and silica⁴¹.

The solution based synthesis of photonic structures based on ChG deserves immense application in different fields of optoelectronics. Solution based approach to the $Ga_5Sb_{10}Ge_{25}Se_{60}$, $Ge_{28}Sb_{12}Se_{60}$ and $Ge_{28}Ga_5Se_{60}$ for the fabrication of different photonic structures and their application in different fields of photonics are presented in this thesis.

1.4.2. Chalcogenide /Polymer nano composite films

Presently, great interest has been devoted to the fabrication of new materials suitable for photonics applications. Among these, the amorphous chalcogenide structures are of considerable interest due to their effectiveness in nonlinear optical characteristics. The Quantum wave stacks (QWS) devices based on high refractive index chalcogenides and low refractive index polymers seem to be promising for applications challenging favourable performance ratio⁴². There exist certain challenges associated with the use of chalcogenide glasses in integrated optics like toxicity, durability, large coefficient of thermal expansion (CTE) etc. This can be overcome by making composite films using chalcogenide glass and polymer. As it was shown by many authors⁴³⁻⁵¹ it is reasonable to combine the properties of these two groups of materials by getting nano-composites from polymers and ChG for optimization of the sensitive parameters, simplification of the technology of fabrication, improving the stability of the registration media, solving problems related to ecological outputs etc.

Tomas Kohoutek⁴⁵ recently fabricated Ge-Se/Polystyren (PS) dielectric and Au/Ge-Se/PS /dielectric reflectors from amorphous chalcogenide and polymer films with the optical reflectivity (R) higher than $R > 99\%$ near $\lambda \sim 1550$ nm using low-temperature and inexpensive deposition techniques. Thin polymer films anchored to ChG are widely used for modulation of the surface properties and for fabrication of versatile adaptive surfaces capable of responding to

changes in the environment. Diffractive structures by holographic and e-beam recording technologies were recently reported by Andriesh et al.⁵¹ using rare-earth-doped chalcogenide glasses and polymer nanocomposite.

1.4.3. Chalcogenide glasses fibers

Optical fibers need low-phonon-energy materials which exhibit excellent resistance to moisture corrosion and good glass-forming ability. The only vitreous materials that accomplish these requirements are glasses based on sulphur, selenium, or tellurium⁵². Chalcogenides fibers and ChG fibers doped with rare earths have been studied for active applications in the near- and mid-IR⁵³⁻⁵⁹. The low phonon energy of chalcogenide glasses activates many mid-IR transitions for rare-earth ions that are usually absent in materials with higher phonon energies. Arsenic trisulfide glasses suffer from poor rare-earth solubility and shows signs of crystallization coinciding with the temperature for fiber-drawing. Ge-As-Ga-Sb-S glass doped with neodymium chalcogenide fibers exhibited an optical amplification at 1.083 μm with a maximum internal gain of 6.8 dB achieved for a pump power of 180 mW⁵⁸. ChG fibers find application in all optical switches and fiber lasers⁵⁹. Holey fibers based on Ga-La-S glasses chalcogenide glasses are recently demonstrated⁶⁰. In these structures, the holes generate a low effective index in the cladding and permit light guiding in the solid core by internal reflection at the core-clad interface. Review on chalcogenide holey fibers by J. Trolès et al.⁶¹ says holey fibers possess the potential

for new applications in the fields of high nonlinear optics and large-mode-area propagation together with single-mode operation at all wavelengths.

1.4.4. Nano composite chalcogenide glass fiber

Yu et al.⁶² have reported on optical properties of quantum dots incorporated into PMMA fibres fabricated by physical methods. Nanoscale reinforcements found far-reaching interests in the polymer field, because reinforced materials (composites) display better structural mechanical properties compared to the pure polymers. Semiconducting nanoparticles (quantum dots) have been materials of curiosity when it comes to polymer reinforcement due to their exciting properties, particularly their remarkable size-dependent optical properties⁶³. The tunable optical properties of quantum dots introduced into polymers may enhance light emission from the polymer. Quantum dots (QD) have an advantage over other dopants because of their small size distribution and high surface area which allows better distribution within the fibres. Studies on quantum dots and other dopants in polymer optical fibers (POF) are already been undertaken by many researchers⁶²⁻⁶⁹. But the reinforcement of chalcogenide nano colloid in polymer fibers is not yet reported. The development and studies on novel chalcogenide nano colloid doped PMMA fiber is presented in this thesis in Chapter 7.

1.5. Properties of Chalcogenide glasses

Some of the important properties of chalcogenide glass like structural, electrical, thermal and optical properties are as follows.

1.5.1. Structural Property

The atomic structure and related properties in chalcogenide glasses depend upon preparation methods and history after preparation⁷⁰. This prehistory dependence is common in all non-equilibrium glass systems. Various experimental techniques like X-ray, neutron, electron diffractions, the anomalous x-ray scattering, the molecular vibrational (IR and Raman) spectra, the Electron Spin Resonance (ESR), the Nuclear Magnetic Resonance (NMR) and the Extended X-ray Absorption Fine Structure (EXAFS) are used to probe the microscopic structures of ChG.

Amorphous chalcogenide materials are reported to have a disordered structure even though the disorder in the structure of an amorphous material is not complete on the atomic scale¹. ChG lacks a long range periodic ordering of the constituent atoms. Chemical ordering has a significant effect on the control of the atomic correlation in these glassy solids. This is particularly important if one approaches from the nonstoichiometric to the stoichiometric compositions. The chemical bonding between atoms, which result in the short-range order, is responsible for most of the properties of amorphous materials. The semiconducting property of chalcogenide glasses is, however, a direct consequence of the covalent bonding existing in these materials. In chalcogenide glasses the covalent bonded atoms are arranged in an open network with order extending up to the third or fourth nearest neighbours. So chalcogenide glasses are also referred to as network glasses². Various structural models

have been developed for amorphous materials depending upon their chemical nature. The Continuous Random Network (CRN) or Zachariasen model⁷¹ was developed for directional bonding, present in covalent solids. Another model Random Close Packing (RCP) or Bernal model⁷² was developed for non-directional bonding present in metallic solids. The Random Coil (RC) [Flory model]⁷³ deals with one dimensional bonding present in polymers.

The CRN model¹ suggested for amorphous semiconductors is based on certain features of these materials like directional nature of bondings, well-defined SRO (the bond length and bond angle) and the topological constraints. The main drawback of the CRN model is that it assumes that all constituent atoms satisfy their valence requirements (8-N), where N is the valency. Hence, the structural defects such as dangling bonds, voids etc. are not taken into account.

The Random Close Packed (RCP) model¹⁵ is applicable for non-directional bonding present in metallic solids providing a satisfactory model for the structure of amorphous metals. Like the CRN model and RCP model, Random Coil model, is essentially a homogeneous single-phase model. This model is widely applied to one-dimensional bonding present in polymers.

To understand the chemical ordering and structural model consider the simple case of binary alloy $A_x B_{100-x}$. The atoms A and B, say belongs to the 'a' and 'b' groups of the periodic table, respectively. There are two models to count the fraction of A-A, A-B and B-B

bonds by assuming that all atoms satisfy the (8-N) rule. These are the Random Covalent Network (RCN) model and the Chemically Ordered Network (CON) model. The RCN considers these bond distributions as purely statistical and neglects the relative bond energies i.e. in random. The fraction of these bonds depends upon their coordination numbers (8-a), (8-b) and the concentration x . Therefore it gives A-A, A-B and B-B bonds at all the concentrations except at $x = 0$ and 1. Where as the CON model considers the preferential ordering i.e. the heteropolar A-B bonds are more preferred entities. Thus, this model predicts a chemically ordered phase at critical composition $X_c = Y_a / (Y_a + Y_b)$ (the coordination of the A and B atoms are $Y_a = 8 - a$ and $Y_b = 8 - b$ respectively). The structural controversy is less for selenium.

1.5.2. Electrical properties and Electronic band structure

Structural defects play an important role in electrical properties than the role of impurities in ChG. The band of the states existing near the centre of the gap arise from specific defect characteristics of the material like dangling bonds, interstitials etc¹⁵. Thus the band structure of the ChG specifically defines its property. Density of states (DOS) diagram is used to explain or predict the properties of a material in the band theory. It denotes the number of electron states per unit energy per electron a material will have at an energy level and it is used successfully to describe many of the characteristic found in a crystalline solids. Band theory for amorphous materials was first explained by Mott⁷⁰ by extending the

band theory of crystalline materials. Mott suggested that the spatial fluctuations in the potential caused by the configurational disorder in amorphous materials could lead to the formation of localized states based on Anderson's localization principle⁷⁴. The diagram of the DOS for crystalline and the modification of it for amorphous materials by Mott is given in Figure 1.7⁷⁵.

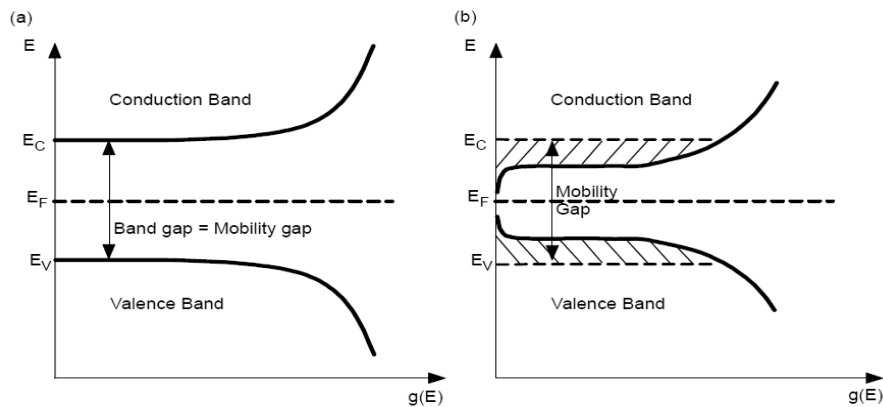


Figure 1.7: (a) DOS of a crystalline semiconductor, (b) DOS models proposed by Mott for amorphous semiconductors.

These localized states do not occupy all the energy states in the band but they form a tail above and below the band. An electron in a localized state will not diffuse at zero temperature to other allowed states with corresponding potential fluctuations. Several models have been proposed for the band structure of amorphous semiconductors using the concept of localized states in band tails. The first diagrammatic representation of the band structure of amorphous semiconductor was given by Cohen⁷⁶ and is referred to as the Cohen-Fritzsche-Ovshinsky (CFO) model. This model suggests that the tail

states extend across the gap in a structure-less distribution. The band picture of CFO model is shown in Figure 1.8. The relevant features of this model are 1) continuous tailing of the localized states, which is so high that they overlap in the middle of the gap. Thus some of the normally filled valence band tails would be at a higher energy than the normally empty conduction tails. Obviously, a redistribution of charge carriers must take place. Thus electrons transfer takes place from the high lying valence band tails to the low-lying conduction band tails. Hence, there is a deep electron trap above and below the E_F which is shown in Figure 1.8 a. (2) This model predicts the existence of the average mobility gap between the valence and conduction bands. (3) There is a finite density of these states $g(E_F)$ at E_F . If $g(E_F) > g(E_c)$, it would make materials to be metallic otherwise they would remain as semiconductors. The existence of high density of $g(E_F)$ turns materials into undopable ones. The band picture of model proposed by Marshall and Owen⁷⁷ is given in Figure 1.8.b.

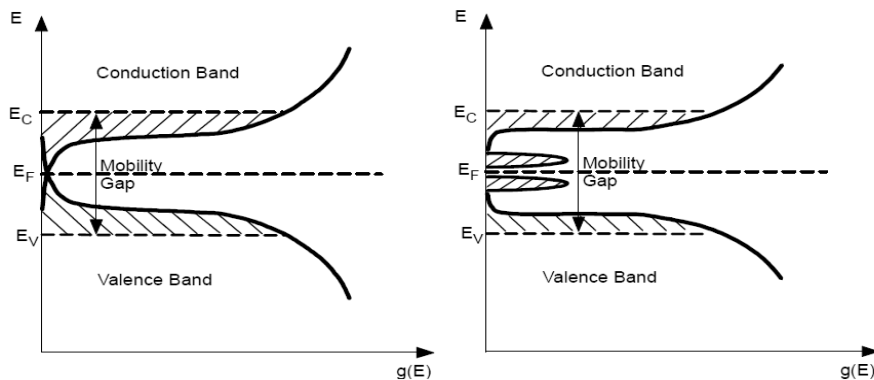


Figure 1.8: DOS models proposed by Cohen, Fritzsche and Ovshinski (CFO) and DOS models proposed by Marshall and Owen. The hatched regions denote localized states.

The main difference between the CFO and the David Mott (DM) model⁷⁰ is the origin of deep traps in the middle of the gap. There is also another model proposed by Emin called Small polaron model⁷⁸. Emin⁷⁸ suggested that the extra free carriers in some amorphous semiconductor may enter as a self trapped (small polaron) state as a result of the surrounding atomic lattice. All of the chalcogenide glasses appear to share a common electronic band structure. The chalcogen atoms all have six valence electrons in an s^2p^4 configuration. The two half-filled p shells participate in the formation of covalent bonds, so the chalcogen atoms are normally two fold coordinated. The valence band of chalcogenide glasses consists of states from the p bonding (σ) and lone pair (LP) orbitals. The LP electrons have higher energy than the bonding electrons, so the full LP band forms the top of the valence band. The conduction band is formed by the antibonding (σ^*) band. The LP band falls between the σ and σ^* bands, so the bandgap is about half of the bonding-antibonding splitting energy. Because the electrical properties are determined by the LP band, these chalcogenide glasses are called lone-pair semiconductors¹⁵.

1.5.3. Thermal properties

Glass transition, crystallisation and melting temperatures, along with the coefficient of thermal expansion, thermal diffusivity etc are the thermal properties associated with chalcogenide glass. The glass transition temperature of ChG is related to the magnitude of cohesive forces within the network and these forces must be

overcome to allow atom movement. Thermal conductivity is critical to many electronic devices^{79,80}. Thermal conductivity, of a material results from transport of energy via electrons or via lattice vibrations (phonons). The total thermal conductivity is the sum of both. Thermal conductivity is related to phonon mean free path. Phonon mean free path in ChG is considerably shorter and correspondingly thermal conductivity is less. Thermal diffusivity (T_D) has a major role in switching exhibited by a chalcogenide glass⁸¹. T_D decides the rate at which heat can be dissipated away from the conducting channel. It has been recently pointed out that there is a strong correlation between the thermal diffusivity and the switching behaviour of chalcogenide glasses⁸⁰. ChG with low thermal diffusivity are likely to exhibit memory behaviour and those with higher values of thermal diffusivity may show threshold-type switching. Consequently, the measurement of thermal diffusivity of switching glasses is important for identifying suitable materials for phase change memory applications. Like optical absorption coefficient, thermal diffusivity is unique for each material and is often ideal over conductivity measurements due to its insensitivity to radiative heat losses as the latter involves heat fluxes that are difficult to control.

1.5.4. Optical Properties

Chalcogenide glasses are promising candidates for photonic applications due to their attractive optical properties, such as high refractive index, high photosensitivity and large optical nonlinearity. The investigation of the optical properties of chalcogenide glasses is

of considerable interest and affords critical information about the electronic band structure, optical transitions and relaxation mechanisms. The optical and electrical properties of chalcogenide glasses are generally much less sensitive to non stoichiometry and the presence of impurities is less sensitive than crystalline semiconductors.

1.5.4.1. Absorption Spectroscopy

The typical absorption spectra of chalcogenide glass is shown in Figure 1.9. In amorphous semiconductors, the optical absorption edge spectra generally contain three distinct region^{2,15}: A) High absorption region ($\alpha=10^4 \text{ cm}^{-1}$), which involves the optical transition between valence band and conduction band and determines the optical bandgap, B) Spectral region with $\alpha=10^2\text{-}10^4 \text{ cm}^{-1}$ is called Urbach's exponential tail (In this region most of the optical transitions take place between localized tail states and extended band states) and C) The region $\alpha \geq 10^2 \text{ cm}^{-1}$ involves low energy absorption and originates from defects and impurities.

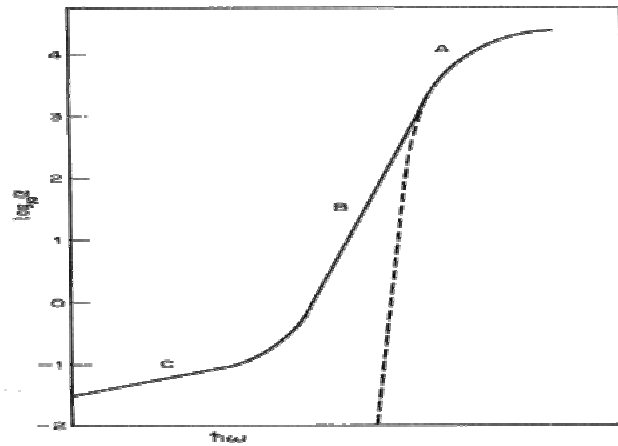


Figure 19: Regions A,B,C of a typical absorption curve of chalcogenide glass.

1.5.4.2. Photoinduced properties

The photoinduced phenomena exhibited in ChG can be grouped into three categories¹⁵: the photon mode, in which the photoelectronic excitation directly induces atomic structural changes; the photothermal mode, in which photoelectronic excitation induces some structural changes with the aid of thermal activation; and the heat mode, in which the temperature rise induced by optical absorption is essential. Interestingly, these three kinds of phenomena are likely to appear in sulfides, selenides, and tellurides, respectively^{2,15,82}. The photon effects are of particular interest from the viewpoint of fundamental science and modern applications.

One of the interesting properties of the chalcogenide materials is their sensitivity to the action of light and other electromagnetic radiations. Therefore, many effects discovered in chalcogenide disordered materials are

based on the action of light. Some of the important photoinduced effects^{15,82-85} are **photo-darkening**, photo-bleaching, photo-plastic effect, photo-induced fluidity, photo-induced ductility, optomechanical effect, polarization-dependent photoplastic, light-stimulated interdiffusion effect, photo-expansion, photocontraction, athermal photo-induced transformation effect, photo-induced amorphisation effect, laser-induced suppression of photocrystallization, photoinduced softening and hardening effect, photo-amplified oxidation effect, photo-dissolution, photo-doping effects, photo-polymerization effect, photo-anisotropy effect, photo-induced dichroism, photoinduced scattering of light, photo-elastic birefringence effect, switching (Ovshinsky) effect, **photoluminescence** etc.

Many types of photosensitive processes observed in the chalcogenide glasses are accompanied by changes in the optical constants, i.e., changes in the electronic band gap, refractive index and optical absorption coefficient. These light-induced changes are favoured in chalcogenide glasses due to their structural flexibility (low coordination of chalcogens) and also due to their high-lying lone-pair p states in their valence bands. Annealing chalcogenide glasses can affect the photoinduced changes, in particular irreversible effects occur in as-deposited films, while reversible effects occur in well-annealed films as well as bulk glasses. Changes in local atomic structure are observed on illumination with light having photon energy near the optical band gap of the chalcogenide.

➤ *Photodarkening*

In chalcogenide glasses the *photodarkening (PD)* process refers to a shift of the optical absorption edge to lower energies upon the application of light whose energy is near that of the band gap. All chalcogenide glasses appear to exhibit the PD process to varying degrees⁸⁴⁻⁹⁰. The role of specific defects in the photodarkening process has yet to be established because a microscopic description of this effect does not exist yet. Several specific defect models have been proposed to account for photoinduced effects. The first defect model was proposed by Mott, Davis and Street (MDS model)¹⁵. This model identifies the defects with negative correlation energy. According to Street and Mott model, chalcogenide glasses contain 10^{18} - 10^{19} cm⁻³ dangling bonds. These bonds are point defects where normal coordination is not satisfied due to the constraint of local topography. The defect creation proposed by them is shown in Figure 1.10.

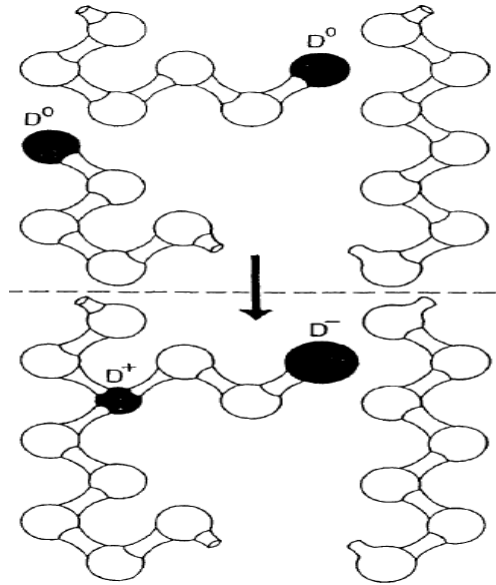
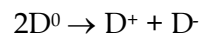


Figure 1.10: A schematic representation of the formation of charged defects D^+ and D^- from two neutral defects D^0 , in accordance with Street and Mott model.

The formation of a D^+ , D^- pair from a broken Se-Se bond (i.e., from two Se dangling bonds) is governed by the reaction,



where the reaction is exothermic because of strong lattice distortions.

These strong lattice distortions mean that the effective electron-electron correlation energy is negative (negative U). Kastner, Adler and Fritzsche¹⁵ (KAF model) have emphasized that the coordinations of the positively and negatively-charged diamagnetic defects are three and one, respectively. These authors also have presented arguments which suggest that these D^+ and D^- defects may require only modest electron interaction energy for stability. In the KAF

version of the model D^- is termed C^{3-} and D^+ is termed C^{3+} in order to show explicitly the coordination of 4 e defect.

Various possible configurations of chalcogen atoms are shown in Figure 1.11. Each possible configuration is denoted C_z^v where C stands for chalcogen atom and v and z are its charge and valence states.

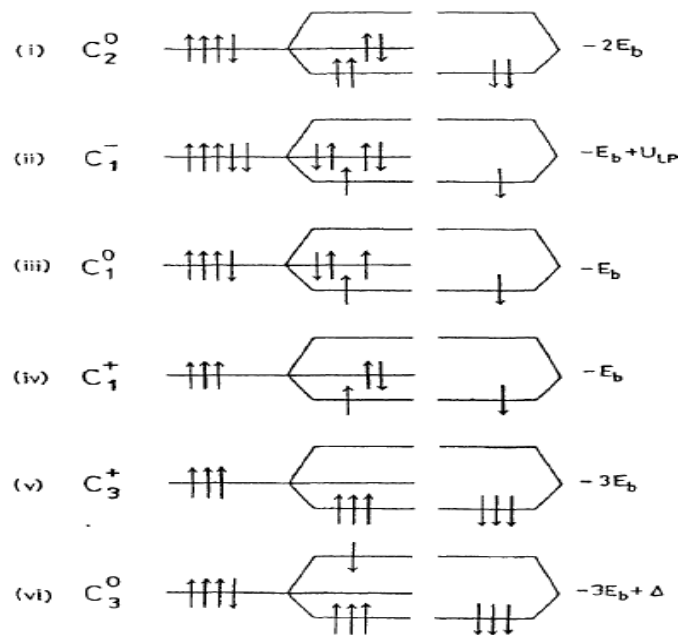


Figure 1.11: The Kastner, Adler and Fritzsche (KAF) model of defects in chalcogenide glasses. E_b is the bond energy, UL_p is the correlation energy. The arrows indicate the spin state of the electrons.

Considering all the defects model for ChG and band models Tanaka and Ohtsuka⁸⁴ have proposed a phenomenological model of PD in which the increase in absorption at a fixed wavelength is proportional to the intensity and a factor ensuring saturation at some maximum absorption. The kinetic model for PD was further

generalized by Liu and Taylor⁸⁴. They assumed that the increase of the absorption is proportional to a general, but unspecified function of the absorption and to a power of intensity. Two types of defect creation are considered, a direct process and an indirect process. The creation of metastable defects can be represented by a configurational diagram as shown in Figure 1.12.

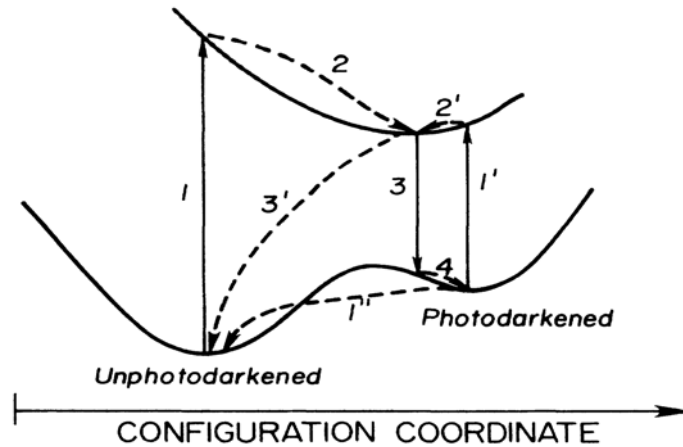


Figure 1.12: Configurational diagram showing the creation of metastable defects.

The ground and excited state energies of an electron vary with a continuous distortion of the atomic configuration. The direct process begins with an electronic excitation by a photon absorbed at non photodarkened site (step 1 in Figure 1.12). These sites may be preexisting defects or the sites may be an ordinary atom or bond in an ideal glass. Excitation is followed by atomic relaxation into a new local atomic configuration (step 2), by electronic relaxation (step 3), and further by relaxation into a metastable configurational defect (step 4). There is a finite probability for relaxation to the unphotodarkened minimum

energy configuration at any point in the defect –creation process. The relaxation to the ground state can be by any of these processes before a metastable state is formed by single quantum efficiency for defect creation per photon absorbed. Defects can be erased by the light by electronic excitation (step 1') followed by relaxation (step 2') and recombination (step 3') or by thermal process (step 1'').

➤ *Photoluminescence (PL)*

The defect states in the band-gap of ChG are expected to play an important role in the occurrence of most of the photo-induced phenomena, since the defects are considered to alter their charge conditions or their mutual interactions by trapping photo-excited carriers. To investigate these gap-states, photoluminescence (PL) measurement is an effective tool since their spectra provide detailed information on the relaxation process of photo-excited electron-hole pairs⁹¹. Kolmeits and co-workers^{9,15} first observed PL spectra in bulk ChG. Recently the Munetoshi Seki et al.⁹² has proposed the conduction band model for the origin of PL in Ge-S glass by the recombination of electron localized at the bottom of conduction band and holes trapped by the charged defects. The observation of double peak lifetime distributions in g-As₂S₃ and a-Se chalcogenides was explained through self-trapped exciton model by T Aoki et al.⁹³. According to this model the double peak life time distribution in the short-lived component is attributed to radiative recombination of singlet excitons, and the long-lived component is assigned to triplet excitons. States in the gap of ChG and the electron-phonon

interaction are the important factors affecting the luminescence of chalcogenides glasses. The dominant feature seen in luminescence spectra of chalcogenide glasses is a broad band centered at about half the band-gap energy. The broad luminescence peak is due to the strong electron phonon coupling. Luminescence in semiconductors occurs due to the electron-hole recombination and its origin can be traced to six different transitions⁹¹ as shown in Figure 1.13. The transitions are (1) a free electron and a free hole (2) an electron trapped in a shallow level and a free hole, (3) an electron trapped in a deep level and a free hole (4) electron-hole pairs trapped in defect pairs deep in the gap, (5) a free electron and a hole trapped in deep level and (6) a free electron and a hole trapped in shallow level. Factors that may influence the shape of the spectrum are the absorption depth, the presence of surface recombination and an excitation-energy-dependent quantum efficiency. A suitable way to represent luminescence processes in ChG is the configurational coordinate diagram representation shown in Figure 1.14 where $E(\text{energy})$ is plotted versus R (distance) with parabolic shape. The difference of chemical bond length in the excited state and the ground state causes a difference in the equilibrium distances in the ground and excited state parabolas.

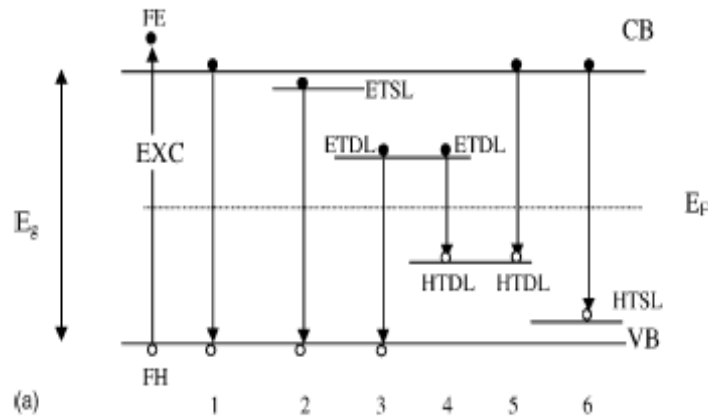


Figure 1.13: Schematic representation of the transition involved in chalcogenide glasses. The abbreviations used are free electron (FE) and a free hole (FH), electron/hole trapped in a shallow level (ETSL/HTSL), electron/hole trapped in a deep level (ETDL/HTDL), electron-hole pairs trapped in defect pairs deep in the gap (ETDL and HTDL).

The most possible optical absorption occurs at $R = 0$ of ground state and brings the centre to a high vibrational level of the excited state. The centre then relaxes to the lowest vibrational level of the excited state from where it can suddenly return to the ground state under emission of radiation. Due to the relaxation processes emission occurs at a lower energy than the absorption energy⁹⁴. The energy difference between the maximum of the lowest excitation band and that of the emission band is the Stokes shift. Along these lines, multiple transitions identified above can be better represented with a configurational coordinate diagram as illustrated in Figure 1.14

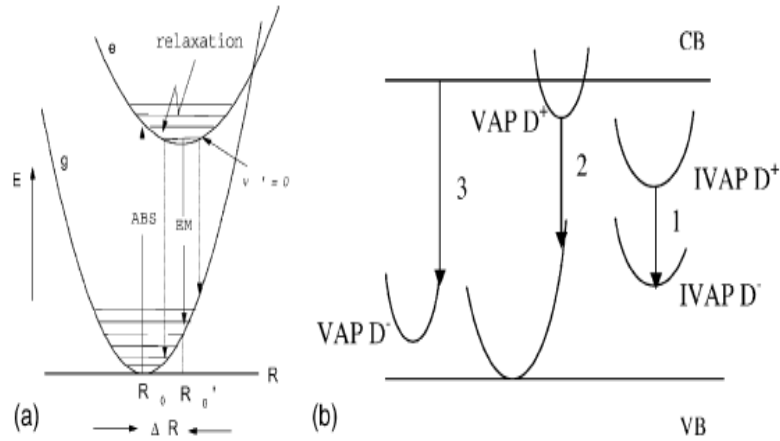


Figure 1.14 : (a) Configurational coordinate diagram representation of absorption and emission transitions, (b) the configurational coordinate diagram representation of multiple transitions in a chalcogenide glass semiconductor. VAPs are Valence Alteration pairs and IVAPs are Inverse Valence alteration Pairs that contribute to luminescence in chalcogenide glasses.

1.5.5. Optical Non linearity

Different techniques, such as two-photon absorption spectroscopy, degenerate four wave mixing (DFWM), Z-scan, third-harmonic generation (THG) and optical Kerr shutter (OKS) have been used to measure the non-linear refractive index as well as the nonlinear absorption coefficient of chalcogenide materials^{8,95}. The origin of optical non linearity in chalcogenide glasses are discussed else were in⁸. Spectral dependence of different nonlinear parameters like two-photon absorption (β) and intensity-dependent refractive index (n_2) on linear absorption and refractive index for an ideal amorphous semiconductor is shown in Figure 1.15.

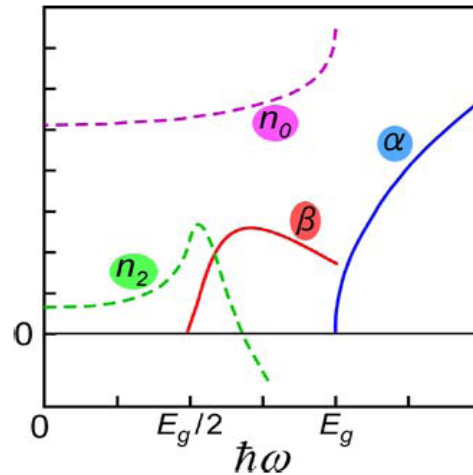


Figure 1.15: Spectral dependence of linear absorption α , linear refractive index n_0 , two-photon absorption β , and intensity-dependent refractive index n_2 in an ideal amorphous semiconductor with energy gap E_g .

J.S. Sanghera et al.⁹⁵ have compared the nonlinear optical properties of these chalcogenide glasses in both bulk and fiber form. The first investigations of the non-linear absorption of nanosecond laser pulses with $h\nu < E_g$ in ChG were reported by Lisitsa et al.⁸. The dynamics of such induced absorption with subpicosecond and picosecond time resolution have been investigated by Fork, Shank et al.⁸ and by Ackley, Tauc et al.⁸. These authors showed that as a result of strong excitation of ChG with excitation energy less than bandgap, an additional induced absorption appears, which exhibits maximum amplitude during the excitation pulse and relaxes with several time constants. This kind of photo-induced absorption (when $h\nu$ is far from the absorption edge E_g) appears only at strong laser excitation of ChG. The mechanisms of two-photon (or two-step) absorption and of the carrier localization and redistribution on states in the gap were

proposed to explain the photo-induced absorption in ChG. In telecommunications based applications, chalcogenide glasses stand out because they exhibit third-order optical nonlinearities (Kerr, Raman and Brillouin) between two to three orders of magnitude greater than silica.

Microscopically, the nonlinear terms arise through several mechanisms such as electronic, atomic (including molecular motions), electrostatic, and thermal processes. Among these, the electronic process can provide the fastest response with nano second and lower time scales, which will be needed for optical information technologies. The nonlinear absorptions usually exhibited in amorphous semiconductors are shown in Figure 1.16. Nonlinear absorption refers to the change in transmittance of a material as a function of intensity or fluence.

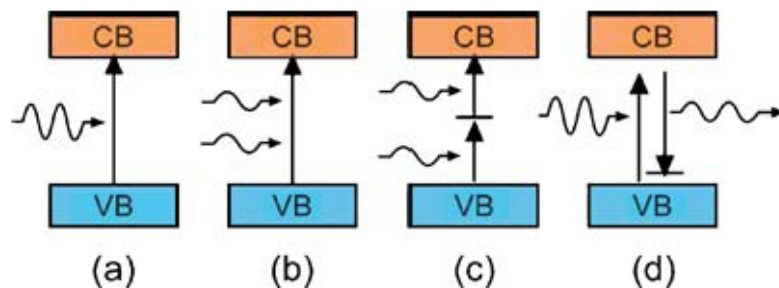


Figure 1.16: Schematic illustrations of (a) one-photon absorption, (b) twophoton absorption, (c) two-step absorption via a midgap state, and (d) Raman-scattering process in a semiconductor with a valence (VB) and a conduction band (CB).

At sufficiently high intensities, the probability of a material absorbing more than one photon before relaxing to the ground state can be greatly enhanced. In addition, population redistribution induced by intense laser fields leads to interesting counterplays of stimulated emission and absorption, complicated energy transitions in complex molecular systems and the generation of free carriers in solids. These phenomena are manifested optically in a reduced (saturable) or increased (reverse saturable) absorption. In addition to the non linear absorptions presented in Figure 1.16 there exist other non linear absorptions like multiphoton absorption, excited state absorption, free carrier absorption etc^{8,95}.

Many reports indicate that a two-photon absorption process is responsible for the optical non-linearities observed in chalcogenide glasses⁹⁶⁻⁹⁸. Studying on the spectral dependence of absorption using a tunable source, showed that two-photon and two-step absorption occurs in As_2S_3 , and the two-photon absorption spectrum appeared to vary exponentially with energy⁸. This exponential form implies that the two photon process is resonantly enhanced by the gap states which cause the weak absorption tail found in this glass.

1.6. Applications of ChG

Much more must be learned about the structure-property relationships in chalcogenide glasses before we know the true potential for these glasses. Chalcogenide glasses have been studied as promising integrated optics materials since early 1970's^{9,15}. The IR transparency of chalcogenide glasses (ChGs) leads to a wide variety

of optical applications as shown in Figure 1.17. Chalcogenide glasses have the potential to be the basis for future optical computers, much as silicon is the basis for today's microprocessors and computer memories⁹⁵. Any optical microcircuit will require passive devices such as waveguides and gratings to control the flow of optical information between the active elements. These elements can be fabricated in a chalcogenide glass by several methods including photodarkening and photodoping⁹⁶. Grating can be recorded on chalcogenide bulk and thin films. The photosensitive response of the chalcogenide glasses can be used to produce high-resolution images and photolithographic resists¹⁶. High-speed optical switching has been demonstrated with chalcogenide glasses⁹⁷. Demultiplexing signals of 50 Gbit/s was achieved and the system has the potential to exceed 100 Gbit/s operations. Infrared fibers based on ChG are of great technological importance for communication, imaging, remote sensing and laser power delivery⁹⁸. ChG fibers find application in the various fields due to their high bandgap, longwavelength multiphonon edge and low optical attenuation⁹⁹. They are also chemically stable in air and can be drawn into long core-clad fibers. They also have the potential to permit new applications that are unachievable with current infrared materials⁹⁹⁻¹⁰². The ChG find application in different fields as shown in Figure 1.17.

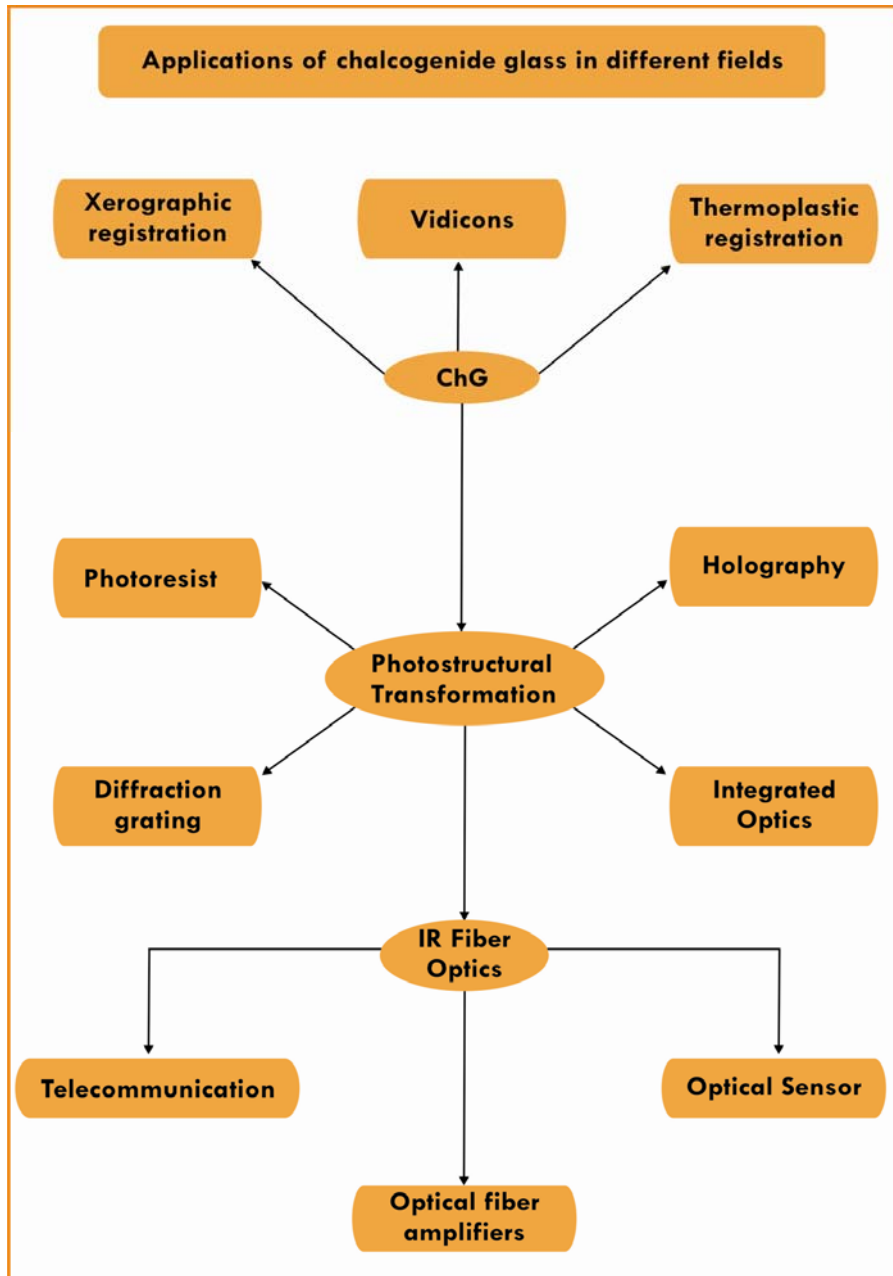


Figure 1.17: Applications of chalcogenide glass in different fields.

1.7. Scope of the thesis

Chalcogenide glasses (ChGs), well known for their large optical nonlinearities and high infrared transparency will enhance or revolutionize many of the products that operate with or on infrared light. Even though ChG's meet all of these criteria like high IR transparency, low phonon energy, high refractive index, good photosensitivity etc and are well suited to various applications, researches are going on for the development of advanced new chalcogenide glass and polymer composite films and fibers for photonic applications. Most of the applications depend on our ability to engineer glass compositions to meet the specific requirements of the system. It is the intent of this research work in this thesis to develop a simple, low cost and tunable solution-based method for the fabrication of ChG films and fibers. This method offers the opportunity to tightly control film chemistry through control of the solution chemistry, preparation of novel material systems such as hybrids and composites and nano composite fibers that opens the door to new types of structures and optical components for photonic applications. It was shown that it is possible to tune the optical and mechanical properties of these coatings by tailoring the glass chemistry (concentration of ChG dissolved in the solvent) or ChG/polymer content over a broad range making them important for applications in IR optical coatings and as interfacial materials where thermal and mechanical property matching is critical. These results may lead directly to applications, or more likely, they may provide a

foundation for other research into the optical behaviour of more new nano composites based on different ChG's for different applications..

1.8. Conclusions

The importance of chalcogenide glasses and its structural, electronic, thermal and optical properties have been reviewed. Recent trends on the fabrication method of chalcogenide glass based materials and polymer nano composites of ChG's are also discussed. Photoinduced optical properties like photodarkening and photoluminescence are found to be very interesting in ChG due to their band gap structure with the presence of localized states and different defects.

1.9. Reference

1. S.R. Elliot, "Physics of Amorphous Materials", Essex: Longman (1990).
2. Valentina Kokorina, "Glasses for Infrared Optics", CRC Press, Boca Raton, Fla (1996).
3. Y. S. Chiang, S. W. Ing Jr., "Studies on selenium-organic polymer interfaces", 13, 883-897 (1969).
4. W. Zhao, D.C. Hunt, T. Kenkichi, J.A. Rowlands, "Amorphous selenium flat panel detectors for medical applications", Nuclear Instruments & Methods in Physics Research A., 549, 205-209 (2005).
5. S.O Kasap, J.A. Rowlands, "Review x-ray photoconductors and stabilized a-Se for direct conversion digital-at-panel x-ray image detectors", Journal of Materials Science: Materials in Electronics., 11, 179-198 (2000).
6. M. Kubota, T. Kato, S. Suzuki, H. Maruyama, K. Shidara, K. Tanioka, K. Sameshima, T. Makishima, K. Tsuji, T. Hirai and T. Yoshida, "Ultra high sensitivity New Super-HARP camera", IEEE Transaction on broadcasting., 42, 3 (1996).
7. R. Golovchak, "Structural Models of Long- And Short-Term Physical Ageing In Selenium-Rich Glasses", Ser. Physics., 43, 209-225(2009).

8. A. Zakery and S.R. Elliott, "Optical Nonlinearities in Chalcogenide Glasses and their Applications", Springer-Verlag Berlin, Heidelberg (2007).
9. Rorert Fairman and Boris Ushkov, "Semiconducting Chalcogenide Glass 1", Elsevier Academic Press, Netherlands (2004).
10. A.M.Andriesh, "Chalcogenide glasses in optoelectronics", Semiconductors., 32, 867-872 (1998).
11. Robert Fairman, Boris Ushkov, "Semiconducting ChG 11: Properties of Chalcogenide glass", Elseiver Accademic Press, Netherlands (2004).
12. N. Mehta, "Applications of chalcogenide glasses in electronics and optoelectronics: A review", Journal of Scientific and Industrial research ., 65, 777-786 (2006).
13. Kimmo Paivasaari, Victor K. Tikhomirov, Jari Turunen, "High refractive index chalcogenide glass for photonic crystal applications", Optics Express., 15, 2336 (2007).
14. Rudolph Frerichs, "New Optical Glasses with Good Transparency in the Infrared", Opt. Soc. Am., 43, 1153 (1953).
15. Dr. A. Ray Hilton, "Chalcogenide Glasses for Infrared Optics", McGraw-Hill Companies, Inc. (2010).
16. R. A. Street and N. F. Mott, "States in the Gap in Glassy Semiconductors", Physical Review Letters., 35, 1293 (1975).
17. A. Urena, A. Piarristeguy, M. Fontana, C. Vigreux-Bercovicic, A. Pradel and B. Arcondo, "Characterisation of thin films obtained by laser ablation of $Ge_{28}Se_{60}Sb_{12}$ glasses", Journal of Physics and Chemistry of Solids., 68, 993-997 (2007).
18. V. Balan, C. Vigreux, A. Pradel, "Chalcogenide Thin Films Deposited By Radio-Frequency Sputtering ", Journal of Optoelectronics and Advanced Materials., 6, 875-882 (2004).
19. C.C Huang, D.W.Heak, "High purity germanium sulphide glass for optoelectronic applications synthesized by chemical vapor deposition", Electronic Letters., 40, 863-865 (2004).

20. R. Tintu, V.P.N. Nampoory, P. Radhakrishnan, Sheenu Thomas "Photoinduced changes in optical properties of Ga-Sb-Ge-Se glasses", *Optics Communications.*, 284, 222-225(2011).
21. E. Márquez, A. M. Bernal-Oliva, J. M. González-Leal, T. Prieto-Alcón, and R. Jiménez-Garay,"On the irreversible photo-bleaching phenomenon in obliquely evaporated GeS₂ glass films", *Journal of Non-Crystalline Solids.*, 222, 250 (1997).
22. Ulrich Siemann, "Solvent cast technology - a versatile tool for thin film production", *Progr Colloid Polym Sci.*, 130, 1-14 (2005).
23. Litty Irimpan, Bindu Krishnan, A Deepthy, V P N Nampoory and P Radhakrishnan, "Size dependent enhancement of nonlinear optical properties in nano colloids of ZnO", *Journal of Applied Physics.*, 103, 033105 (2008).
24. Litty Irimpan, A. Deepthy, Bindu Krishnan, V. P. N. Nampoory and P Radhakrishnan, "Size dependent fluorescence spectroscopy of nanocolloids of ZnO", *Journal of Applied Physics.*, 102, 063524 (2007).
25. Litty Irimpan, Bindu Krishnan, A. Deepthy, V. P. N. Nampoory and P Radhakrishnan, "Excitation wavelength dependent fluorescence behaviour of nano colloids of ZnO", *Journal of Physics D: Applied Physics.*, 40, 5670-5674 (2007).
26. Litty Irimpan, V. J. Dann, Bindu Krishnan, A. Deepthy, V. P. N. Nampoory and P Radhakrishnan, "Backscattering of laser light from colloidal silica", *Laser Physics .*, 18 (7), 882-885 (2008).
27. R. Tintu, V. P. N. Nampoory, P. Radhakrishnan, and Sheenu Thomas,"Nonlinear optical studies on nanocolloidal Ga-Sb-Ge-Se chalcogenide Glass", *Journal of Applied Physics.*, 108, 073525 (2010).
28. R A. Ganeeva. I Ryasnyansky and T Usmanov,"Nonlinear refraction and nonlinear absorption of As₂S₃ aqueous solution", *Optical and Quantum Electronics.*, 35, 211-219(2003).
29. (1) Berzelius, J. J. *Ann. Chim. Phys.*, 32, 166 (1826).(2) Bineau, A. *Ann. Chim. Phys.*, 70, 54 (1839).

30. T.Kohoutek, T.Wagner, M. Frumar, A.Chrissanthopoulos, O. Kostadinova, and S. N. Yannopoulos, "Effect of cluster size of chalcogenide glass nano colloidal solutions on the surface morphology of spin-coated amorphous films", *Journal of Applied Physics*, 103, 063511 (2008).
31. S. Shtutina, M. Klebanov, S. R. V. Lyubin, and V. Volterra, "Photoinduced phenomena in spin-coated vitreous As_2S_3 and $AsSe$ films," *Thin Solid Films*, 261, 263–265 (1995).
32. S.B. Mamedov and M.D. Michailov, "Dissolution kinetics of glassy and crystalline As_2S_3 in aqueous sodium sulfide and hydroxide" *Journal of Non-Crystalline Solids*, 221, 181-186 (1997).
33. M.D. Michailov, S.B. Mamedov, and S.V. Tsventarnyi, "Dissolution Kinetics of Glassy Arsenic Sulfide in Alkali and Amine Solutions" , *Journal of Non-Crystalline Solids*, 176, 258-262 (1994).
34. J. Orava, T. Wagner, M. Krbal, T. Kohoutek, M. Vlcek, and M. Frumar, "Selective wet-etching of undoped and silver photodoped amorphous thin films of chalcogenide glasses in inorganic alkaline solutions", *Journal of Non-Crystalline Solids*, 352, 1637-1640 (2006).
35. S. Song, N. Carlie, J. Boudies, L. Petit, K. Richardson, and C. B. Arnold, "Spin-coating of $Ge_{23}Sb_7S_{70}$ chalcogenide glass thin films," *Journal of Non-Crystalline Solids*, 355, 2272–2278 (2009).
36. G. C. Chern, and I. Lauks, "Spin-coated amorphous chalcogenide films," *Journal of Applied Physics*, 53(10), 6979 (1982).
37. G. C. Chern, I. Lauks, and A. R. McGhie, "Spin coated amorphous chalcogenide films: Thermal properties," *Journal of Applied Physics*, 54(8), 4596 (1983).
38. G. C. Chern, and I. Lauks, "Spin coated amorphous chalcogenide films: Structural characterization" , *Journal of Applied Physics*, 54, 2701 (1983).
39. Nathan A. Carlie, "A Solution-Based Approach To The Fabrication Of Novel Chalcogenide Glass Materials And Structures", PhD thesis, Graduate School of Clemson University (2010).
40. S. Song, S. S. Howard, Z. Liu, A. O. Dirisu, C. F. Gmachl, and C. B. Arnold, "Mode tuning of quantum cascade lasers through optical processing of chalcogenide glass claddings," *Applied Physics Letters* ., 89(4), 041115 (2006).

41. Tomas Kohoutek , Jiri Orava , Tsutomu Sawada, Hiroshi Fudouzi, "Inverse opal photonic crystal of chalcogenide glass by solution processing", *Journal of Colloid and Interface Science.*, 353 , 454–458(2011).
42. S. H. Kim and C.K. Hwangbo, "Design of Omnidirectional High Reflectors with Quarter-Wave Dielectric Stacks for Optical Telecommunication Bands," *Optics Letters.*, 23, 1573-1575 (1998).
43. T. Kohoutek, J.Orava, M.Hrdlicka, T.Wagner, Vlcek Mil. & M.Frumar, "Planar Quarter Wave Stacks Prepared from Chalcogenide Ge-Se and Polymer Polystyrene Thin Films", *J. Phys. Chem. Solids.*, 68, 2376-2380 (2007).
44. V. Balan, C. Vigreux, A. Pradel, M. Ribes "Waveguides Based Upon Chalcogenide Glasses", *Journal of Optoelectronics and Advanced Materials.*, 3, 367 – 372 (2001).
45. T.Kohoutek, T.Wagner, J.Orava, M.Krbal, Mir.Vlcek, J.Ilavsky, Mil.Vlcek and M.Frumar, "Multilayer Planar Structures Prepared from Chalcogenide Thin Films of As-Se and Ge-Se Systems and Polymer Thin Films using Thermal Evaporation and Spincoating Techniques", *Journal of Non-Crystalline Solids.*, 354, 529-532 (2008).
46. S.H. Kim and C. K. Hwangbo, "Design of omnidirectional high reflectors with quarter-wave dielectric stacks for optical telecommunication bands," *Applied Optics.*, 41, 3187-3192 (2002).
47. R. G. DeCorby, H. T. Nguyen, P. K. Dwivedi, and T. J. Clement, "Planar omnidirectional reflectors in chalcogenide glass and polymer," *Optics Express.*, 13, 6228-6233 (2005).
48. R. G. DeCorby, N. Ponnampalam, M. M. Pai, H. T. Nguyen, P. K. Dwivedi, T. J. Clement, C. J. Haugen, J.N. McMullin, and S. O. Kasap, "High index contrast waveguides in chalcogenide glass and polymer," *IEEE J. Sel. Top. Quantum Electron.*, 11, 539-546 (2005).
49. T. J. Clement, N. Ponnampalam, H. T. Nguyen, and R. G. DeCorby, "Improved omnidirectional reflectors in chalcogenide glass and polymer by using the silver doping technique", *Optics Express.*, 14, 1789 (2006).

50. Edward Bormashenko, Roman Pogreb, Zosya Pogreb and Semion Sutovski, "Development of new near infrared filters based on the "sandwich" polymer-chalcogenide glass-polymer composites", *Optical Engineering*, 40, 661 (2001).
51. Andrei Andriesh and Mihail Iovu, "Diffraction and luminescent structures based on chalcogenide glasses and polymers", *Phys. Status Solidi B*, 246, 1862-1865 (2009).
52. B. Bendow, H. Rast, and O. H. El-Bayoumi, "Infrared fibers: an overview of prospective materials, fabrication methods, and applications", *Optical Engineering*, 24 (6), 1072-1078 (1985).
53. P. Klocek, M. Roth, and R. D. Rock, "Chalcogenide glass optical fibers and image bundles: properties and applications", *Optical Engineering*, 26 (2), 88 (1987).
54. J. Troles, Q. Coulombier, G. Canat, M. Duhant, W. Renard, P. Toupin, L. Calvez, G. Renversez, F. Smektala, M. El Amraoui, J. L. Adam, T. Chartier, D. Mechin, and L. Brilland, "Low loss microstructured chalcogenide fibers for large non linear effects at 1995 nm", *Optics Express*, 18(25), 26647 -26654 (2010).
55. M. El-Amraoui, G. Gadret, J. C. Jules, J. Fatome, C. Fortier, F. Désévéday, I. Skripatchev, Y. Messaddeq, J. Troles, L. Brilland, W. Gao, T. Suzuki, Y. Ohishi, and F. Smektala, "Microstructured chalcogenide optical fibers from As_2S_3 glass: towards new IR broadband sources", *Optics Express*, 18(25), 26655 -26665 (2010).
56. R. J. Weiblen, A. Docherty, J. Hu, and C. R. Menyuk, "Calculation of the expected bandwidth for a mid-infrared supercontinuum source based on As_2S_3 chalcogenide photonic crystal fibers", *Optics Express*, 18(25), 26666 -26674 (2010).
57. A. B. Seddon, Z. Tang, D. Furniss, S. Sujecki, and T. M. Benson, "Progress in rare-earth-doped mid-infrared fiber lasers", *Optics Express*, 18(25), 26704-26719 (2010).
58. Atsushi Mori, Yasutake Ohishi, Terutoshi Kanamori, and Shoichi Sudo, "Optical amplification with neodymium-doped chalcogenide glass fiber", *Applied Physics Letters*, 70, 1230 (1997).

59. J. Kim, U-C. Paek, B. H. Lee, J. Hu, B. Marks, and C. R. Menyuk, "Impact of interstitial air holes on a wide bandwidth rejection filter made from a photonic crystal fiber," *Optics Letters* ., 31, 1196-1198 (2006).
60. Monro, T. M., West, Y. D., Hewak, D. H., Broderick, N. G., and Richardson," *Holey optical fibers: an efficient modal model*" D. J, *Electronic Letters*., 36 (1998.)
61. J.Troles, L. Brilland, F. Smektala, P. Houizot, F. Desevedavy, Q.Coulombier, N.Traynor, T.Chartier, J. L. Adam and G. Renversez, "Chalcogenide microstructured fibers for infrared systems, elaboration modelization and characterization", *Fiber and Integrated Optics*., 28, 11-26 (2008).
62. H.C.Y. Yu, M.A. van Eijkelenborg, S.G. Leon-Saval, A. Argyros and G.W. Barton, "Enhanced magneto-optical effect in cobalt nanoparticle doped optical fibre," *Applied Optics*., 47, 6497-6501(2008).
63. X. Yang and L. Wang, "Silver nanocrystals modified microstructured polymer optical fibres for chemical and optical sensing ", *Optics Communication*., 280, 368-373 (2007).
64. M. C. J.Large, S. Ponrathnam, A. Argyros, N. S. Pujari, and F. Cox, "Solution doping of microstructured polymer optical fibres" , *Optics Express*., 12(9), 1966-1971 (2004).
65. M. C. J. Large, A. Argyros, F. Cox, M. A. van Eijkelenborg, S. Ponrathnam, N. S. Pujari, I. M. Bassett, R. Lwin, and G. W. Barton, "Microstructured polymer optical fibres: New opportunities and challenges," *Mol. Cryst. Liq. Cryst.*, 446, 219-231 (2006).
66. H. C. Y. Yu, A. Argyros, G. Barton, M. A. van Eijkelenborg, C. Barbe, K. Finnie, L. Kong, F. Ladouceur, and S. McNiven, "Quantum dot and silica nanoparticle doped polymer optical fibers," *Optics Express*., 15(16), 9989-9994 (2007).
67. G. de Bastida, F. J. Arregui, J. Goicoechea, and I. R. Matias, "Quantum dots-based optical fiber temperature sensors fabricated by layer-by-layer," *IEEE Sens. J.*, 6(6), 1378-1379 (2006).
68. T.P. Mthethwa, M.J. Moloto , A. De Vries , K.P. Matabola "Properties of electrospun CdS and CdSe filled poly(methyl methacrylate) (PMMA) nanofibres", *Materials Research Bulletin*., 46, 569-575(2011).

69. Cheng Cheng and Xuefeng Peng, "Spectral Characteristics of a Quantum -Dot (CdSe/ZnS)-Doped Fiber in Low Concentration", *Journal Of Lightwave Technology.*, 27, 1362-1369 (2009).
70. N.F.Mott, "Electrons in disordered structures", *Advances in Physics.*, 16, 49-57 (1967).
71. W. H. Zachariasen, "The Atomic Arrangement in Glass", *J. Arner. Chem. Soc.*, 54, 3841(1932).
72. J.D. Berna, "Structure, Properties, Solid Interactions", Elsevier, Amsterdam (1965).
73. P. J. Flory "Spatial configuration of macromolecular chains", *Science.*, 188, 1268 (1975).
74. P. W. Anderson, "Absence of Diffusion in Certain Random Lattices", *Physical Review.*, 109, 1492 (1958).
75. Wee Chong Tan, "Optical Properties of Amorphous Selenium Films", PhD thesis , University of Saskatchewan (2006).
76. Cohen M.H., Fritzsche H. and Ovshinski S.R., "Simple band model for amorphous semiconductor alloys", *Physical Review Letters.*, 22, 1065-1072 (1969).
77. J.M. Marshall and A.E.Owen, "Drift mobility studies in vitreous arsenic triselenide", *Philosophical Magazine.*, 24, 1281-1290 (1971).
78. David Emin, "Correlated Small-Polaron Hopping Motion", *Phys. Rev. Lett.*, 25, 1751-1755 (1970).
79. K. Tanaka, T. Gotoh, N. Yoshida and S. Nonomura "Photothermal deflection spectroscopy of chalcogenide glasses", *Journal of Applied Physics.*, 91, 125 (2002).
80. P. Boolchand, D. G. Georgiev, and B. Goodman, "Discovery of the intermediate phase in chalcogenide glasses", *J. Optoelectron Materials.*, 3(3), 703-720 (2001).
81. A Redaelli, A Pirovano, F. Pellizzer, AL. Lacaíta, D. Ielmini and R. Bez, "Electronic Switching Effect and Phase-Change Transition in Chalcogenide Materials", *IEEE Electron Device Letters.*, 25, 648-686(2004).

82. K. Tanaka, "Photoinduced structural changes in chalcogenide glasses", *Reviews of Solid State Sci.*, 4 (2 & 3), 511 (1990).
83. G. Pfeiffer, M. A. Paesler, and S. C. Agarwal, "Reversible photodarkening of amorphous arsenic chalcogens", *J. Non-Cryst. Solids.*, 130, 111 (1991).
84. L. Tichy, H. Ticha, P. Nagels, and R. Callaerts, "Photoinduced optical changes in amorphous Se and Ge-Se films, *Journal of Non-Crystalline Solids.*, 240, 177 (1998).
85. V. M. Lyubin and V. K. Tikhomirov, "Novel photo-induced effects in chalcogenide glasses", *Journal of Non-Crystalline Solids.*, 135, 37 (1991).
86. M. Popescu, "Disordered Chalcogenide Optoelectronic Materials: Phenomena And Applications", *Journal of Optoelectronics and Advanced Materials.*, 7, 2189 – 2210 (2005).
87. G.B Turpin and L.E McNeil, "Photodarkening in $Ge_{1-x} Sn_x Se$ films", *Physical Review B.*, 39, 8750 (1989).
88. Stephen Ducharme, J Hautala and P.C.Taylor, "Photodarkening profile and kinetics in chalcogenide glass", *Physical Review B.*, 41, 12250-12261 (1990).
89. A. A. Othman, H. H. Amer , M. A. Osman , A. Dahshan. " Reversible photodarkening in amorphous $Ga_{20}S_{75}Sb_5$ and $Ga_{20}S_{40}Sb_{40}$ thin films", *Radiation Effects & Defects in Solids.*, 159, 659–666(2004).
90. M. Štábl, L. Tichý "Giant" photo-darkening in $Ge_{16}As_{26}S_{58}$ amorphous thin film", *Solid State Sciences.*, 7, 201–207(2005)
91. R. A. Street, "Luminescence in amorphous semiconductors" *Advances In Physics.*, 25, 397-454(1976).
92. Munetoshi Seki, Kan Hachiya , Katsukuni Yoshida, " Photoluminescence excitation process and optical absorption in Ge-S chalcogenide glasses" *Journal of Non-Crystalline Solids.*, 324 , 127–132(2003).
93. T. Akoi, S. Komedoori, S Kobayashi, T.Shimisu, A.Ganjoo and K.Shimkaea , "Photoluminescence life time distribution of chalcogenide glass obtained by wide band frequency resolved spectroscopy", *Journal of Non-Crystalline Solids.*, 326, 273-278 (2003).

94. S.G.Bishop and D.L Mitchell, "Photoluminescence excitation spectra in chalcogenide glass", *Physical Review B.*, 8, 5696-5701 (1973).
95. J.S. Sanghera , C.M. Florea , L.B. Shaw , P. Pureza , V.Q. Nguyen ,M. Bashkansky , Z. Dutton , I.D. Aggarwal, " Non-linear properties of chalcogenide glasses and fibers", *Journal of Non-Crystalline Solids .*, 354, 462-467 (2008).
96. R. A. Ganeev, A. I. Ryasnyanski and T. Usmanov, "Effect of Nonlinear Refraction and Two-Photon Absorption on the Optical Limiting in Amorphous Chalcogenide Films", *Physics of the Solid State.*, 45, 207-213 (2003).
97. R A Ganeev, A Ryasnyansky, M K Kodirov and T Usmanov, "Two-photon absorption and nonlinear refraction of amorphous chalcogenide films", *J. Opt. A: Pure Appl. Opt.*, 4, 446-451(2002).
98. H. Nasu, K. I. Kubodera, M. Kobayashi, M. Nakamura, and K. Kamiya, "Thirdharmonic generation from some chalcogenide glasses", *J. Am. Ceram. Soc.*, 73, 1794-1796 (1990).
99. A.M. Andriesh, V. V. Ponomar', V. L. Smirnov, and A. V. Mironos, "Applications of chalcogenide glasses in integrated and fiber optics (review)", *Sov. J. Quantum Electron.*, 16 (6), 721-736(1986).
100. A. Andriesh, "Chalcogenide Glasses As Multifunctional Photonic Materials", *Journal of Optoelectronics and Advanced Materials.*, 7, 2931 - 2939(2005).
101. D. Lezal, "Chalcogenide Glasses- Survey And Progress", *Journal of Optoelectronics and Advanced Materials*, 5, 23 - 34 (2003).
102. J. S. Sanghera and I. D. Aggarwal, "Active and passive applications of chalco-genide glass fibers a review," *J. Non-Cryst. Solids.*, 2573 (6), 1794 (1990).



Chapter 2

MATERIALS AND METHODS

- 2.1. *Section 1. Preparation techniques*
 - 2.2. *Section 2. Experimental tool and techniques used for characterization of ChG*
 - 2.3. *Conclusions*
 - 2.4. *References*
-

This chapter is divided in to two sections namely the preparation techniques and the experimental tools and techniques used for the characterization of ChG in the present work.

2.1. Section 1. Preparation techniques

The techniques used for the preparation of bulk ChG, thin films, nano colloid solutions, ChG/Polyvinyl Alcohol nano composite film, stacked hybrid films of ChG and polymer and nano colloid ChG doped polymer fiber are discussed in this section.

2.1.1. Chalcogenide bulk glass preparation

Bulk glasses were prepared using melt quenching method. Melt quenching technique was the only method used for the preparation of bulk glasses before the development of chemical vapour deposition and sol gel technique^{1,2}. One of the important features of the melt quenching technique is the high flexibility of geometry and composition and the advantage of obtaining materials of large size in comparison to other methods. The doping or codoping of active ions or transition metals are quiet easy using this method. This method can be used for the preparation of silicate, borate, phosphate, oxide or non oxide systems¹. One of the main disadvantages of this method is the lack of ultra high purity as compared to other chemical methods. In order to avoid contamination, the crucibles made of noble metals can be used.

Melt quenching method applied for chalcogenide glass preparation is as follows. This method is based on the fusion of raw materials in to a viscous solid, followed by forming in to a shape and quenching to a glass. The electronic grade (5N purity) constituent elements are weighed in proportion to their atomic weight

percentages. The raw materials used in the present study are Ge, Se, Sb, Ga and Er which are all purchased from Alfa Aesar having a grade of 5N purity. For each composition approximately around 4gm of material is transferred to clean quartz ampoules of 8 mm diameter and 8cm length.

The ampoule is then evacuated at a pressure of 10^{-3} m bar for half an hour and then flame sealed at this vacuum using oxygen - indane flame torch. Pre-cleaning and evacuating helps to avoid the presence of impurities. The ampoule is then placed in a rocking and rotating furnace as shown in Figure 2.1.



Figure 2.1: Rocking and rotating furnace used for the preparation of ChG glasses.

The furnace can attain a maximum temperature of 1100°C. The temperature controller in this unit is C961 Blind Temperature Controller with single thermocouple or RTD input and one relay output with user specific control action and relay logic. Before keeping the ampoule, the furnace can be programmed to the desired temperature. The samples presented in this thesis are prepared at a temperature of 1050°C. In order to homogenize the melt continuous rotation and rocking in an interval of

1 hour is given. The melt is then rapidly quenched to ice cold water. The samples are then taken out from the sealed ampoules by dipping it in Hydrofluoric acid (HF) solution. HF solution etches the quartz ampoule leaving the bulk glass.

2.1.2. Thin film preparation

Thin film preparation can be based on physical deposition or chemical deposition method^{3,4}. Depositions that happen because of a chemical reaction are Chemical Vapour Deposition (CVD), Electro deposition, Epitaxy, Thermal oxidation etc and depositions that happen because of a physical reaction are Physical Vapour Deposition, Evaporation, Sputtering and Casting. The vapour deposition methods such as thermal evaporation, sputtering and chemical vapour deposition methods can yield amorphous thin films deposited on a substrate.

2.1.2. a) Thermal evaporation technique

It is perhaps the simplest vapour deposition technique which involves resistive or electron beam heating in vacuum of a reservoir containing the material to be evaporated. The melt so produced then evaporates and the vapour is condensed on to a substrate, forming a thin film. In chalcogenide glass the deposition of the film at the oblique incidence may result to structural inhomogeneity which may lead to formation of columnar growth morphology for the films⁵.

The making of an amorphous chalcogenide thin film by thermal evaporation in vacuum coating unit is done in the following

way. The unit used for coating is India High Vacuum pumps (12A4-D). Firstly, bulk sample is loaded in tungsten boat in the system as shown in Figure 2.2. After than the bell jar is closed and the system pumped down to around 2×10^{-5} torr through a diffusion pump. At this level of air pressure, the entire environment inside the deposition chamber is free of impurities and the sample is ready for deposition. The chamber is evacuated by INDVAC Diffpak pump Model 114D abd backed by 250 liters per minute, doublestage, direct driven, Rotary vacuum pump, Model:IVP.

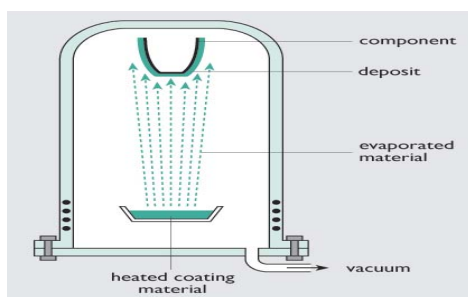


Figure 2.2: Schematic representation of the Bell jar in thermal evaporation unit.

With the shutter in the closed position, the temperature of the substrate is set to the desired level heated till the sample loaded starts to evaporate. The heating element in the system is conal sheated nichrome having a power rating of 500 watts, 120 V to 140V. Once the evaporation rate is stabilized and the substrate reaches its desired temperature, the vapour is allowed to come into contact with the substrate. The rate of evaporation is maintained to be $10 \text{ \AA}^0/\text{s}$. The evaporation rate as well as the film thickness can be controlled using a quartz crystal in Digital thickness Monitor Model-CTM-200

attached to the bell jar. When the desired thickness is reached, the shutter is closed. The amorphous film is maintained at the substrate temperature until the boat and the chamber cooled down to a level suitable for the film to be removed from the system.

2.1.2 b) Spin coating and drop casting

➤ Spin coating

SPIN 150-v3 was used for spin coating the films. Spin Coating involves the acceleration of a liquid puddle on a rotating substrate⁶. In this technique the coating material is deposited in the center of the substrate either manually or by a robotic arm. The physics behind spin coating involve a balance between centrifugal forces controlled by spin speed and viscous forces which are determined by solvent viscosity⁶. Some variable process parameters involved in spin coating are Solution viscosity, Solid content, Angular speed and Spin Time. The method of spin coating is given in Figure 2.3.

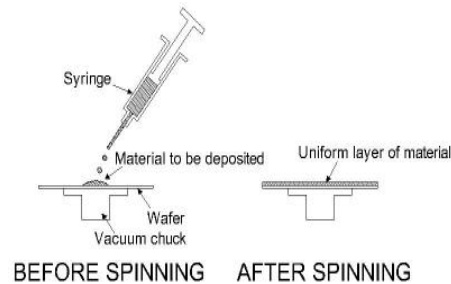


Figure 2.3: Schematic diagram of spin coating.

➤ Drop casting

The drop casting technique is a simple method to deliver drops of liquid in the micromolar to millimolar range⁷. The drops are deposited mostly by means of micropipettes onto solid surfaces. The

stirred solution is taken in a micro glass syringe and placed in a cleaned glass slide. The films were then allowed to dry and kept in dark in desiccators.

2.1.3. Chalcogenide Nano colloid preparation

Chalcogenide nano colloids were prepared by dissolving the bulk glasses in *n*-butylamine solution (Alfa Aesar). *n*-Butylamine is an organic compound⁸ (specifically, an amine) with the formula $\text{CH}_3\text{CH}_2\text{CH}_2\text{CH}_2\text{NH}_2$. This colourless liquid is one of the four isomeric amines of butane, the others being *sec*-butylamine, *tert*-butylamine and *isobutylamine*. At standard temperature and pressure, *n*-butylamine is a liquid having the fishy, ammonia-like odor common to amines¹⁶.

The bulk glasses were grounded to fine powders and weighed. After that solutions of different concentrations were made by dissolving the ChG in *n*-butylamine in a sealed bottle. The solutions were given continuous stirring at an ambient temperature (35°C) for expediting the dissolution mechanism. The solutions were then kept in refrigerator.

Chern and Luck⁹⁻¹¹ has described the dissolution of the bulk glass in amine solvents as follows, the dissolution of the continuous network of the bulk glass chalcogenide glass in butylamine leads the bulk glass to get fragmented possibly along the weakly bonded interlayer planes in the form of clusters. The surface of these clusters react with the solvent to form amine salts. It is interesting to point out that the chalcogenide glasses are found to be both stable in neutral and acidic (non-oxidizing) solutions, but begin to dissolve quite

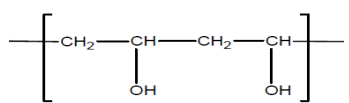
rapidly in basic solutions. The dissolution mechanism of the chalcogenide glass in solvents primarily centers on general acid-base chemistry. Amines are usually considered to be bases.

According to the Brönstead-Lowry (B-L)¹² concept an acid is defined as a substance which is able to donate a proton while a base as a proton acceptor; whereas the Lewis concept¹² defines acids as capable of accepting a lone pair in order to form a coordinate covalent bond and bases are the lone pair donors. This concept is equivalent in aqueous solutions but in nonaqueous solutions and particularly when the acid does not possess hydrogen atoms, the B-L concept becomes awkward¹³.

In our case the glass is considered as the acid. Another important thing is nucleophilicity, which is distinct from basicity. Nucleophilicity is the focus of the Pearson hard-soft acid base (HSAB) concept¹³⁻¹⁵. This concept defines the chemical hardness (η) as equal to one half of the derivative of the chemical potential of a system with respect to the total number of electrons. In other words it relates to the difference between the ionization potential and electron affinity¹⁴. Hardness is therefore a measure of the energy needed to alter the electron cloud through addition or removal of an electron. Here species with extreme electronegativities or high charge densities would be considered hard while those with intermediate electronegativities and high polarizabilities would be considered soft. Thus hard-hard interactions will tend to be ionic in nature while soft-soft interactions are covalent, making soft bases generally better nucleophiles¹⁵.

2.1.4. Composite film preparation

Chalcogenide/Polymer composite films were prepared by drop casting method. The prepared nano colloid solutions of different glasses and the polymer are mixed together. The polymer used for making films is polyvinyl alcohol¹⁶. Polyvinyl alcohol (PVOH, PVA, or PVAL) is a water-soluble synthetic polymer. Unlike many vinyl polymers, PVA is not prepared by polymerization of the corresponding monomer. The monomer, vinyl alcohol, almost exclusively exists as the tautomeric form, acetaldehyde. PVA instead is prepared by partial or complete hydrolysis of polyvinyl acetate to remove acetate groups. The chemical formula for PVA is,



The nano colloid solutions of chalcogenide glass and poly Vinyl Alcohol were mixed in different proportions using a magnetic stirrer. The mixture was then carefully drop casted on to a cleaned glass slide. The films were then allowed to dry by keeping in desiccators.

2.1.5. Multilayers of chalcogenide glass

Multilayers of chalcogenide glass were prepared by coating the bulk chalcogenide glass by thermal evaporation on to composite films of chalcogenide glass and polymer prepared by drop casting method. The composite films are also coated on to the thermally evaporated films.

2.1.6. Fiber fabrication

Drawing of fiber directly from melts of material in crucibles or fiber drawing by Vapor phase oxidation are the basic techniques used in the fabrication of Polymer Optical fibers (POF)¹⁷⁻¹⁹.

2.1.6.1. Continuous extrusion method

Plastic optical fibers are produced in a simple extrusion process, which is similar to the double crucible method used for fabricating glass fibers. The disadvantage of this method is the possibility of introducing contaminants during the melting process. The most economical method for making polymer optical fiber that is also amenable to high-volume processing is the extrusion process. In this method, a purified monomer (methyl methacrylate), an initiator and a chain transfer agent are fed into a reaction chamber where the monomer is polymerized. The material is partially polymerized into a thick fluid, which is typically 80% polymer and 20% monomer. The temperature of the reactor chamber is typically 180°C. This concentrated solution is directed to the screw extruder, which pushes the material through a nozzle that creates the fiber. Remaining monomer is evaporated in the core extruder and recovered for further use. Subsequently, the core of the fiber runs into a second chamber and then through a nozzle where the cladding is coated onto the fiber-also using an extrusion process. This leads to the formation of a continuous fiber. Effectively, then, material is fed into one end and the fiber comes out the other end. The most important advantage of continuous extrusion is high production rate¹⁷.

2.1.6.2. Vapor phase oxidation

With direct drawing, it is difficult to get pure and homogeneous fibers; therefore this method is not commonly used^{19,20}. The vapor phase oxidation processes have proven to be more successful. These processes are usually done in two steps:

- ✚ The first being the preparation of the Preform.
- ✚ The second being the drawing of the fiber.

This method is used for the preparation of nano colloid ChG doped polymer fiber.

➤ *Preform method*

The preform drawing process can be used for making single mode step index fiber, multimode fiber and graded index fiber²⁰. So this method is very advantageous compared to other fiber fabricating methods. Fabrication of POFs by preform method involves two stages. In the first stage, a cylindrical preform of required diameter and length is made. In the second stage, the preform is drawn into fiber by the heat-drawing process.

Preform making is the most important part of making a POF because it decides the optical quality of the fiber. The fiber drawing process relies on the smooth flow of softened polymer. Since thermoplastics are polymers that flow at an elevated temperature, they are well suited as fiber materials. An important property of the polymer is its molecular weight, which is a measure of the average chain length. If the molecular weight is too high, the chains are too

long to permit them to slip and flow²¹. The result is that the polymer remains rubbery even at temperatures that are high enough to cause the material to decompose. The ideal molecular weight allows the material to flow without dripping. In making the polymer, a chain transfer agent is used to control the molecular weight.

A cylindrical tube, which serves as the cladding layer, is made by polymerizing a cladding material inside a rotating cylindrical reactor. Materials that can be polymerized by the radical polymerization reaction are used and the reaction is induced thermally or by UV radiation using photoinitiator²². Due to the fast rotational speed of the reactor about its axis, a tube of uniform thickness is formed once the reaction is complete. This tube is then removed from the reactor and filled with a core material mixed with an initiator and a chain transfer agent. The core material is then polymerized to make a preform that is drawn to a fiber by heat-drawing process.

There are two other commonly used methods for preform fabrication. First is the rod-in-tube method, in which a pre-fabricated polymer core rod is inserted into a pre-fabricated polymer cladding tube with a tight-fitting²³. The disadvantage of this method is that the rod diameter is usually too large for the drawn fiber to achieve a single-mode operation. Also bubbles may be trapped at the core-cladding interface. The second method is the hole-in-rod technique^{23,24} where a hole is drilled into a cladding polymer rod followed by pouring in core monomer. A polymerization process is then initiated

to obtain a composite core-cladding polymer preform. The core-cladding interface of this preform may not be smooth because of drilling. This could lead to excessive loss.

The most successful technique that can be used for the fabrication of the preform is “Teflon technique”²⁴. In this technique a thin teflon string is properly fixed in the center of a glass tube. The thermal polymerization of the filled tube is carried out in a temperature controlled oil bath. After the monomers are fully polymerized and heat treated, the teflon string is removed and we obtain a polymer tube (polymer rod with a small hole in its center). The bottom side of the core is sealed and the hole is then filled with the initiated monomers for the core. Again it is kept in an oil bath for further polymerization.

➤ *Heat drawing process*

The heat drawing process is shown schematically in Figure 2.4. The solid preform is then drawn or pulled into an optical fiber by a process called fiber drawing.

The fiber drawing process begins by feeding the preform into the drawing furnace. The drawing furnace softens the end of the preform to the melting point. The preform is positioned vertically in the middle of the furnace (or oven) where its lower portion is heated locally to the drawing temperature^{20,25}. Both convective and radiative heat transfer mechanisms are important in heating the preform in the furnace. When the lower part of the preform reaches a temperature beyond its softening point, it necks downward by its own weight due

to gravity. Once this initiation of the drawing process is achieved, tension is applied to the fiber by drawing rollers and the fiber is drawn continuously while the preform is fed at a predetermined rate.

The fiber diameter is continuously measured and the desired value is maintained by controlling the preform feed speed and the drawing roller speed. Another design of the fiber drawing system is the horizontal drawing rig. The only difference in this case from the conventional drawing system is that the whole drawing procedure is horizontal. GD Peng et al.²⁵ have widely used this type of configuration and have observed no fiber sagging during drawing and the fiber diameter was kept at an acceptable tolerance. The horizontal machine offers an additional advantage of convenience of saving the need of climbing up and down the ladder during the draw initiation phase.

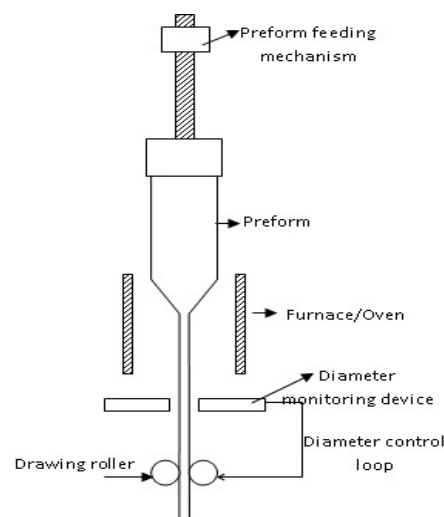


Figure 2.4: Schematic diagram of heat drawing process of polymer optical fiber.

2.2. Section 2. Experimental tool and techniques used for characterization of ChG

In this section the structural, thermal and optical characterization and the tools used for characterizing chalcogenide based materials are included.

2.2.1. Structural Characterization

The structural characterization of the investigated samples of chalcogenide glass was done using X-Ray diffraction technique, Scanning electron microscopy, Atomic force Microscopy, NMR Spectroscopy and Confocal microscopy.

2.2.1. a) X-Ray diffraction (XRD)

Macroscopically, the distinction between crystalline solids and non crystalline solids can be made just by observation. The crystals have definite shapes which reflect the regular atomic arrangement in the atomic scales for example the cubic faces of common salt and glasses on the other hand have curved surfaces²⁶. Microscopically, the distinction can be made using X-ray diffraction (XRD). It is a rapid analytical technique primarily used for phase identification of a crystalline material and can provide information on unit cell dimensions. The analyzed material is finely ground, homogenized, and average bulk composition is determined. Hence it is also called the powder diffraction method. Max von Laue, in 1912, discovered that crystalline substances act as three-dimensional diffraction gratings for X-ray wavelengths similar to the spacing of planes in a

crystal lattice. X-ray diffraction is now a common technique for the study of crystal structures and atomic spacing. X-ray diffraction is based on constructive interference of monochromatic X-rays and a crystalline sample. The interaction of the incident rays with the sample produces constructive interference (and a diffracted ray) when conditions satisfy Bragg's Law²⁶ ($n\lambda=2d \sin \theta$). This law relates the wavelength of electromagnetic radiation to the diffraction angle and the lattice spacing in a crystalline sample. These diffracted X-rays are then detected, processed and counted. By scanning the sample through a range of 2θ angles, all possible diffraction directions of the lattice should be attained due to the random orientation of the powdered material. Conversion of the diffraction peaks to d-spacings allows identification of the mineral because each mineral has a set of unique d-spacings. If a material does not show this diffraction peaks it proves that the material is not a crystal and must be non crystalline. We have used the Bruker AXS D8 Advance diffractometer whose source of X rays is Cu, Wavelength 1.5406 Å°.

2.2.1 b) Scanning electron microscopy (SEM)

Surface imaging of the chalcogenide nano clusters in the spin coated thin films are studied using Scanning electron microscope (JEOL Model JSM - 6390LV) equipped with EDS (JEOL Model JED - 2300) for the qualitative elemental analysis²⁷.

2.2.1. c) Atomic force microscopy (AFM)

The atomic force microscopy (AFM) include in the family of scanning probe microscopes which has grown steadily since the

invention of the scanning tunneling microscope. Veeco, Nanoscope III, made by Digital Instruments Inc., USA base-style atomic force microscopes (AFMs) which uses the basic software element NanoScope is used in the present work to study the distribution of nano clusters in the composite films. The AFM can work either in contact mode or in Tapping Mode. In contact AFM, the tip – that part which directly interacts with the sample – is usually mounted on the end of a support (the cantilever) to create a unified probe. The cantilever provides a support for the tip and is deflected by pressure upon the tip²⁸. By monitoring how the cantilever is deflected, the tip's travel over surface features is interpreted, and then rendered into an electronic image. In tapping mode the tip does not interact directly with the sample. The composite films prepared are studied in tapping mode.

2.2.1 d) Bruker Avance III 400MHz NMR spectrometer

Bruker Avance III 400MHz NMR spectrometer includes a inverse broadband probe fitted with a Z-axis gradient and with automatic tuning and matching. The inner coil is optimized for ¹H and the outer coil can be tuned from ³¹P to ⁹⁷Mo (and others in between). So X-frequencies are ranging from 162 to 27 MHz. The whole system is controlled by Bruker's Topspin software. A B-ACS 60 sample changer is present to be flexible in non-working hours²⁹.

2.2.1. e) Confocal microscope

Leica TCS SP5 II laser scanning confocal microscope is used for the imaging of emission from nano clusters in the nano colloids of

ChG. The system is a Leica TCS SP5, a point scanning spectral confocal with five channels³⁰. The system runs on a Windows XP platform with Leica LAS AF system software. The microscope is enclosed in a Ludin environmental chamber with temperature, humidity, and CO₂ control. It has the following lasers: Blue diode 50mW 405nm, Multiline argon: 5 mW 458 nm, 5 mW 476 nm, 20 mW 488 nm, 5 mW 496 nm, 20 mW 514 nm, He-Ne 1 mW 543 nm, He-Ne 2 mW 594 nm, He-Ne 10 mW 633 nm.

2.2.2. Thermal Characterization

Thermal characterization of the prepared bulk ChG's was done using Differential scanning Calorimetry (DSC). A Mettler-Toledo DSC model 822e³¹ is used to follow the thermal behavior of the samples. The apparatus is equipped with a ceramic sensor FRS5 (heat-flux sensor with 56 thermocouples Au-Au/Pd). The differential scanning calorimeter was previously calibrated using indium and zinc standards for temperature and power calibration. The autosampler available on the Mettler-Toledo DSC 822e is used to automate the experimental procedure.

10 mg of the samples were sealed in a pierced aluminum crucible and heated under nitrogen flow (200 mL/min outside the oven, 100 mL/min inside the oven). Sample was then given temperature at heating rates of 10°C /min. This heating rate improves the calorimetric response (without a decrease of accuracy) and reduces the time of the analysis and, consequently, the risk of sample degradation.

2.2.3. Thickness measurement

Thickness is one of the most important thin film parameter to be characterized since it plays an important role in the film properties unlike a bulk material. Thickness measurement of the thin films prepared by thermal evaporation were carried out at the time of coating itself using a DTM thickness monitor attached in the vacuum system. After fabrication the thickness of the films were found using stylus profiler (Dektak 6M). The stylus profiler³² takes measurements electromechanically by moving the sample beneath a diamond tipped stylus. The high precision stage moves the sample according to a user defined scan length, speed and stylus force. The stylus is mechanically coupled to the core of a linear variable differential transformer (LVDT). The stylus moves over the sample surface. Surface variations cause the stylus to be translated vertically. Composite films of micrometer range were measured using a Mitutoyo digital outside micrometer, series 193 with a resolution ± 0.001 mm.

2.2.4. Optical characterization

2.2.4 a) Absorption, reflection and transmission measurements

JASCO V-570 UV/VIS/NIR Spectrophotometer was used for the absorption, transmission and reflectance measurements of the samples. The spectrometer consist of Optical system³³: single monochromatic, UV/ VIS region 1200 lines/ mm plane grating, NIR region: 300 lines/ nm plane grating, Czerny -Turner mount double beam type Resolution: 0.1 nm (UV/ VIS region) 0.5 nm (NIR region).

Light source: 30 mW deuterium discharge tube in 190 nm to 350 nm region, 20 W tungsten iodine lamp in 330 to 2500 nm region, Wavelength range: 190 nm to 2500 nm. The beam from the light source is converged and enters the monochromator. It is dispersed by the grating in the monochromator and the light passes out through the exit slit. This light is split into two light paths by a sector mirror, one incident on the sample to be measured and the other on the reference sample such as solvent. The light that has passed through the sample or reference sample is incident on the photomultiplier tube and PbS photoconductive cell which are the detectors. In the reflectance measurement the set up has to be changed.

The Model SLM-468 single reflection attachment is designed to measure the relative reflectance of sample using the forward reflected light from the aluminum-deposited plane mirror as reference³⁴. It permits the measurement of the reflectance of metal deposited film, metal plating etc. The wavelength range is 220 nm to 2200 nm with a beam port diameter of 7 mm and angle of incidence approximately 5°.

2.2.4 b) *Optical absorption spectroscopy of amorphous semiconductors*

Absorption spectroscopy of the materials investigated in this thesis was studied using Jasco V570 spectrophotometer. The typical absorption spectrum of chalcogenide glass is shown in Figure 2.5. In amorphous semiconductors, the optical absorption edge spectra generally contain three distinct region³⁵:

- A) High absorption region ($\alpha=10^4 \text{ cm}^{-1}$), which involves the optical transition between valence band and conduction band

which determines the optical bandgap. The absorption coefficient in this region is given by

$$\alpha_{h\nu} = B(h\nu - E_g)^p \quad 2.1$$

where E_g is the optical bandgap and B is a constant related to band tailing parameter. In the above equation, $p=1/2$ for a direct allowed transition, $p=3/2$ for a direct forbidden transition, $p=2$ for an indirect allowed transition and $p=3$ for an indirect forbidden transition.

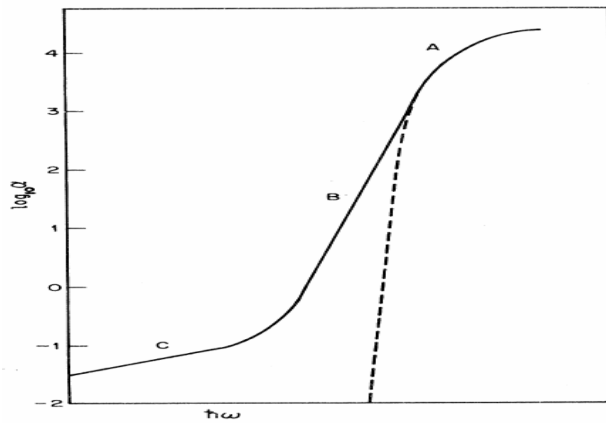


Figure 2.5: Regions A,B,C of a typical absorption curve of chalcogenide glass.

B) Spectral region with $\alpha=10^2-10^4 \text{ cm}^{-1}$ is called Urbach's exponential tail region in which absorption depends exponentially on photon energy ³⁶and is given by

$$\alpha_{h\nu} = \alpha_0 \exp(h\nu/E_e) \quad 2.2$$

where α_0 is a constant and E_e is interpreted as band tailing width of localized states, which generally represents the degree of

disorder in amorphous semiconductors. In this region most of the optical transitions take place between localized tail states and extended band states.

C) The region with $\alpha \geq 10^2 \text{ cm}^{-1}$ involves low energy absorption and originates from defects and impurities.

2.2.4. c) Analysis of Transmission Spectra of thin films using Swanepoels method

Basically, the amount of light that gets transmitted through a thin film material depends on the amount of reflection and absorption that takes place along the light path. The transmission spectrum which depends on the material will have two distinctive features, it will either have interference fringes or it will not. The schematic representation of behaviour of light passing through the material is shown in Figure 2.6.

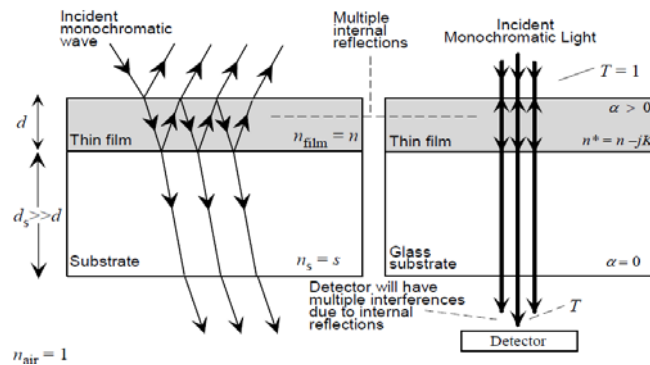


Figure 2.6: Schematic sketch of the typical behaviour of light passing through a thin film on a substrate. On the left, oblique incidence is shown to demonstrate the multiple internal reflections. In most measurements, the incident beam is nearly normal to the film as shown on the right.

The optical constants can be measured by examining the transmission through a thin film deposited on a transparent glass or other (e.g. sapphire) substrate. Figure 2.7 shows a spectrum taken from a thin film on glass substrate. Swanepoel³⁷ has critically reviewed how a single transmission spectrum as shown in figure can be used to extract the optical constants of a thin film.

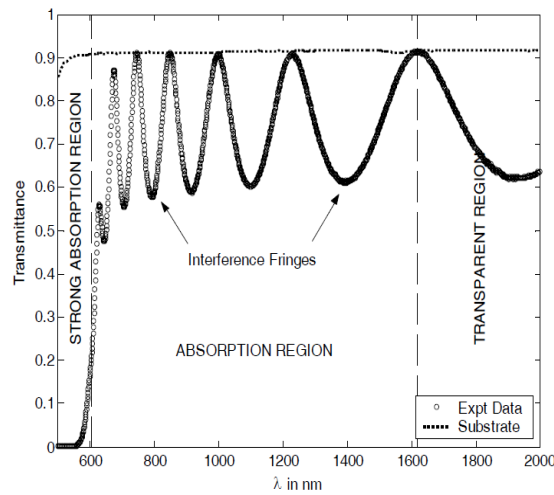


Figure 2.7: Transmission spectra showing the interference fringes.

The refractive index of the thin film with uniform thickness can be calculated from the two envelopes, $T_M(\lambda)$ and $T_m(\lambda)$, by considering the extremes of the interference fringes³⁸:

$$\text{Maxima: } T_M = \frac{Ax}{B - Cx + Dx^2}, \quad 2.3$$

$$\text{Minima: } T_m = \frac{Ax}{B + Cx + Dx^2} \quad 2.4$$

Subtracting the reciprocal of above first equation 2.3 from second equation 2.4 yields an expression that is independent of the absorbance, x ,

$$\frac{1}{T_m} - \frac{1}{T_M} = \frac{2C}{A} \quad 2.5$$

Where $A = 16n^2s$, 2.6

$$C = 2(n^2 - 1)(n^2 - s^2). \quad 2.7$$

Rearranging it for n ,

$$n = \sqrt{\left(N + \sqrt{(N^2 - s^2)} \right)}, \quad 2.8$$

Where $N = \left[\frac{2s}{T_M T_m} \right] - \frac{s^2 + 1}{2}$ 2.9

In this equation, s is the refractive index of glass substrate and its values are obtained from transmission spectra of substrate T_s , using the relation.

$$s = \frac{1}{T_s} + \left(\frac{1}{T_s} - 1 \right)^{1/2} \quad 2.10$$

In the region of weak and medium absorption, where $\alpha \neq 0$, transmittance decreases mainly due to the effect of absorption coefficient, α and Eq.(2.9) modifies to

$$N = 2s \left[\frac{T_M - T_m}{T_M T_m} \right] + \frac{s^2 + 1}{2} \quad 2.11$$

where T_M and T_m are the transmission maximum and corresponding minimum at a certain wavelength .

If n_1 and n_2 are refractive indices of two adjacent maxima or two adjacent minima at wavelengths λ_1 and λ_2 , respectively, then the thickness d_1 of the film is given by³⁶

$$d_1 = \frac{\lambda_1 \lambda_2}{2(\lambda_1 n_2 - \lambda_2 n_1)} \quad 2.12$$

The accuracy of the above equation can also be increased by taking into consideration the basic interference equation,

$2nd_2 = m\lambda$, where n is the order number, m is an integer for maxima and half integer for minima.

2.2.4. d) Refractive index of films without interference fringes

When light gets transmitted through a material at normal incident with multiple reflections at both surfaces of the material, the absorptivity, the reflectance and the transmittance can be expressed by the following relationships³⁹

$$R = r + \frac{(1-r^2)re^{-2\alpha d}}{1+r^2e^{-2\alpha d}} \quad 2.13$$

$$A = (1-r) \frac{1-e^{-\alpha d}}{1-re^{-\alpha d}} \quad 2.14$$

With:

$$r = \frac{(n-1)^2 + k^2}{(n+1)^2 + k^2} \quad 2.15$$

and
$$\alpha = \frac{4\pi k}{\lambda} \quad 2.16$$

where r is the reflectivity in a single reflection, α is the absorption coefficient, k is the extinction coefficient or also called the absorption constant, d is the thickness and n is the refractive index. By definition the absorptivity $A = I_A / I_0$, the reflectance $R = I_R / I_0$ and the transmittance $T = I_T / I_0$, where I_A , I_R and I_T are the intensities of the respective absorption, reflection and transmission activities, and I_0 is the original intensity of the light.

2.2.4 e) Dispersive analysis of the refractive index using Wemple-DiDomenico model

The spectral dependence of the refractive index has been analyzed in terms of Wemple-DiDomenico (WDD) model⁴⁰, which is based on the single effective oscillator approach having the expression, where $h\nu$ is the photon energy, E_0 is the single oscillator energy (also called average energy gap) and E_d is the dispersion energy, which is a measure of average strength of the inter band optical transitions. The oscillator parameters are determined by plotting refractive index factor $(n^2-1)^{-1}$ versus $(h\nu)^2$ and by fitting a straight line to the points. Slope gives $(E_0 E_d)^{-1}$ and the intercept on vertical axis gives (E_0/E_d) .

The effective oscillator energy E_0 , which can be directly correlated with optical energy gap by an empirical formulas proposed by Tanaka as⁴¹

$$E_0 \approx 2 E_g \quad 2.17$$

The values for the static refractive index (n_0) have been calculated from WDD dispersion parameters E_0 and E_d by using the formula

$$n_0 = (1 + E_d / E_0)^{1/2} \quad 2.18$$

The values of n_0 can be calculated by extrapolating the WDD dispersion equation with $h\nu \rightarrow 0$. The high frequency dielectric constant (ϵ_∞) (static dielectric constant) has been calculated from the relation⁴²

$$\epsilon_\infty = (n_0)^2 \quad 2.19$$

2.2.4. f) Calculation of Nonlinear susceptibility and refractive index using Generalized Millers rule and WDD model

Simple empirical relation based on generalized Miller's rule⁴³ can be used for the estimation of the non linear refractive index (n_2) and susceptibility ($\chi^{(3)}$). The non linear refractive index (n_2) and susceptibility ($\chi^{(3)}$) can be calculated by combining Miller's generalized rule⁴⁴ and low-frequency linear refractive index estimated from Wemple-DiDomenico⁴⁰ single effective oscillator model. The linear optical susceptibility in the case of chalcogenide glasses is given by relation: $\chi^{(1)} = (n_2-1)/4\pi$. Using generalized Miller's rule we obtain

$$\chi^{(3)} = A(\chi^{(1)})^4 \quad 2.20$$

Estimated A value⁴⁴ is 1.7×10^{-10} (for $\chi^{(3)}$ in (esu)).

The n_2 can be calculated from the relation,

$$n_2 = \frac{12\pi\chi^{(3)}}{n_0} \quad 2.21$$

2.2.4. g) Absorption coefficient , extinction coefficient, dielectric constants and optical conductivity

The absorption coefficient (α) of these materials strongly depends on optical transmission (T) and reflection (R) and is evaluated using the relation ³⁸

$$\alpha = \frac{2.303}{d} \log \frac{(1-R)^2}{T} \quad 2.22$$

The optical energy gap (E_g) of the thin films has been determined from absorption coefficient data as a function of photon energy. Once the absorption coefficient is calculated the band gap and the width of localized states can be found using Eqs (2.1) and (2.2).

The extinction coefficient (k) and refractive index (n) are important parameters characterizing photonic materials. Values of n and k are calculated using the experimental data obtained for the samples under study has been calculated using the relation³⁹

$$k = \alpha \lambda / 4 \pi \quad 2.23$$

The knowledge of real part and imaginary part of the dielectric constant provide information about the loss factor³⁷. The real part of the dielectric constant is associated with the term that shows how much it will slow down the speed of light in the material and the imaginary part shows how a dielectric absorbs energy from an electric field due to dipole motion.

The dielectric constant (ϵ_r) and dielectric loss (ϵ_i) have been determined from³⁹

$$\varepsilon_r = n^2 - k^2 \quad 2.24$$

$$\varepsilon_i = 2nk \quad 2.25$$

The optical response of a material is most conveniently studied in terms of the optical conductivity. It has dimensions of frequency which are valid only in a Gaussian system of units. The optical conductivity (σ) has been determined from the relation³⁹

$$\sigma = \alpha nc / 4\pi \quad 2.26$$

where α is the absorption coefficient, n is the refractive index and c is the velocity of light.

2.2.4. h) Photodarkening experiment

Photoinduced darkening experiments were done on the thin films using the experimental set up⁴² as shown in Figure 2.8.

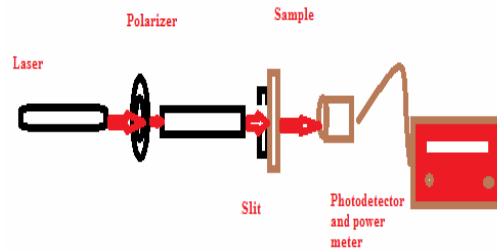


Figure 2.8: Experimental set up used for photodarkening experiment.

Photoinduced studies were carried out using above band gap and near band gap laser sources. We have used 4 mW, 10 mW and 20mW He-Ne laser (1.96 eV) and Sacher Semiconductor laser (1.53 eV) to study the photosensitivity of the unannealed films. The laser power was made stable during exposure to avoid significant

uncertainty in the total supplied energy. The laser beam was expanded from an initial beam waist of 1.0 mm (FWHM) using a plano-concave lens and collimated with a second plano-convex lens. At the sample stage an aperture (1 cm²) was used to admit only the central maximum of the laser beam, so as to assure irradiating the sample with a fairly uniform intensity.

The transmittance and reflectance spectra of the films at normal incident condition in the spectral range 250–2500 nm were recorded by a double beam UV–VIS–NIR spectrophotometer (Jasco V 570) after and before exposure. All the measurements were executed at room temperature and the samples were kept in the dark between experiments.

2.2.4. i) *Photoluminescence spectroscopy*

Photoluminescence studies on nano colloid chalcogenide glasses were carried out using Varian Spectro fluoremeter. The fluorescence excitation and emission spectrum of the samples were taken using Cary Eclipse Fluorescence spectrophotometer of VARIAN⁴⁵. It has a single cell holder for liquid sample analysis and a solid sample holder accessory to perform fluorescence measurements on solid samples. The solid sample holder accessory provides both rotational and translational adjustment of the sample. The angle of incidence of the excitation may be varied from 20°- 35°. This is the angle between the exciting light and a line perpendicular to the surface of the sample mounting slide. The source of excitation is xenon lamp.

➤ *Laser induced photoluminescence*

Laser induced photoluminescence is spontaneous emission from atoms or molecules that have been excited by laser radiation. Two radiative transitions are involved in the Laser induced photoluminescence process. First, absorption takes place, followed by a photon-emission step. Laser induced photoluminescence has a large range of applications in spectroscopy⁴⁶. Laser induced photoluminescence is a dominant laser spectroscopic technique in the probing of unimolecular and bimolecular chemical reactions. This technique serves as a sensitive monitor for the absorption of laser photons in fluorescence excitation spectroscopy. It is well suited to gain information on molecular states if the fluorescence spectrum excited by a laser on a selected absorption transition is dispersed by a monochromator.

The pump beam is taken from a Quanta Ray Q-switched Nd:YAG laser which emits pulses of 7 ns duration at 532 nm and at a repetition rate of 10 Hz⁴⁷. A cylindrical lens is used to focus the pump beam in the shape of a stripe on the sample. In the present case it is adjusted to a pump beam width of 7 mm. The output is collected from the edge of the front surface of the cuvette using an optical fiber in a direction normal to the pump beam. The emission spectra are recorded with Acton monochromator attached with a CCD camera (Figure 2.9). Princeton Instruments NTE/CCD air cooled detectors have three distinct sections⁴⁸. The front vacuum enclosure contains the CCD array seated on a cold finger. This finger is in turn seated on a four-stage Peltier thermoelectric cooler. The back enclosure contains the heat exchanger. An internal fan cools the heat

exchanger and the heat exits the unit through openings in the housing. The CCD array used is Roper Scientific NTE/CCD-1340/100-EM. The electronics enclosure contains the preamplifier and array driver board. This keeps all signal leads to the preamplifier as short as possible, and also provides RF shielding. SPEC-10 controller of Princeton Instruments controls the CCD.

SpectraPro-500i is a 500 mm focal length monochromator/spectrograph. It features an astigmatism-corrected optical system, triple indexable gratings and triple grating turret. The SpectraPro-500i includes a direct digital grating scan mechanism with full wavelength scanning capabilities, plus built-in RS232 and IEEE488 computer interfaces. The 1200 grooves/mm grating has an aperture ratio $f/6.5$. The scan range is 0 to 1400 nm (mechanical range) and an operating range of 185 nm to the far IR and a resolution of 0.05 nm at 435.8 nm. WinSpec, the spectroscopic software, of Princeton Instruments⁴⁹ is used for collecting, storing and processing data from the Roper Scientific system.

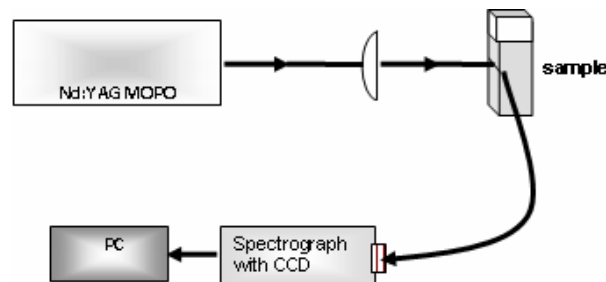


Figure 2.9: Laser induced luminescence experimental set up.

Luminescence studies on the fibers are also carried out using the above setup. Instead of the sample in the cuvette the fiber is inserted axially in a fiber holder and studied.

Luminescence studies on fiber are also carried out transversely in the prepared fiber using the set up as shown in Figure 2.10. More information regarding the experiment is given in chapter 7. Studies are made on excitation with LED as excitation source also.

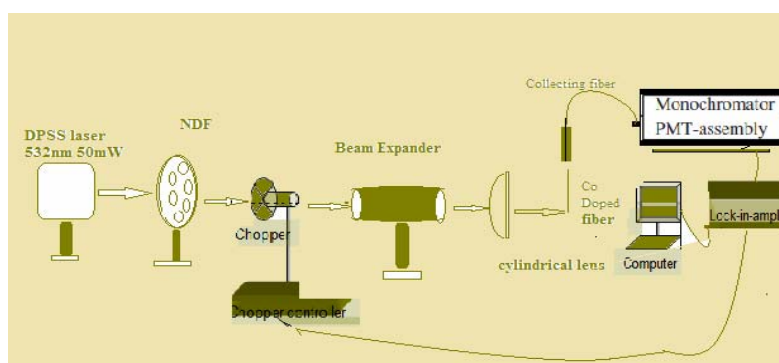


Figure 2.10: Experimental set up for luminescence studies on fiber.

2.2.5. Thermal lens technique for diffusivity measurement

Thermal lens technique is based on the optical measurement of the thermal energy released by a sample subsequently to light absorption and nonradiative relaxation of the excited species⁵⁰. In this method, sample is illuminated using a gaussian beam. A part of the incident radiation is absorbed by the sample and subsequent nonradiative decay of excited state population results in local heating of the medium⁵⁰. The temperature distribution in the medium mimics the beam profile of the excitation beam and hence a refractive index gradient is created in the medium. Due to this modification in

refractive index, the medium act as a lens, called thermal lens (TL). The thermal lens generally has a negative focal length since most materials expand upon heating and hence have negative temperature coefficient of refractive index. The formation of the thermal lens causes the probe beam to expand and is detected as a time dependent decrease in power at the centre of the beam at far field. Most of the currently employed techniques for thermal parameter evaluation are mainly depending upon the heat exchange mechanism or on temperature gradients. However, the thermal lens technique depends upon change in refractive index due to nonradiative deexcitation of sample following the optical excitation which can offer accurate results. The experimental set up used for the studies is given in Figure 2.11. This method offers certain advantage such as its response to even small absorption coefficient as well as accurate measurement of thermal parameters.

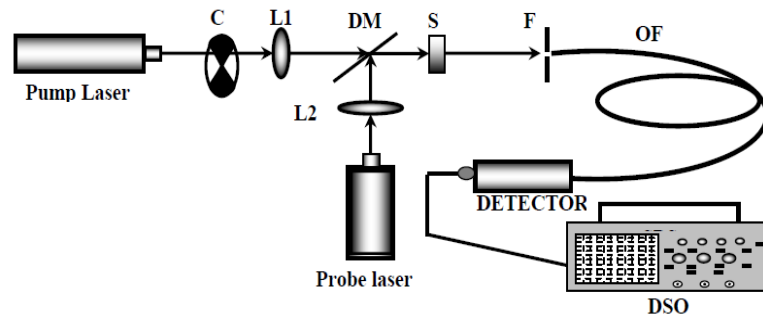


Figure 2.11: Schematic diagram of the experimental set up. BS1, BS2- Beam Splitters, C - Chopper, L1, L2 - Lenses, DM - Dichroic Mirror, S - Sample, F- Filter, OF- Optical fiber, DSO- Digital Storage Oscilloscope.

Laser radiation at 532 nm wavelength from a Diode Pumped Solid state laser (50mW) is used as the pump beam to generate the thermal lens in the medium. Micro DPSS laser model BWT-50 (B&W) at 532 nm was also used⁵⁰. BWT series are miniature diode-pumped Nd: YVO₄ lasers with integrated internal thermoelectric cooler. They can be operated over a temperature range of -10 to 50°C.

It has TEM₀₀ mode with a spectral line width <0.1 nm and a beam size of 1 mm JDS Uniphase He-Ne gas laser emitting at 633 nm with 4 mW power was used as the probe beam in studies. The pump beam is intensity modulated using a mechanical chopper. The probe beam is made to pass collinearly through the sample using a dichroic mirror. An optical fiber mounted on XYZ translator serves as the finite aperture. The other end of the fiber is coupled to a fast photodetector. The signal output from detector is processed using a digital storage oscilloscope. Mechanically chopped optical radiation from pump laser is focused using a lens L1 to the sample in a cuvette of 1cm length. The sample holder is placed in a micrometer translational stage and the position of the sample holder is adjusted along the optic axis to obtain the maximum intensity change of the probe beam (one confocal length away from the beam focus). When the chopper allows impinging of pump beam on the sample, it creates a thermal lens within the sample. The chopper used in the study for light beam modulation is HMS/ITHACO model 230 light beam chopper⁵¹ with a set of three interchangeable blades of slots 2, 10 or 30 providing three frequency ranges. The frequency ranges from 4 to

200 Hz, 20 to 1 kHz and 60 to 3 kHz for 2, 10 and 30 slotted blades respectively. The probe beam from the He-Ne laser which travel collinearly with pump beam experience a diverging lens and the beam shape expands in the presence of thermal lens. The change in intensity of the probe beam is measured using a fast photodetector using fiber which is fixed on the optic axis of the experimental set up. The TL signal is recorded from which the relative change in intensity and initial slope is measured. The value of θ and t_c are determined. From these values, the thermal diffusivity of the sample under investigation is evaluated.

Theory

The magnitude of the effective thermal lens produced by propagation of a cw Gaussian laser beam of spot size ω is governed by the steady state balance between laser heating and solvent or matrix heat dissipation. If the beam is suddenly turned on at time $t=0$, the lens approach to steady state governed by⁵²

$$f(t) = f_{\infty} \left(1 + \frac{t_c}{2t} \right) \quad 2.27$$

and the steady state focal length f_{∞} of such a lens is derived as

$$f_{\infty} = \frac{\pi k \omega^2}{PA \left(\frac{dn}{dt} \right)} \quad 2.28$$

where k is the thermal conductivity ($\text{W cm}^{-1} \text{K}^{-1}$), P is the laser power (W), A is the sample absorbance, dn/dt is the refractive index change with temperature and t_c is the time response to attain the steady state focal length given by

$$t_c = \frac{\omega^2}{4T_D} \quad 2.29$$

from which thermal diffusivity (T_D) can be calculated. The thermal diffusivity in the sample is detected by its effect on the propagation of the probe laser beam aligned with the centre of the lens. The expression relating the intensity as a function of time is given as

$$I(t) = I(0) \left[1 - \frac{\theta}{1 + t_c/2(t)} + \frac{\theta^2}{2 \left(1 + t_c/2(t) \right)^2} \right] \quad 2.30$$

The modified equation for continuous wave laser source is,

$$I(t) = I(0) \left[1 - \frac{\theta}{1 + t_c/2(t-t_0)} + \frac{\theta^2}{2 \left(1 + t_c/2(t-t_0) \right)^2} \right]^{-1} \quad 2.31$$

where t_0 is the time at $t=0$, θ is directly proportional to P_{th} by the relation

$$\theta = \frac{P_{th} \left(\frac{dn}{dT} \right)}{\lambda k} \quad 2.33$$

where P_{th} is the laser power degraded to heat and λ is the laser wavelength. For a given solvent or matrix the experimental parameter of interest is θ , which may be obtained from the initial intensity I_0 and the intensity after the steady state has been established, I_∞ , so that

$$\theta = 1 - (1 + 2I)^{1/2} \quad 2.34$$

$$I = \frac{I_0 - I_\infty}{I_\infty} \quad 2.35$$

$$\text{The initial slope of the decay curve, } m = \frac{2\theta}{I_0 t_c} \quad 2.36$$

from which the value of t_c and hence T_D is calculated.

2.2.6. Z-scan technique for the analysis of nonlinear optical properties of the samples investigated

Z-scan technique introduced by Sheik Bahae⁵³ is a single beam method for measuring the sign and magnitude of nonlinear refractive index that has a sensitivity compared to interferometric methods. It provides direct measurement of nonlinear absorption coefficient. Previous measurements of nonlinear refraction have used a variety of techniques⁵⁴ including nonlinear interferometry, degenerate four wave mixing, nearly degenerate three wave mixing, ellipse rotation and beam distortion measurements. The first three methods namely nonlinear interferometry and wave mixing are potentially sensitive techniques, but all require complex experimental apparatus. The propagation of laser beam inside such a material and the ensuing self refraction can be studied using the z-scan technique. Thus it enables one to determine the third order nonlinear properties of solids, ordinary liquids, and liquid crystals. The experimental set up for single beam z-scan technique is given in Figure 2.12. In the ordinary single beam configuration, the transmittance of the sample is measured, as the sample is moved along the direction of the focussed

gaussian beam. A laser beam propagating through a nonlinear medium will experience both amplitude and phase variation. If transmitted light is measured through an aperture placed in the far field with respect to focal region, the technique is called closed aperture z-scan. In this case, the transmitted light is sensitive to both nonlinear absorption and nonlinear refraction. In a closed aperture z-scan experiment, phase distortion suffered by the beam while propagating through the nonlinear medium is converted into corresponding amplitude variations. On the other hand, if transmitted light is measured without an aperture, the mode of measurement is referred to as open aperture z-scan. In this case, the output is sensitive only to nonlinear absorption. Closed and open aperture z-scan graphs are always normalized to linear transmittance i.e., transmittance at large values of $|z|$.

Closed and open aperture z-scan methods yield the real part and imaginary part of nonlinear susceptibility $\chi(3)$ respectively. Usually closed aperture z-scan data is divided by open aperture data to cancel the effect of nonlinear absorption contained in the closed aperture measurements. The new graph, called divided z-scan, contains information on nonlinear refraction alone.

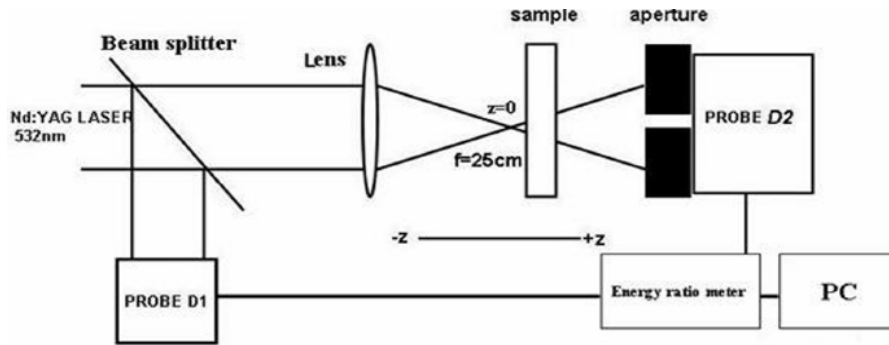


Figure 2.12: Z Scan set up.

An important requirement in the z-scan measurement is that, it is assumed that the sample thickness is much less than Rayleigh's range z_0 (diffraction length of the beam [$z_0 = k \omega_0^2 / 2$, where k is the wave vector and ω_0 is the beam waist radius. The beam waist radius ω_0 is given by $\omega_0 = f\lambda / D$, where f is the focal length of the lens used, λ is the wavelength of the source and D is the beam radius at the lens. This is essential to ensure that the beam profile does not vary appreciably inside the sample because z-scan technique is highly sensitive to the profile of the beam and also to the thickness of the sample. Any deviation from gaussian profile of the beam and also from thin sample approximation will give rise to erroneous results.

2.2.6.1. Open aperture z- Scan.

Non linear absorption of a sample is manifested in the open aperture z- Scan measurement. If the sample is having nonlinear absorption such as two photon absorption (TPA)⁵⁵, it is manifested in the measurement as a transmission minimum at the focal point. Otherwise if the sample is a saturable absorber, the transmission

increases with increase in incident intensity and results in transmission maximum at the focal region.

Theory of open aperture z-scan technique

In the case of an open aperture z-scan, the aperture as shown in Figure 2.12 is absent. In the absence of an aperture the transmitted light measured by the detector is sensitive only to intensity variations. Hence, phase variations of the beam are not taken into consideration. The intensity dependent nonlinear absorption coefficient $\alpha(I)$ can be written in terms of linear absorption coefficient α and TPA coefficient β as⁵³

$$\alpha(I) = \alpha + \beta I \quad 2.37$$

The irradiance distribution at the exit surface of the sample can be written as

$$I_r(z, r, t) = \frac{I(z, r, t)e^{-\alpha l}}{1 + q(z, r, t)} \quad 2.38$$

Where $q(z, r, t) = \beta I(z, r, t)L_{\text{eff}}$. L_{eff} is the effective length given in terms of sample length l and α by the relation

$$L_{\text{eff}} = \frac{(1 - e^{-\alpha l})}{\alpha} \quad 2.39$$

The total transmitted power $p(z, t)$ is obtained by integrating Eq 2.38 over z and r and is given by

$$P(z, t) = P_I(t)e^{-\alpha l} \frac{\ln[1 + q_0(z, t)]}{q_0(z, t)} \quad 2.40$$

$P_I(t)$ and $q_0(z, t)$ are given by the following equations respectively.

$$P_I(t) = \frac{\pi\omega_0^2 I_o(t)}{2} \quad 2.41$$

$$q_0(z,t) = \frac{\beta I_0(t) L_{eff} Z_0^2}{Z^2 + Z_0^2} \quad 2.42$$

For a pulse of gaussian temporal profile, Eq 2.40 can be integrated to give the transmission as

$$T(z) = \frac{C}{q_0 \sqrt{\pi}} \int_{-\infty}^{\infty} \ln(1 + q_0 e^{-t^2}) dt \quad 2.43$$

Non linear absorption coefficient is obtained from fitting the experimental results to the Eq (2.43).

If $|q_0| < 1$, the Eq 2.42 can be simplified as

$$T(z, S=1) = \sum_{m=0}^{\infty} \frac{[-q_0(z,0)]^m}{(m+1)^{1/2}} \quad 2.44$$

where m is an integer. Once an open aperture z -scan is performed, the parameter q_0 can be obtained by fitting the experimental results to equation (2.42). Then the nonlinear absorption coefficient β can be unambiguously deduced using equation (2.43). The imaginary part of third order susceptibility ($\chi^{(3)}$) determines the strength of the nonlinear absorption. The TPA coefficient is related to $\text{Im}(\chi^{(3)})$ by the relation⁵⁶

$$\text{Im}(\chi^{(3)}) = \frac{\varepsilon_0 n_0^2 c^2 \beta}{\omega} (m2V - 2) = \frac{n_0^2 c^2 \beta}{240 \pi^2 \omega} \quad (esu) \quad 2.45$$

where λ is the excitation wavelength, n_0 is the linear refractive index, ε is the permittivity of free space and c the velocity of light in vacuum.

2.2.7. Two Photon absorption

Two-photon absorption (TPA) is the phenomenon in which two photons of identical or different frequencies are absorbed simultaneously such that a molecule from one state (usually the ground state) will be excited to a higher energy electronic state. Schematic representation of TPA is shown in Figure 2.13. Two-photon absorption can be broadly classified into two types, one is called the resonant TPA and the other one belongs to non resonant TPA. The non resonant TPA is the process in which two photons combine to bridge an energy gap larger than the energies of individual photons. When there exists an intermediate state in the gap, the transition happens through two separate one photon transitions and the process is now described as resonant TPA (sequential TPA).

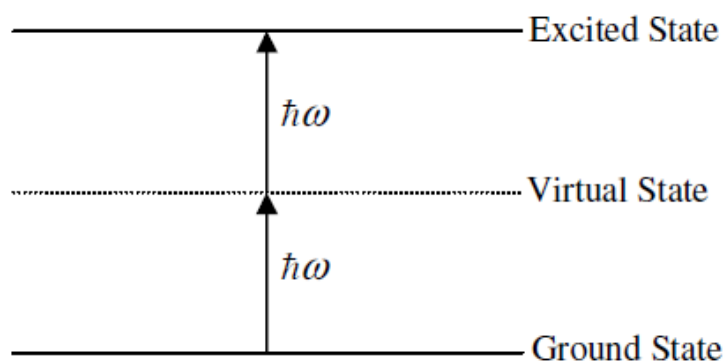


Figure 2.13: Schematic representation of TPA.

In non resonant TPA there need not be an intermediate state for the atom to reach before arriving at the final excited state (as if it were moving up two stair steps by stepping one at a time). Instead,

the atom is excited to a “virtual state” which need not correspond to any electronic or vibrational energy eigen state. The nonlinear absorption in this case is proportional to the square of the instantaneous intensity and is given by⁵⁷

$$\frac{dI}{dZ} = -\alpha I - \beta I^2 \quad 2.46$$

where α is the linear absorption coefficient and β is the two photon absorption coefficient.

2.2.8. Optical limiting studies

The optical limiting behaviour of the samples and the threshold value of optical limiting are understood by keeping the sample in a fixed position and measuring the transmittance as a function of input fluence⁵⁸. The optical limiting properties of a material can also be estimated from its z-scan plots for various input fluence. For this, the nonlinear transmission has to be plotted as a function of input fluence and such plots can be generated from the z-scan measurements. From the value of fluence at the focus, fluence level at other sample positions can be calculated using the standard equation for Gaussian beam waist given by⁵⁸,

$$\omega^2(z) = \omega_0^2 \left(1 + \frac{z^2}{z_0^2} \right)$$

Generally it is found that the threshold value of optical limiting is not sharp for material⁵⁸. One will be able to find an exact value for threshold from the Z-scan plot for the transmission in terms of input fluence.

2.3. Conclusions

The preparation method used in the research work for bulk, thin film, nano colloid, composite film, stacked film and nano colloid doped polymer fiber from ChG are discussed in detail. The characterization tools and experimental set up along with theory used for the study of absorption spectroscopy, photoinduced darkening, photoluminescence mechanism, thermal diffusivity measurement and z-scan technique used for investigating ChG based samples are also discussed.

2.4. References

1. Masayuki Yamane and Yoshiyuki, "Glasses for Photonics", Cambridge University Press, Spain (2000).
2. Valentina Kokorina, "Glasses for Infrared Optics", CRC Press, Boca Raton, Fla (1996).
3. Frey, Harmut and H.R Khan, "Hand Book of thin film technology", Springer (2011).
4. A. Goswami, "Thin Film Fundamentals", New Age International (P) Limited, New Delhi (1996).
5. H.E. Atyia, "Electrical and optical properties of thermally evaporated $Ge_{20}In_{15}Se_{75}$ films", Physica B., 403, 16–24(2008).
6. URL:<http://www.clean.cise.columbia.edu/process/spintheory.pdf%20%20>
7. Guozhrng Cao, "Nano structures and Nano materials. Synthesis, Properties and Applications", Imperial college press, London (2004).
8. URL:<http://en.wikipedia.org/wiki/N-Butylamine>.
9. G. C. Chern, and I. Lauks, "Spin-coated amorphous chalcogenide films," Journal of Applied Physics., 53(10), 6979 (1982).
10. G. C. Chern, I. Lauks, and A. R. McGhie, "Spin coated amorphous chalcogenide films: Thermal properties," Journal of Applied Physics., 54(8), 4596 (1983).

11. G. C. Chern, and I. Lauks, "Spin coated amorphous chalcogenide films: Structural characterization", *Journal of Applied Physics.*, 54, 2701 (1983).
12. Puri, Sharma, Pathania, "Principles of Physical Chemistry", Vishal Publishing Co, Jalandhar (2003).
13. R.G. Parr and R.G. Pearson, "Absolute Hardness: Companion Parameter to Absolute Electronegativity", *J. Am. Chem. Soc.*, 105, 7512-7516 (1983)
14. R.G. Pearson, "Hard and soft acids and bases, HSAB, part I: Fundamental principles", *J. Chem. Educ.*, 45, 581-586 (1968).
15. R.G. Pearson, "Hard and soft acids and bases, HSAB, part II: Underlying theories", *J. Chem. Educ.*, 45, 643-648 (1968).
16. C.A.Fenich, "Poly Vinyl Alcohol: Properties and Applications", John and Wiley \$ Sons, London (1973).
17. Nicholas P Chremisinoff and Chremisinoff, "Handbook of polymer science and technology ", CRC Press, Taylor and Francis (1989).
18. Gary E. Winik, Debra J.Trantola, Thomas M.Cooper, Joseph D.Gresser, "Photonic polymer systems, Fundamentals: methods and application", CRC Press, Taylor and Francis (1998).
19. Werner Daum, Jrgen Krauser, Peter E Zamzow, Olaf Ziemann, "Pof - Polymer Optical Fibers for Data Communication", Springer, Verlag Berlin Heidenberg ,Newyork (2002).
20. Sheeba M, " Fabrication and Characterization of Polymer Optical Fibers for Photonic Device Applications", PhD Thesis, CUSAT, Cochin (2008).
21. H. P. A. van den Boom, W. Li, P. K. van Bennekom, Tafur Monroy, and Giok-Djan Khoe, "High-Capacity Transmission Over Polymer Optical Fiber", *IEEE J Sel Top Quan Elec.*, 7, 461-470 (2001).
22. Takaaki Ishigure, Yasuhiro Koike, and James W. Fleming, "Optimum Index Profile of the Perfluorinated Polymer-Based GI Polymer Optical Fiber and Its Dispersion Properties", *J Lightwave.Tech.*, 18, 959 - 965 (2000).
23. T. Ishigure, E. Nihei, and Y. Koike, "Optimum refractive-index profile of the graded-index polymer optical fiber, toward gigabit data links", *Applied Optics.*, 35, 2048(1996).

24. Andreas Neyer, Bjorn Wittmann, and Matthias Johnck, "Plastic-Optical-Fiber-Based Parallel Optical Interconnects", IEEE J. SEL TOP QUAN ELEC., 5, 393(1999).
25. Gang Ding Peng Chu, P.K. Zhengjun Xiong Whitbread, T.W. Chaplin, R.P., "Dye-doped step-index polymer optical fiber for broadband optical amplification", Journal Lightwave Technology., 14, 2215-2223(1996).
26. A.L. Patterson, "The Sherrer formula for X-Ray particle size determination" Phys.Rev. , 56(10), 978-982 (2002).
27. Scanning electron microscope (JEOL Model JSM - 6390LV) equipped with EDS (JEOL Model JED - 2300), Japan. Manual.
28. Veeco, Nanoscope III, made by Digital Instruments Inc., USA. Manual
29. Bruker Avance III 400MHz NMR spectrometer, Germany. Manual.
30. Leica TCS SP5 II laser scanning confocal microscope Manual.
31. Mettler-Toledo DSC model 822e, Switzerland. Manual.
32. Veeco Dektak 6M Manual (2004)
33. Model V-550/560/570 Spectrophotometer Hardware/Function manual (data station type).JASCO Corporation, Tokyo, Japan. (1996).
34. Model SLM-468 single reflection attachment instruction manual. JASCO Corporation, Tokyo, Japan. (1994).
35. S.R. Elliot, "Physics of Amorphous Materials", Essex: Longman Group Limited, New York (1990).
36. Franz Urbach "The Long-Wavelength Edge of Photographic Sensitivity and of the Electronic Absorption of Solids", Physical Review., 92, 1324-1324 (1953).
37. R. Swanepoel, "Determination of the thickness and optical constants of amorphous silicon," Journal Physics E., 16(12), 1214-1222 (1983).
38. Ambika, P.B.Barman," An optical study of vacuum evaporated $Se_{85-x}Te_{15}Bi_x$ chalcogenide thin films", Physica., B405 ,822-827(2010).
39. R Tintu, K Sulakshna, K Saurav, V P N Nampoore, P Radhakrishnan and Sheenu Thomas "Ge₂₈Se₆₀Sb₁₂ /PVA Composite Films For Photonic Applications", Journal of Non-Oxide Glasses., 2, 167- 174 (2010).

40. S. H. Wemple and M. DiDomenico, "Behavior of the Electronic Dielectric Constant in Covalent and Ionic Materials," *Physical Review B.*, 3, 1338-1351 (1971).
41. A. Zakery and S.R. Elliot, "Optical Properties and Applications of Chalcogenide Glasses: A Review" *J. Non-Cryst. Solids.*, 330(1), 1-12 (2003).
42. R. Tintu, V.P.N. Nampoory, P. Radhakrishnan, Sheenu Thomas "Photoinduced changes in optical properties of Ga-Sb-Ge-Se glasses", *Optics Communications.*, 284, 222-225 (2011).
43. Wang C, "Empirical Relation between the Linear and the Third-Order Nonlinear Optical Susceptibilities," *Phys. Rev. B.*, 2 [6], 2045-2048(1970).
44. Ticha H and L.Tichy, "Semiempirical relation between non-linear susceptibility (refractive index), linear refractive index and optical bandgap and its application to amorphous semiconductors", *Journal of Optoelectronics and Advanced Materials.*, 4[2], 381 - 386 (2002).
45. Cary Eclipse Hardware operation manual. VARIAN. Australia (2000).
46. Wolfgang Demtrder 'Laser spectroscopy: Basic concepts and instrumentation'. (3rd edition) Springer, New Delhi, India (2004).
47. Quanta-Ray, Pulsed Nd:YAG lasers User's manual GCR-100 series, Spectra-Physics, USA (1997).
48. Princeton Instruments NTE/CCD, Manual, Roper Scientific, Inc. USA (2001).
49. WinSpec, spectroscopic software of Princeton Instruments, Roper Scientific, USA (2001).
50. Instruction manual. Diode pumped solid state lasers. BWH/ BWT-xx series.
51. HMS light beam chopper instruction manual Ithaco model 230. New York (1985).
52. A.C.Tam, "Photothermal Investigation of Solids and Fluids, Academic press, Inc., New York (1989).
53. M S Bahae, A A Said, T H Wei, D J Hagan and E W Van Stryland, "Sensitive measurement of optical nonlinearities using a single beam", *IEEE J. Quantum Electron.*, 14, 760 (1990).

54. A. Zakery and S.R. Elliott, "Optical Nonlinearities in Chalcogenide Glasses and their Applications", Springer, Berlin. (2007).
55. R. Tintu, V. P. N. Nampoore, P. Radhakrishnan, and Sheenu Thomas "Nonlinear optical studies on nanocolloidal Ga-Sb-Ge-Se chalcogenide Glass", Journal Of Applied Physics., 108, 073525 (2010).
56. R. Tintu, V. P. N. Nampoore, P. Radhakrishnan, and Sheenu Thomas, "Nano composite Thin films of $Ga_5 Sb_{10} Ge_{25} Se_{60}$ chalcogenide glass for optical limiting applications ", Optical Materials., 33 ,1221-1225 (2011).
57. S Sapra and D D Sarma; "Evolution of the electronic structure with size in II-VI semiconductor nanocrystals", Phys. Rev., B 69, 125304 (2004)
58. J. Troles, F. Smektala, G. Boudebs, A. Monteila, B. Bureau, J. Lucas, "Optical limiting behaviour of chalcogenide glasses", Journal of Optoelectronics and Advanced Materials ., 4,729 - 735(2002) .



Chapter 3

STUDIES ON $\text{Ga}_5\text{Sb}_{10}\text{Ge}_{25}\text{Se}_{60}$ CHALCOGENIDE GLASS

- 3.1. Section 1. Studies on Bulk and thin film $\text{Ga}_5\text{Sb}_{10}\text{Ge}_{25}\text{Se}_{60}$
- 3.2. Section 2. Photoinduced darkening in thermally evaporated $\text{Ga}_5\text{Sb}_{10}\text{Ge}_{25}\text{Se}_{60}$ films
- 3.3. Section 3. Studies on Nano colloid $\text{Ga}_5\text{Sb}_{10}\text{Ge}_{25}\text{Se}_{60}$ chalcogenide glass
- 3.4. Section 4. Optical Characterization of nano composite $\text{Ga}_5\text{Sb}_{10}\text{Ge}_{25}\text{Se}_{60}$ /PVA films
- 3.5. Conclusions
- 3.6. References

This chapter deals with the studies on $\text{Ga}_5\text{Sb}_{10}\text{Ge}_{25}\text{Se}_{60}$ chalcogenide glass and it is divided in to four sections. Section 1 includes the preparation, structural, thermal and optical characterization of bulk and thin films of $\text{Ga}_5\text{Sb}_{10}\text{Ge}_{25}\text{Se}_{60}$ glass. The kinetics of photoinduced effects on $\text{Ga}_5\text{Sb}_{10}\text{Ge}_{25}\text{Se}_{60}$ thin film exposed to continuous wave laser radiations are studied as a function of exposure time, laser intensity and laser wavelength (near band gap and above band gap) in section 2. Section 3 deals with the preparation and characterization of nano colloid $\text{Ga}_5\text{Sb}_{10}\text{Ge}_{25}\text{Se}_{60}$ glass solutions. Section 4 introduces a new low-cost, scalable method method for the fabrication of nano composite $\text{Ga}_5\text{Sb}_{10}\text{Ge}_{25}\text{Se}_{60}$ /PVA films for optical applications. Results of the structural and optical investigation of the nano composite films are also included in section 4.

The results of this chapter are published in

1. R. Tintu et al, *Optics Communications*, 284, 222–225(2011).
2. R. Tintu et al, *Journal of Applied Physics*, 108, 073525 (2010).
3. R. Tintu et al, *Optical Materials*, 33, 1221-1225 (2011).

3.1. Section 1. Studies on bulk and thin film Ga₅Sb₁₀Ge₂₅Se₆₀ ChG

This section deals with the preparation and characterization of bulk and thermally evaporated thin films of Ga₅Sb₁₀Ge₂₅Se₆₀.

3.1.1. Introduction

Germanium-containing glasses show interesting thermal, mechanical and optical properties due to their strong chemical bond¹. These glasses have significantly high glass transition temperature, lower thermal expansion coefficient and higher mechanical strength. Ga-Ge-Sb-Se has been studied in detail for potential applications in the 8–12 μm regions by H.L. Ma et al.². The glass-forming region in Ga-Ge-Sb-Se system with two different atomic percentages of Ga (5% and 10%) is represented as in Figure 3.1. The system forms macroscopically homogeneous glasses over a wide range of compositions. Studies on different compositions of Ga-Ge-Sb-Se systems show that Ga₅Sb₁₀Ge₂₅Se₆₀ glass has a high enough glass transition temperature (283°C), a relatively high refractive index (2.63 at 10 μm) and is found to be very stable towards crystallization².

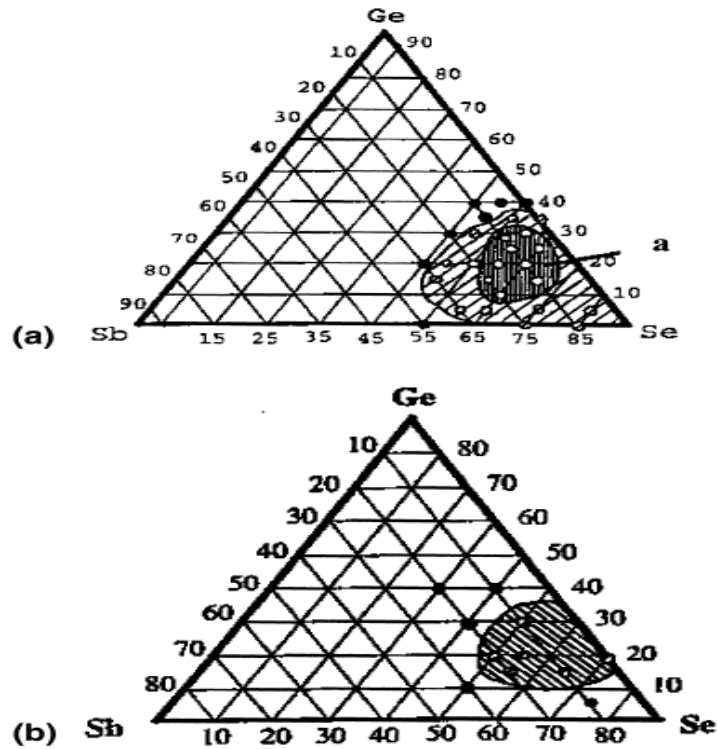


Figure 3.1: Glass-forming region of the Ga-Ge-Sb-Se system. Open dots: glassy sample; filled dots: crystalline samples. (a) Diagonal lines: glassy material region; vertical lines: glasses with no crystallisation phenomena (b) Diagonal lines: glassy material.

Thermal and mechanical properties are generally the weak point of vitreous materials and this is particularly true for the infrared transmitting chalcogenide glasses. Therefore the physical properties have to be considered before using the chalcogenide glass for any optical applications. The transmission spectra of $Ga_5Sb_{10}Ge_{25}Se_{60}$ glass is shown in Figure 3.2. $Ga_5Sb_{10}Ge_{25}Se_{60}$ is found to have transmission in the range $0.8 \pm 15 \mu m^3$.

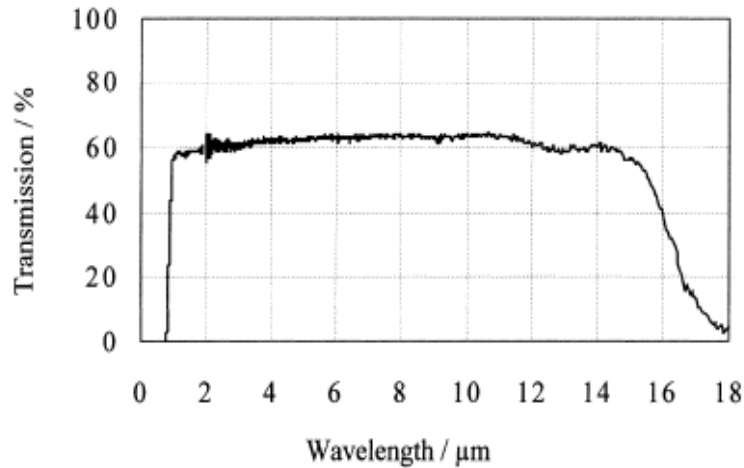


Figure 3.2: Transmission spectra of $\text{Ga}_5\text{Sb}_{10}\text{Ge}_{25}\text{Se}_{60}$ glass.

Chemical durability studies under different conditions indicates that this glass is strongly resistant to dilute acid solutions and less resistant towards corrosion when immersed in basic solutions. Another important parameter to be considered is the stability towards different environmental conditions. $\text{Ga}_5\text{Sb}_{10}\text{Ge}_{25}\text{Se}_{60}$ glass is found to be very stable in normal environmental conditions and even in hot water during several hours². Some of the important mechanical properties of $\text{Ga}_5\text{Sb}_{10}\text{Ge}_{25}\text{Se}_{60}$ glass are tabulated in Table 3.1.

Table 3.1: Mechanical properties of $\text{Ga}_5\text{Sb}_{10}\text{Ge}_{25}\text{Se}_{60}$ glass.

Elastic constant (GPa)	Young's moduls (GPa)	Poisson's constant	Themal expansion coefficient (K ⁻¹)	Density (g/Cm ²)
9.5±0.1	23.9±0.3	0.262±0.005	155±5×10 ⁻⁷	4.69±0.02

To achieve an acceptable usability of chalcogenide glass fibers, some tradeoffs are necessary between the optical properties and the thermo-mechanical properties. Since $\text{Ga}_5\text{Sb}_{10}\text{Ge}_{25}\text{Se}_{60}$ glass has a significantly higher glass transition temperature and better thermal

and mechanical properties it will lead to stronger fibers. Studies on $\text{Ga}_5\text{Sb}_{10}\text{Ge}_{25}\text{Se}_{60}$ glass fiber show that these fibers are much stronger, more flexible and can withstand almost the same excited laser power without much attenuation⁴. $\text{Ga}_5\text{Sb}_{10}\text{Ge}_{25}\text{Se}_{60}$ glass fiber is also a potential candidate for applications such as remote spectroscopy, temperature sensing, laser power delivery and thermal image transfer due to the wide transmission region of these fibers from about 3 up to 13 μm , covering the fundamental absorptions of many chemical and biological species.

3.1.2. Preparation and characterization of $\text{Ga}_5\text{Sb}_{10}\text{Ge}_{25}\text{Se}_{60}$ bulk glass

Appropriate amounts of high purity (99.999%) constituent elements Ge, Sb, Se, Ga were sealed in a quartz ampoule at about 10^{-3} m barr and loaded in a rotary furnace. The ampoule was kept at 1050°C for 24 h with continuous rotation and rocking for homogenizing the mixture. It was then quenched in to ice water. The amorphous nature of the sample was confirmed by X - ray diffraction studies.

A typical normalized signal versus 2θ plot of x-ray diffraction studies is shown in Figure 3.3. The diffractogram shows no sharp peaks (signifying crystallinity). However, the broad humps, which are characteristic of the short-range order in these glasses, are observed.

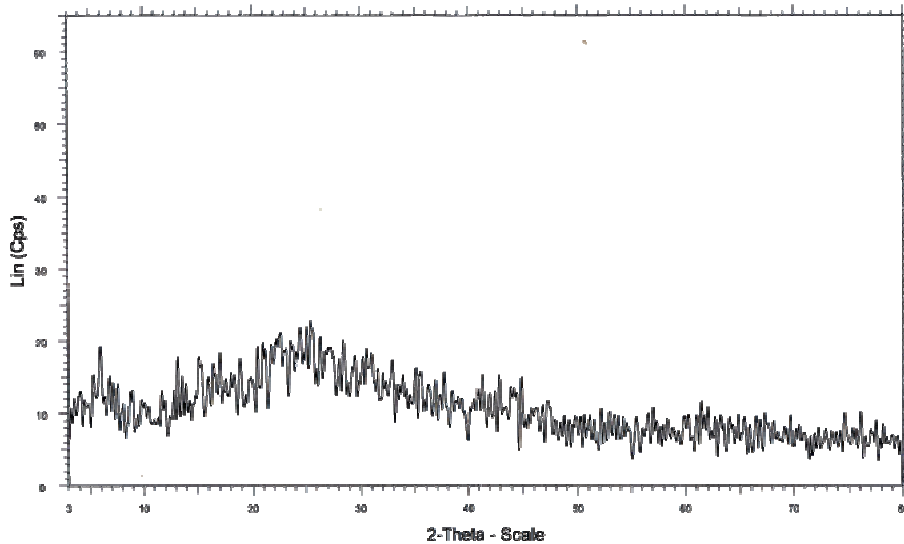


Figure 3.3: Normalized signal versus 2θ plot of the $\text{Ga}_5\text{Sb}_{10}\text{Ge}_{25}\text{Se}_{60}$ glass.

Figure 3.4 show the Differential Scanning Calorimetry (DSC) analysis of this glass, indicating a glass transition temperature T_g as 316°C , which will make this glass usable at temperatures as high as 200°C . The T_g values reported in this thesis correspond to the on-set of the glass transition. This value is estimated as the temperature corresponding to the intercept of the tangent drawn to the baseline and the endothermic baseline shift as shown in Figure 3.4. It can also be seen that there is no exothermic peak associated with crystallization phenomena, indicating that this glass is thermodynamically very stable towards de-vitrification. $\text{Ga}_5\text{Sb}_{10}\text{Ge}_{25}\text{Se}_{60}$ glass has high T_g indicating they would be good candidates for higher temperature fibre sensing applications (above 200°C).

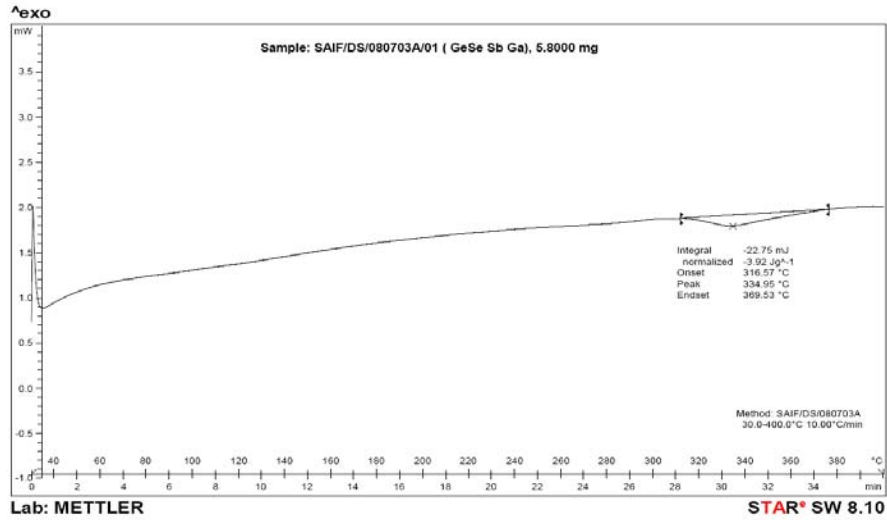


Figure 3.4: DSC curve of the $Ga_5Sb_{10}Ge_{25}Se_{60}$ glass, showing its stability towards the crystallization.

The band gap of the bulk $Ga_5Sb_{10}Ge_{25}Se_{60}$ glass was estimated to be 1.52eV from the absorption spectra as shown in Figure 3.5.

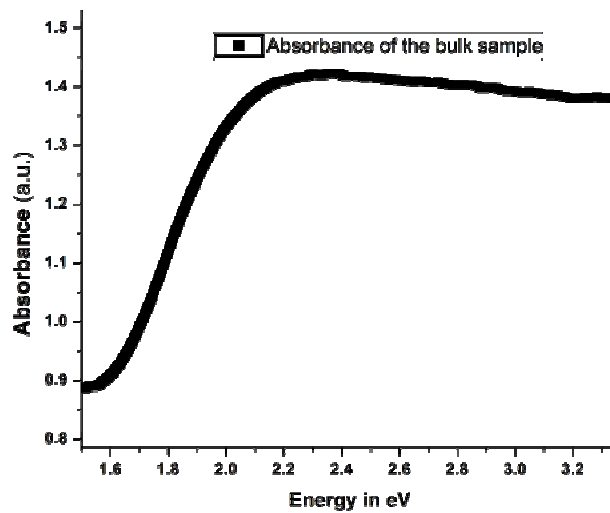


Figure 3.5: Plot of absorption spectra of $Ga_5Sb_{10}Ge_{25}Se_{60}$ glass.

3.1.3. Fabrication and Optical characterisation of $\text{Ga}_5\text{Sb}_{10}\text{Ge}_{25}\text{Se}_{60}$ thin film

$\text{Ga}_5\text{Sb}_{10}\text{Ge}_{25}\text{Se}_{60}$ thin films have been directly deposited on to glass substrate using thermal evaporation technique. The evaporation was done at a pressure of 2×10^{-5} m bar and at a rate of $10 \text{ \AA}/\text{s}$. The thickness of the films was controlled to 325 nm by the shutter with the help of a quartz crystal growth monitor. Figure 3.6 shows the XRD patterns of the $\text{Ga}_5\text{Sb}_{10}\text{Ge}_{25}\text{Se}_{60}$ thin film. The absence of sharp structural peaks in these XRD traces confirmed the amorphous nature of thin film.

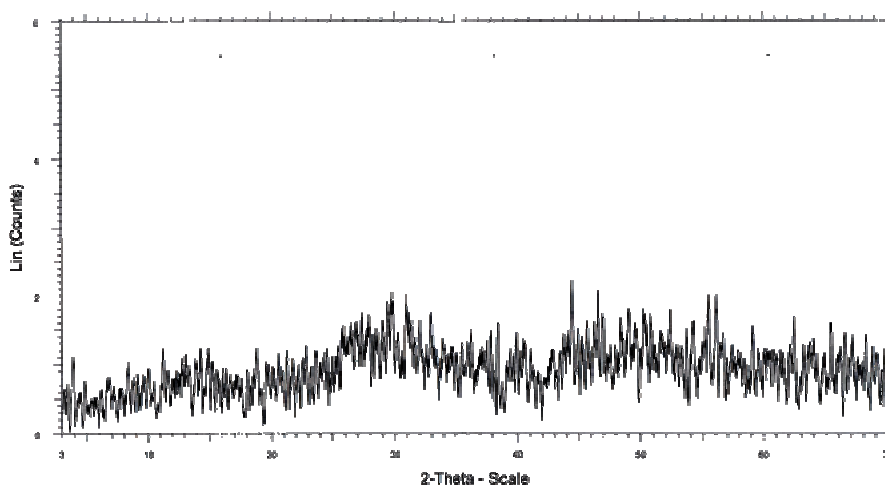


Figure 3.6: XRD pattern for $\text{Ga}_5\text{Sb}_{10}\text{Ge}_{25}\text{Se}_{60}$ thin film.

The transmission spectrum and reflection spectra of the samples fabricated obtained from a spectrometer is as shown in Figure 3.7. The plot shows fringes due to interference at various wavelengths. A continuously oscillating maxima and minima at different wavelengths confirm the optical homogeneity of deposited

thin films. Optical transmission (T) and reflection (R) are very complex functions and strongly depend on the absorption coefficient. Various optical parameters are calculated for the prepared thin film as given in Chapter 2 (section 2.2.4) using a straight forward method proposed by Swanepoel⁵, which is based on the use of extrema's of the interference fringes of the transmittance spectrum.

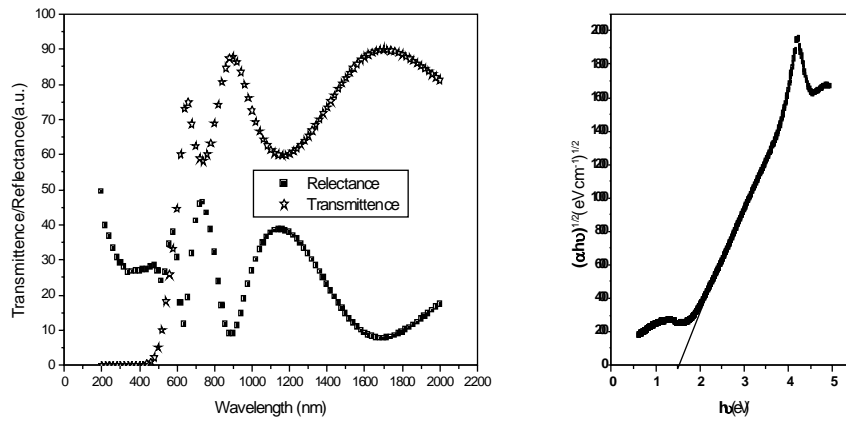


Figure 3.7: a) Reflectance and transmittance spectra of $Ga_5Sb_{10}Ge_{25}Se_{60}$ thin film. b) Plot of $(\alpha hv)^{1/2}$ versus $h\nu$ for the film.

The optical energy gap has been determined from plot 3.7(b) by the intercepts of extrapolations to zero with the photon energy axis $(\alpha hv)^{1/2} \rightarrow 0$ (i.e. Tauc extrapolation). The optical energy gap has been found to 1.72eV. The variation of refractive index (n) with wavelength for the thin film is shown in Figure 3.8(a). The decrease in refractive index with wavelength shows the normal dispersion behavior of the material⁶. The real (ϵ_r) and imaginary (ϵ_i) parts of the dielectric constants for a thin film are calculated with the help of refractive index and extinction coefficient⁶. Real part of dielectric

constant is calculated using the relation $\epsilon_r = n^2 - k^2$ while the imaginary part is calculated using, $\epsilon_i = 2nk$. The complex dielectric constant is fundamental intrinsic material property. The real part is associated with the term that how much it will slow down the speed of light in the material and imaginary part shows how much a dielectric absorb energy from electric field due to dipole motion.

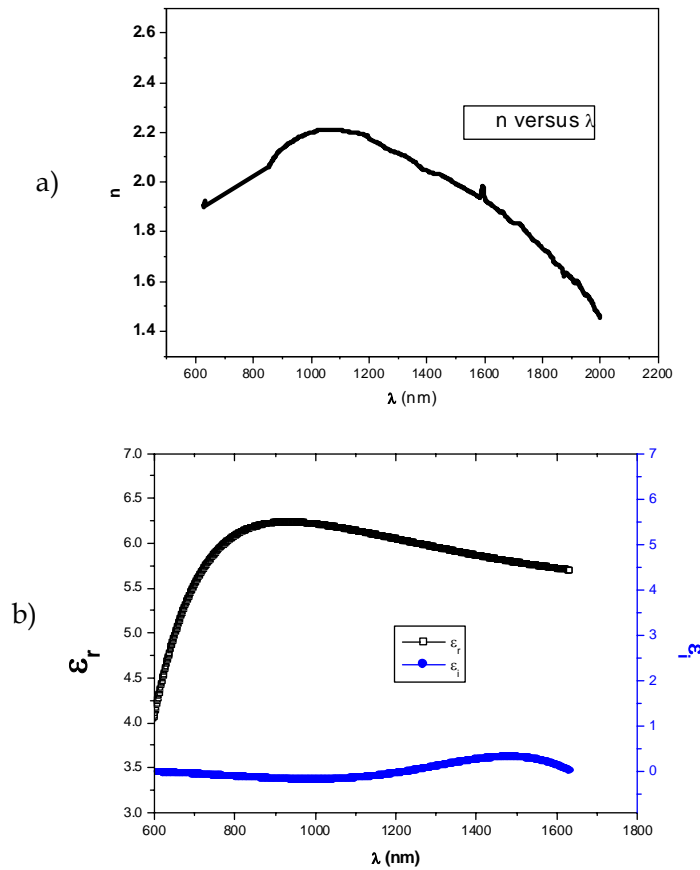


Figure 3.8: a) Plot of refractive index (n) versus wavelength (λ) and b) ϵ_r and ϵ_i with λ for $\text{Ga}_5\text{Sb}_{10}\text{Ge}_{25}\text{Se}_{60}$ thin films.

The variation of both ϵ_r and ϵ_i with λ for thin film under consideration is shown in Figure.3.8 (b). The variation of both ϵ_r and ϵ_i with λ follows the same trend as that of refractive index and extinction coefficient. The optical conductivity is determined using the relation $\sigma = \alpha n c/4\pi$ where 'c' is the velocity of light. Optical response is most conveniently studied in terms of optical conductivity and it has the dimensions of frequency, which are valid only in Gaussian system of units. The optical conductivity directly depends on the absorption coefficient and refractive index and is found to increase sharply for higher energy values due to large absorption coefficient as well as refractive index.

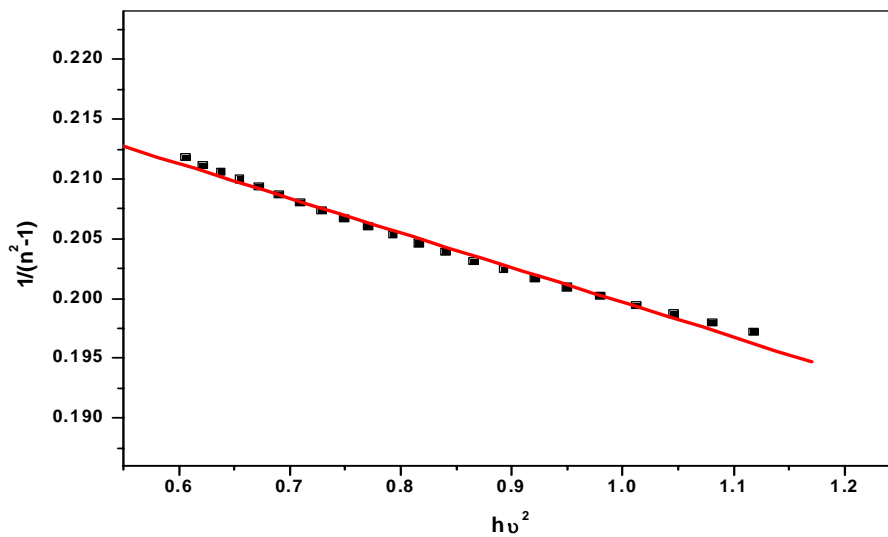


Figure 3.9: Plot of refractive index factor $(n^2 - 1)^{-1}$ versus $(h\nu)^2$

The refractive index dispersion, $n(h\nu)$ of film was analysed using the single effective-oscillator model⁷. Plotting $(n^2 - 1)^{-1}$ versus $(h\nu)^2$ as shown in Figure 3.9 yields a straight line. The fit of the linear parts of the plot is used for calculating the values of E_0 and E_d from the slope $(E_0E_d)^{-1}$ and the intercept (E_0/E_d) , respectively.

Table 3.2: The bandgap (E_g),width of localized states (E_e),optical conductivity (σ at 1000nm),extinction coefficient (k at 1000nm),dispersion energy(E_d), effective oscillator energy (E_0), static refractive index (n_0), third order non linear susceptibility ($\chi^{(3)}$) and non linear refractive index (n_2) of Ga₅Sb₁₀Ge₂₅Se₆₀ thin films.

E_g (eV)	E_e (eV)	σ *10 ¹¹ (s ⁻¹)	k	E_d (eV)	E_0 (eV)	n_0	$\chi^{(3)}$ *10 ⁻¹² (esu)	n_2 *10 ⁻¹¹ (esu)
1.5	0.51	2.94	0.44	12.24	2.59	2.39	3.37	5.31

Dispersion energy (E_d) measure the average strength of interband optical transitions and is associated with the changes in the structural order of the material and the effective oscillator energy (E_0) is directly correlated with optical energy gap by an empirical formula. Generalized Miller's rule and linear refractive index as discussed in section 2.2.4 are used to find the nonlinear susceptibility and non linear refractive index of thin film⁸.

3.2. Section 2. Photoinduced darkening in thermally evaporated Ga₅Sb₁₀Ge₂₅Se₆₀ films

3.2.1. Introduction

Chalcogenide glasses when exposed to above- and near-bandgap light, absorption coefficient over a broad range of frequencies increases⁹. The amount of increase depends on the

wavelength of the inducing light, the duration of exposure and the intensity of the light. The photodarkening process involves a shift of the optical absorption edge to lower energy and an increase in the band tail absorption. The absorption change is permanent and can only be removed by annealing the glass at a temperature near its glass transition temperature. Because the optical changes can be removed this is known as reversible photodarkening. Reversible photodarkening has been observed in bulk glasses and well as in thin films⁹. The photodarkening can be induced with above-bandgap or below-bandgap light, so long as the light has sufficient energy to excite electrons from the LP band. The index of refraction of the glass also changes with photodarkening. The associated index change may prove useful for the fabrication of optical structures in bulk glasses and in thin films.

A.S Tverjanovicha et al. have reported⁹ that in Ga-Ge-S system, exposure with an energy higher than band gap leads to photoinduced bleaching. The replacement of S by Se brings about photoinduced darkening (PD). In $\text{Ge}_{20}\text{Se}_{72.5}\text{Bi}_{7.5}$ films, exposure of above band gap light leads to a decrease in the values of the optical band gap¹⁰. This was explained as arising due to an increase in disorder due to the formation of an impurity band adjacent to a band and formation of tails of states extending the band into the mobility gap. The structural bond change and distribution of bonds is well established in Se based chalcogenide glasses and the possibility of both PD and photoinduced bleaching (PB, blue shift in band gap) in Ge-Se films prepared by thermal evaporation is also

reported^{10,11}. It was recognized that the excitation of electrons from spatially localized states in the band tail induces the formation of several types of defects in the glass structure¹². Structural defects such as transient bonds, ESR active sites, and valence alternation pairs also called self-trapped excitons are thought to play a role in the photoinduced modifications¹². Thanak and Ohtsuka¹³ have proposed a phenomenological model of photodarkening in which the increase in absorption at a fixed wavelength is proportional to the intensity and a factor ensuring saturation at some maximum absorption. The kinetic model was further generalized by Liu and Taylor¹⁴ who assumed that the increase of the absorption is proportional to a general, but unspecified, function of the absorption itself and to a power of the intensity.

Possible structural models for photodarkening phenomena can be as shown in Figure 3.10. a and b show defect model and c represent distortion model.

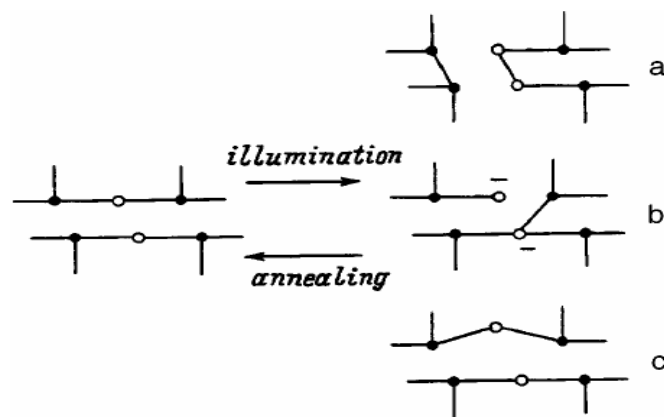


Figure 3.10: Structural models for photodarkening phenomena. a) and b) show defect model and c) represent distortion model.

3.2.2. Experimental

The photodarkening experiment was arranged as shown in Figure.3.11. He-Ne laser (633 nm) of 4 mW, 10 mW and 20 mW and semiconductor laser (810 nm, 20 mW) were used to study the photosensitivity of the films. The laser power was made stable during exposure to avoid significant uncertainty in the total supplied energy. The laser beam was expanded from an initial beam waist of 1.0 mm (FWHM) using a plano-concave lens and collimated with a second plano-convex lens. At the sample stage an aperture was used to admit only the central maximum of the laser beam, so as to assure irradiating the sample with a fairly uniform intensity. The transmittance and reflectance spectra of films at normal incident condition in the spectral range 250–2500 nm were recorded by a double beam UV-VIS-NIR spectrophotometer (Jasco V 570).

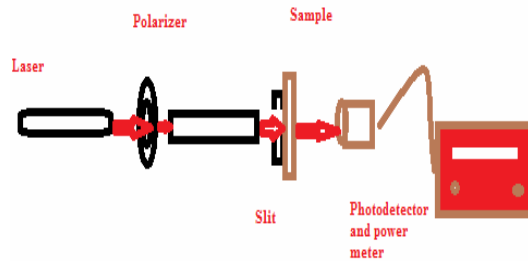


Figure 3.11: Experimental set up for photodarkening.

The thickness of thin films before and after illumination were analyzed using surface profiler [DEKTAK 6M Stylus Profiler]. The thickness of the films was found to be around 325nm before and after irradiation. All the measurements were executed at room temperature and the samples were kept in the dark between experiments.

3.2.3. Results and Discussion

In order to study the kinetics involved in the photoinduced process, time and intensity dependence of bandgap and refractive index of the sample on laser irradiation were made. The band gap and the optical constants like absorption coefficient (α) and refractive index (n) were found before and after illumination with 633 nm laser. The transmission spectra of the thin film with different exposure time with radiation intensity, 632 nm, 4 mW is given in Figure 3.12.

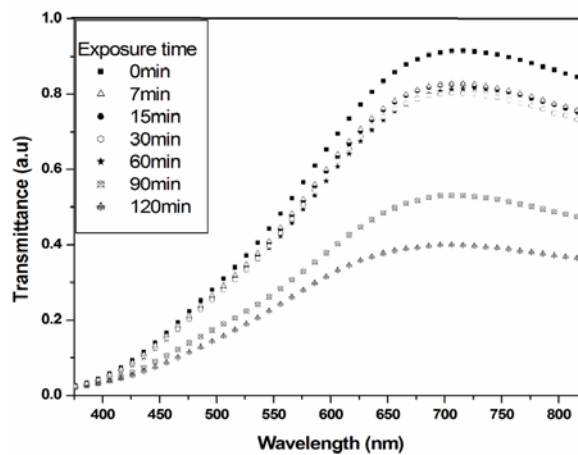


Figure 3.12: Plot of transmittance versus wavelength of the initial and the irradiated $\text{Ga}_5\text{Sb}_{10}\text{Ge}_{25}\text{Se}_{60}$ thin films at different times ranging from 7 min to 120 min using 4 mW He-Ne laser.

The transmission spectra of the films prior to and after laser irradiations shows that laser illumination shifts the optical transmission edge to higher wavelength. Since the transmission through the thin film decreases by exposure it is clear that there is no possibility of formation of cracks and pinholes in the films^{15,16}. AFM analysis was also done to

check the surface of illuminated films. The analysis confirms the absence of any holes or cracks after illumination. AFM image of the illuminated film (4mW, 30min) is shown in Figure 3.13. The image confirms the absence of cracks or holes due to irradiation.

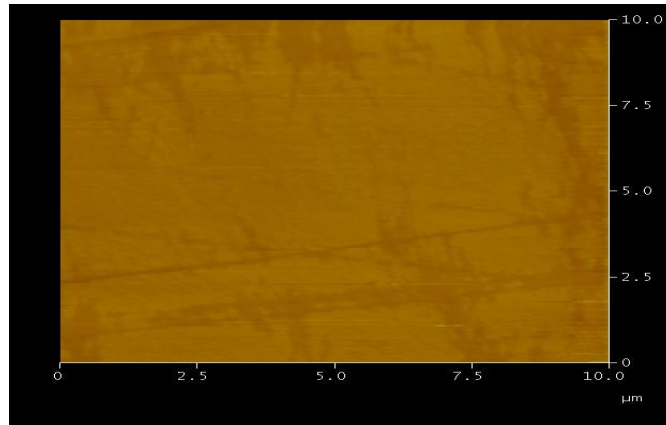


Figure 3.13: AFM image of 4mW (He Ne, 632nm) illuminated film showing the absence of cracks or holes due to irradiation.

The change in transmittance as shown in Figure 3.12, indicates a change in the structure of the samples during illumination. This change in structure leads to a change in the electronic properties of the material. The optical band edge may shift or a new absorption process may occur by the formation of new defects. Thus, the change in physical structure leads to a change in optical properties¹⁶. To further characterize the photoinduced change in structure, the optical properties must be calculated from the transmittance and reflectance.

The absorption coefficient (α) of these materials strongly depends on optical transmission (T), reflection (R) and thickness of film (d) which is evaluated using the relation¹⁶,

$$\alpha = [\ln (1-R)^2/T]/d. \quad (1)$$

The Ga₅Sb₁₀Ge₂₅Se₆₀ films thickness (d) remained constant before and after illumination showing the absence of photo induced contraction or photo expansion in films. Another important parameter for characterizing amorphous semiconductors is the width of the band tail (E_e), which measures the degree of disorder. E_e can be found from the plot of $\ln(\alpha)$ versus $h\nu$. The plot of band gap (E_g) vs Time (min) for Ga₅Sb₁₀Ge₂₅Se₆₀ films for different exposure time at 4mW He Ne laser is given in Figure 3.14. It is found from the figure that the band gap decreases as the illuminating time is increased i.e., there is a red shift of the absorption edge on illumination, which indicates the narrowing of the optical gap of the chalcogenide film. It is believed to be due to broadening of the valence band, the top of which is formed mainly by states of lone-pair electrons of the chalcogen atom. Optical gap is diminishing due to a broadening of the conduction and valence band, respectively. The origin of such broadening of both the conduction and valence band is due to an increase in the disorder. Plot of refractive index (n) versus Time (min) is given in Figure 3.15. The time evolution of E_g and n reveal that the absorption of photon of energy greater than band gap results in a decrease in bandgap and an increase in refractive index with exposure. The shift in the optical absorption edge to the lower energy

and an increase in band tail absorption can be due to the photoinduced darkening in the films.

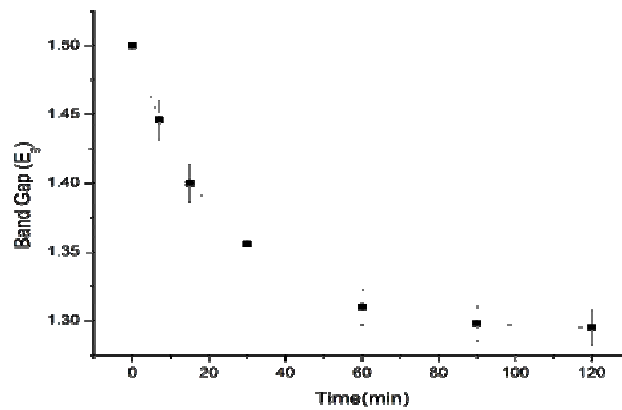


Figure 3.14: Plot of band gap (E_g) against Time (min) for 4 mW laser exposure shows that as the exposure time increases there is a red shift in the band gap and after a particular time it is showing a saturation effect.

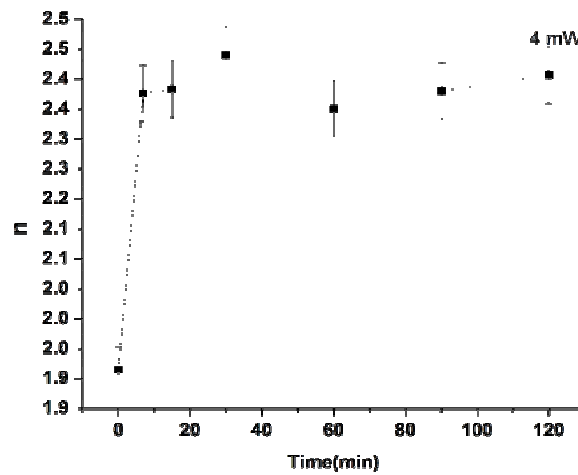


Figure 3.15: Spectral dependence of refractive index (n) with Time showing the increase in refractive index with exposure time.

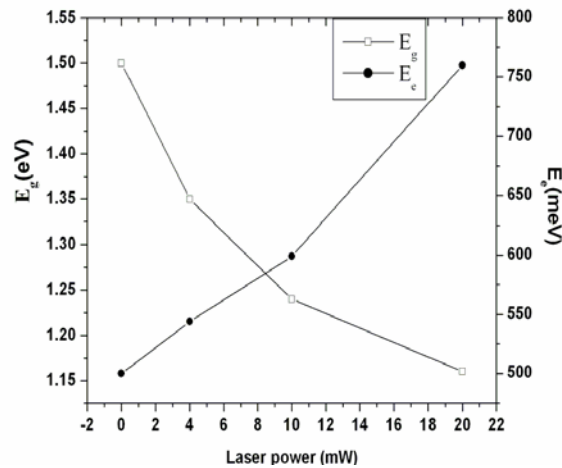


Figure.3.16: Plot of in the band gap (E_g) and width of localized states (E_e) versus laser power. The increase in the degree of disorder (E_e) can be due to the increase in defect states with increases in the laser power.

Although darkening in films has attracted attention for its possible applications in optical memory elements, the mechanism causing the change in optical gap remains unclear. One of the possible mechanisms can be due to the dissociation of the bonds or bonding rearrangement leading to large absorption of light i.e., illumination above the band gap alters the bond statistics resulting in the randomness of the bond distribution and the creation of defect states which leads to an increase in disorder^{17,18}.

He-Ne laser power dependent change in transmission spectra is also analyzed. The laser power dependent change in band gap (E_g) and width of localized states (E_e) are given in Figure 3.16. It shows the photodarkening mechanism as due to the increase in disorder. Band gap and refractive index variation shows saturation effect with

exposure. For longer exposure time the rate of dissociation of bond is slower which may be due the saturation of defect states. The saturation can be due to the finite number of photo darkening sites which cannot be greater than the number of atoms in the glass. The saturated behavior of photo-darkened state in amorphous films is found to be sensitive to the photon flux of the excitation light by Stabl M and Tichy L ¹⁹.

Neither the transmittance nor reflectance is directly related to the structure; however, the dielectric response terms ε_r and ε_i are because they are a linear sum of all of the contributions from the optically active structural elements.

The dispersion parameters are significant factors in optical communication and in designing devices. The spectral dependence of the refractive index, in the visible and near infrared regions, has been analyzed. The dispersion energy (E_d) effective oscillator energy (E_0), static refractive index (n_0), susceptibility ($\chi^{(3)}$) and non linear refractive index (n_2) are tabulated in Table 3.3. Both E_d and n_0 increases while E_0 decreases with increasing exposure time. The increase in the dispersion energy value is usually associated with decrease in the band gap. The nonlinear refractive index (n_2) for $\text{Ge}_{35}\text{Sb}_5\text{Se}_{60}$ system is reported to be 8.47×10^{-11} esu²⁰ and it is observed that by the replacement of Ge by Ga or S by Se in the Ge/Ga-Sb-S/Se system the nonlinear refractive index increases²¹. The studies on the $\text{Ge}_{20}\text{Sb}_{10}\text{S}_{65}\text{Ga}_5$ systems by J Troles et al²² reports n_2 as 3.2×10^{-18} m²/W (1.68×10^{-11} esu). Our studies deal with $\text{Ga}_5\text{Sb}_{10}\text{Ge}_{25}\text{Se}_{60}$ glass system

which shows higher n_2 as 5.31×10^{-11} esu. The variation in n_2 with respect to the composition is pointed out only to stress the fact that by appropriate change in glass composition we will get a glass system with tunable optical nonlinearity. The dependence of n_2 on the total number of electronic lone pairs and to the position of the absorption band gap in Ge/Ga-Sb-S/Se glass system is also reported by L. Petit et al.²¹. Thus depending on the bandgap, the nonlinear refractive index of the investigated films also changes. The high refractive index values of these glasses are advantageous for strong optical confinement and for nonlinear interactions. This property can be utilized for waveguide writing in chalcogenide glasses.

Table 3.3: The dispersion energy (E_d), effective oscillator energy (E_0), static refractive index (n_0), susceptibility ($\chi^{(3)}$) and non linear refractive index (n_2) for films before and after irradiation.

Exposure time (min)	E_d (eV)	E_0 (eV)	n_0	$\chi^{(3)}$ (esu)	n_2 (esu)
0	12.24	2.59	2.39	3.37×10^{-12}	5.31×10^{-11}
7	23.69	1.54	4.05	3.87×10^{-10}	3.60×10^{-11}
15	21.59	1.78	3.62	1.46×10^{-10}	1.53×10^{-9}
30	24.15	1.59	4.04	3.73×10^{-10}	3.48×10^{-9}
60	25.34	1.86	3.82	2.31×10^{-10}	2.28×10^{-9}
90	23.27	1.88	3.66	1.61×10^{-10}	1.66×10^{-9}
120	26.48	1.98	3.76	2.19×10^{-10}	2.17×10^{-9}

The magnitude of photo-darkening induced by 633nm and 810nm wavelength of the excitation light is found to be different for same laser power (20mW) and exposure period. The change in bandgap ($dE_g = E_g$ (before illumination) - E_g (after illumination)) for

633nm illumination for 30 min is 0.33 eV (1.5-1.17) where as the change in bandgap after 810 nm illumination is 0.16 eV. The difference in the magnitude of photodarkening can be due to the difference in effective penetration depth¹⁹. The absorption coefficient for $\lambda = 633$ nm is close to $\alpha = 39416$ cm⁻¹ which corresponds to the effective penetration depth (dp) of photons around 253 nm while α for $\lambda = 810$ nm is close to 15818 cm⁻¹ which implies that in this case $dp \approx 633$ nm. The effective penetration depth of the photons decides the magnitude of photodarkening. The change in bandgap, width of the localised states and refractive index for the films on excitation with different lasers is tabulated in Table 3.4. It is clear that the conditions of illumination play a crucial role in the magnitude of photodarkening in the Ga₅Sb₁₀Ge₂₅Se₆₀ thin films.

Table 3.4: Measured values of Bandgap (E_g), width of the localised states (E_e) and refractive index (n) at 30 minute exposure under different laser power and wavelength.

Conditions	E_g (eV)	E_e (meV)	n
Without irradiation	1.50	480	1.92
He-Ne (4mW)	1.35	525	2.50
He-Ne (10mW)	1.24	578	2.70
He-Ne (20mW)	1.17	762	2.72
Semiconductor (20mW)	1.34	509	2.31

3.3. Section 3. Studies on Nano colloid $\text{Ga}_5\text{Sb}_{10}\text{Ge}_{25}\text{Se}_{60}$ chalcogenide glass

3.3.1. Introduction

Colloidal solutions have found applications due to their fast response and large nonlinearities. Among a variety of preparation methods for nano particle solutions, the most popular are the chemical method²³ and the preparation by laser ablation method²⁴. The local field enhancement of nano particles in colloidal suspensions leads us to expect interesting, new features of semiconductor nano particles²⁵. Interest in the synthesis, characterization and application of colloidal semiconductor ‘quantum dot’ materials has grown markedly²⁶ due to the strong size-related dependences of their optical and electronic properties. However, the dependence of the optical nonlinearities on the size of the semiconductor nanoparticles has yet to be determined.

As early as 1826, Berzelius and Bineau²⁷ recognized that As_2S_3 was soluble in liquid ammonia. They observed that this system resulted in a gelatinous solution. For this study, then, it was assumed that organic base amines would also serve as chalcogenide solvents and possibly lead to gelatinous systems. The solutions were synthesized by dissolution of bulk As_2S_3 in a variety of anhydrous amine solvents. The solvents included ethylenediamine, n-butylamine, n-propylamine, diethylamine, and triethylamine. They suggested that the dissolution mechanism support the model of nitrogen behaving as a Lewis base, donating its lone pair of electrons to the empty d-orbitals of arsenic. But

dissolution of the As_2S_3 in ethylenediamine did not result in any amine salts, sulphur hydride, or sulfur nitride species due to the bidentate nature of ethylenediamine as it chelates two arsenic centers.

Chern and Lauks first reported that amorphous chalcogenide films can be deposited from their solutions and retain many of the solute properties²⁸⁻³⁰. For useful optical device manufacturing, it is important to retain the bulk glass stoichiometry in deposited thin films as glass properties critically depend on material compositions. Hence before studying the thin film properties it is important to characterize the nano colloidal solutions used for the fabrication of thin films. Even though attempts to understand the mechanism of dissolution of chalcogenides in amines and the existence of the presence of chalcogenide clusters with dimensions of several nanometres was reported³¹ earlier, factors such as the use of suitable solvent for bulk glass dissolution solubility, solution viscosity etc have only been studied recently by Shanshan Song et al³². Considering both the ease of dissolving and composition consistency, amine based solvents has been found to be the most appropriate for chalcogenide glasses.

3.3.2. Synthesis of $Ga_5Sb_{10}Ge_{25}Se_{60}$ nano colloids

Chalcogenide glass solutions of five different concentrations $C_0=0.72$ mg/ml, $C_1=0.67$ mg/ml, $C_2=0.540$ mg/ml, $C_3=0.335$ mg/ml and $C_4=0.12$ mg/ml of $Ga_5Sb_{10}Ge_{25}Se_{60}$ were obtained by the dissolution of bulk glass in n- butylamine solvent (Sigma-Aldrich, 99.9%). The dissolution was carried out inside a sealed glass container to prevent

solvent evaporation. A magnetic stirrer was used to expedite the dissolution process. The solutions were characterized by optical absorption measurements recorded by using a spectrophotometer (JascoV-570 UV/VIS/IR). Scanning Electron Microscope (SEM) (JEOL Model JSM - 6390LV) photographs of the two solutions were taken to understand the distribution of the nanoclusters.

3.3.3. Structural Characterization and absorption spectroscopy

a) 1H NMR

The 1H NMR (Bruker Avance III, 400MHz) spectra was taken to check whether amine salts are present in the colloid solutions. 1H NMR was taken for the colloid solution by dissolving the nanocolloids in $CdCl_3$. The chemical shift (around 7.5) as shown in Figure 3.17 shows the presents of salt formation in the solution.

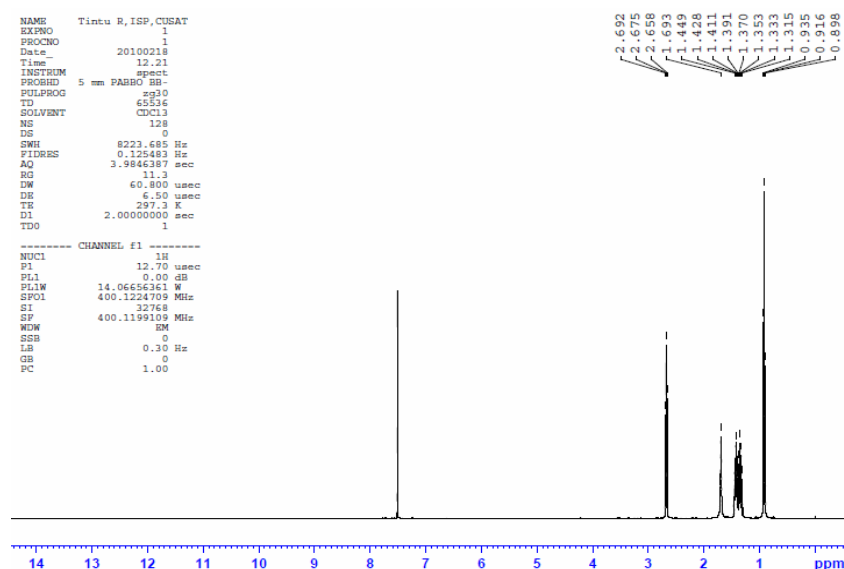


Figure 3.17: 1H NMR spectrum of C_1

b) Scanning electron microscopy

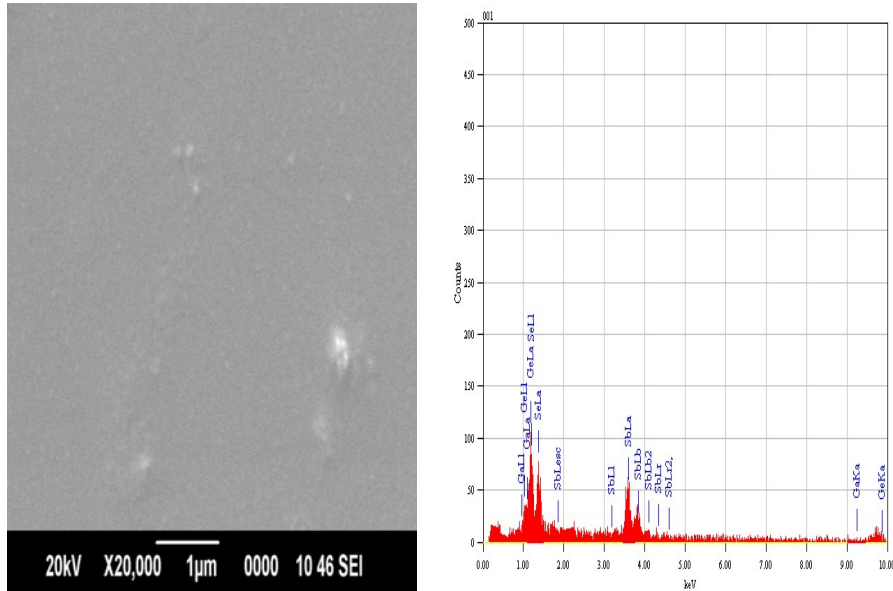


Figure 3.18: SEM with EDAX image showing the nano ranged cluster formation in the chalcogenide glass solution ($C_1=0.67\text{mg/ml}$).

The cluster formation in the solution was confirmed to be of nano range with the SEM analysis (JEOL Model JSM - 6390LV). The SEM photograph of the prepared sample is shown in Figure 3.18. The EDAX confirms the presence of all elements in the cluster. The sample material for SEM analysis was prepared by spin coating the solution on a glass slide. The cluster size from the SEM analysis on spin coated thin films of the solution was found to be around 70 nm and 40 nm for C_1 and C_3 , respectively. The actual cluster size of the solute in solution will be much less than the grain size of the thin films used for SEM analysis as reported by Kohoutek et al³¹. The increase in the grain size of the thin films compared to that in

solution can be due to the agglomeration of chalcogenide clusters during solvent evaporation from the film structure at the time of spin coating of film.

c) Absorption spectroscopy

The colloids were characterized by optical absorption measurements recorded using a spectrophotometer (JascoV-570 UV/VIS/IR). The absorption spectra of semiconductor solutions are presented in Figure 3.19. The absorption edge of the chalcogenide nano colloid solutions is located in the visible range, whereas for bulk semiconductors it is located in the near IR range. It is found that as the concentration of the chalcogenide decreases there is a blue shift in band edge and a change in the slope of absorption spectra³³. The slope of the absorption edge characterizes the width of the localized states which in turn indicates the ordering of the structure.

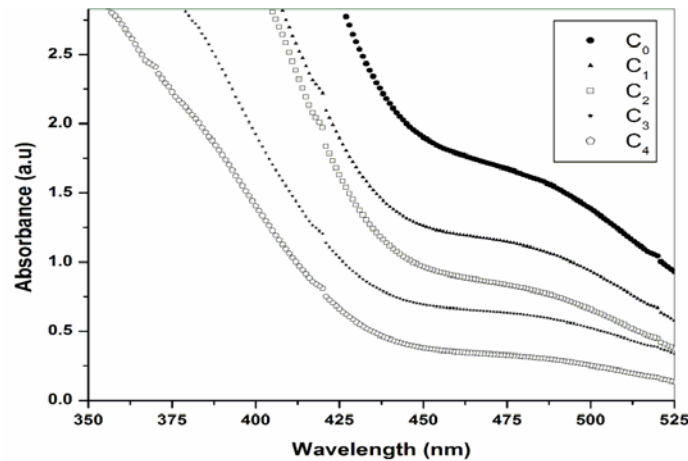


Figure 3.19: Absorption spectra of nano colloids $\text{Ga}_5\text{Sb}_{10}\text{Ge}_{25}\text{Se}_{60}$ chalcogenide glass.

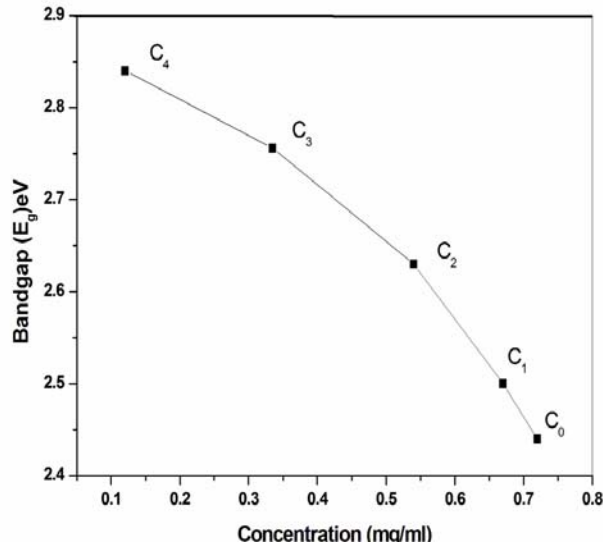


Figure 3.20: The dependence of concentration on the band gap. As the concentration increases the bandgap (E_g) shifts to lower energy.

To evaluate the optical bandgap of the samples, linear absorption measurements were performed. Since glasses are amorphous solids, they lack a sharp absorption edge and the optical bandgap is taken to be the point at which the absorption changes from a quadratic dependence on energy to an exponential dependence (Urbach tail region)³⁴. An exponential fit of data in the Urbach tail region yields the bandgap. The energy gaps (E_g) of the solutions were also estimated using the derivatives of the transmission curves. Eventually, the minimum of the first derivative corresponds to the inflection point of the transmission curve which is usually considered as an accurate estimation of E_g . It is found that with increasing concentration of $\text{Ga}_5\text{Sb}_{10}\text{Ge}_{25}\text{Se}_{60}$ glass the cluster size also increases. The dependence of concentration on the band gap is

given in Figure 3.20. The optical band gap of bulk $Ga_5Sb_{10}Ge_{25}Se_{60}$ glass is 1.56 eV and that of colloidal solution varies from 2.43 eV (C_0) to 2.84 eV (C_4). Thus the optical band gap (E_g) of the material is tunable between 1.56 eV to 2.84 eV.

3.3.4. Photoluminescence from nano colloid $Ga_5Sb_{10}Ge_{25}Se_{60}$ ChG

a) Excitation wavelength dependent Photoluminescence studies

The Photoluminescence (PL) measurements were recorded by using a Cary Eclipse fluorescence spectrophotometer (VARIAN). Figure 3.21 presents the photoluminescence spectra of nano colloidal solutions of $Ga_5Sb_{10}Ge_{25}Se_{60}$ at an excitation of 400 nm. The photoluminescence spectra show a cluster size dependent change in peak wavelength and intensity. It is found that for excitation at 400 nm the photoluminescence intensity increases with decrease in cluster size (due to decrease in concentration). Lesser the concentration smaller will be the broadening of the band tails. Due to these bandgap states in chalcogenide glasses the optical transitions such as photoluminescence (PL) and the optical absorption process are complicated³⁵. The excitation wavelength dependent change in photoluminescence in C_1 is given in Figure 3.22.

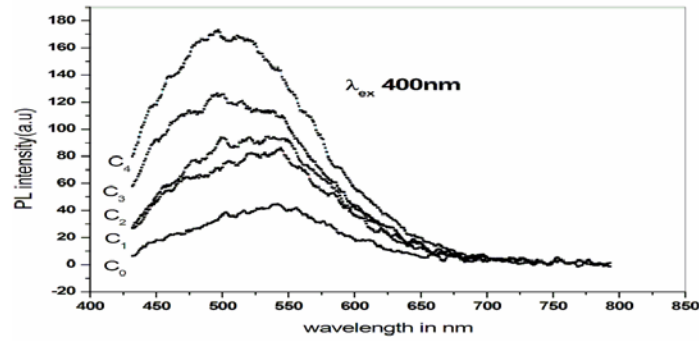


Figure 3.21: PL spectra of nano colloid $\text{Ga}_5\text{Sb}_{10}\text{Ge}_{25}\text{Se}_{60}$ at an excitation of 400nm.

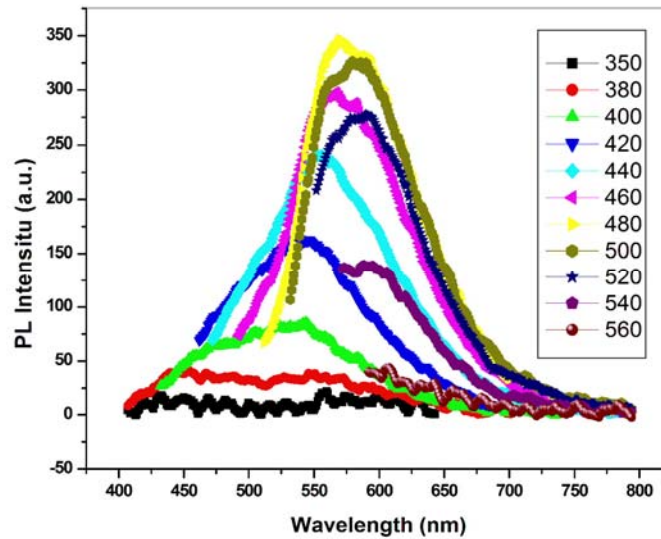


Figure 3.22: Excitation wavelength dependent PL shift for nano colloid $\text{Ga}_5\text{Sb}_{10}\text{Ge}_{25}\text{Se}_{60}$ having a concentration of 0.67mg/ml (C_1).

The spectra show a remarkable dependence on the cluster size and the excitation energy of the nano colloid ChG solution investigated. A strong electron phonon coupling distorts the lattice near the trapped hole and this interaction is responsible for the broadness of the luminescence band³⁵. The excitation energy dependence of

photoluminescence intensity in Ge-S glass was reported by M. Seki et al.³⁶. Studies by Street et al.³⁵ shows that the broad luminescent spectra is common in chalcogenide glasses and they proposed the model of negative-U defects, which can explain many PL-related properties in chalcogenide. These charged defects, which have energy levels in the bandgap with a spectral bandwidth ΔE , are responsible for the PL in chalcogenide glasses. It is to be noted that (Figure 3.22), as the excitation wavelength (λ_{ex}) increases the PL peak intensity increases upon to an optimum wavelength, there after the intensity again decreases. In other words spectra 3.22 help us to gain information regarding the spectral response of the photoluminescence centre. When the excitation is with optimum λ_{ex} only then the electronic transition probability from the charged centres to the conduction band is maximum which leads to maximum PL intensity³⁶. In fact the significance of this band is seen in absorption spectra (Figure 3.19) in the region 400nm-540nm.

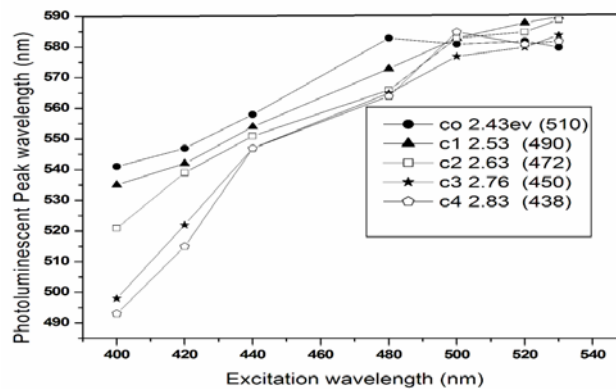


Figure 3.23: PL peak wavelength versus excitation wavelength plots of nano colloids $\text{Ga}_5\text{Sb}_{10}\text{Ge}_{25}\text{Se}_{60}$ chalcogenide glass solution.

PL peak wavelength versus excitation wavelength plots of nano colloids $\text{Ga}_5\text{Sb}_{10}\text{Ge}_{25}\text{Se}_{60}$ chalcogenide glass solutions with different cluster size is given in Figure 3.23. Another important result to be noted is that before the optimum excitation concentrated $\text{Ga}_5\text{Sb}_{10}\text{Ge}_{25}\text{Se}_{60}$ nano colloid solution ie, C_0 is having higher PL intensity whereas after the optimum excitation the PL intensity increases with the decrease in concentration. It is found that at 532nm the higher concentration is having more photoluminescence intensity compared to lower concentrations as shown in Figure 3.24. Here as the concentration increases the non radiative relaxation of the excited state to the defect centres is seen to overcome radiative relaxation above an optimum concentration. The non radiative relaxation originating by the collision process enhances with the concentration therefore when we monitor the PL intensity as the function of concentration PL quenching takes place. In bulk samples the decrease in such quantum efficiency at higher excitation energy has been explained due to strong non radiative surface recombination³⁷.

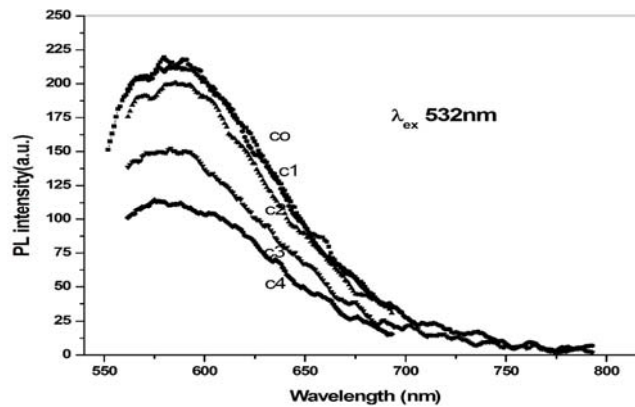


Figure 3.24: PL spectra of nano colloid $\text{Ga}_5\text{Sb}_{10}\text{Ge}_{25}\text{Se}_{60}$ at an excitation of 532nm.

The emission from the clusters were confirmed from the confocal microscopy (Leica TCS SP5 LASER scanning confocal microscope) as shown in Figure 3.25. The spectrum of confocal microscopy shown in the figure for C_0 confirms the emission from the clusters of nanocolloid chalcogenide glass solutions.

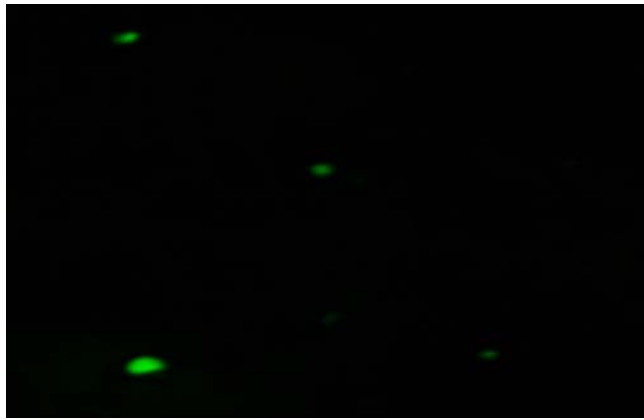


Figure 3.25: Confocal microscope image showing the emission from the nano colloid chalcogenide glass clusters at an excitation with 484 nm.

Thus through size tunability and excitation wavelength, samples can emit narrow colour spectra that are spectrally distinct.

b) Laser induced PL in nano colloid $Ga_5Sb_{10}Ge_{25}Se_{60}$ ChG

Laser induced PL studies were carried out in the nano colloid solutions using a frequency doubled Nd: YAG laser. The samples were transversely pumped using 7 ns pulses from a frequency doubled Nd:YAG laser (532 nm, 10 Hz). The emission from the sample was collected by a fibre and directed to a 0.5 m spectrograph

(SpectraPro-500i) coupled with a cooled CCD array. The experimental set up is given in Figure.3.26.

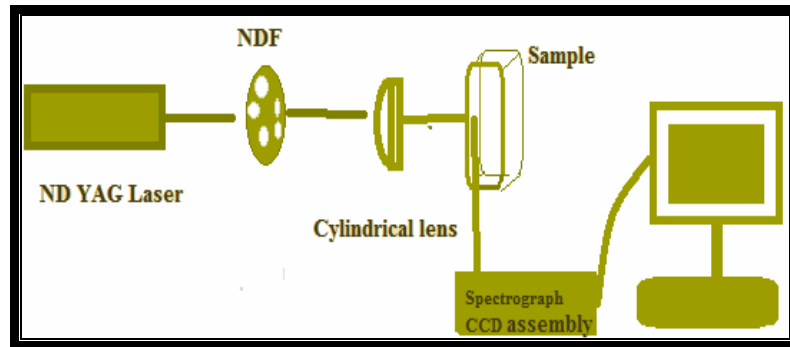


Figure 3.26: The experimental set up for Laser induced PL studies.

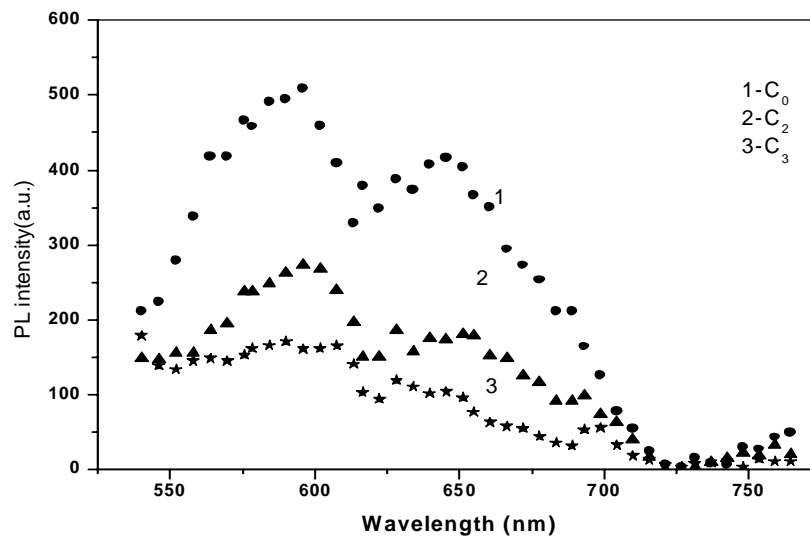


Figure 3.27: Emission from $\text{Ga}_5\text{Sb}_{10}\text{Ge}_{25}\text{Se}_{60}$ nano colloids at pump energy of $10\mu\text{J}$ from an Nd:YAG laser.

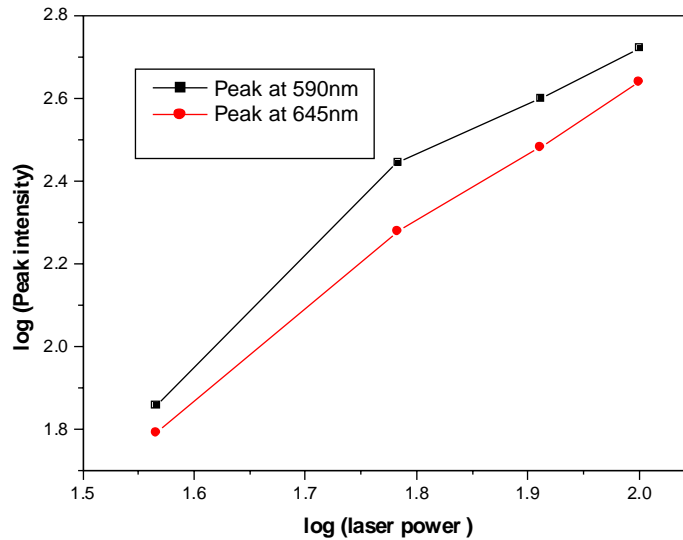


Figure 3.28: Logarithmic plots of PL intensity versus excitation laser power.

PL intensity with concentration and laser power were studied using a Nd: YAG laser beam and the PL spectra obtained for three concentrations is presented in Figure 3.27. It is found that at 532nm the higher concentration (C_0) is having more photoluminescence intensity compared to lower concentration. To verify the origin of the observed luminescence, the PL studies were carried out against the excitation power as shown in Figure 3.28. A fit to the logarithm of the data reveals a slope of 1.97 for peak at 590 nm and 1.94 for peak at 645nm, indicative of a dominant two photon process excitation mechanism for the measured PL^{38,39}.

3.3.5. Thermal diffusivity of $\text{Ga}_5\text{Sb}_{10}\text{Ge}_{25}\text{Se}_{60}$ nano colloids

In order to study the thermal transport properties of poor conductors, thermal diffusivity studies are often preferred due to the

insensitivity to radiative loss. Dual beam mode-matched thermal lens method has been employed to measure the heat diffusivity in nano colloids at 532 nm excitation. The experimental set up used for the study is given in section 2.2.5. The time evolution of TL signal for $\text{Ga}_5\text{Sb}_{10}\text{Ge}_{25}\text{Se}_{60}$ nano colloid at room temperature is shown in Figure 3.29. The solid curve represents the theoretical fit and the dark circles represent the experimental data. Thermal diffusivity, which is directly related to thermal conductivity, depends on the phonon mean free path which in turn depends on the network structure. The absorption coefficient, being related to the phonon mean free path, on the other hand are more sensitive to the change in the network topology^{40,41}.

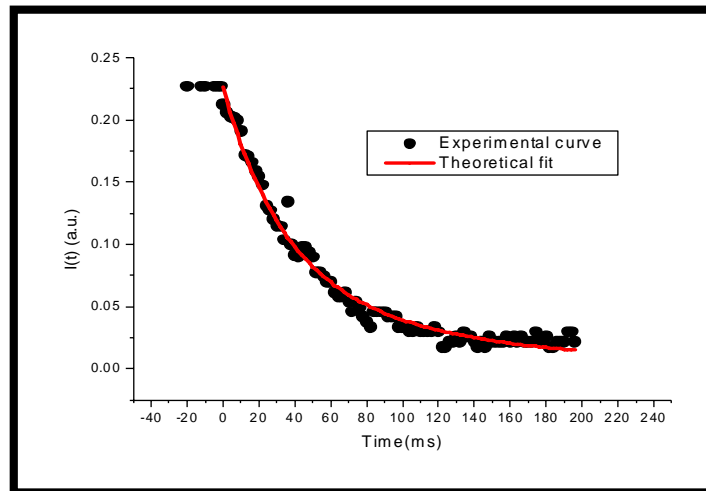


Figure 3.29: Decay curve for $\text{Ga}_5\text{Sb}_{10}\text{Ge}_{25}\text{Se}_{60}$ nano colloid

Table 3.5: Measured values of thermal diffusivity for Ga₅Sb₁₀Ge₂₅Se₆₀ nano colloids with different cluster size.

Samples	Thermal diffusivity (cm ² /s)
C ₀	1.41*10 ⁻⁴
C ₁	1.85*10 ⁻⁴
C ₂	2.79*10 ⁻⁴
C ₃	5.38*10 ⁻⁴
C ₄	12.7*10 ⁻⁴

Thermal diffusivity of the sample is one of the key factors which decide the type of switching exhibited by a chalcogenide glass. Variation of thermal diffusivity for Ga₅Sb₁₀Ge₂₅Se₆₀ nano colloid with different cluster size is tabulated in Table 3.5. Thermal diffusivity value decreases with the increase in concentration of Ga₅Sb₁₀Ge₂₅Se₆₀. It was found from the linear absorption measurement that with decreasing concentration of Ga₅Sb₁₀Ge₂₅Se₆₀ glass (where by cluster size decreases), the E_g value increases. This can be attributed to the decrease in the no. of defect states in the forbidden gap, which can offer minimum resistance to propagating thermal waves due to reduced scattering⁴². This cause an increase in thermal diffusivity. Studies clearly shows that cluster size have great influence on the thermal diffusivity which shows the nonradiative recombination.

3.3.6. Nonlinear optical studies on Ga₅Sb₁₀Ge₂₅Se₆₀ nano colloids

The technique of open-aperture Z-scan scheme (as discussed in section 2.2.6) was employed to study the nonlinear optical properties of the system^{43,44}. The open-aperture curve exhibits a

normalized transmittance valley, indicating the presence of reverse saturable absorption (RSA) in the nano colloidal solutions. Normalized transmittance as a function of the position for C_1 and C_3 in the open aperture scheme at the wavelength of 532 nm with different laser power (182 MWcm^{-2} , 273 MWcm^{-2} , 431 MWcm^{-2} and 539 MWcm^{-2}) is shown in Figure 3.30. The obtained values of nonlinear absorption coefficient at different intensities for the nano colloids are shown in Table 3.6.

Applying a semiconductor concept, it has been shown that nonlinear properties become greater in the materials with smaller optical gaps⁴³. Our observations also support this result showing an increase in nonlinear absorption with lowering of band gap. Generally different processes, such as two photon absorption (TPA), free carrier absorption, transient absorption, interband absorption, photo ejection of electrons, and nonlinear scattering are reported to be operative in nano clusters^{45,46}. Hence the induced absorption can occur due to a variety of such processes. The experimental data shows best fit for two photon absorption confirming that TPA may be the basic mechanism involved in the nonlinear absorption process. Possibility of higher order nonlinear processes such as free carrier absorption contributing to induced absorption cannot be ruled out. The measured value of β for the samples decreases with increasing input intensity due to the removal of an appreciable fraction of photo carriers from the ground state^{33,47}. Thus when the incident intensity

exceeds the saturation intensity, the nonlinear absorption coefficient of the medium decreases.

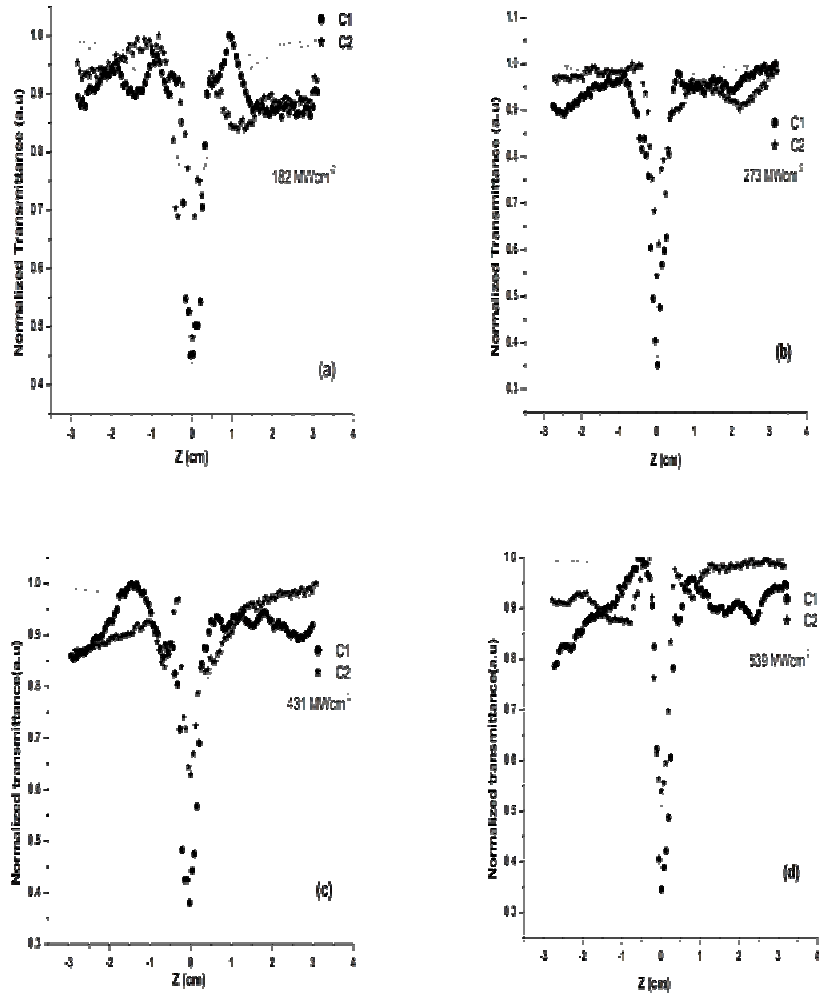


Figure 3.30: Normalized transmittance as a function of the position for concentration C_1 and C_3 in the open aperture scheme at 532 nm with different laser powers. (a) 182 MW cm⁻², (b) 273 MW cm⁻², (c) 431 MW cm⁻², and (d) 539 MW cm⁻². The solid line shows the theoretical fit.

Table 3.6: Measured values of nonlinear absorption coefficient for C_0 , C_1 , C_2 , C_3 and C_4 at wavelength of 532 nm for different irradiation intensity.

Input laser power density (MWcm ⁻²)	β (cm/GW)				
	C_0	C_1	C_2	C_3	C_4
182	20.23	19.61	17.46	15.05	12.89
273	15.05	13.61	14.65	12.45	9.70
431	10.65	8.42	7.96	7.02	6.41
539	8.36	6.80	6.76	6.68	5.97

3.3.7. Optical limiting

The reverse saturable absorption, which is generally associated with a large cross section of absorption from excited levels, brings about optical limiting effects in colloidal solutions^{48,49}. In semiconductor materials the optical limiting is governed by two-photon absorption as observed in the present studies. An important parameter in the optical limiting phenomena is the limiting threshold. It is obvious that lower the optical limiting threshold, better the efficiency of optical limiting material. Figure 3.31 illustrates the optical limiting response of C_1 and C_3 at an input laser intensity of 273 MWcm⁻². The fluence value corresponding to the onset of optical limiting (optical limiting threshold) is found to be higher in the case of C_3 (210 MW/cm²) in comparison with that of C_1 (166 MW/cm²). The limiting threshold at different laser intensities is tabulated in Table 3.7. As given in the table the nonlinear response of the medium depends on both pump power as well as in the concentration. As the concentration is increased there will be enhancement in the cluster

size resulting in to larger magnitude of optical nonlinear interaction between radiations and the sample. This results in lowering of the optical threshold.

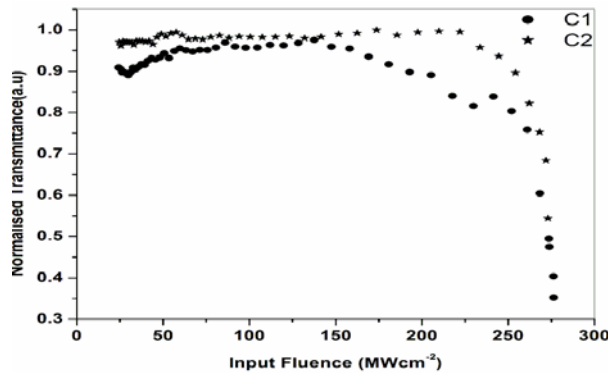


Figure 3.31: Optical limiting response of C_1 and C_3 at 532 nm at an Input power density of 273MWcm^{-2} . The optical limiting threshold (onset of optical limiting) is found to be higher in the case of C_3 (210 MW/cm^2) in comparison with that of C_1 (166 MW/cm^2).

Thus cluster size has a significant effect on limiting performance. Increasing the concentration results in the enhancement of the cluster size which results in the reduction of the limiting threshold thereby enhancing the optical limiting performance.

Table 3.7: Measured values of optical limiting threshold for different concentrations of $\text{Ga}_5\text{Sb}_{10}\text{Ge}_{25}\text{Se}_{60}$ nano colloids.

Input laser power density(MWcm^{-2})	optical limiting threshold (MWcm^{-2})				
	C_0	C_1	C_2	C_3	C_4
182	64	92	101	123	128
273	144	166	192	210	218
431	161	178	188	226	258
539	435	472	486	500	512

3.4. Section 4. Optical Characterization of nano composite $Ga_5Sb_{10}Ge_{25}Se_{60}/PVA$ films

3.4.1. Introduction

Novel combinations of materials become available by taking advantage of the solution phase of chalcogenide glasses. Most of the optical nonlinear studies were done on thin films prepared by thermal evaporation, sputtering or pulsed laser deposition⁴³. Now-a-days, inorganic/polymeric composites have assured importance as a growing class of materials with promising physical and optical characteristics^{50,51}. The realisation of thin films using less conventional techniques such as spin-coating of glassy films from solution is advantageous for realizing large area, thick film, or localized material deposition with less cost^{52,53}. The primary advantage in combining these two materials into a composite or hybrid system is the combination of high hardness from the glass phase with ductility from the polymer phase for increased mechanical durability. Another important use of conducting polymers as an organic guest for preparing such organoinorganic hybrid materials attractive for electrochemical applications mainly for electronic conducting properties.

3.4.2. Fabrication of $Ga_5Sb_{10}Ge_{25}Se_{60}/PVA$ composite films

The composite films were obtained from the solution of $Ga_5Sb_{10}Ge_{25}Se_{60}$ glasses and polyvinyl alcohol (PVA) $[-CH_2CH(OH)-]_n$ in different proportions. The different concentrations of nano colloid

solutions used for drop casting C_1 , C_2 , C_3 films were 0.700 mg/ml, 0.500 mg/ml and 0.251 mg/ml respectively. The composite films were made from these nanocolloid solutions and PVA in the ratio 1 : 1 and named as C_1 +PVA, C_2 +PVA and C_3 +PVA respectively. The films were prepared from the homogeneous solutions of different concentrations by the drop casting method. Best films having thickness 100 μm were used for the optical studies. The thickness of the films was measured using a Mitutoyo Micrometer (series 193). The Atomic Force Microscope (AFM) images of $\text{Ga}_5\text{Sb}_{10}\text{Ge}_{25}\text{Se}_{60}$ /PVA composite films surfaces were recorded using an Atomic Force Microscope (Veeco, Nanoscope III, made by Digital Instruments Inc.,USA). To understand the composition of the each cluster in the prepared new composite films SEM along with EDAX was taken for $\text{Ga}_5\text{Sb}_{10}\text{Ge}_{25}\text{Se}_{60}$ /PVA composite films.

3.4.3. Determination of the optical parameters

In order to characterize the prepared composite thin film, the optical transmission spectra and reflection spectra have been recorded by using a spectrophotometer (JascoV-570 UV/VIS/IR). Transmission and reflection spectra have been used for the study of optical properties. The transmission spectra of the $\text{Ga}_5\text{Sb}_{10}\text{Ge}_{25}\text{Se}_{60}$ /PVA composite films with three different concentrations are given in Figure 3.32. It is clear from figure that as the concentration of the $\text{Ga}_5\text{Sb}_{10}\text{Ge}_{25}\text{Se}_{60}$ component in the polymer decreases the transmission edge gets shifted towards the short wavelength side. The importance of this feature is that it is possible to shift the spectral range of photosensitivity of amorphous composites from ultraviolet to infrared. The increase in bandgap with decrease in

$\text{Ga}_5\text{Sb}_{10}\text{Ge}_{25}\text{Se}_{60}$ can be attributed to the dependence of the cluster size of the corresponding solution used for making composite films.

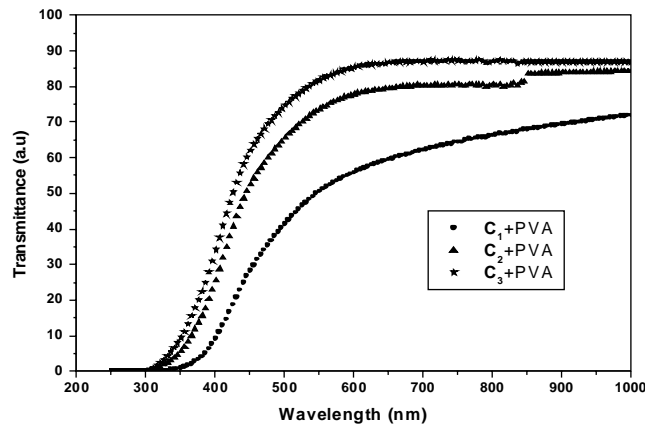


Figure 3.32: Transmission spectra of $\text{Ga}_5\text{Sb}_{10}\text{Ge}_{25}\text{Se}_{60}$ /PVA composite films with different concentrations. The transmission edge and the slope shifts with respect to the concentration of the $\text{Ga}_5\text{Sb}_{10}\text{Ge}_{25}\text{Se}_{60}$ glass.

The optical band gap, a decisive parameter determining the nonlinear optical properties in amorphous semiconductors, can be estimated from the absorption coefficient data. The calculated bandgap for the composite films are tabulated in Table 3.8. The increase in bandgap with decrease in $\text{Ga}_5\text{Sb}_{10}\text{Ge}_{25}\text{Se}_{60}$ can be attributed to the dependence of the cluster size of the corresponding solution used for making composite films.

AFM image of the $\text{Ga}_5\text{Sb}_{10}\text{Ge}_{25}\text{Se}_{60}$ /PVA composite films for C_1 +PVA and C_3 +PVA is presented in Figure 3.33. The distribution of the nano colloid in PVA matrix is less in C_3 +PVA compared to the other. The EDAX plot of C_3 +PVA is given in Figure 3.34. It shows the atomic percentage of elements involved in its formation. The EDAX

analysis done on other films show that as the concentration of the chalcogenide glass decreases the atomic percent contributing to a particular cluster also decreases.

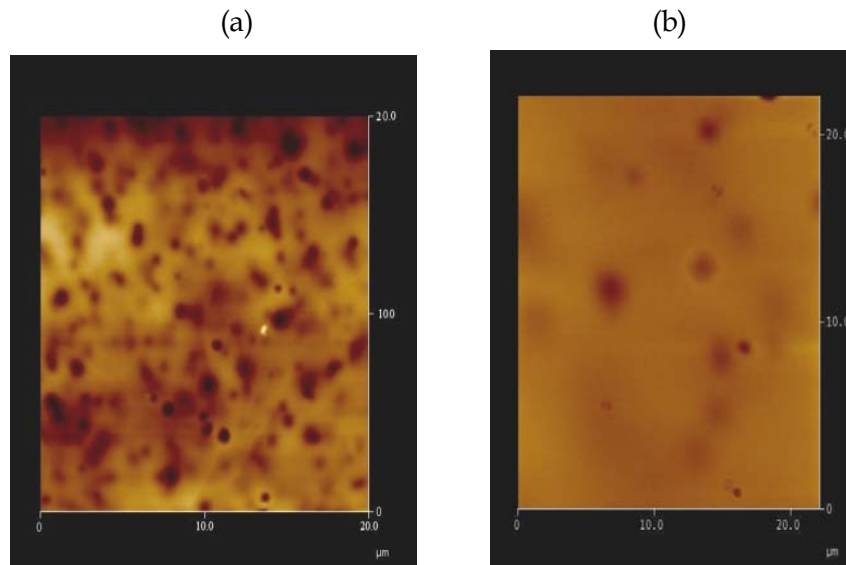


Figure 3.33: AFM images showing the distribution of nanoclusters in the composite films (a) C_1+PVA (b) C_3+PVA

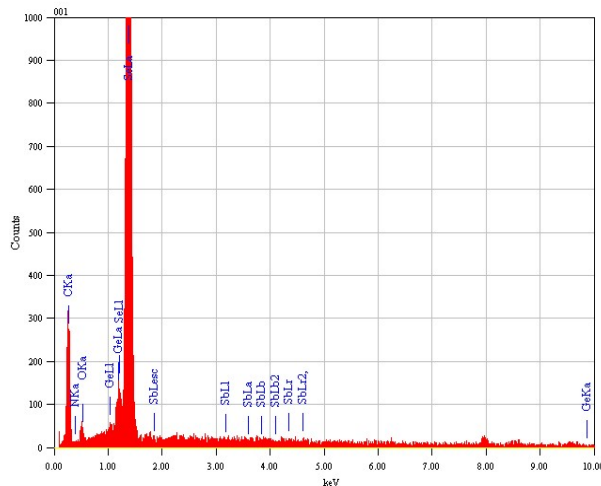


Figure 3.34: EDAX spectrum from a cluster of C_3+PVA film.

3.4.3. a) Refractive index and dispersion analysis of refractive index

Dispersion of refractive index was studied using the WDD single oscillator model⁷. Band gap (E_g), the slope parameter of the Urbach region (E_e), static refractive index (n_0), and the refractive index (n) (at 1.8 eV) are tabulated in Table 3.8. The static refractive index has been found to increase with decrease in Ga₅Sb₁₀Ge₂₅Se₆₀ concentration in PVA. The oscillator energy (E_0) was found to follow the empirical relation with the optical energy gap. The non linear susceptibility ($\chi^{(3)}$), non-linear refractive index (n_2), the dispersion energy and the energy of effective oscillator have been calculated for the composite films and tabulated in Table 3.8.

Table 3.8: Values of Band gap (E_g), the slope parameter of the Urbach region (E_e), static refractive index (n_0), and the refractive index (n) (at 1.8 eV) for the films, Values of dispersion energy (E_d), the single-oscillator energy or Wemple–Di Domenico gap (E_0), and the static dielectric constant (ϵ_∞), non linear susceptibility ($\chi^{(3)}$) and non linear refractive index (n_2) for Ga₅Sb₁₀Ge₂₅Se₆₀/PVA films.

Samples	E_g (eV)	E_e (meV)	n	E_0 (eV)	E_d (eV)	n_0	ϵ_∞	$\chi^{(3)}$ *10 ⁻¹³ (esu)	n_2 *10 ⁻¹² (esu)
C ₁ +PVA	2.46	478	1.82	4.47	7.45	1.78	3.17	1.52	3.22
C ₁ +PVA	2.76	347	1.74	5.47	11.41	1.75	3.08	1.28	2.76
C ₁ +PVA	2.90	293	1.52	5.73	12.46	1.63	2.66	0.52	1.21

The refractive index has been found to decrease with the decrease in concentration of the chalcogenide glass content. The static refractive index has been found to increase with decrease in Ga₅Sb₁₀Ge₂₅Se₆₀ concentration in PVA. It is seen from the studies that

the addition of inorganic semiconductor into the polymer results in fabrication of new composite films with low cost. The investigated new composites are prospective for different photonic devices and for nonlinear optical applications⁵⁴.

3.4.4. NLO studies on $Ga_5Sb_{10}Ge_{25}Se_{60}/PVA$ composite films

The nonlinear optical properties of the thin film samples were studied using the technique of open-aperture z-scan scheme Z-scan technique applying a frequency doubled Nd:YAG laser (Spectra Physics LAB-1760) as the light source with a repetition rate of 10 Hz having a pulse width of 7 ns and wavelength of 532nm. In order to ensure that no permanent photoinduced change has occurred to the sample during laser irradiation, we have repeated the experiment by illuminating the sample on the same position.

The experimental conditions used in our study are such that the laser beam intensity at 532 nm corresponds to the two-photon absorption process because the photon energy of the 532nm laser radiation is within the range⁵⁴ $E_g < 2h\nu < 2E_g$, where $h\nu = 2.33$ eV and E_g of thin films are 2.46 eV, 2.76eV, 2.90 eV for C_1+PVA , C_2+PVA , C_3+PVA respectively. The open-aperture curve exhibits a normalized transmittance valley, indicating the presence of reverse saturable absorption (RSA). Normalized transmittance as a function of the position for the composite films in the open aperture scheme at the wavelength of 532 nm with laser power (539 MWcm^{-2}) are shown in inset of Figure 3.35. From these theoretical fits as described in section 2.2.6, the β values were calculated for the composite films. In general, induced absorption can occur due to a variety of processes. The

theory of two photon absorption processes fitted well with the experimental curve and two photons of 532 nm radiation lie below the absorption band-edge of the films under investigation. This confirms that TPA is the basic mechanism involved in the nonlinear absorption process.

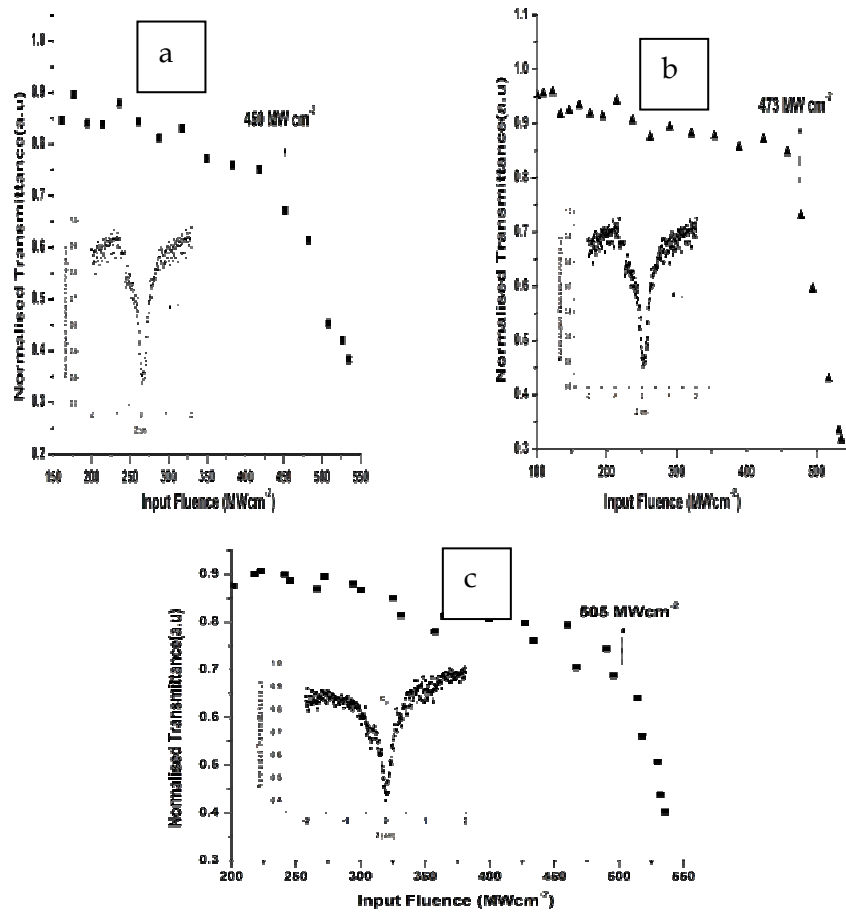


Figure 3.35: Optical limiting response of nano composites film a) C_1 +PVA, b) C_2 +PVA and c) C_3 +PVA at a wavelength of 532nm for a laser power density 539 MW/cm². Inset shows the corresponding z-scan curve.

The obtained values of nonlinear absorption coefficient at different intensities for composite films with different grain size are shown in Figure 3.36. Our results show that the two-photon absorption coefficient increases when the energy gap of the films become closer to the photon energy corresponding to the excitation wavelength, which is consistent with the theoretical work of Sheik-Bahae et al.⁵⁵. This decrease in β with input intensity can be due to the removal of an appreciable fraction of photo carriers from the ground state.

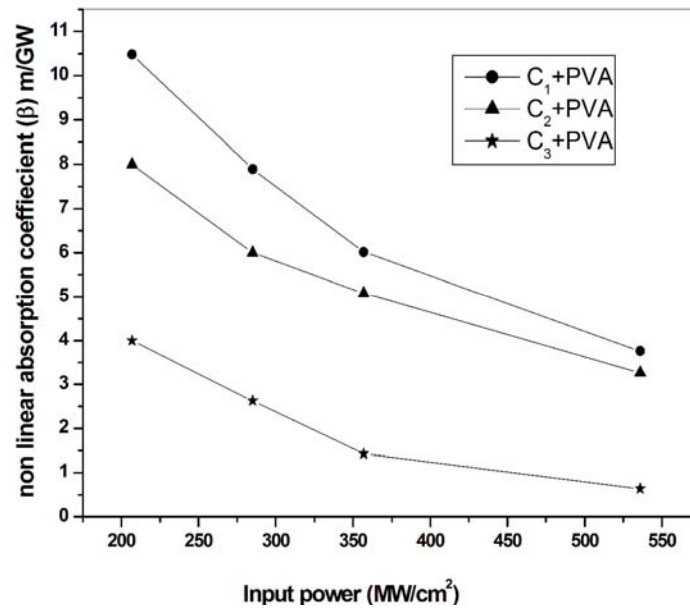


Figure 3.36: Plot of dependence of nonlinear absorption coefficient of films on input power density.

From the value of β , the imaginary part of susceptibility can be calculated and β is related to $\text{Im}(\chi^{(3)})$ through the relation⁵⁶

$$\text{Im} \chi^{(3)} = \frac{n_0^2 \varepsilon_0 c^2 \beta \lambda}{4\pi} \quad (5)$$

where n_0 is the linear refractive index of films, ϵ_0 is the permittivity of free space, c is the velocity of light in vacuum, ω is the angular frequency of the radiation used, β the nonlinear absorption coefficient. The linear refractive index found from the transmission and reflection spectra is presented in Table 3.8. The obtained values of the $\text{Im } \chi^3$ for the composite films are given in Table 3.9. The susceptibility values vary to a great extent depending on the excitation wavelength, pulse duration, experimental technique, and concentration of the molecular species in the sample etc⁵⁶. So one has to be very careful while comparing these values with the literature.

Z scan data used to study the optical limiting property of films show that the $\text{Ga}_5\text{Sb}_{10}\text{Ge}_{25}\text{Se}_{60}/\text{PVA}$ composite film can be considered as almost non-investigated possible applicants for optical limiting applications. The limiting response has been studied for three concentrations with four different laser powers. The Figure 3.35 represents the limiting response of C_1+PVA , C_2+PVA and C_3+PVA at an input power density of $536 \text{ MW}/\text{cm}^2$. The optical limiting threshold for different concentrations of films at a laser power density of $357 \text{ MW}/\text{cm}^2$ is tabulated in Table 3.9. The fluence value corresponding to the onset of optical limiting is less for C_1+PVA compared to C_2+PVA and C_3+PVA which is clear from the limiting response graphs shown in Figure 3.35. Studies show that nonlinear response of the medium depends on both pump power as well as in the concentration of the chalcogenide glass. As the concentration is increased there will be enhancement in the

optical nonlinear efficiency of the samples which result in lowering of the limiting threshold.

Table 3.9: Measured values of imaginary part of the third-order susceptibility ($\text{Im } \chi^3$) and optical limiting threshold (at wavelength of 532nm for intensity of 357MW/cm²) for the Ga₅Sb₁₀Ge₂₅Se₆₀ / PVA composite films.

Samples	$\text{Im } \chi^3 \cdot 10^{-9}$ (m/GW)	Limiting Threshold (MW/cm ²)
C ₁ +PVA	2.24	275
C ₂ +PVA	1.73	300
C ₃ +PVA	0.42	341

3.5. Conclusions

- ✓ Ga₅Sb₁₀Ge₂₅Se₆₀ bulk glass having transparency above 620nm was prepared and was found to be stable. The glass was found to have a glass transition temperature of 316°C. Ga₅Sb₁₀Ge₂₅Se₆₀ thin films fabricated from thermal evaporation technique were optically characterized using different models. Various parameters related to optical properties have been calculated for the thin film. The optical absorption in the given system seems to be of non-direct transition.
- ✓ The photo induced studies on the Ga₅Sb₁₀Ge₂₅Se₆₀ thin films shows that there is a laser power, wavelength and duration of laser radiation dependent shift in the band gap and refractive index. The red shift in bandgap and the increase in refractive index can be due to the photo darkening mechanism in the material. Studies show that a low power radiation is sufficient enough to provide a shift in the absorption edge

and a change in the refractive index. This mechanism in $\text{Ga}_5\text{Sb}_{10}\text{Ge}_{25}\text{Se}_{60}$ glasses can be used to realize continuous wave laser written waveguide and for fabricating photosensitive optical components for various applications

- ✓ Nano colloidal solutions of $\text{Ga}_5\text{Sb}_{10}\text{Ge}_{25}\text{Se}_{60}$ glass were synthesised and investigated. The energy gap of the dispersed chalcogenide nanoclusters were found to depend on cluster size which is inversely proportional to concentration. The photoluminescence emission characteristic from nano colloidal $\text{Ga}_5\text{Sb}_{10}\text{Ge}_{25}\text{Se}_{60}$ chalcogenide glass solutions were investigated and the results show a remarkable dependence on the glass concentration and the excitation energy. PL studies show that the localized states differ with the concentration and those defect states play an important role in the luminescence spectra.
- ✓ Thermal diffusivity of colloid solutions at an excitation of 532nm (DPSS-50mW) for different concentrations were studied using Dual beam mode-matched thermal lens method and the investigated samples show cluster size dependent change in thermal diffusivity.
- ✓ Nonlinear optical response of investigated samples shows that they are highly nonlinear exhibiting reverse saturable absorption. The studies show that materials are promising candidates for light-emitting devices, optoelectronic devices and optical limiters for the development of nonlinear optical devices with a relatively small limiting threshold.
- ✓ The band gap of the thin film samples prepared from colloidal solutions of $\text{Ga}_5\text{Sb}_{10}\text{Ge}_{25}\text{Se}_{60}$ glasses at different concentration exhibit varying bandgap from 2.46eV ($C_1=0.700\text{mg/ml}$) to 2.90eV ($C_3=0.251\text{mg/ml}$). This enables us to realize special requirements by engineering their

concentration. Nonlinear optical characterisation of the films studied by the z-scan technique shows reverses saturable absorption, which makes it useful for optical limiting applications. Thus depending on the concentration of the nano colloid solution used for the fabrication of nano composite films, varying nonlinear response can be obtained, enabling a pathway to new materials for optoelectronic devices.

3.6. References

1. R. Ganesan, "Thermal and optical properties of Ge-Se glass matrix doped with Te, Bi and Pb", PhD thesis, Indian Institute of Science, Bangalore (2004).
2. H.L. Ma, Y. Guimond, X.H. Zhang, J. Lucas, "Ga-Ge-Sb-Se based glasses and influence of alkaline halide addition", *Journal of Non-Crystalline Solids.*, 256&257, 165-169 (1999).
3. Xianghua Zhang, Hongli Ma, Jean-Luc Adam, Jacques Lucas, Guorong Chen, Donghui Zhao, "Thermal and optical properties of the Ga-Ge-Sb-Se glasses", *Materials Research Bulletin.*, 40, 1816-1821 (2005).
4. Xiang Hua Zhang, Hongli Ma, Jacques Lucas, "Evaluation of glass fibers from the Ga-Ge-Sb-Se system for infrared applications", *Optical Materials* 25, 85-89 (2004).
5. R. Swanepoel, "Determination of the thickness and optical constants of amorphous silicon," *Journal Physics E.*, 16(12), 1214-1222 (1983).
6. R. Tintu, K. Sulakshna, K. Saurav, V. P. N Nampoory, P. Radhakrishnan and Sheenu Thomas, " $\text{Ge}_{28}\text{Se}_{60}\text{Sb}_{12}$ /PVA Composite Films For Photonic Applications", *Journal of Non-Oxide Glasses.*, 2, 167- 174 (2010).
7. S. H. Wemple and M.DiDomenico, "Behavior of the Electronic Dielectric Constant in Covalent and Ionic Materials," *Physical Review B.*, 3 1338-1351 (1971).
8. Y. A. El-Gendy, "Refractive index, oscillator parameters and optical band gap of e-beam evaporated $\text{Ga}_{10}\text{Ge}_{10}\text{Te}_{80}$ films", *J. Phys. D: Appl. Phys.*, 42, 115408 (2009).

9. A. S. Tverjanovich, E. N. Borisov, O. Volobueva, S. B. Mamedov and M. D. Mikhailov, "Photoinduced Bleaching in Ga-Ge-S(Se) Vitreous Films", *Glass Physics and Chemistry.*, 32, 677-680 (2006).
10. M. M. Hafiz, A. A. Othman, M. M. EL-Nahass and A. T. AL-Motasem, "Photoinduced effects on the optical constants of a-Ge-Se-Bi chalcogenide glassy thin films", *Radiation Effects & Defects in Solids.*, 162, 669-676 (2007).
11. G.B Turpin and L.E McNeil, "Photodarkening in $Ge_{1-x} Sn_x Se$ films", *Physical Review B.*, 39, 8750 (1989).
12. K. Tanaka, "Photoinduced structural changes in amorphous semiconductors", *Semiconductors.*, 32, 861-867 (1998).
13. Keji Tanak and Yoshihiro Oshtsuka, "Composition dependence of photoinduced refractive index change in amorphous as-s films", *Thin Solid Films.*, 57, 59-64 (1979).
14. J.Z.Liu and P.C.Taylor, "Defects in Glasses", *Material Research Society.*, 61, 223 (1986).
15. V. M. Lyubin and V. K. Tikhomirov, "Novel photo-induced effects in chalcogenide glasses", *Journal of Non-Crystalline Solids.*, 135, 37 (1991).
16. R. Tintu, V.P.N. Nampoore, P. Radhakrishnan, Sheenu Thomas "Photoinduced changes in optical properties of Ga-Sb-Ge-Se glasses", *Optics Communications.*, 284, 222-225(2011).
17. Stephen Ducharme, J Hautala and P.C.Taylor, "Photodarkening profile and kinetics in chalcogenide glass", *Physical Review B.*, 41, 12250-12261 (1990).
18. A. A. Othman, H. H. Amer, M. A. Osman, A. Dahshan, " Reversible photodarkening in amorphous $Ga_{20}S_{75}Sb_5$ and $Ga_{20}S_{40}Sb_{40}$ thin films" *Radiation Effects & Defects in Solids.*, 159, 659-666 (2004).
19. M. Štábl, L. Tichý, "Giant" photo-darkening in $Ge_{16}As_{26}S_{58}$ amorphous thin film", *Solid State Sciences.*, 7, 201-207(2005).

20. Ticha H and L.Tichy, "Semiempirical relation between non-linear susceptibility (refractive index), linear refractive index and optical bandgap and its application to amorphous semiconductors", *Journal of Optoelectronics and Advanced Materials*, 4[2], 381 – 386 (2002).
21. L. Petit, N. Carlie, K. Richardson, A. Humeau, S. Cherukulappurath, G. Boudebs, "Non linear Optical properties of glasses in the system Ge/Ga-Sb-S/Se", *Optics Letters*, 31, 1495-1498 (2006).
22. J. Troles, L. Brilland, F. Smektala, P. Houizot, F. Desevedavy, Q. Coulombier, Traynor, T. Chartier, T.N. Nguyen, J.L. Adam, G. Renversez, "Chalcogenide Microstructured fibers for Integrated Systems, Elaboration Modelization and Characterization", *Fiber and Integrated Optics*, 28, 11 (2009).
23. U. Woggon, "Optical properties of semiconductor quantum dots", Springer Verlag Berlin, Heidelberg (1997).
24. R. A. Ganeeva, I. Ryasnyansky and T. Usmanov, "Nonlinear refraction and nonlinear absorption of As_2S_3 aqueous solution", *Optical and Quantum Electronics*, 35, 211-219 (2003).
25. Herve Rigneault, Jean-Michel Lourtioz, Claude Delalande and Ariel Levenson, "Nanophotonics", ISTE Ltd. London, UK (2006).
26. T Yao and J C Woo, "Physics and applications of semiconductor quantum structures", IOP publishing Bristol and Philadelphia (2001).
27. (1) Berzelius, J. J. *Ann. Chim. Phys.*, 32, 166 (1826). (2) Bineau, A. *Ann. Chim. Phys.*, 70, 54 (1839).
28. G. C. Chern, and I. Lauks, "Spin-coated amorphous chalcogenide films," *J. Appl. Phys.*, 53(10), 6979 (1982).
29. G. C. Chern, I. Lauks, and A. R. McGhie, "Spin coated amorphous chalcogenide films: Thermal properties", *J. Appl. Phys.*, 54(8), 4596 (1983).
30. G. C. Chern, and I. Lauks, "Spin coated amorphous chalcogenide films: Structural characterization", *Journal of Applied Physics*, 54, 2701 (1983).

31. T. Kohoutek, T. Wagner, M. Frumar, A. Chrissanthopoulos, O. Kostadinova and S. N. Yannopoulos, "Effect of cluster size of chalcogenide glass nanocolloidal solutions on the surface morphology of spin-coated amorphous films", *Journal of Applied Physics*, 103, 063511 (2008).
32. S. Song, N. Carlie, J. Boudies, L. Petit, K. Richardson, and C. B. Arnold, "Spin-coating of $\text{Ge}_{23}\text{Sb}_7\text{S}_{70}$ chalcogenide glass thin films", *J. Non-Cryst. Solids*, 355(45-47), 2272-2278 (2009).
33. R. Tintu, V. P. N. Nampoori, P. Radhakrishnan, and Sheenu Thomas "Nonlinear optical studies on nanocolloidal Ga-Sb-Ge-Se chalcogenide Glass", *Journal Of Applied Physics*, 108, 073525 (2010).
34. F. Urbach, *Phy.Rev.*, 1324 (1953).
35. R. A. Street, "Luminescence in amorphous semiconductors", *Advances In Physics*, 25, 397-454 (1976).
36. Munetoshi Seki, Kan Hachiya, Katsukuni Yoshida, "Photoluminescence excitation process and optical absorption in Ge-S chalcogenide glasses", *Journal of Non-Crystalline Solids*, 324, 127-132 (2003).
37. S.G. Bishop and D.L. Mitchell, "Photoluminescence excitation spectra in chalcogenide glass", *Physical Review B*, 8, 5696-5701 (1973).
38. K. Imura, T. Nagahara, and H. Okamoto, "Near-field two-photon-induced photoluminescence from single gold nanorods and imaging of plasmon modes," *J. Phys. Chem. B*, 109, 13214-13220 (2005).
39. N. J. Durr, T. Larson, D. K. Smith, B. A. Korgel, K. Sokolov, and A. Ben-Yakar, "Two-photon luminescence imaging of cancer cells using molecularly targeted gold nanorods," *Nano Letters*, 7(4), 941-945 (2007).
40. Pulok Pattanayak, N. Manikandan, M. Paulraj and S. Asokan, "Photo-thermal deflection and electrical switching studies on Ge-Te-I chalcogenide glasses", *J. Phys. Condens. Matter*, 19, 036224 (2007).
41. K. Tanaka, T. Gotoh, N. Yoshida and S. Nonomura, "Photothermal deflection spectroscopy of chalcogenide glasses", *Journal of Applied Physics*, 91, 125 (2002).

42. N. Manikandan, M. Paulraj, S. Asokan, "Thermal diffusivity measurements on As-Te-Ga glasses by photo-thermal deflection technique: Composition dependence and topological thresholds", *Journal of Non-Crystalline Solids.*, 355, 58–60(2009).
43. A. Zakery and S.R. Elliott, "Optical Nonlinearities in Chalcogenide Glasses and their Applications", *Springer Series in Optical Sciences*, Springer: Berlin (2007).
44. K. S. Bindra, H. T. Bookey, A. K. Kar, B. S. Wherrett X. Liu and A. Jha, "Nonlinear optical properties of chalcogenide glasses: Observation of multiphoton absorption", *Applied Physics Letters.*, 79, 1939-1941 (2001).
45. Litty Irimpan, A Deepthy, Bindu Krishnan, L M Kukreja, V P N Nampoori and P Radhakrishnan, "Effect of self assembly on the nonlinear optical characteristics of ZnO thin films", *Optics Communications.*, 281 (10), 2938-2943 (2008).
46. Richard L Sutherland, "Handbook of nonlinear optics", CRC press (2003).
47. R.Tintu, V.P.N. Nampoori, P. Radhakrishnan and Sheenu Thomas, "Reverse saturable absorption in nano colloidal $\text{Ge}_{28}\text{Sb}_{12}\text{Se}_{60}$ chalcogenide glass", *J. Non-Crys. Solids.* doi:10.1016/j.jnoncrysol.2011.03.028 .
48. Kazuhiko Ogusu, Jun Yamasaki, Shinpei Maeda, Michihiko Kitao and Makoto Minakata, "Linear and nonlinear optical properties of Ag-As-Se chalcogenide glasses for all-optical switching", *Optics Letters.*, 29 , 265-268 (2004).
49. J. Troles, F. Smektala, G. Boudebs, A. Monteila, B. Bureau, J. Lucas, "Optical limiting behaviour of chalcogenide glasses", *Journal of Optoelectronics and Advanced Materials .*, 4, 729 – 735 (2002).
50. T.Kohoutek, T.Wagner, J.Orava, M.Krbal, Mir Vlcek, J.Ilavsky, Mil. Vlcek and M. Frumar, "Multilayer Planar Structures Prepared from Chalcogenide Thin Films of As-Se and Ge-Se Systems and Polymer Thin Films using Thermal Evaporation and Spincoating Techniques", *J. Non-Cryst. Solids.*, 354, 529-532 (2008).

51. R. G. DeCorby, H. T. Nguyen, P. K. Dwivedi and T. J. Clement, "Planar omnidirectional reflectors in chalcogenide glass and polymer," *Opt. Express.*, 13, 6228-6233 (2005).
52. M. S. Iovu, A. M. Andries, S. A. Buzurniuc, V. I. Verlan, E. P. Colomeico, St. V. Robu," *New $\text{As}_2\text{S}_3:\text{Pr}^{3+}$ - polymer composite materials*", *Journal of Optoelectronics and Advanced Materials.*, 8, 257-260 (2006).
53. M. S. Iovu, A. M. Andriesh, S. A. Buzurniuc, V. I. Verlan," *Optical Properties Of $\text{As}_2\text{S}_3: \text{Pr}$ And $\text{As}_2\text{S}_3: \text{Dy}$ Amorphous Composites*", *Digest Journal of Nanomaterials and Biostructures.*, 2, 201-206 (2007).
54. R. Tintu, V. P. N. Nampoore, P. Radhakrishnan, and Sheenu Thomas," *Nano composite Thin films of $\text{Ga}_5\text{Sb}_{10}\text{Ge}_{25}\text{Se}_{60}$ chalcogenide glass for optical limiting applications* ", *Optical Materials.*, 33 ,1221-1225 (2011).
55. M S Bahae, A A Said, T H Wei, D J Hagan and E W Van Stryland, " *Sensitive measurement of optical nonlinearities using a single beam*", *IEEE J. Quantum Electron.*, 14, 760 (1990).
56. R. Tintu, V.P.N. Nampoore, P. Radhakrishnan, Sheenu Thomas," *Preparation and optical characterization of novel Ge-Se-Sb/PVA composite films for optical limiting application*", *J. Phys. D: Appl. Phys.*, 44, 025101(2011).



Chapter 4

STUDIES ON $\text{Ge}_{28}\text{Sb}_{12}\text{Se}_{60}$ CHALCOGENIDE GLASS

4.1. Introduction

4.1. Section 1. Studies on bulk and thin films of $\text{Ge}_{28}\text{Se}_{60}\text{Sb}_{12}$.

4.2. Section 2. Photoinduced darkening in $\text{Ge}_{28}\text{Se}_{60}\text{Sb}_{12}$ films.

4.3. Section 3. Studies on Nano colloid $\text{Ge}_{28}\text{Sb}_{12}\text{Se}_{60}$ chalcogenide glass

4.4. Section 4. $\text{Ge}_{28}\text{Se}_{60}\text{Sb}_{12}$ /PVA nano composite films for photonic applications

4.5. Conclusions

4.6. References

This chapter presents the results obtained from the investigation on $\text{Ge}_{28}\text{Se}_{60}\text{Sb}_{12}$ glass. Four sections are included in this chapter. Structural and optical characterization done on bulk and thin film samples of $\text{Ge}_{28}\text{Sb}_{12}\text{Se}_{60}$ glass is presented in first section. Photoinduced studies carried out on the thin films with near and above band gap illumination is included in section 2. The synthesis and structural, thermal linear and non linear optical studies carried out for the nano colloid $\text{Ge}_{28}\text{Se}_{60}\text{Sb}_{12}$ glass are discussed in section 3. Section 4 deals with fabrication and characterization of $\text{Ge}_{28}\text{Se}_{60}\text{Sb}_{12}$ glass/PVA composite films for non linear applications.

The results of this chapter are published in

- 1.R. Tintu et al., *Journal of Non-Oxide Glasses.*, 2, 167- 174(2010).
- 2.R Tintu et al., *J. Phys. D: Appl. Phys.*, 44, 025101(2011).
- 3.R. Tintu et al., *Journal of Non-Crystalline Solids.*, (doi:10.1016/j.jnoncrsol. 2011.03.028).

4.1. Introduction

Germanium based chalcogenide glasses containing heavy metal species such as Sb has shown their potential as glasses with high non-linear optical properties¹. The physical properties of germanium chalcogenide glasses have attracted much interest for physical and technical reasons. Ge–Sb–Se glasses are attractive candidates for applications requiring low transmission losses, as they are transparent to IR radiation from 2 to 16 μm ²⁻⁴. Recently, IR optical fibres have been successfully made from these glasses⁵. This group of materials is perhaps the only family that fulfils the material requirements for the fabrication of optical fibres, such as large bandgap, low material dispersion, low light scattering, long wavelength multi phonon edge along with good thermal, mechanical and chemical properties³. It is reported that for a planar optical waveguide in the Ge–Sb–Se glass system on a silica glass substrate, an optical propagation loss⁴ of 27 dB/cm was measured at 1.2 μm . Various studies related to the physical properties such as electron spin resonance, optical properties, thermodynamic properties, chemical ordering, electrical conduction, photo-electrical properties, and the effect of pressure on the electrical properties have already been reported for Ge–Sb–Se glasses⁶⁻¹⁰. All these properties have been related to the existence of the quasi-binary $\text{GeSe}_2\text{–Sb}_2\text{Se}_3$ system.

The glass-forming area of Ge–Sb–Se system is enclosed by the dashed line in Figure 4.1. Glass compositions near the dashed edge of the glass-forming region in above figure were found to be crystalline or partially crystalline. In the Ge–Sb–Se system, the glass-forming region was found to extend from about 5 to 35 at. % germanium, 5 to

40 at.% antimony, with the rest being selenium. It is reported that the $\text{Ge}_{28}\text{Se}_{60}\text{Sb}_{12}$ glasses which is in the center of the area enclosed is a good glass former. The glass transition temperature, thermal expansion, density and Vickers hardness as reputed by J. A. Savage¹¹ are 277°C , 13.79×10^6 , 4.68×10^{-3} and 206 kg mm^{-2} respectively. The Young's modulus of the glass is reported to be 19.23 GPa .

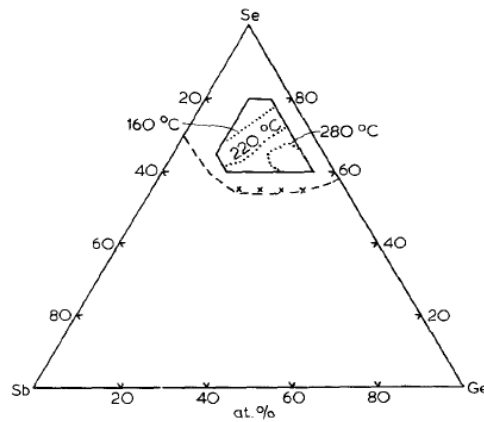


Figure 4.1: Glass-forming region of Ge-Sb-Se system.

The structure of $\text{Ge}_{28}\text{Se}_{60}\text{Sb}_{12}$ is as shown in figure 4.2. In $\text{Sb}_x\text{Ge}_y\text{Se}_z$ system we can find that Ge represents any fourfold coordinated atom, Sb any threefold coordinated atom and Se any twofold coordinated atom. The composition $\text{Ge}_{28}\text{Se}_{60}\text{Sb}_{12}$ can be also considered as Ge_2Se_3 (Ge-Se and GeSe_2 components) in which Ge is gradually replaced by Sb. It is reported⁷ that in $\text{Ge}_{28}\text{Se}_{60}\text{Sb}_{12}$, the disorder around Sb is the smallest and that around Se is the largest; the disorder around Ge being at an intermediate level. The bonding for Sb is heteropolar Sb-Se bonds, and also these are relatively stable bonds. The larger disorder around Se is observed because Se is

bonded to Ge and Sb (see Figure 4.2) with different bond distances. The formation of both Se-Ge and Se-Sb bonds increases the disorder around Se.

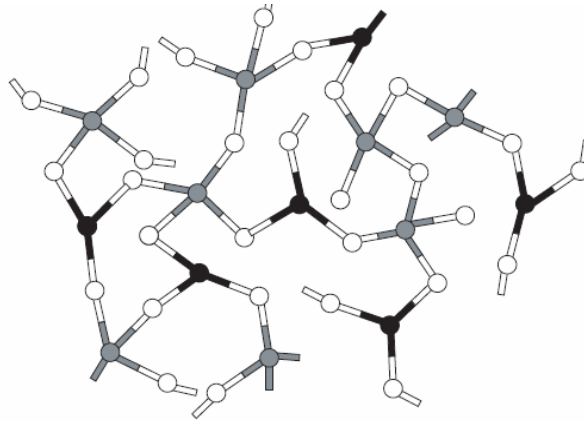


Figure 4.2: Structure of Ge-Sb-Se glass. Solid grey, white and black circles represent Ge, Se and Sb atoms respectively.

Optical studies were carried out on $\text{Ge}_{28}\text{Se}_{60}\text{Sb}_{12}$ thin films prepared by thermal evaporation, RF-sputtered films, chemical vapour deposition, pulsed laser deposition and laser ablation⁷⁻¹². One of the main disadvantages of the films prepared by above mentioned techniques is the failure to reproduce the stoichiometry of the films.

4.1. Section 1. Studies on bulk and thin films of $\text{Ge}_{28}\text{Se}_{60}\text{Sb}_{12}$

4.1.1. Preparation and characterization of $\text{Ge}_{28}\text{Se}_{60}\text{Sb}_{12}$ bulk glass

$\text{Ge}_{28}\text{Se}_{60}\text{Sb}_{12}$ glasses were synthesized by melting the mixture of Ge, Sb, and Se elements (5N purity, Sigma Aldrich) in an evacuated fused-quartz ampoule. The ampoule was placed in a rotating and rocking furnace at 1050 °C for 24 h for thorough mixing and homogenization of the melt and then rapidly quenched to ice

cold water. Using X-ray diffraction (XRD) technique (Bruker AXS D8 Advance X-ray Diffractometer) the amorphous nature was confirmed as shown in Figure 4.3.

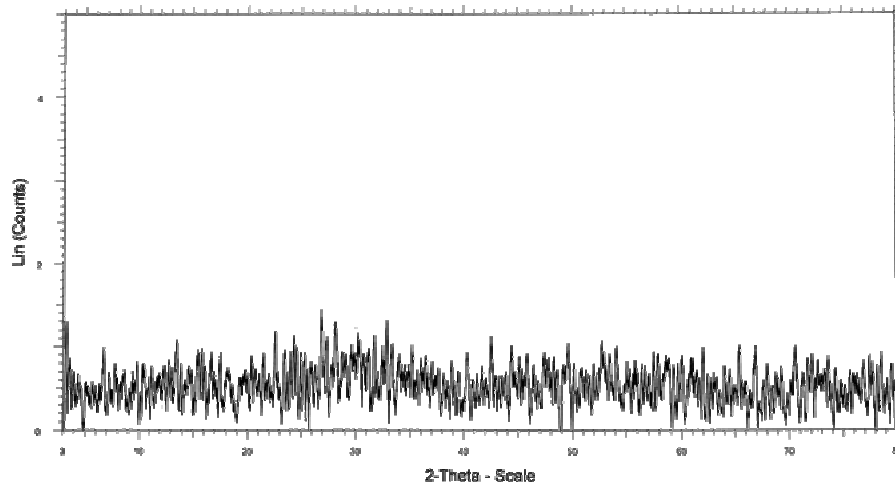


Figure 4.3: Normalized XRD signal versus 2θ plot of the $\text{Ge}_{28}\text{Se}_{60}\text{Sb}_{12}$ glass showing amorphous nature of sample.

Thermal studies carried out on melt quenched $\text{Ge}_{28}\text{Se}_{60}\text{Sb}_{12}$ glass by Differential Scanning Calorimetric method (DSC) show glass transition temperature (T_g), which is the temperature for transition from glass solid phase to glass liquid phase, to be 274°C . This value is estimated as the temperature corresponding to the intercept of the tangent drawn to the baseline and the endothermic baseline shift as shown in Figure 4.4.

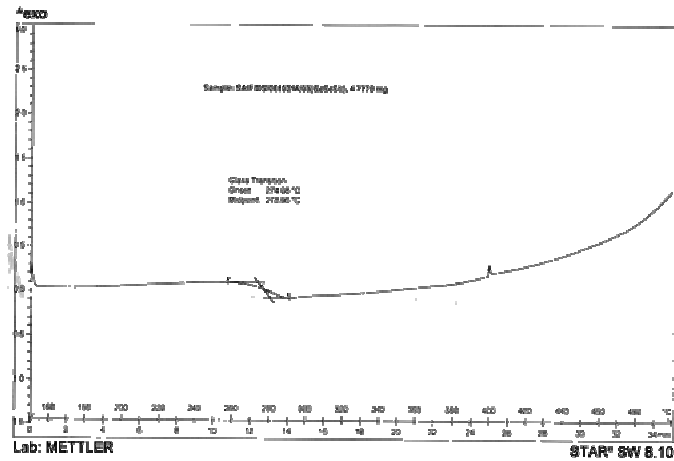


Figure 4.4: DSC curve of $\text{Ge}_{28}\text{Se}_{60}\text{Sb}_{12}$ glass.

Optical absorption measurements recorded using a spectrophotometer (JascoV-570 UV/VIS/IR) is presented in Figure 4.5. $\text{Ge}_{28}\text{Se}_{60}\text{Sb}_{12}$ glass is highly absorbing throughout much of the visible spectrum and the band edge absorption spectrum is characterized by an exponential Urbach tail¹³. The absorption in the sample above 1.60 eV corresponds to the band-to-band transition and the band gap is evaluated to be about 1.60 eV.

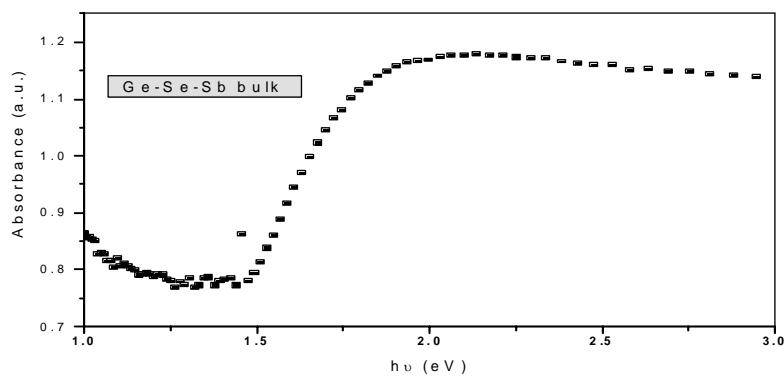


Figure 4.5: Plot of absorption spectra of $\text{Ge}_{28}\text{Se}_{60}\text{Sb}_{12}$ glass.

4.1.2. Fabrication and Optical characterisation of Ge₂₈Se₆₀ Sb₁₂ thin films.

Thermal evaporation technique was used to prepare thin films at a pressure of 2×10^{-5} mbar and rate of $10 \text{ \AA}^0/\text{S}$ using a vacuum system. The films having a thickness of 325nm were deposited on a microscopic glass slide. X-ray diffraction data reveals the amorphous nature of the as-prepared thin films as shown in Figure 4.6. The figure does not show any diffraction peaks and the broad features indicate that the thin films are amorphous in nature.

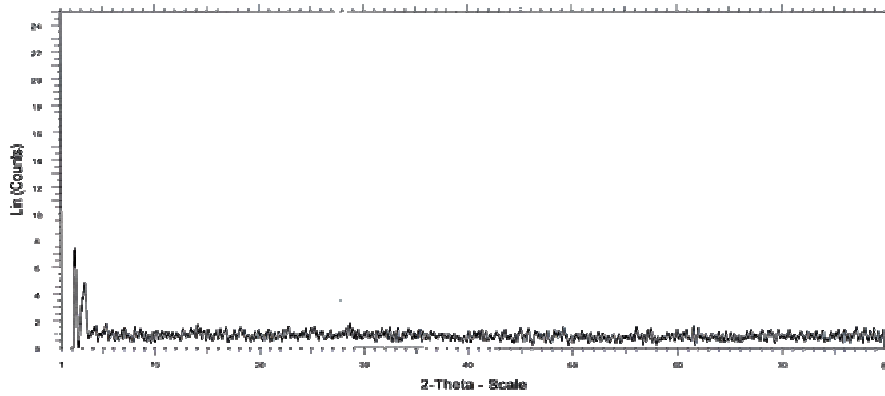


Figure 4.6: XRD spectra for Ge₂₈Se₆₀ Sb₁₂ chalcogenide glass film.

The optical properties of the thin films were analysed through the transmission spectrum and reflection spectra of the thin films obtained from spectrophotometer (JascoV-570 UV/VIS/IR). The transmission and reflection spectrum is presented in Figure 4.7. The interference fringes at the transparency wavelengths have been used to extract index of refraction and other optical parameters of the films using the Swanepoel's method¹⁴. The dispersion of the refractive index is discussed in terms of the single-oscillator Wemple-Di

Domenico model¹⁵. The optical-absorption edge is described using the non-direct transition model proposed by Tauc and the optical band gap is calculated from the absorption coefficient values by Tauc's extrapolation procedure¹⁶. Different Optical parameters measured for the thin film are tabulated in Table 4.1. The parameters are calculated as discussed in Section 2.2.4.

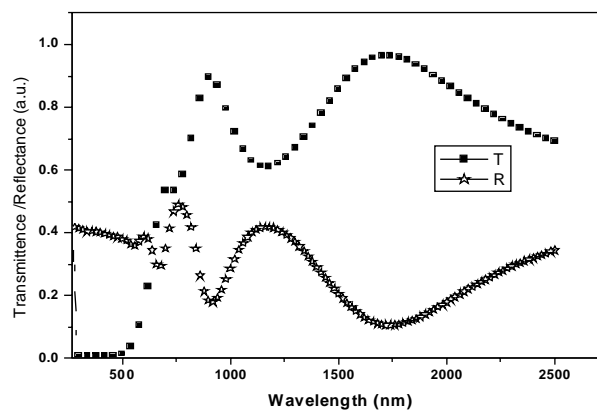


Figure 4.7: Plot of reflectance and transmittance spectra of $\text{Ge}_{28}\text{Se}_{60}\text{Sb}_{12}$ thin films.

The obtained values of E_g for indirect allowed transitions are given in Table 4.1. The analysis of both refractive index and extinction coefficient show a decrease with the increase of wavelength. The decrease of refractive index and extinction coefficient with the increase of wavelength may be correlated with decrease of absorption coefficient. The decrease in the value of refractive index with increasing wavelength shows the normal dispersion behavior of the material within the worked spectral region. The decrease of extinction coefficient with increasing wavelength shows that the fraction of light lost due to scattering and absorbance decreases. The knowledge of real and imaginary part of dielectric constant provides

information about the loss factor which is the ratio of imaginary part of dielectric constant to real part of dielectric constant, i.e. larger the imaginary part of dielectric constant or smaller the real part of dielectric constant, larger is the loss factor.

Table 4.1: The bandgap(E_g), width of localized states (E_e), refractive index (n at 1000nm), extinction coefficient (k at 1000nm), optical conductivity (σ at 1000nm), real part of dielectric constant(ϵ_r), imaginary part of dielectric constant(ϵ_i), dispersion energy(E_d), effective oscillator energy (E_0), static refractive index (n_0), high frequency dielectric constant (ϵ_∞) susceptibility ($\chi^{(3)}$) and non linear refractive index (n_2) of thermally evaporated Ge₂₈Se₆₀Sb₁₂ thin film.

Optical parameters of Ge ₂₈ Se ₆₀ Sb ₁₂ thin film	
E_g (eV)	1.66
E_e (meV)	371
n	3.30
k	0.02
σ (s ⁻¹)	2.09*10 ⁻¹¹
ϵ_r (eV)	10.90
ϵ_i (eV)	0.14
n_0	3.29
ϵ_∞	10.82
E_d (eV)	29.14
E_0 (eV)	3
$\chi^{(3)}$ *10 ⁻¹¹ (esu)	6.08
n_2 *10 ⁻¹⁰ (esu)	6.96

The non linear refractive index (n_2) and susceptibility ($\chi^{(3)}$) calculated by combining Miller's generalized rule and low-frequency linear refractive index estimated from Wemple-Di Domenico single effective oscillator model is presented in Table 4.1. The prepared thin film is showing high non linear refractive index.

4.2. Section 2. Photoinduced darkening in $\text{Ge}_{28}\text{Se}_{60}\text{Sb}_{12}$ films

4.2.1. Introduction

Amorphous semiconductors containing appreciable proportions of the chalcogens Se and S (eg., Ge-Se or Ge-S alloys) exhibit a variety of structural changes on illumination with subband gap light (or other ionizing radiation)¹⁷. These structural alterations produce several effects such as a shift of the optical absorption edge, volume changes, and changes of refractive index¹⁸⁻²⁰. Chalcogenide glasses have been found to exhibit a change in refractive index under the influence of light, which makes it possible to use these materials to record not only the magnitude but also the phase of illumination. Current interest in the chalcogenide compounds and their photo-darkening under laser irradiation approximated to their band gap energy show considerable impact on making many optical devices. In $\text{Ge}_{28}\text{Sb}_{12}\text{Se}_{60}$ films, the disorder around Sb is the smallest and that around Se is the largest; the disorder around Ge being at an intermediate level. In order to use chalcogenide glasses in integrated optics, including wavelength selective devices for WDM networks, it is important to know the optical constants and how they can be changed with band-gap illumination.

4.2.2. Experimental

The photosensitivity of the films was studied using He-Ne laser (633-nm) of 4mW, 10mW and 20mW and semiconductor laser (810nm, 20mW). The laser power was made stable during exposure to avoid significant uncertainty in the total supplied energy. The laser beam was expanded from an initial beam waist of 1.0 mm (FWHM) using a plano-concave lens and collimated with a second plano-convex lens. At the sample stage an aperture was used to admit only the central maximum of the laser beam, so as to assure irradiating the sample with a fairly uniform intensity. The transmittance and reflectance spectra of films at normal incident condition in the spectral range 250–2500 nm were recorded by a double beam UV-VIS-NIR spectrophotometer (Jasco V 570). The thickness of thin films before and after illumination were analyzed using surface profiler [DEKTAK 6M Stylus Profiler]. The thickness of the film was found to be around 325nm and remained constant before and after illumination. All the measurements were executed at room temperature and the samples were kept in the dark between experiments.

4.2.3. Results and discussion

Figure 4.8 shows the spectral distribution of optical transmittance (T) for as-deposited and illuminated Ge₂₈Sb₁₂Se₆₀ films. It is observed that the optical transmittance decreases with exposure, indicating the occurrence of photodarkening. The change in the width of tail states (E_e) is very small. The parameter E_e is thought to provide

information about the extent of disorder or randomness in amorphous chalcogenide glasses. Absorption in this region is related to the transition between extended states in one band and localized states in the exponential tail of the band; hence disorder here refers more towards that of electronic states within the material as compared to irregularity in atomic arrangement²¹.

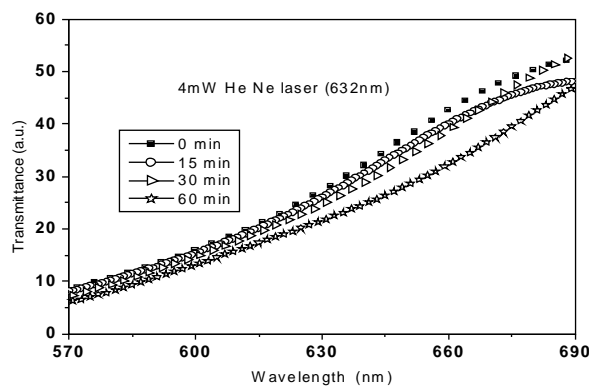


Figure 4.8: Optical transmittance edge of unexposed and exposed $\text{Ge}_{28}\text{Sb}_{12}\text{Se}_{60}$ films using a 4mW He-Ne laser.

Table 4.2: Measured values of bandgap (E_g), width of localised states (E_c) and refractive index (n) under different exposure conditions for $\text{Ge}_{28}\text{Sb}_{12}\text{Se}_{60}$ films.

	Exposure Time (min)	E_g (eV)	E_c (meV)	n
4 mW 633 nm	0	1.66	250	2.67
4 mW 633 nm	15	1.64	298	2.69
4 mW 633 nm	30	1.63	304	2.70
4 mW 633 nm	60	1.59	330	2.72
10 mW 633 nm	30	1.60	346	2.75
20 mW 633 nm	30	1.55	380	3.29
20 mW 810 nm	30	1.57	337	2.83

The optical band gap decreases with the increase in exposure time and laser intensity which may be due to an increase in the density of state in the band gap. The exposure may also create localized states in the band gap. This will lead to a shift in absorption edge towards lower photon energy and consequently decrease in the optical energy gap can be explained by the increased tailing of the conduction band edge into the gap. Our results are in good agreement with the results reported in ^{22,23}. Moreover, optical band gap is in good approximation with WDD parameter E_0 through the relation $E_0 \approx 2 \times E_g$ obtained by Tanaka²⁴. The change in bandgap by exposure with 20mW near bandgap and above band gap shows that photodarkening mechanism is more with above bandgap illumination.

The photoinduced change in the refractive index demonstrated large variation with exposure time, intensity and wavelength. After 30 min exposure, we observed a change of 2.99%, 23.2% and 5.99% in the refractive index of film at 10 mW, 633 nm, 20 mW, 633 nm and 20 mW 810 nm respectively.

The average strength of interband optical transitions and the dispersive energy parameter which is associated with the changes in the structural order of the material is found to change from 29.14 eV without illumination to 9.05 eV for 30 min exposure, using 20 mW Semiconductor laser (810 nm). It is observed that the variation in the transition strength, E_d , results primarily from changes in the nearest neighbor coordination number. So, the decrease in the dispersion

energy value is usually associated with the decrease of coordination number.

The oscillator energy, E_0 , is independent of the scale of dielectric loss and is subsequently the average energy gap. The oscillator energy is found to vary as 3eV to 2.35eV after irradiating with 20mW He-Ne laser. The oscillator energy after irradiating with 20mW Semiconductor laser is found to be 2.47eV.

The nonlinear refractive index (n_2) for unexposed Ge₂₈Se₆₀Sb₁₂ film is 6.69×10^{-10} esu. The n_2 reported for Ge₃₅Sb₅Se₆₀ system² is 8.47×10^{-1} esu and that for Ge₂₈Sb₇Se₆₅ is 7.10×10^{-11} esu. The results show that the thermally evaporated Ge₂₈Se₆₀ Sb₁₂ is having higher n_2 and it is found to increase up to 2×10^{-10} with exposure (633 nm, 20 mW, 30 min).

4.3. Section 3. Studies on Nano colloid Ge₂₈ Sb₁₂Se₆₀ chalcogenide glass

4.3.1. Introduction

Ternary chalcogenide Ge-Sb-Se bulk and thin films have drawn attention for their high non-linear optical properties and compositional dependencies of various properties either within the Ge-Sb-Se glass system⁷⁻⁹. Solution method can be used for making thin films of Ge-Sb-Se. Solution method offers low cost, scalable method for chalcogenide glass thin film production²⁵⁻²⁸. This method has the advantage that the same solutions can be adopted for other precision dispensing techniques such as ink jet or laser direct write²⁸,

giving spatial control over the location of the added material with programmable patterns. In order to retain the attractive optical properties of Ge-Sb-Se glasses while enabling new fabrication routes and hybrid and composite material systems, we have developed a novel technique for the deposition of Ge-Sb-Se based materials through dissolution of bulk glasses in n-butyl amine. The prospect of using solution-based methods offers the opportunity to tightly control film chemistry through control of the solution chemistry. As a first step here we present the structural and optical characterization of the Ge₂₈Se₆₀Sb₁₂ nano colloid solution.

4.3.2. Synthesis of Ge₂₈Se₆₀Sb₁₂ nano colloids

Nano colloid solutions of Ge₂₈Se₆₀Sb₁₂ were prepared by dissolving bulk Ge₂₈Se₆₀Sb₁₂ pieces in n-butyl amine solvent. The bulk glass sample were manually ground into a fine powder to increase the surface area and therefore to shorten the dissolution time. The dissolution was carried out inside a sealed glass container to prevent solvent evaporation. Detailed description of the preparation is given in section 2.1.3. Five different concentrations S₀ =1.2 mg ml⁻¹, S₁ =0.9 mg ml⁻¹ and S₂=0.540 mg ml⁻¹, S₃=0.24 mg ml⁻¹and S₄=0.12 mg ml⁻¹ of Ge₂₈Se₆₀Sb₁₂ were prepared.

4.3.3. Results and discussion

4.3.3. 1. Structural Characterization and absorption spectroscopy

a) Scanning electron microscopy and EDAX

The typical SEM image analysed using JEOL Model JSM - 6390LV for S₀ is presented in Figure 4.9.

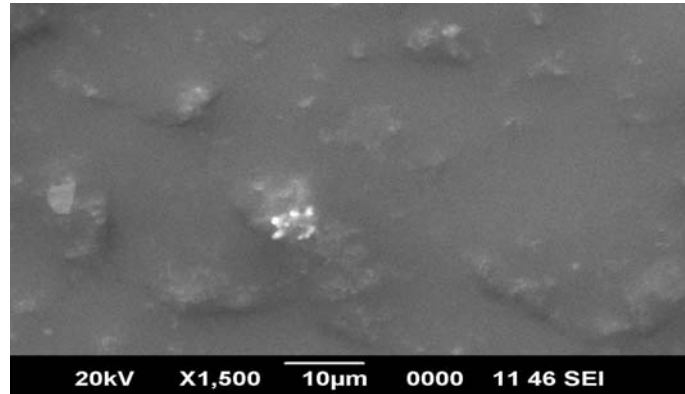


Figure 4.9: SEM image showing the distribution of nanoclusters in the S_0 .

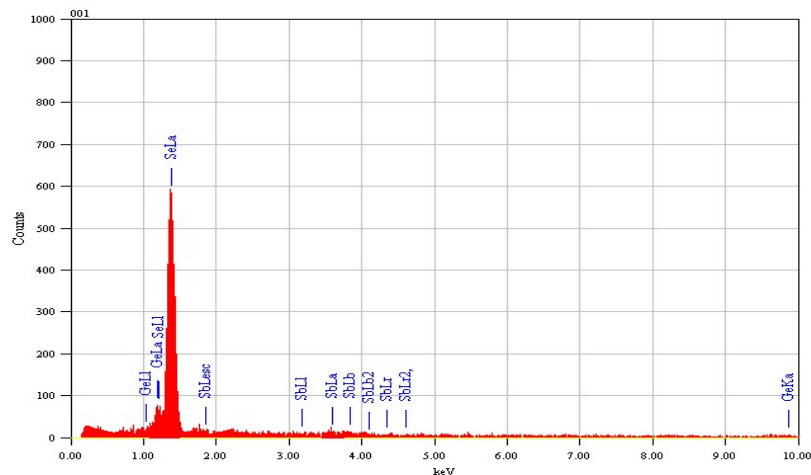


Figure 4.10: EDAX spectrum from a cluster of S_0 .

The SEM picture was taken by spin coating the nano colloid solutions on to a glass slide. The cluster size of spin coated film seems to be large compared to the cluster size in the solution. This can be due to aggregation during solvent evaporation. The EDAX plot of S_0 from a particular cluster given in Figure 4.10 shows the atomic percentage of elements involved in its formation.

b) Absorption spectroscopy

The absorption spectra of Ge₂₈Se₆₀Sb₁₂ nano colloid solutions obtained from spectrophotometer (JascoV-570 UV/VIS/IR) are presented in Figure 4.11. The absorption edge of the nano colloid solutions is located in the 350-550 nm, whereas for bulk semiconductors it is located in the near infrared range. The absorption edge is found to be blue shifted (500-370 nm) with decreasing concentration of ChG. Bulk Ge₂₈Se₆₀Sb₁₂ ChG glass is having bandgap 1.46 eV. The variation in the bandgap of the nano colloid solution is tabulated in Table 4.3.

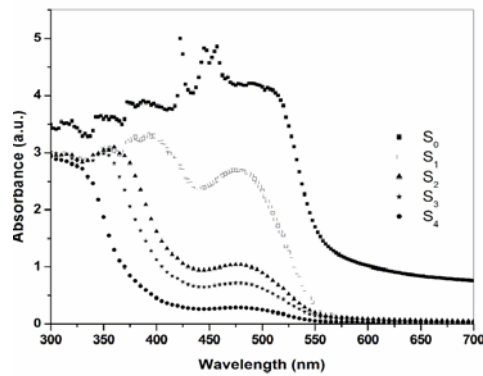


Figure 4.11: Absorption spectra of Ge₂₈Se₆₀Sb₁₂ nano colloids with different concentrations ($S_0=1.2$ mg ml⁻¹, $S_1=0.9$ mg ml⁻¹ and $S_2=0.540$ mg ml⁻¹, $S_3=0.24$ mg ml⁻¹ and $S_4=0.12$ mg ml⁻¹).

Table 4.3: Measured values of optical band gap (E_g) for Ge₂₈Se₆₀ Sb₁₂ nano colloids with different concentration.

Samples	Band gap (eV)
S_0	2.12
S_1	2.36
S_2	2.81
S_3	2.93
S_4	3.27

The slope of the absorption edge characterizes the width of the localized states which in turn indicates the ordering of the structure. It is believed that the charged defects exist in the bandgap²⁸ and the localized states and around the bandgap.

4.3.3.2. Photoluminescence from nano colloid $\text{Ge}_{28}\text{Se}_{60}\text{Sb}_{12}$ ChG

a) Excitation wavelength dependent PL studies

Due to the bandgap states in chalcogenide glasses the optical transitions such as photoluminescence (PL) and the optical absorption process are complicated^{29,30}. Confocal microscopic images of S_0 shown Figure 4.12 it corresponds to the photoluminescence image from each clusters.

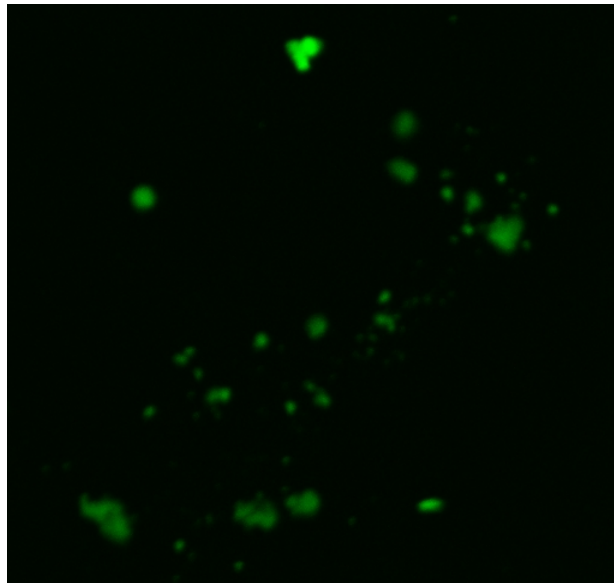
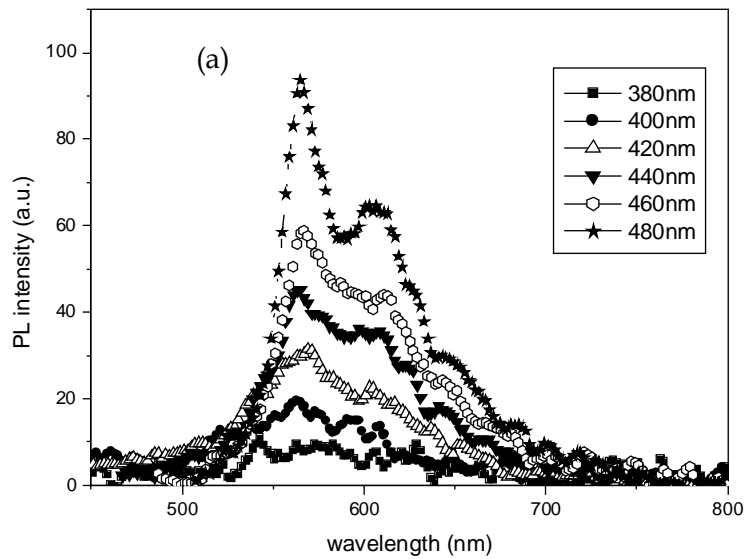


Figure 4.12: Confocal microscope image showing the emission from the $\text{Ge}_{28}\text{Se}_{60}\text{Sb}_{12}$ nano colloid chalcogenide glass clusters at an excitation with 484nm.

The PL measurements were recorded using a Cary Eclipse fluorescence spectrophotometer (VARIAN). The excitation wavelength depended change in PL for S_2 is shown in Figure 4.13. Figure 4.13 (a) represents the emission spectrum corresponding to the excitation from 380 nm to 480 nm. Figure 4.133 (b) represents the emission spectrum corresponding to the excitation from 500 nm to 600 nm. From the figure it is clear that up to 460 nm excitation the emission spectrum is broad. A strong electron phonon coupling distorts the lattice near the trapped hole and this interaction may be responsible for the broadness of the luminescence band²⁹.



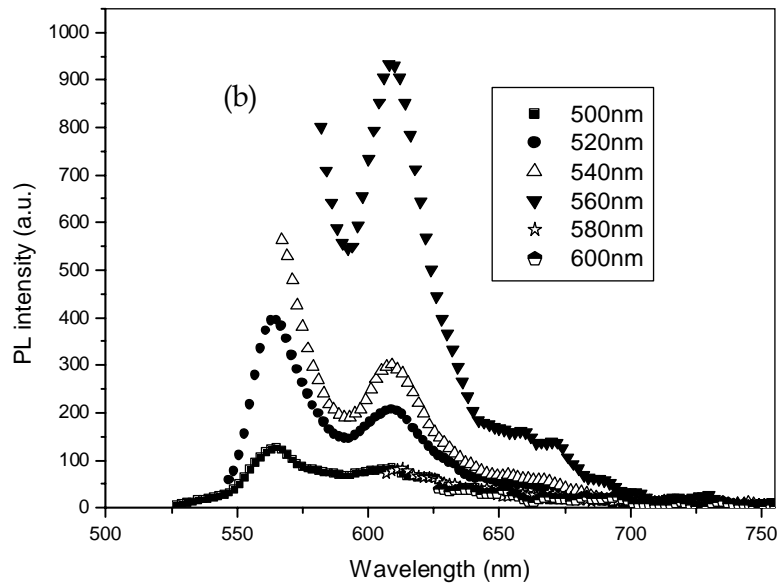
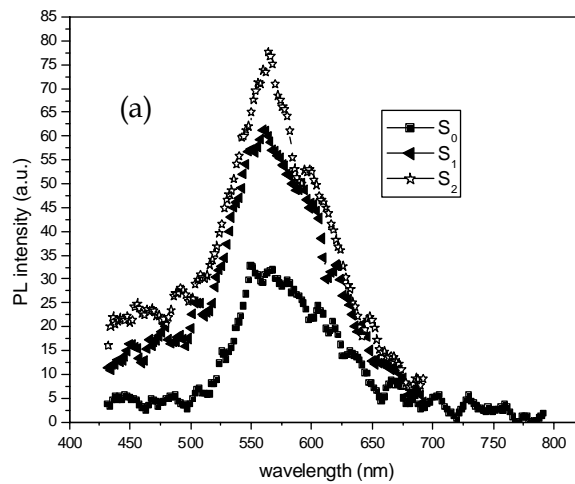


Figure 4.13: Excitation wavelength dependent luminescence behaviour for S₂ on excitation with a) 380 nm to 480 nm b) 500 nm to 600 nm.



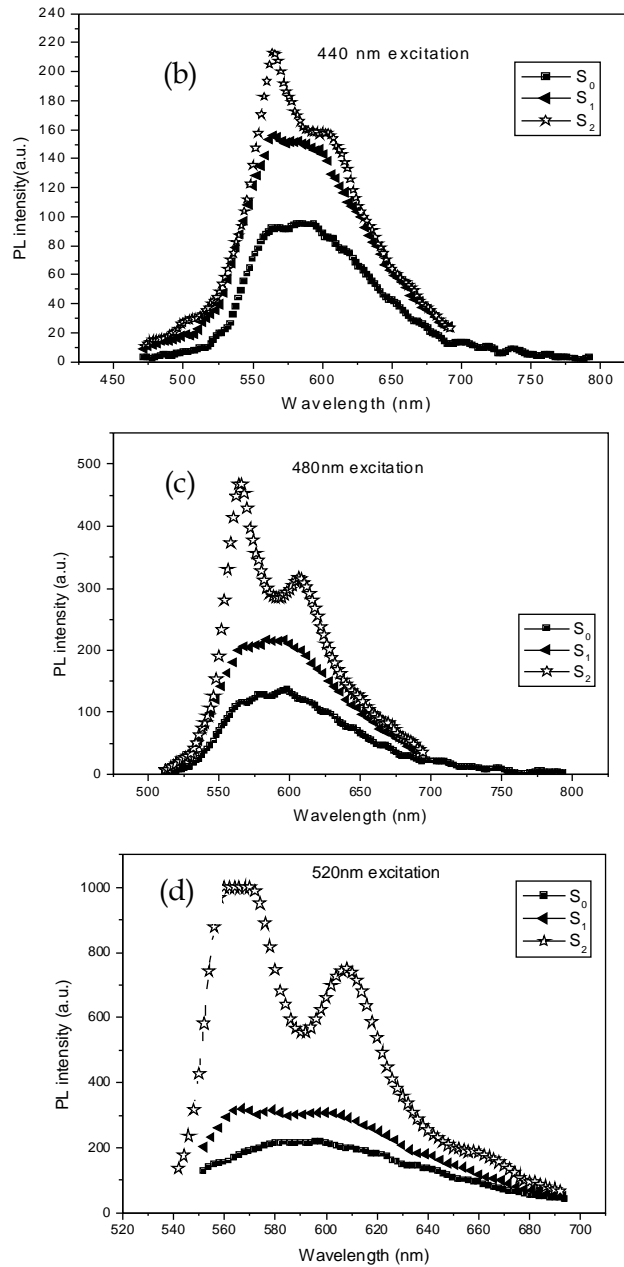


Figure 4.14: Cluster size dependent PL spectra for S_0 , S_1 , S_2 at an excitation of a) 400nm, b) 440nm, c) 480nm and d) 520nm.

From the Figure 4.13 it is clear that at 440 nm excitation there exists a peak at 566 nm and a shoulder at 608 nm. After 440 nm excitation the shoulder at 608 nm enhances up to an excitation of 560 nm. At 560 nm excitation the emission peaks at 566nm and 608nm is of same intensity. The cluster size dependent change in emission characteristics for four different excitation wavelengths is shown in Figure 4.14. At 400nm excitation S_0 , S_1 and S_2 is having emission peak at 566 nm. In the case of 440 nm and 480 nm excitation, S_2 is showing double peak at 566 nm and 608 nm. At 520 nm excitation S_2 is shows a shoulder at 655 nm in addition to the peaks at 566 nm and 608 nm. These charged defects, which have energy levels in the bandgap with a spectral bandwidth ΔE , are responsible for the PL in chalcogenide glasses³⁰.

The potential advantage shown by the $\text{Ge}_{28}\text{Se}_{60}\text{Sb}_{12}$ nano colloid chalcogenide glass solutions is that it possesses strong photoluminescence in the visible region which can be attributed to the quantum size effect. The photoluminescence intensity of nano colloidal solutions of $\text{Ge}_{28}\text{Se}_{60}\text{Sb}_{12}$ glass change almost in proportion to changes to bandgap which in turn is related to the cluster size. Another important observation is that depending upon the cluster size the peak at 608nm enhances. The studies show that nano colloidal solutions of $\text{Ge}_{28}\text{Se}_{60}\text{Sb}_{12}$ glass are promising candidates for light-emitting devices, optoelectronic devices and other photonic devices.

b) Laser induced PL in nano colloid $\text{Ge}_{28}\text{Se}_{60}\text{Sb}_{12}$ ChG

The laser induced emission studies were carried out using a 7 ns pulses from a frequency doubled Nd:YAG laser (532 nm, 10 Hz). A set of calibrated neutral density filters was used for varying the pump energy. The pump energy was varied from 2.2 mW to 30 mW. The beam was focused using a cylindrical lens of focal length 8cm. The emission from the sample was collected by a fiber and directed to a 0.5 m spectrograph (SpectraPro-500i) coupled with a cooled CCD array.

Luminescence studies carried out for the solutions using Nd:YAG laser beam is presented in Figure 4.15. The samples show strong luminescence peak at 595 nm and 645nm. As the cluster size increases the nonlinear absorption coefficient increases which results in greater PL intensity. The cluster size dependence on the nonlinear absorption coefficient is discussed in coming section. Two photon absorption is usually regarded as the third order nonlinear optical process although the intensity of two photon absorption depends quadratically upon the intensity of incident excitation light³². The two photon absorption coefficient (β) for the colloid solutions S_0 , S_1 and S_2 were measured by us using the open aperture z- scan technique at 532nm. Measured β for the S_0, S_1, S_2 at a laser (Nd:YAG, 532nm) power of 178W/m² are 17.92 cm/GW, 11.43 cm/GW, 5.26 cm/GW respectively. Applying a semiconductor concept, it has been shown that nonlinear properties become greater in the materials with smaller optical gaps.

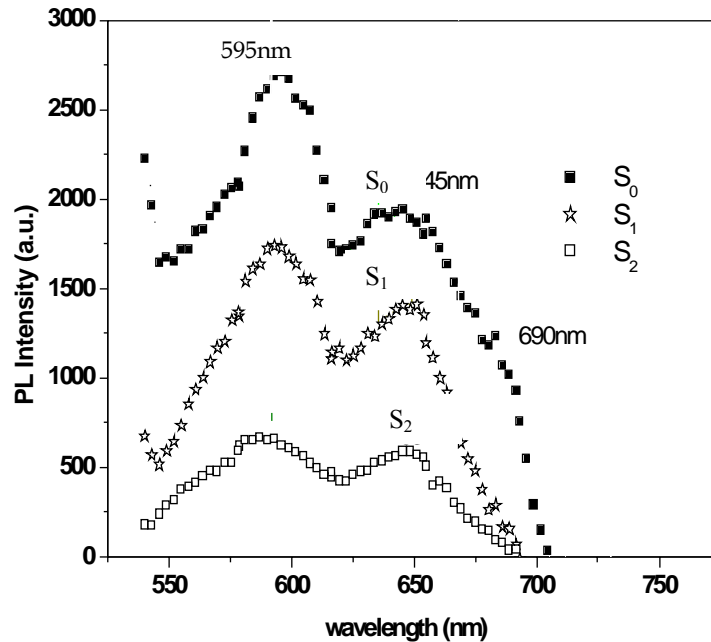


Figure 4.15: Cluster size dependent PL spectra for S_0 , S_1 , S_2 at an excitation 532 nm, Nd: YAG laser.

Our observations also support this result showing an increase in nonlinear absorption with lowering of band gap. As the concentration is increased there will be enhancement in the cluster size resulting in a larger magnitude of optical nonlinear interaction between radiations and the sample.

In order to check the origin of the emission peak the studies were carried out at different laser intensities. The exciting laser intensity dependent change in photoluminescence intensity for S_0 is shown in Figure 4.16. The observed PL is investigated by plotting the logarithm of PL intensity versus the logarithm of laser intensity as

shown in Figure 4.17. The plot obeys the square law dependence where the slope is about 1.94. This confirms that the absorption is a typical two photon process at the excitation wavelength of 532nm.

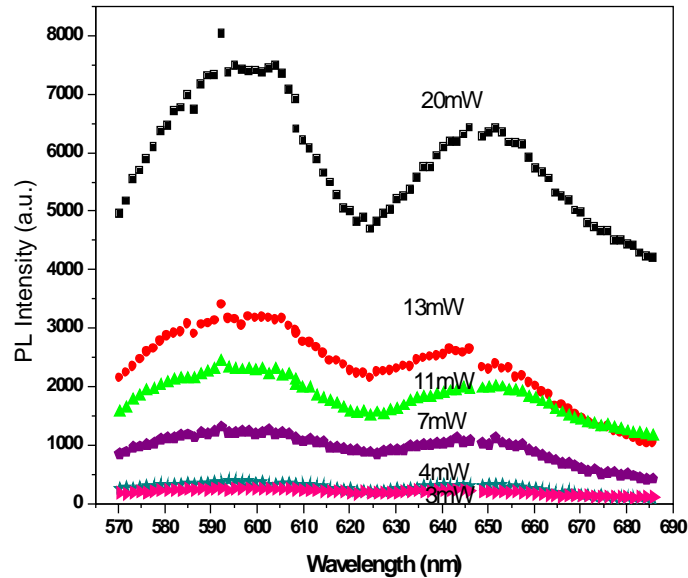


Figure 4.16: PL spectra for S_0 at different laser powers.

Luminescence peak at 595 nm and 645 nm shows quadratic dependence on laser intensity. Two-photon absorption is assumed to be a resonant process involving levels midway between the valence and conduction bands³¹. At large intensities the intermediate state becomes almost filled, with absorption dominating over transitions back to the valence band.

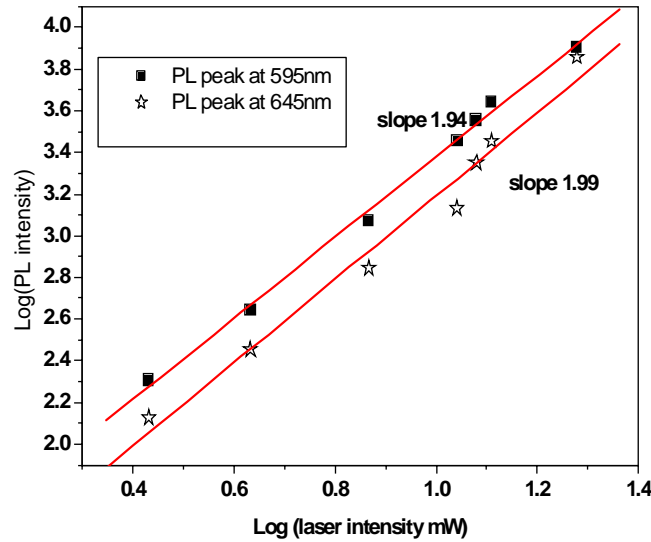


Figure 4.17: Quadratic dependence of luminescence intensity on the excitation powers at 532 nm.

These strong two photon induced photoluminescence signals can be used to image molecularly targeted colloids for cancer cells in vitro and to image biological samples^{32, 33}.

4.3.3.3. Thermal diffusivity of $\text{Ge}_{28}\text{Se}_{60}\text{Sb}_{12}$ ChG nano colloids

Properly designed Thermal Lens technique was used to study the measure the heat transfer through diffusion in $\text{Ge}_{28}\text{Se}_{60}\text{Sb}_{12}$ nano colloid solutions. In the technique as discussed in section 2.2.5, a point heat source is generated by laser and the essential idea is to indirectly measure the speed of heat dissipation^{34,35}. Thermal diffusivity values obtained from the thermal lens studies on the nano colloids are tabulated in Table 4.4.

Table 4.4: Measured values of thermal diffusivity (T_D) for Ge₂₈Se₆₀ Sb₁₂ nano colloid with different cluster size

Samples	$T_D * 10^4 \text{ cm}^2/\text{s}$
S ₀	1.07
S ₁	1.35
S ₂	1.89
S ₃	2.55
S ₄	3.04

Studies show that the thermal diffusivity varies with the concentration. Thermal energy formation is mainly due to non radiative recombination and neutral defects play an important role in non-radiative recombination centers. An increase in the number of neutral defects, D^0 results in an increase in non radiative recombination centers. Finite frequency modes/frequency due to defects gives rise to scattering of thermal waves by the phonon mode causing reduction in thermal diffusivity³⁶. A theoretical model based on the Brownian motion of the nanoparticles was also proposed by some researchers to describe the heat transfer performance of nanofluids³⁶.

4.3.3.4 Non Linear Optical studies on Ge₂₈Se₆₀ Sb₁₂ nano colloids.

The change in optical parameters with concentration can also lead to variations in their nonlinear optical characteristics. So considering the importance of the nonlinear absorption studies, the open aperture z- scan was done using the standard z-scan technique at 532 nm. Figure 4.18 presents the results of normalized

transmittance measurements as a function of the position of the nano colloid solution in the open aperture scheme.

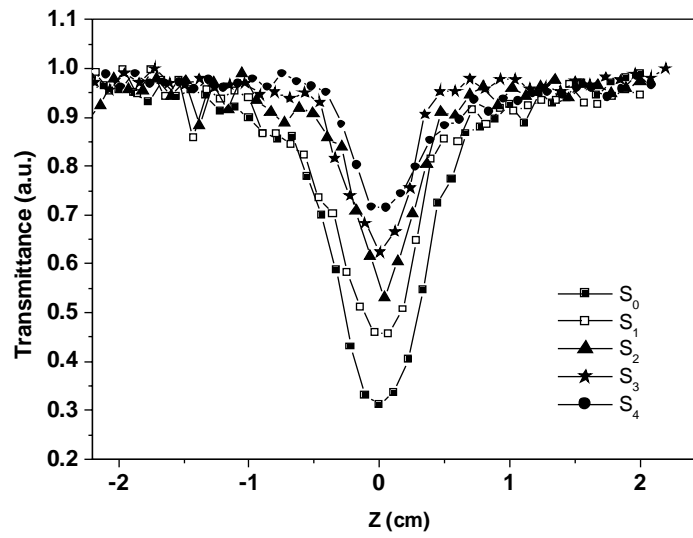


Figure 4.18: Normalized transmittance as a function of the position for different concentration $S_0=1.2 \text{ mgml}^{-1}$, $S_1=0.9 \text{ mgml}^{-1}$, $S_2=0.540 \text{ mgml}^{-1}$, $S_3=0.24 \text{ mgml}^{-1}$ and $S_4=0.12 \text{ mgml}^{-1}$ in the open aperture scheme at 532 nm with laser power of 571 W/m^2 .

The theory of two photon absorption (TPA) processes fitted well with the experimental curve and two photons of 532 nm radiation lie below the absorption band-edge of the sample under investigation. This confirms that TPA is the basic mechanism involved in the nonlinear absorption process. From these fits, the β values were calculated for S_0, S_1, S_2, S_3 and S_4 . The obtained values of nonlinear absorption coefficient at different laser intensities for colloid solutions with different concentrations are tabulated in Table

4.5. As in the case of nonlinear absorption, the experimental investigations of the optical limiting in samples were performed using open aperture Z Scan.

The z-scan curve demonstrates a strong nonlinear absorption that is regarded as the reverse saturable absorption for the absorption at 532 nm. As shown in Figure 4.11, this wavelength is close to that of the absorption cut-off, so the repetition rate 10Hz can avoid the influence of the accumulative thermal changes which can change the refractive index at high intensity laser beam at 532nm.

The nonlinearity in semiconductors is determined completely by E_g . β is strongly dependent³³ upon E_g as $\beta \propto 1/(E_g)^3$ and our result are also in good agreement with this. Measured value of β for S_0 is of the order of 17.9 cm/GW at 178 W/m² laser fluence and 6.2 cm/GW at 571 W/m². The decrease in β by increase in laser fluence can be due to the removal of an appreciable fraction of photo carriers from the ground state²⁸. S_4 is having a nonlinear absorption coefficient of 0.9 cm/GW at a laser fluence of 571 W/m². To be considered as a good candidate for ultrafast optical switch, the material should have small value of β ³³. L. Petit et al.³⁷ has recently reported the compositional dependence on the nonlinear absorption coefficient (β) of the bulk Ge-Sb-Se chalcogenide glasses. Ge₂₈Sb₇₅Se₆₅ glass is reported to have a nonlinear absorption coefficient of 4.9 cm/GW. The nonlinear absorption coefficient of the prepared nano colloid samples are in the same order as that of the bulk glasses. We were able to tune β from 6.2cm/GW to 0.9 cm/GW by simply varying the

concentration of $\text{Ge}_{28}\text{Sb}_{12}\text{Se}_{60}$ in the butylamine from 1.2 mg ml^{-1} to 0.12 mg ml^{-1} .

Table 4.5: Measured values of bandgap (E_g) and nonlinear absorption coefficient (β) at wavelength of 532nm for different irradiation intensity.

Sample	Bandgap (eV)	β (cm/GW)				
		178	267	357 (W/m ²)	500	571
S ₀	2.19	17.92	12.43	8.90	6.91	6.24
S ₁	2.36	11.34	8.52	6.62	5.14	4.35
S ₂	2.81	5.26	2.70	5.01	4.03	3.84
S ₃	2.93	-	-	-	3.25	2.16
S ₄	3.27	-	-	-	1.15	0.90

Figure 4.19 illustrates the influence of nano colloid composition on the optical limiting response. The limiting threshold is different for different samples as shown in figure. Optical limiting results for cluster size dependent nonlinear optical (NLO) properties of samples presented in Figure 4.19 clearly shows the variation in the fluence value corresponding to the onset of optical limiting threshold. The largest limiting is observed in S₀. It can be seen that with the progressive red shift of the absorption edge, i.e., the increase of cluster size, the degree of optical limiting is enhanced and the limiting threshold is reduced. Larger particles have better optical limiting performance. The reverse saturable absorption, which is generally associated with a large cross section of absorption from

excited levels, brings about optical limiting effects in colloidal solutions³⁸.

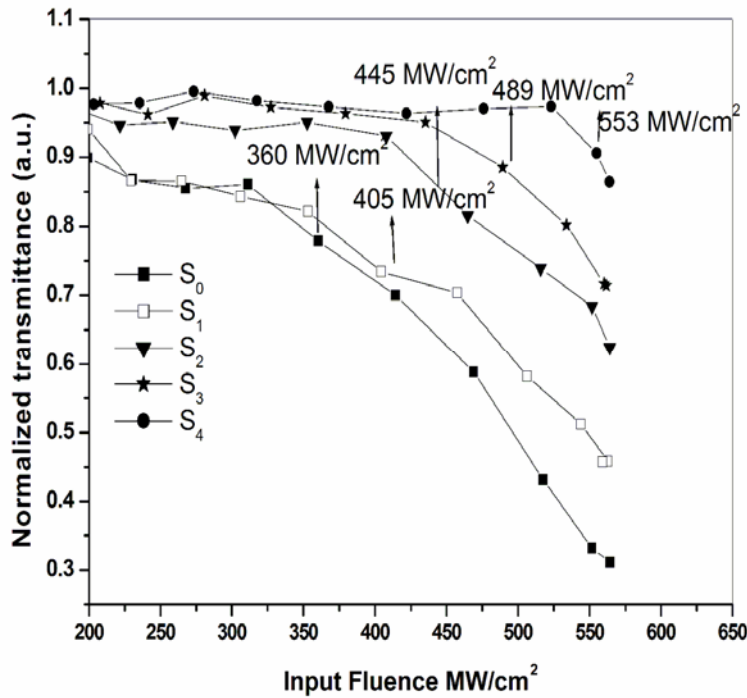


Figure 4.19: Optical limiting response of S_0 , S_1 , S_2 , S_3 and S_4 at 532 nm at an input power density of 571 MW/cm².

In this case, the optical limiting is due to two-photon absorption. This property is desirable for protection of sensors and human eyes from being affected by intense laser radiation. It occurs when the optical transmission in a material decreases with increasing laser fluence³⁸. Therefore it is important to determine the magnitude of the nonlinearity of materials to select suitable materials as optical limiting media.

4.4. Section 4: $\text{Ge}_{28}\text{Se}_{60}\text{Sb}_{12}$ /PVA nano composite films for photonic applications

4.4.1. Introduction

Solution-derived thin films in the chalcogenide system are shown to possess similar molecular structure to the parent bulk glass, and vacuum heat treatment allows the preservation of IR transparency through the removal of residual organics. Chalcogenide glass-polymer hybrid materials may be created through the incorporation of compatible polymers in the co solution phase. It is shown that it is possible to tune the optical and mechanical properties of these coatings by tailoring the glass chemistry/polymer content over a broad range, important for applications in IR optical coatings and as interfacial materials where thermal and mechanical property matching is critical³⁹. This technique was shown to be a promising route towards the preparation of novel IR optical materials and structures.

4.4.2. Experimental

The composite films were obtained from the solution of $\text{Ge}_{28}\text{Se}_{60}\text{Sb}_{12}$ glasses and polyvinyl alcohol (PVA) $[-\text{CH}_2\text{CH}(\text{OH})-]_n$ in different proportions. The concentrations of the ChG in the colloid solutions are as follows 1.2 mg/ml, 0.9 mg/ml and 0.24 mg/ml for S_1 , S_2 and S_3 respectively. The films were prepared from the homogeneous solutions of different concentrations by drop casting method. The composite films were made from these nano colloid solution and PVA in the ratio 1:1.

The thickness of the films was measured using Metutoyo, Micrometer (series 193). The Atomic Force Microscope (AFM) images of Ge₂₈Se₆₀Sb₁₂/PVA composite films surfaces were recorded using an Atomic Force Microscope (Veeco, Nanoscope III, made by Digital Instruments Inc., USA). In order to characterize the prepared thin film composites; the optical absorption for different film composition of the chalcogenide glass /polymer was investigated. The optical transmission spectra and reflection spectra have been recorded by using a spectrophotometer (JascoV-570 UV/VIS/IR). Transmission and reflection spectra have been used for the study of optical properties. The dispersion of refractive index has been studied using the Wemple–Di Domenico (WDD) single oscillator model. Some important parameters (dielectric constant, dielectric loss, optical conductivity etc) have also been determined using n , k and absorption coefficient (α). Generalized Miller's rule and linear refractive index were used to find the nonlinear susceptibility and non linear refractive index of thin films.

4.4.3. Results and Discussion

4.4.3.1. Optical parameters

The transmission spectra of the chalcogenide glass/composite films with different concentrations are presented in Figure 4.20. The composite films are transparent in the visible range compared to thermally evaporated thin film. It is clear from Figure 4.20 that as the concentration of the Ge₂₈Se₆₀Sb₁₂ component in the polymer composition decreases the absorption edge gets shifted towards the short wavelength side.

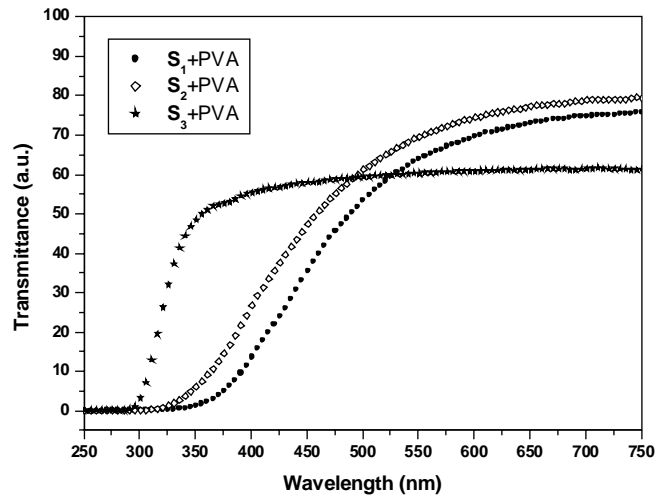


Figure 4.20: Transmission curves of $\text{Ge}_{28}\text{Sb}_{12}\text{Se}_{60}$ /PVA composite films S_1 +PVA, S_2 +PVA, S_3 +PVA.

The importance of this feature is related to the possibility to move the spectral range of photosensitivity of amorphous composites from ultraviolet to infrared⁴⁰.

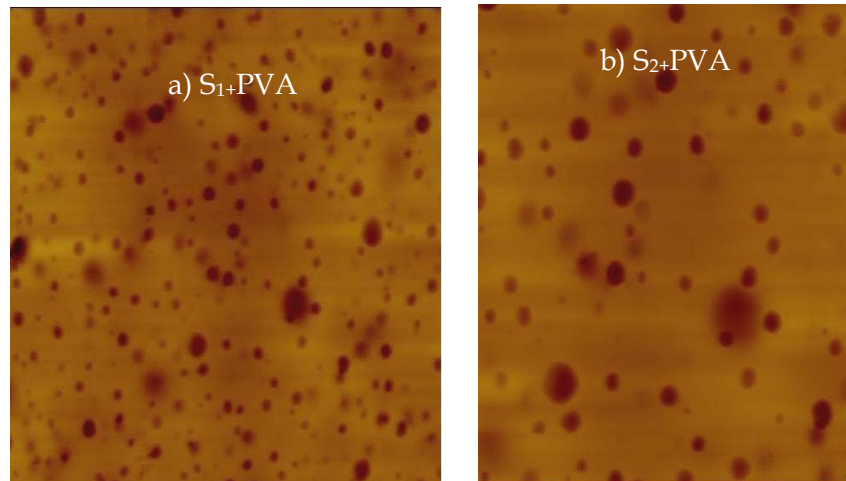


Figure 4.21: AFM images showing the distribution of nano clusters in the composite films (a) S_1 +PVA, (b) S_2 +PVA.

AFM image of the composite films for S_1 +PVA and S_2 +PVA are presented in Figure 4.21. The AFM scans confirm the existence of the chalcogenide nano clusters in the prepared films. The optical energy gap (E_g) of the thin films has been determined from absorption coefficient data as a function of photon energy. From the linear plots of $(\alpha h\nu)^{1/2}$ against $(h\nu)$ for these samples as shown in Figure 4.22, the optical energy gap has been determined from the intercepts of extrapolations to zero with the photon energy axis $(\alpha h\nu)^{1/2} \rightarrow 0$ (i.e. Tauc extrapolation). From the results obtained, it is seen that an increase of concentration of $\text{Ge}_{28}\text{Sb}_{12}\text{Se}_{60}$ in the system leads to a decrease in the optical band gap. It shows that it is possible to tune the optical properties of the thin film by varying the concentration of nano colloid solution used for casting the films.

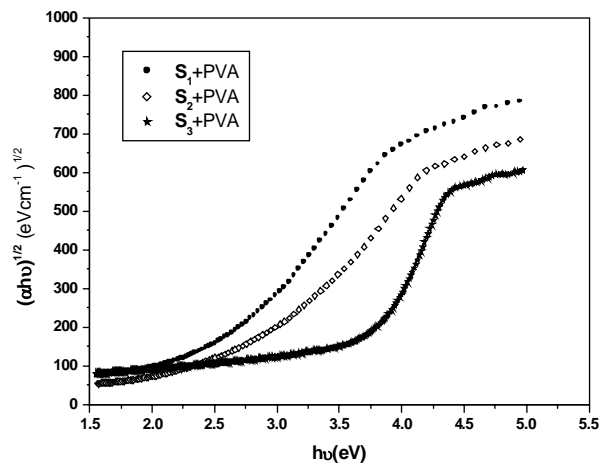


Figure 4.22: Plot of $(\alpha h\nu)^{1/2}$ against $(h\nu)$ for $\text{Ge}_{28}\text{Se}_{60}\text{Sb}_{12}$ /PVA composite films with three different concentrations.

Table 4.6: Values of optical energy gap (E_g), width of the tails of localized states in the band gap (E_e), refractiveindex (n) (at 1000nm), dielectric constant (ϵ_r) (at 1000nm) and dielectric loss (ϵ_i) (at 1000nm) for $\text{Ge}_{28}\text{Se}_{60}\text{Sb}_{12}$ / PVA composite films .

Sample	E_g (eV)	E_e (meV)	n	ϵ_r	ϵ_i $\times 10^{-5}$
S ₁ +PVA	2.51	543	1.74	3.00	42
S ₂ +PVA	2.74	477	1.72	2.97	33
S ₃ +PVA	3.56	200	1.66	2.80	16

The grainy surface pattern was found to be related to the cluster size of the dissolved chalcogenide material in the parent solution and as the grain size increases the band gap decreases. It is found that as the concentration of the chalcogenide decreases the band gap gets blue shifted. The the slope of absorption spectra also changes with the concentration. The values of width of the localized states (E_e) obtained for the different compositions are listed in Table 4.6. The width of the localized states for $\text{Ge}_{28}\text{Se}_{60}\text{Sb}_{12}$ /PVA composite films is found to decrease with decrease in concentration which shows the ordering of the structure. The extinction coefficient (k) and refractive index (n) which are important parameters characterising photonic materials has been calculated as discussed in section 2.2.4. Values of n and k calculated from transmission and reflection spectra using the relation are also tabulated in Table 4.6. The extinction coefficient decreases with an increase in wavelength which shows the fraction of light lost due to scattering. The high refractive index values of these glasses are advantageous for strong optical

confinement and enhance the optical intensities for nonlinear interactions.

The optical response of a material studied in terms of the optical conductivity, the dielectric constant (ϵ_r) and dielectric loss (ϵ_i) have been determined and are given in Table 4.6. The dispersion parameters, effective oscillator energy (E_0), dispersion energy (E_d), static refractive index (n_0) oscillator strength, f ($f = E_0 E_d$), the static dielectric constant, ϵ_∞ ($\epsilon_\infty = n_0^2$), non linear refractive index (n_2) and susceptibility ($\chi^{(3)}$) are tabulated in Table 4.7.

Table 4.7: The effective oscillator energy (E_0), dispersion energy (E_d), static refractive index (n_0), oscillator strength (f), static dielectric constant (ϵ_∞), non linear susceptibility ($\chi^{(3)}$) and non linear refractive index (n_2) for Ge₂₈Se₆₀Sb₁₂/PVA films.

Sample	E_0 (eV)	E_d (eV)	n_0	f (eV) ²	ϵ_∞	$\chi^{(3)}$ *10 ⁻¹³ (esu)	n_2 *10 ⁻¹² (esu)
S ₁ +PVA	3.81	7.94	1.76	30.30	3.08	1.29	2.76
S ₂ +PVA	4.67	9.31	1.72	43.43	2.99	1.07	2.35
S ₃ +PVA	6.57	12.48	1.70	81.97	2.90	0.89	1.97

It is found that depending on the band gap the nonlinear refractive index of the investigated films also changes. The addition of inorganic semiconductor into the polymer results in fabrication of new composite films with low cost. The investigated new composites are prospective for different photonic devices and for nonlinear optical applications³³.

4.4.3.2 .NLO studies on $\text{Ge}_{28}\text{Se}_{60}\text{Sb}_{12}/\text{PVA}$ composite films

The technique of open-aperture z-scan scheme was employed to study the nonlinear optical properties of the system. In order to ensure that no permanent photoinduced change has occurred to the sample during laser irradiation, we have repeated the experiment by illuminating the sample on the same position. Under the experimental conditions, laser beam illumination at 532 nm usually corresponds to the two-photon absorption process because the photon energy of the 532 nm laser is within the range $E_g < 2h\nu < 2E_g$ where $h\nu = 2.33$ eV and the optical band gap is 2.51 eV, 2.74 eV, 3.56 eV for $S_1 + \text{PVA}$, $S_2 + \text{PVA}$, $S_3 + \text{PVA}$ respectively. Z-scan traces were made for three different concentrations of thin films with four different input power densities. The z-scan traces for a laser power density of 536 MWcm^{-2} are shown in Figure 4.23. In semiconductors, it has been shown that nonlinear properties become greater in the materials with smaller optical gaps³³. It is reported that the nonlinear absorption coefficient is determined completely by bandgap. β depend inversely on $(E_g)^3$. Our observations also shows an increase in nonlinear absorption with lowering of band gap.

The experimental data shows the best fit for two photon absorption confirming that TPA may be the basic mechanism involved in the nonlinear absorption process. From these fits, the β values were calculated and are plotted against input power density in Figure 4.24. For samples $S_1 + \text{PVA}$, $S_2 + \text{PVA}$ and $S_3 + \text{PVA}$ the measured values of β decrease with increasing input intensity due to the removal of an

appreciable fraction of photo carriers from the ground state⁴¹. Thus, when the incident intensity exceeds the saturation intensity, the nonlinear absorption coefficient of the medium decreases.

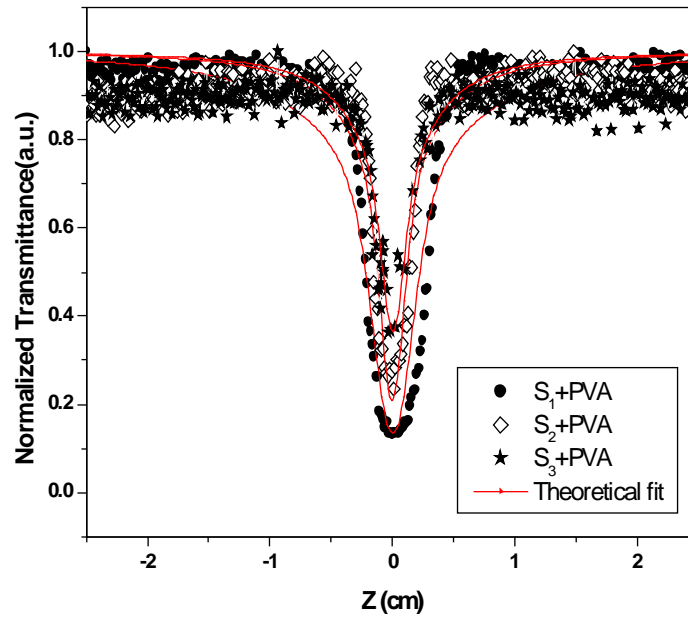


Figure 4.23: Normalized transmittance as a function of the position for $S_1 + \text{PVA}$, $S_2 + \text{PVA}$ and $S_3 + \text{PVA}$ in the open-aperture scheme at 532 nm for a laser power density of 536 MW cm^{-2} . The solid line shows the theoretical fit.

The imaginary part of the third-order susceptibility, $\text{Im } \chi^3$, is related through the equation linear refractive index of films, permittivity of free space, velocity of light in vacuum and wavelength of radiation used. The nonlinear absorption coefficient, β is tabulated in Table 4.8.

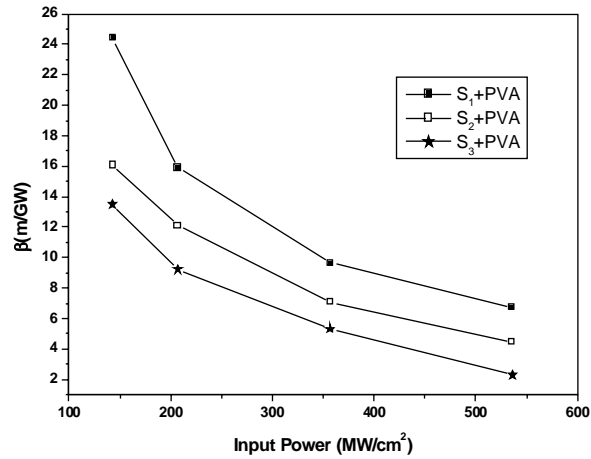


Figure 4.24: Dependence of nonlinear absorption coefficient on input power density.

Table 4.8: Measured values of optical bandgap and imaginary part of the third-order susceptibility ($\text{Im}\chi^3$) at a wavelength of 532 nm for different irradiation intensity.

Sample	E_g (eV)	$\text{Im}\chi^3 \cdot 10^{-9}$ (m ² /GV ²)			
		143	207	357	536
S ₁ +PVA	2.51	8.31	5.41	3.28	2.29
S ₂ +PVA	2.74	5.35	4.03	2.35	1.48
S ₃ +PVA	3.56	4.12	2.86	1.65	0.71

Optical limiting studies show that the $\text{Ge}_{28}\text{Se}_{60}\text{Sb}_{12}/\text{PVA}$ composite film can be considered as almost non-investigated possible applicants for optical limiting. The optical limiting response has been studied from the Z scan data for three concentrations with different powers. The Figure 4.25 represents the limiting response of S₁+PVA, S₂+PVA and S₃+PVA at an input power density of 536 MW/cm². The arrow in the figure indicates the approximate fluence at which the normalized transmission begins to deviate from linearity.

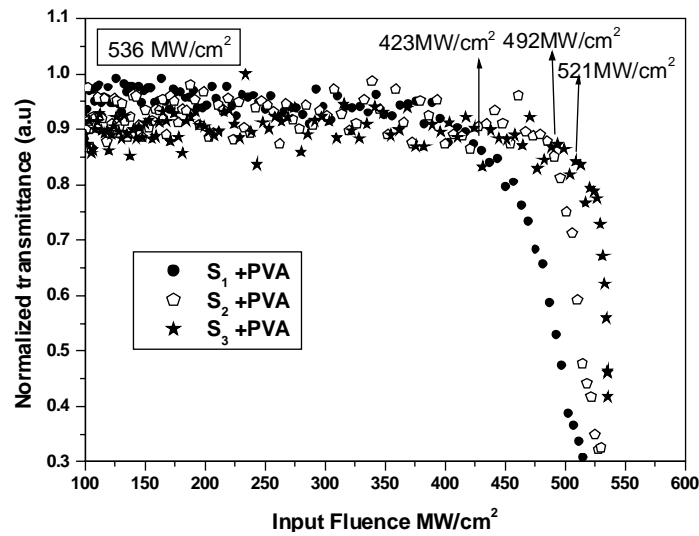


Figure 4.25: Optical limiting response of $\text{Ge}_{28}\text{Se}_{60}\text{Sb}_{12}/\text{PVA}$ composite films at 532 nm.

Table 4.9: Measured values of optical limiting threshold for $\text{Ge}_{28}\text{Se}_{60}\text{Sb}_{12}/\text{PVA}$ composite films at a wavelength of 532nm with different irradiation intensity.

Sample	Optical limiting threshold at			
	143	207	357	536
	(MW/cm ²)			
$\text{S}_1 + \text{PVA}$	119	150	305	423
$\text{S}_2 + \text{PVA}$	131	161	318	492
$\text{S}_3 + \text{PVA}$	140	184	336	521

The limiting threshold at different laser intensities is tabulated in Table 4.9. As given in the table, the nonlinear response of the medium depends on both pump power as well as the concentration. The larger magnitude of optical nonlinear interaction with increasing concentration of $\text{Ge}_{28}\text{Se}_{60}\text{Sb}_{12}$ can be attributed to the enhancement in

the grain size. This results in a lowering of the optical limiting threshold thereby enhancing the optical limiting performance⁴¹. Thus cluster size of the parent solution has a significant effect on the performance of samples as optical limiters.

4.5. Conclusions

- ✓ *The $\text{Ge}_{28}\text{Sb}_{12}\text{Se}_{60}$ bulk sample prepared by melt quenching was found to be amorphous in nature by XRD analysis.*
- ✓ *The optical constants of $\text{Ge}_{28}\text{Sb}_{12}\text{Se}_{60}$ thin films were calculated from the transmission spectra and reflection spectra using Swanepoel method. The optical parameters, refractive index (n) and extinction coefficient (k) have been calculated in the wavelength range 700–2000 nm by analysing the transmission spectrum. The dispersion of the refractive index is described in terms of a Wemple–Di Domenico single oscillator model.*
- ✓ *The photo induced studies on the $\text{Ge}_{28}\text{Sb}_{12}\text{Se}_{60}$ thin films shows that there is a power, wavelength and duration of laser radiation dependent shift in the band gap and refractive index resulting due to photodarkening.*
- ✓ *Nano colloids of $\text{Ge}_{28}\text{Sb}_{12}\text{Se}_{60}$ were prepared and characterized. The absorption edge and the slope shifts with respect to the concentration of the $\text{Ge}_{28}\text{Sb}_{12}\text{Se}_{60}$ glass in the nano colloid solutions. The band gap gets blue shifted with decrease in $\text{Ge}_{28}\text{Sb}_{12}\text{Se}_{60}$ concentration.*
- ✓ *The z-scan spectra reveal a strong non linear absorption (reverse saturable absorption) for the nano colloid $\text{Ge}_{28}\text{Sb}_{12}\text{Se}_{60}$ solutions. Observation of optical limiting at excitation wavelength suggests the potential of these materials to be used as optical limiters.*

- ✓ New Ge₂₈Sb₁₂Se₆₀/PVA composite films were synthesised and investigated. The optical energy gap has been estimated using the Tauc method. The energy gap of the films were found to depend on grain size which is inversely proportional to concentration of the colloidal solution used.
- ✓ Nonlinear response of Ge₂₈Sb₁₂Se₆₀/PVA samples studied using nanosecond laser pulses show high nonlinearity exhibiting reverse saturable absorption.

4.6. References

1. Dr. A. Ray Hilton, "Chalcogenide Glasses for Infrared Optics", McGraw-Hill Companies, Inc. (2010).
2. J. A. Savage, P. J. Webber and A. M. Pitt, "An assessment of Ge-Sb-Se glasses 8 to 12 μ m infra-red optical materials", Journal of Material Science ., 13, 859-864 (1978).
3. A.H. Moharram, "Structural and optical properties of Ge₂₀Sb_xSe_{80-x} films", Applied Physics A., 66, 515-519 (1998).
4. S M El-Sayed, "Far-infrared studies of the amorphous Sb_xGe_{28-x}Se₇₂ glassy semiconductor", Semiconductor Science Technology., 18, 337-341(2003).
5. P. Klocek, M. Roth and R.D. Rock, "Chalcogenide Glass Optical Fibers and Image Bundles: Properties and Applications," Optics Engineering., 26, 88 (1987).
6. R.M. Mehra, Rajesh Kumar and P.C. Mathur, "Electrical and optical properties of Ge₂₀Sb_xSe_{80-x} thin films", Thin Solid Films., 170, 15-26(1989).
7. A. Ganjoo, H. Jain, S.Khalid and C. G. Pantano, "Structural modification of Ge-Se amorphous films with the addition of Sb", Philosophical Magazine Letters., 85, 503-512 (2005).
8. A. Srinivasan, K. N. Madhuoodanan, E. S. R Gopal and J. Philip, "Observation of threshold behaviour in the optical band gap and thermal diffusivity of Ge- Sb- Se glasses", Physical review B., 45, 8112-8115 (1992).

9. V. Balan, C. Vigreux, A. Pradel, A. Llobera, C. Dominguez, M.I. Alonso, M. Garriga, "Chalcogenide glass-based rib ARROW waveguide," *J. Non-Crystalline Solids.*, 326–327, 455–459 (2003).
10. D.R. Goyal and A. S. Maan, "Far-infrared absorption in amorphous $\text{Sb}_{15}\text{Ge}_x\text{Se}_{85-x}$ glasses," *Journal of Non-Crystalline Solids.*, 183, 182-185(1995).
11. A. Ray Hilton, "Chalcogenide glasses for Infrared Optics", Mc Graw Hill professional (2010).
12. A. Urena, A. Piarristeguy, M. Fontana, C. Vigreux-Bercovicic, A. Pradel and B. Arcondo, "Characterisation of thin films obtained by laser ablation of $\text{Ge}_{28}\text{Se}_{60}\text{Sb}_{12}$ glasses", *Journal of Physics and Chemistry of Solids.*, 68 ,993–997(2007).
13. Franz Urbach, "The Long-Wavelength Edge of Photographic Sensitivity and of the Electronic Absorption of Solids", *Physical Review.*, 92, 1324–1324 (1953).
14. R. Swanepoel, "Determination of the thickness and optical constants of amorphous silicon," *Journal Physics E.*, 16(12), 1214–1222 (1983).
15. S. H. Wemple and M. Di Domenico, "Behavior of the Electronic Dielectric Constant in Covalent and Ionic Materials," *Physical Review B.*, 3 1338-1351 (1971).
16. J. Tauc, "Absorption edge and internal electric fields in amorphous semiconductors," *Material Research Bulletin.*, 5(8), 721–729 (1970).
17. K. Petkov, P.J.S. Ewen, "Photoinduced changes in the linear and non-linear optical properties of chalcogenide glasses," *Journal of Non-Crystalline Solids.*, 249, 150-159 (1999).
18. M. Popescu, "Disordered Chalcogenide Optoelectronic materials: Phenomena and Applications", *Journal of Optoelectronics and Advanced Materials.*, 7, 2189 - 2210 (2005).
19. H. Fritzsche, "Toward understanding the photoinduced changes in chalcogenide glasses", *Semiconductors.*, 32, 850-855 (1998).
20. A. S. Tverjanovich, E. N. Borisov, O. Volobueva, S. B. Mamedov and M. D. Mikhailov, "Photoinduced Bleaching in Ga-Ge-S(Se) Vitreous Films", *Glass Physics and Chemistry.*, 32, 677–680 (2006).

21. R. Tintu, V.P.N. Nampoore, P. Radhakrishnan and Sheenu Thomas "Photoinduced changes in optical properties of Ga-Sb-Ge-Se glasses", *Optics Communications.*, 284, 222-225(2011).
22. G.B Turpin and I.E McNeil, "Photodarkening in amorphous $\text{Ge}_{1-x}\text{Sn}_x\text{Se}_2$ films", *Physical review B.*, 39, 8750-8756 (1989).
23. A. Ganjoo, K. Shimakawa, "Transient and metastable photodarkening in amorphous chalcogenides", *Journal of Optoelectronics and Advanced Materials.*, 3, 221-226 (2001).
24. K. Tanaka, "Photoinduced structural changes in amorphous semiconductors", *Semiconductors.*, 32, 861-867 (1998).
25. S. Song, N. Carlie, J. Boudies, L. Petit, K. Richardson and C. B. Arnold, "Spin-coating of $\text{Ge}_{23}\text{Sb}_7\text{S}_{70}$ chalcogenide glass thin films," *J. Non-Crystalline Solids.*, 355(45-47), 2272-2278 (2009).
26. B. Singh, G. C. Chern, and I. Luaks, "Application of spin-coated As_2S_3 thin films in a high resolution trilayer resist system," *Applied Physics Letters.*, 45(1), 74 (1984).
27. J. J. Santiago, M. Sano, M. Hamman and N. Chen, "Growth and optical characterization of spin-coated As_2S_3 multilayer thin films", *Thin Solid Films.*, 147(3), 275-284 (1987).
28. R.Tintu, V.P.N. Nampoore, P. Radhakrishnan and Sheenu Thomas, "Reverse saturable absorption in nano colloidal $\text{Ge}_{28}\text{Sb}_{12}\text{Se}_{60}$ chalcogenide glass", *J. Non-Crys. Solids.* doi:10.1016/j.jnoncrysol.2011.03.028 .
29. R. A. Street, "Luminescence in amorphous semiconductors", *Advances In Physics.*, 25, 397-454 (1976).
30. Munetoshi Seki, Kan Hachiya, Katsukuni Yoshida, "Photoluminescence excitation process and optical absorption in Ge-S chalcogenide glasses", *Journal of Non-Crystalline Solids.*, 324, 127-132 (2003).
31. K. Imura, T. Nagahara, and H. Okamoto, "Near-field two-photon-induced photoluminescence from single gold nanorods and imaging of plasmon modes," *J. Phys. Chem. B.*, 109, 13214-13220 (2005).
32. N. J. Durr, T. Larson, D. K. Smith, B. A. Korgel, K. Sokolov, and A. Ben-Yakar, "Two-photon luminescence imaging of cancer cells using molecularly targeted gold nanorods," *Nano Letters.*, 7(4), 941-945 (2007).

33. A. Zakery and S.R. Elliott, "Optical Nonlinearities in Chalcogenide Glasses and their Applications", in Springer Series in Optical Sciences, Springer: Berlin (2007).
34. Pulok Pattanayak, N Manikandan, M Paulraj and S Asokan," Photo-thermal deflection and electrical switching studies on Ge-Te-I chalcogenide glasses", J. Phys. Condens. Matter., 19, 036224 (2007).
35. K. Tanaka, T. Gotoh, N. Yoshida and S. Nonomura" Photothermal deflection spectroscopy of chalcogenide glasses", Journal of Applied Physics., 91, 125 (2002).
36. N. Manikandan, M. Paulraj, S. Asokan,"Thermal diffusivity measurements on As-Te-Ga glasses by photo-thermal deflection technique: Composition dependence and topological thresholds", Journal of Non-Crystalline Solids., 355, 58-60 (2009).
37. L. Petit, N. Carlie, H. Chen, S. Gaylord, J. Massera, G. Boudebs, J. Huc, A. Agarwal, L. Kimerling, K. Richardson, "Compositional dependence of the nonlinear refractive index of new germanium-based chalcogenide glasses", Journal of Solid State Chemistry., 182, 2756-2761(2009).
38. J. Troles, F. Smektala, G. Boudebs, A. Monteila, B. Bureau, J. Lucas, "Optical limiting behaviour of chalcogenide glasses", Journal of Optoelectronics and Advanced Materials., 4, 729 - 735(2002) .
39. R. G. DeCorby, H. T. Nguyen, P. K. Dwivedi and T. J. Clement, "Planar omnidirectional reflectors in chalcogenide glass and polymer," Opt. Express., 13, 6228-6233 (2005).
40. R Tintu, K Sulakshna ,K Saurav, V P N Nampoore, P Radhakrishnan and Sheenu Thomas, " $\text{Ge}_{28}\text{Se}_{60}\text{Sb}_{12}$ /PVA Composite Films For Photonic Applications", Journal of Non-Oxide Glasses., 2, 167- 174 (2010).
41. R. Tintu, V.P.N. Nampoore, P. Radhakrishnan, Sheenu Thomas" Preparation and optical characterization of novel Ge-Se-Sb/PVA composite films for optical limiting application", J. Phys. D: Appl. Phys., 44, 025101-025106 (2011).



Chapter 5

STUDIES ON $\text{Ge}_{28}\text{Ga}_5\text{Se}_{60}$ CHALCOGENIDE GLASS

- 5.1. *Introduction*
 - 5.2. *Studies on bulk and thin film $\text{Ge}_{28}\text{Ga}_5\text{Se}_{60}$ glass.*
 - 5.3. *Studies on Nano colloids of $\text{Ge}_{28}\text{Se}_{60}\text{Ga}_5$ chalcogenide glass*
 - 5.4. *Fabrication and characterization of $\text{Ge}_{28}\text{Se}_{60}\text{Ga}_5$ /PVA nano composite films*
 - 5.5. *Conclusions*
 - 5.6. *References*
-

This chapter deals with the studies on $\text{Ge}_{28}\text{Se}_{60}\text{Ga}_5$ chalcogenide glass. Optical characterization of the $\text{Ge}_{28}\text{Se}_{60}\text{Ga}_5$ thin film fabricated by thermal evaporation technique is discussed along with the characterization of bulk glass. Synthesis and optical properties of $\text{Ge}_{28}\text{Se}_{60}\text{Ga}_5$ nano colloids are also presented in this section. Absorption spectroscopy of the nano colloids are analyzed using a UV visible spectrophotometer. The band gap estimated from the absorption spectra of the nano colloids show cluster size dependent change in band gap. Luminescence mechanism in the colloid solutions are studied and the results show cluster size and excitation energy dependent change in the luminescence peak. The non linear optical properties of the nano colloids are studied using an open aperture z- scan technique. $\text{Ge}_{28}\text{Se}_{60}\text{Ga}_5$ /PVA composite films are fabricated from the nano colloid solutions and are optically characterized.

5.1. Introduction

Ternary Ge–Se–Ga glasses are promising infrared transmitting chalcogenide glasses with low phonon energy¹. They can dissolve up to 1–2 at% of rare earths. The Ge–Ga–Se system is known to form bulk glasses up to about 35 at.% Ge, 20 at.% Ga and remaining being Se. The glass forming region for Ge–Ga–Se system¹ is shown in Figure 5.1.

The chemically ordered covalent network model proposed for Ge–Ga–Se glasses says that GeSe_2 and the Ga_2Se_3 units in the glass are connected with extra Se atoms. The excess Se atoms are connected in chains. Ga–Se bond energy (65 kcal/mol) is higher than Ge–Se bond energy (55.4 kcal/mol), which indicates that with the increase of the Ga content, the average bond energy of the system will increase^{2,3}.

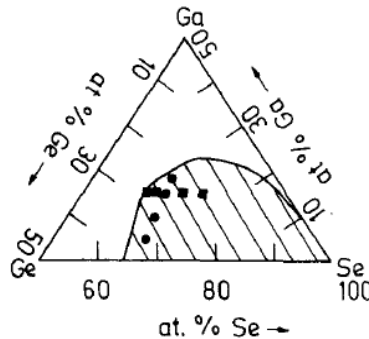


Figure 5.1: Glass forming region of Ge–Ga–Se system.

Optical studies on different compositions of Ge–Ga–Se thin films prepared by thermal evaporation technique are reported by Y. Nedeva et al.⁴. They found that the optical band gap of the thin films increases with the addition of gallium in to the system. The increase in band gap is explained by the increase in average bond energy of the system. The

average bond energy in the system increase due to the addition of the gallium alloy⁴. Optical nonlinearities in the Ge-Ga-Se system are less studied. Most of the studies were done on the system by the incorporation of rare earths into the system since gallium is a good network modifier. Ge-Ga-Se system is a promising candidate for optical amplifiers and integrated optics⁵.

5.2. Studies on bulk and thin film $\text{Ge}_{28}\text{Ga}_5\text{Se}_{60}$ glass

5.2.1. Preparation and characterization of bulk $\text{Ge}_{28}\text{Ga}_5\text{Se}_{60}$ ChG

$\text{Ge}_{28}\text{Ga}_5\text{Se}_{60}$ glass was synthesized by melting mixtures of the constituent elements Ge, Se and Ga with 5N purity in evacuated and flame sealed fused quartz ampoules at 1050°C for 24 h in a rocking furnace. The ampoule was quenched into ice cold water. A more detailed description of the preparation method can be found in section 2.2.1. The amorphous nature of the bulk sample is confirmed by X-ray diffraction studies. Figure 5.2 shows the plot of normalized signal versus 2θ for the bulk sample. The diffractogram shows no sharp peaks showing the absence of crystallinity.

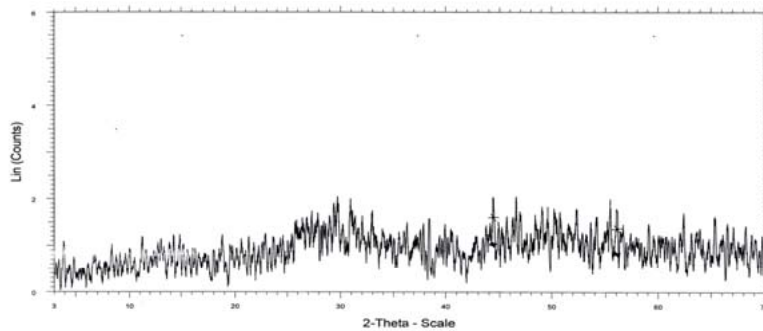


Figure 5.2: XRD pattern for $\text{Ge}_{28}\text{Ga}_5\text{Se}_{60}$ bulk glass.

In order to understand the glass transition temperature of the prepared glass, differential scanning calorimetric technique measurements were done. The glass transition temperature (T_g), which is the temperature for transition from glass solid phase to glass liquid phase is estimated to be about 276.93°C from the DSC graph.

Dependence of optical absorption with wavelength for bulk $\text{Ge}_{28}\text{Se}_{60}\text{Ga}_5$ glass is presented in Figure 5.3. Plot shows three regions: high absorption, exponential and tail region as that of a typical chalcogenide glass. The band gap estimated from the plot arising due to the transition from the extended states is 1.68 eV.

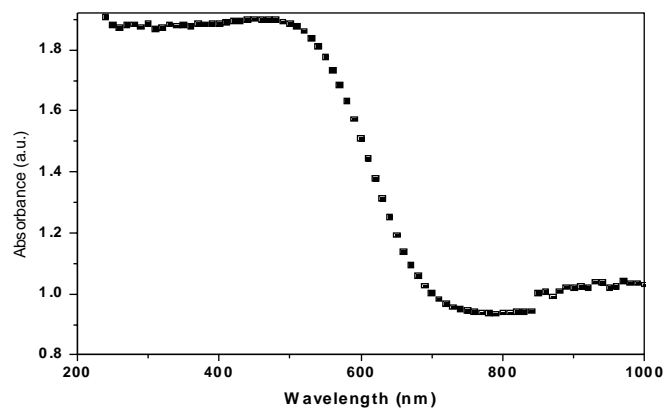


Figure 5.3: Plot of dependence of optical absorption with wavelength for bulk $\text{Ge}_{28}\text{Se}_{60}\text{Ga}_5$ glass.

5.2.2. Optical characterization of $\text{Ge}_{28}\text{Se}_{60}\text{Ga}_5$ thin films prepared by thermal evaporation

$\text{Ge}_{28}\text{Se}_{60}\text{Ga}_5$ thin film was evaporated on glass substrates in a standard vacuum installation, using the respective bulk composition as a source material. The residual pressure was 1.5×10^{-5} Torr. The

prepared films have a thickness of 325 nm. The transmission and reflection of the thin film were measured in the energy range of 200nm to 2000 nm using UV-VIS-NIR spectrophotometer (Jasco V 570). The scanned transmission and reflection spectra were used to analysis the refractive index and dispersive analysis of refractive index using Swanepoel's method ⁶ as discussed in section 2.2.4. The analysis of the optical absorption coefficient has revealed the presence of an indirect optical transition for the as-deposited film. The band gap of the thin film is measured to be 2.19 eV from the plot of $(\alpha h\nu)^{1/2}$ versus $h\nu$ as shown in Figure 5.4.

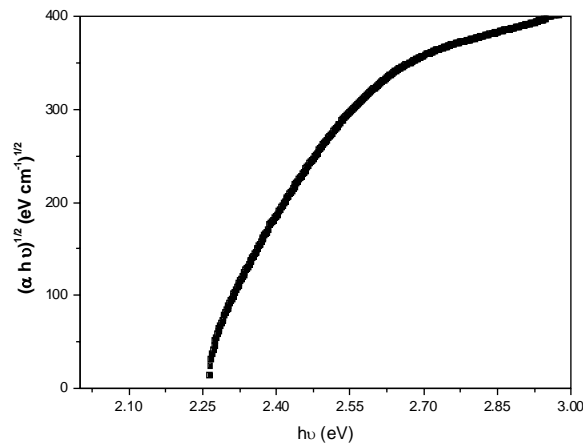


Figure 5.4: Plot of $(\alpha h\nu)^{1/2}$ versus $h\nu$ for Ge₂₈Se₆₀Ga₅ thin film.

Other optical constants of the thin film were also calculated and are tabulated in Table 5.1. The refractive index and the extinction coefficient studied for wavelength above band gap shows the normal dispersion behaviour. The dispersive analysis of the refractive index gives the average bond energy and the oscillator strength of the

system. The oscillator energy (E_0) is found to be 3.97 eV. E_0 is an average energy gap, as it scales with the Tauc gap⁷ (E_g) as $2E_g$.

Table 5.1: Calculated values of optical band gap (E_g), width of localized states (E_e), refractive index(n), extinction coefficient (k), optical conductivity(σ), dielectric constants (ϵ_r , ϵ_i), dispersive parameters (E_d , E_0), effective oscillator strength (f), third order nonlinear susceptibility (χ^3) and nonlinear refractive index(n_2).

Optical parameters of Ge ₂₈ Ga ₅ Se ₆₀ thin film	
E_g (eV)	2.21
E_e (meV)	170
n	2.27
k	-0.02
σ (s ⁻¹)	2.06×10^{-4}
ϵ_r	5.18
ϵ_i	0.134
E_d (eV)	8.54
E_0 (eV)	3.97
f (eV) ²	31.7
χ^3 (esu)	1.13×10^{-13}
n_2 (esu)	2.44×10^{-12}

The nonlinear refractive index and third order nonlinear susceptibility calculated for the film are less compared to Ge₂₈Se₆₀Sb₁₂ thin film. The replacement of 5% Ga to Ge-Se system leads to an increase in the band gap and decrease in refractive index of the film. The increase in

optical band gap may be correlated with the electro negativity difference of the elements involved. The decrease in the nonlinearity can be due to the increase in band gap, since the nonlinearity of a semiconductor is inversely proportional to the band gap⁸.

5.3. Studies on Nano colloids of Ge₂₈Se₆₀Ga₅ chalcogenide glass

5.3.1. Synthesis, structural analysis and absorption spectroscopy of Ge₂₈Se₆₀Ga₅ nano colloids

Nano colloid solutions of Ge₂₈Se₆₀Ga₅ with three different concentrations A₁= 1.2 mg/ml, A₂= 0.9 mg/ml and A₃= 0.24 mg/ml were prepared by dissolution of bulk Ge₂₈Se₆₀Ga₅ glass in n-butylamine solvent (Sigma-Aldrich, 99.9%). The dissolution was carried out inside a sealed glass container to prevent solvent evaporation. A magnetic stirrer was used to expedite the dissolution process. The solutions were kept in refrigeration to avoid moisture. Detailed description is given in 2.1.3.

The cluster formation in the colloid solution was confirmed by the SEM analysis. The solvent evaporation results in the agglomeration of the clusters during SEM analysis. The SEM image of A₁, the solution with higher concentration is given in Figure 5.5. EDAX of the higher concentrated sample is taken to understand the constituents of each cluster. The result of EDAX analysis shown in Figure 5.6 confirms the presence of Ge, Se and Ga in the cluster.

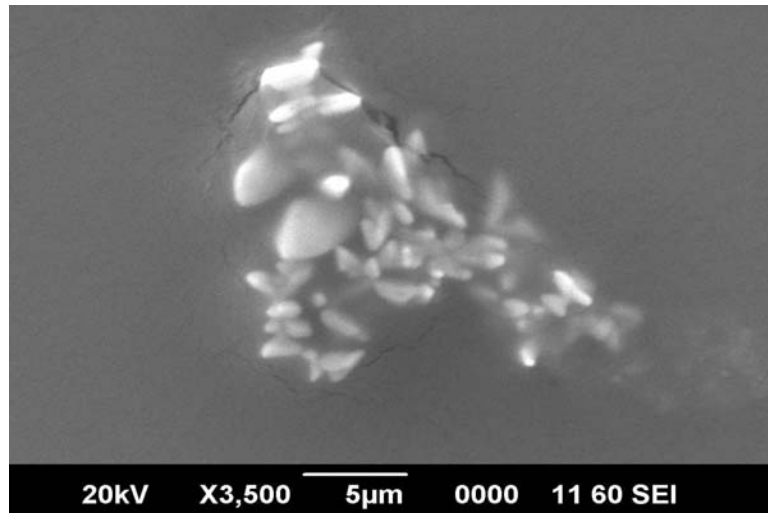


Figure 5.5: SEM image of A_1 .

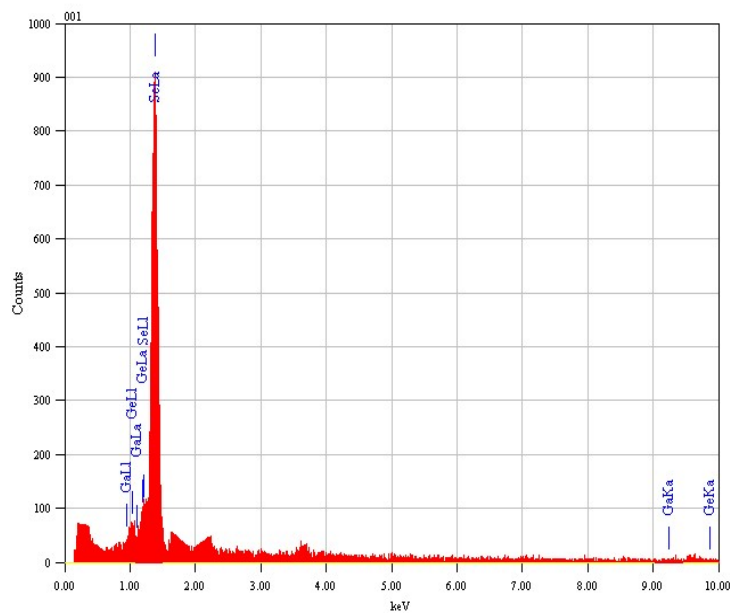


Figure 5.6: EDAX Spectrum from the cluster of A_1 .

The UV-visible absorption spectra of the nano colloids are shown in Figure 5.7. The band gap is calculated from the point of

inflection of the first derivative curve of the absorption spectra. An increase in the band gap with decrease in cluster size is observed which is attributed to the quantum size effect. Bulk glass is having a band gap of 1.68 eV. In the case of nano colloids the band gap have increased from 1.68 eV to 2.39 eV, 2.95 eV and 3.56 eV for A_1 , A_2 and A_3 respectively. The slope change for different colloid solutions is clear from the spectra. The slope indicates the ordering of the structure⁹. Here the solution with higher concentration of $\text{Ge}_{28}\text{Se}_{60}\text{Ga}_5$ is having more disorder compared to the other two.

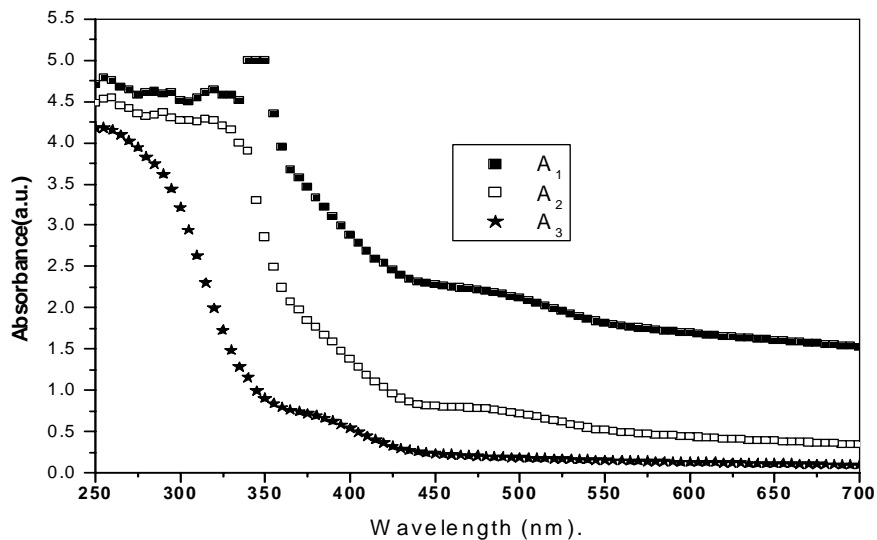


Figure 5.7: Plot of absorption spectra of A_1 , A_2 , A_3 .

5.3.2. Excitation wavelength and cluster size dependent change in photoluminescence spectra of $\text{Ge}_{28}\text{Se}_{60}\text{Ga}_5$ nano colloids

The photoluminescence studies were carried out on the nano colloid samples using a Varian Cary Eclipse spectrofluorimeter at

room temperature. The excitation wavelength dependent change in the A_2 nano colloid solution is presented in Figure 5.9 a, b, c and d. Figure 5.8 (a) shows the emission spectra corresponding to 250 nm (4.96 eV) and 270 nm (4.59 eV) excitation. The excitation results to the emission at 425nm, 484nm and 537 nm. Higher band gap excitation leads to three emission peaks and a shoulder at 581 nm. The luminescence at 425 nm, 484 nm and 537 nm is observed up to an excitation of 295 nm. For an excitation from 300 nm (4.13 eV) to 370nm (3.35 eV) the luminescence peaks are observed both at 425 nm (2.92eV) and 575 nm (2.16 eV). The excitation with 370 nm to 400 nm results in a small shift in the luminescence peak wavelength. The band gap excitation (2.95 eV) of the A_2 nanoclusters results in the luminescence peak at 575 nm (2.16 eV). The luminescent intensity decreases as the excitation energy decreases from 4.96 eV to 4.28 eV and increases afterward up to 3.45 eV excitation. Thereafter up to bandgap energy (2.95 eV), peak intensity decreases and increases afterwards up to an excitation of 2.58 eV.

The luminescence intensity depends on the number of electron hole pair recombination taking place in the sample. Here the recombination takes place in the excited state, localized state and in the charged defect state in between the extended states¹⁰. The luminescence peak is broadened in shape due to the electron phonon coupling¹¹.

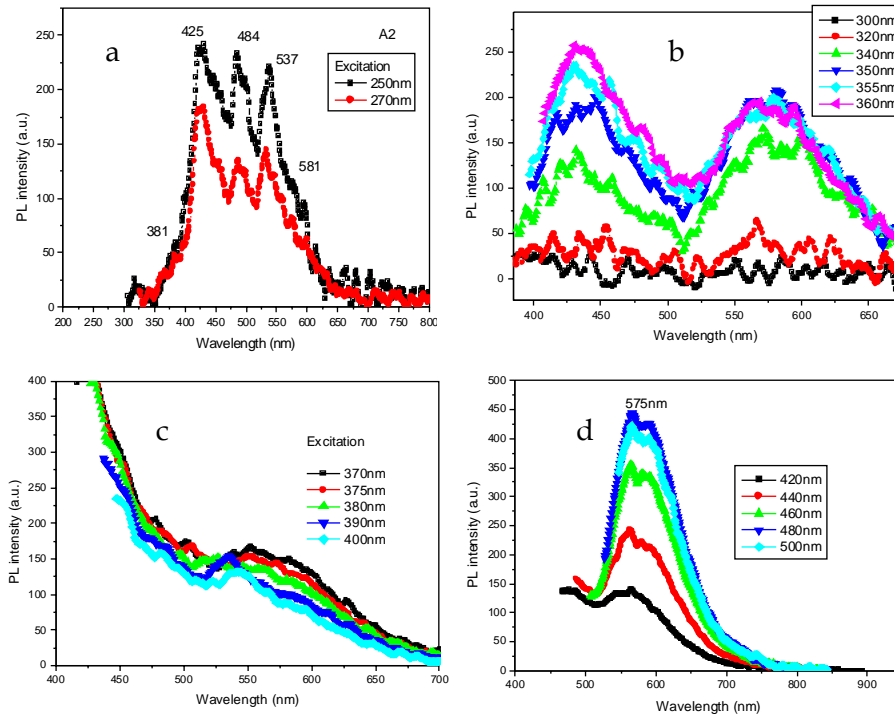


Figure 5.8: The excitation wavelength dependent emission behaviour for A_2 Luminescence corresponding to an excitation of, (a) 250nm and 270nm, (b) 300nm to 360nm (c) 370 nm to 400nm (d) 420nm to 500nm.

Cluster size dependent luminescence studies on the $\text{Ge}_{28}\text{Se}_{60}\text{Ga}_5$ nano colloids at an excitation wavelength of 400 nm and 500 nm are presented in Figure 5.9 a, b. Photoluminescence from A_1 , A_2 and A_3 shows a red shift in the emission peak with cluster size of the nano colloid solutions. Such size dependent optical properties of semiconductor particle suspensions in the quantum regime are well known and similar observations have previously been made for several quantum particle systems¹². With the decrease in the cluster size, the band gap energy gets shifted from 2.39 eV to 3.56 eV. The

shift of band gap energy is related to the shift in the luminescence peak wavelength. These unique properties are observed in the chalcogenide glasses due to their electronic states¹³⁻¹⁵.

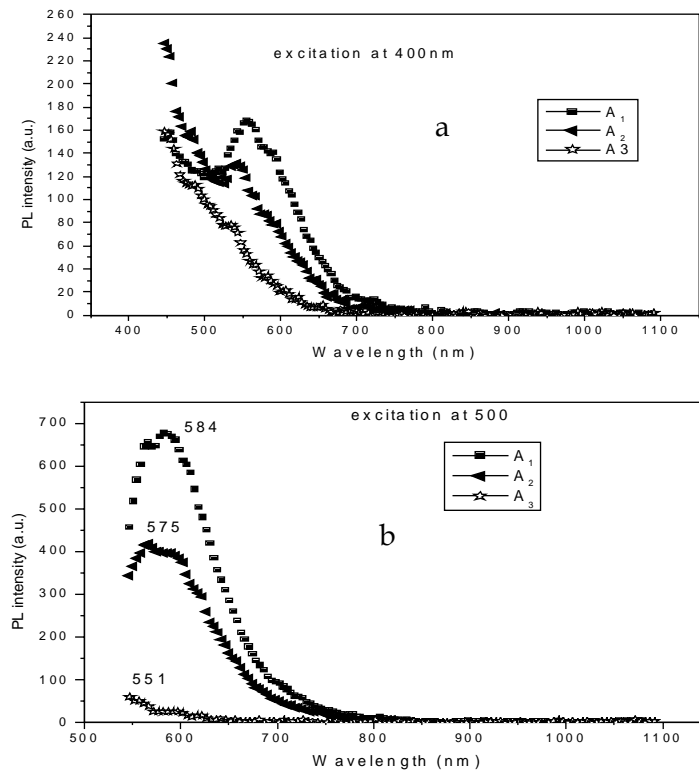


Figure 5.9: Cluster size dependence on the photoluminescence with an excitation of (a) 400 nm and (b) 500 nm.

5.3.3. Nonlinear optical studies on $Ge_{28}Se_{60}Ga_5$ nano colloids

Open aperture z-scan technique was used to study the nonlinear optical absorption coefficient of the colloid solutions. The open aperture curve for $Ge_{28}Se_{60}Ga_5$ colloids is shown in Figure 5.10. It exhibits a normalized transmittance valley, indicating the presence of reverse saturable induced absorption in the colloids. The z-scan

traces show best fit for the two photon absorption confirming that two photon absorption may be the main mechanism involved in nonlinear absorption of A_1, A_2 and A_3 . The calculated non linear absorption coefficients (β) are 2.52 cm/GW, 1.79 cm/GW and 0.73 cm/GW for A_1, A_2 and A_3 respectively.

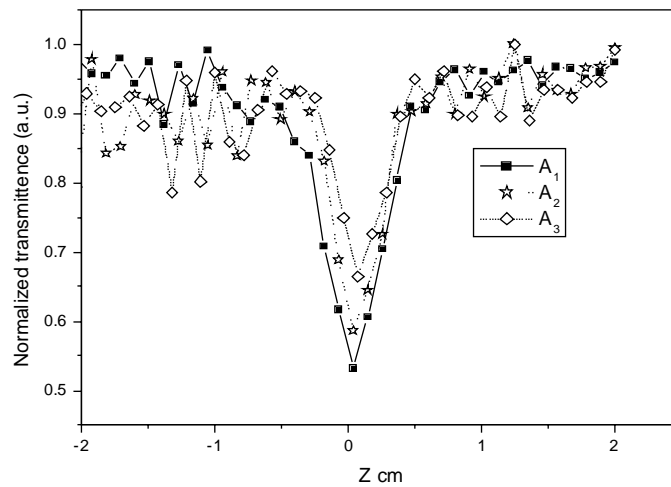


Figure 5.10: The open aperture z-scan traces of $\text{Ge}_{28}\text{Se}_{60}\text{Ga}_5$ colloids of different cluster sizes at an input power density of 571 MW/cm^2 .

From the z- scan curves, it is found that as the band gap decreases (increase in cluster size) the non linear optical absorption coefficient (β) of the colloid solutions increases. The rate of two photon absorption increases with cluster size which is attributed to an inverse proportionality between β and third power of band gap (E_g)¹⁶.

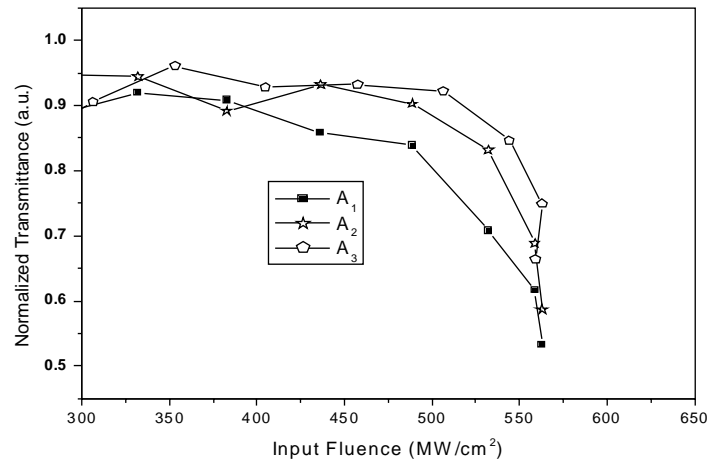


Figure 5.11: Optical limiting response of A_1 , A_2 and A_3 at 532 nm at an input power density of 571MWcm^{-2} .

The optical limiting property occurs mostly due to absorptive nonlinearity¹⁷. Thus it is possible to generate optical limiting curves from open aperture z-scan data. The plot of fluence versus transmittance represents the optical limiting curve and Figure 5.11 illustrates the influence of cluster size on the optical limiting response. Optical limiting threshold is the approximate fluence at which the normalized transmission begins to deviate from linearity¹⁸. The optical limiting threshold is found to be high for A_3 (544MW/cm^2) as compared to the A_2 (530MW/cm^2) and A_1 (486MW/cm^2). Cluster size has a significant effect on the limiting performance of chalcogenide nano colloids. Increasing particle size reduces the limiting threshold and enhances the optical limiting performance. From the measured values of β for the colloids, it can be seen that the colloids with larger particle size is a better nonlinear absorber and hence a good optical limiter.

5.4. Fabrication and characterization of Ge₂₈Se₆₀Ga₅ /PVA nano composite films

5.4.1. Preparation and optical parameters of Ge₂₈Se₆₀Ga₅/PVA nano composite films

The Ge₂₈Se₆₀Ga₅/PVA composite films were prepared from the nanocolloidal Ge₂₈Se₆₀Ga₅ solution and polyvinyl alcohol (PVA) [-CH₂CH(OH)-]ⁿ in various proportions. The concentrations of the ChG in the colloid solutions are as follows 1.2 mg/ml, 0.9 mg/ml and 0.24 mg/ml for A₁, A₂ and A₃ respectively. The films were prepared from the homogeneous solutions of different concentrations by drop casting method. The composite films were made from these nano colloid solutions of Ge₂₈Se₆₀Ga₅ and PVA in the ratio 1:1. The thickness of the films were measured using Metutoyo, Micrometer (series 193) and found to be around 100µm. The optical transmission spectra and reflection spectra have been recorded by using a spectrophotometer (JascoV-570 UV/VIS/IR). Transmission and reflection spectra of the composite films have been used for the study of optical properties. The dispersion of refractive index has been studied using the Wemple-Di Domenico (WDD) single oscillator model. The band gap of the composite films was found to increase with decrease in concentration of the nano colloid used for the preparation of films. The increase in band gap with decrease in concentration can be due to the decrease in cluster size of the parent solution as reported earlier^{16,17}. It is found that as the concentration of the chalcogenide decreases there is a blue shift in band edge and a change in the slope of absorption spectra.

Table 5.2: The measure values of optical band gap (E_g), refractive index (n), dispersive parameters (E_d , E_0) effective oscillator strength (f), third order non linear susceptibility ($\chi^{(3)}$) and non linear refractive index for Ge₂₈Ga₅Se₆₀ /PVA composite films.

	E_g (eV)	n	E_0 (eV)	E_d (eV)	f (eV) ²	$\chi^{(3)} \cdot 10^{-13}$ (esu)	$n^2 \cdot 10^{-12}$ (esu)
A ₁ +PVA	2.33	1.95	4.53	13.12	59.43	4.80	9.17
A ₂ +PVA	2.58	1.78	4.57	12.88	58.86	4.32	8.31
A ₃ +PVA	2.89	1.60	4.87	11.7	56.97	2.27	4.65

The width of the localized states for Ge₂₈Ga₅Se₆₀ /PVA composite films is found to decrease with decrease in concentration which shows the ordering of the structure. The calculated optical parameters are tabulated in Table 5.2. Some important parameters (dielectric constant, dielectric loss, optical conductivity etc.) have also been determined using n , k and absorption coefficient (α). The extinction coefficients are found to vary from $78 \cdot 10^{-4}$ (A₁+PVA) to $35 \cdot 10^{-4}$ (for A₃ +PVA). The decrease in the extinction coefficients with concentration show that the fraction of light lost through the medium. The dielectric constants show how much it will slow down the speed of light in the material. It is found to change from 3.80 (A₁+PVA) to 2.56 (A₃+PVA). The imaginary part of dielectric constant which shows how a dielectric absorbs energy from an electric field due to dipole motion decreases from $3.04 \cdot 10^{-4}$ (A₁+PVA) to $1.12 \cdot 10^{-4}$ (A₃+PVA). Generalized Miller's rule and linear refractive index were used to find the nonlinear susceptibility and non linear refractive index of thin films¹⁹. The calculated values of non linear refractive index (n^2)

and susceptibility ($\chi^{(3)}$) are tabulated in Table 5.2. It is found that depending on the band gap the nonlinear refractive index of the investigated films also changes.

5.4.2. Nonlinear optical properties of Ge₂₈Se₆₀Ga₅ /PVA nano composite films

The nonlinear optical properties of the composite films are studied using open aperture z-scan technique using a Nd:YAG laser (532nm) as excitation source. Studies show that the thin films have transmittance valley at the focal point which indicates the reverse saturable absorption in the composite films.

Table 5.3: Measured values of non linear absorption coefficient (β), imaginary part of third order nonlinear susceptibility ($\text{Im}\chi^3$) and limiting threshold at 532nm For A₁+PVA, A₂+PVA and A₃+PVA

Samples	β (m/GW)	$\text{Im}\chi^3$ (m ² GV ⁻²)	Limiting threshold (MW/cm ²)
A ₁ +PVA	2.57	2.22	397
A ₂ +PVA	2.10	1.97	420
A ₃ +PVA	1.78	1.14	465

The z-scan traces have good theoretical fit for two photon absorption. Thus as observed in Ge₃₀Se₆₀Sb₅Ga₅ and Ge₂₈Sb₁₂Se₆₀ composite films two photon absorption is the main mechanism contributing to induced absorption. The calculated value for two photon absorption coefficient at a laser power of 571 MW/cm² are tabulated in Table 5.3. The rate of two photon absorption increases

with cluster size which is attributed to an inverse proportionality between β and third power of band gap (E_g) and enhancement in the nonlinear susceptibility due to enhanced oscillator strength with particle size¹⁶. The optical limiting response of the films studied using z- scan data clearly shows an increase in optical limiting threshold as the grain size of films reduces. The imaginary part of third order nonlinear susceptibilities for the composite films are also tabulated in Table 5.3. The third order optical nonlinearity enhances with the increase in the amount of chalcogenide glass in the film.

5.5. Conclusions

- *$\text{Ge}_{28}\text{Ga}_5\text{Se}_{60}$ bulk samples was found to be amorphous from the XRD analysis.*
- *The optical gap of the $\text{Ge}_{28}\text{Ga}_5\text{Se}_{60}$ thin film prepared by thermal evaporation technique was found to be 2.21 eV. The high band gap in compared to other investigated systems can be due to the increase of average bond energy of the alloys that occurs with the addition of Ga.*
- *Nano colloids of $\text{Ge}_{28}\text{Ga}_5\text{Se}_{60}$ ChG solutions show cluster size dependent change in the bandgap and non linear absorption.*
- *The PL studies on the nano colloids show the dependence of the bandgap and the defect states in the emission spectra.*
- *Nano composite $\text{Ge}_{26}\text{Ga}_5\text{Se}_{60}$ films prepared by casting method were characterized using the transmission and reflection spectra.*
- *These nano composites show self-defocusing nonlinearity and good nonlinear absorption behaviour.*

5.6. References

1. A. Giridhar and Sudha Mahadevan, "Chemical ordering in Ge-Ga-Se glasses", *Journal of Non-Crystalline Solids.*, 126, 161-169(1990).
2. A. Lipinski, B. Ziolkowska and W. Mycielski, "Drift Mobility in Ge-Se-Ga Glasses", *Journal of Non-Crystalline Solids.*, 90, 433-436 (1987).
3. K. Maeda , T. Sakai , K. Sakai ,T. Ikari , M. Munzar, D. Tonchev, S. O. Kasap and G. Lucovsky, "Effect of Ga on the structure of Ge-Se-Ga glasses from thermal analysis, Raman and XPS measurements", *J Mater Sci: Mater Electron.*, 18, S367-S370 (2007).
4. Y. Nedev, T. Petkova, E. Mytilineou, P. Petkov, "Compositional Dependence of the Optical Properties of the Ge-Se-Ga Glasses", *Journal of Optoelectronics and Advanced Materials.*, 3, 433 - 436 (2001).
5. C. Koughia, M. Munzar, D. Tonchev, C. Haugen, R. Decorby, J.C. McMullin and S.O. Kasap, "Photoluminescence in Er doped Ge-Ga-Se glasses," *Journal of Luminescence.*, 112, 92-96 (2005).
6. R. Swanepoel, "Determination of the thickness and optical constants of amorphous silicon," *J. Phys. E.*, 16(12), 1214-1222 (1983).
7. J. Tauc, "Absorption edge and internal electric fields in amorphous semiconductors", *Mater. Res. Bull.*, 5(8), 721-729 (1970).
8. A. Zakery and S.R. Elliott, "Optical Nonlinearities in Chalcogenide Glasses and their Applications", *Springer Series in Optical Sciences*, Springer: Berlin (2007).
9. R. Tintu, V.P.N.Nampoori, P. Radhakrishnan, Sheenu Thomas, "Photoinduced changes in optical properties of Ga-Sb-Ge-Se glasses", *Optics Communications.*, 284, 222-225 (2011).
10. R. A. Street, "Luminescence in amorphous semiconductors", *Advances In Physics.*, 25, 397-454 (1976).
11. Munetoshi Seki, Kan Hachiya , Katsukuni Yoshida," Photoluminescence excitation process and optical absorption in Ge-S chalcogenide glasses", *Journal of Non-Crystalline Solids.*, 324 , 127-132(2003).

12. Litty Irimpan, A. Deepthy, Bindu Krishnan, V. P. N. Nampoori and P Radhakrishnan, "Size dependent fluorescence spectroscopy of nanocolloids of ZnO", *Journal of Applied Physics* ., 102, 063524 (2007).
13. M. A Bosch, R.W.Epworth and D.Emin, "Photoluminescence dynamics in chalcogenide glasses and crystals", *Journal of Non-Crystalline Solids.*, 40, 587-594(1980).
14. Munetoshi Seki, Kan Hachiya, Katsukuni Yoshida," *Photoluminescence and states in the bandgap of germanium sulfide glasses*", *Journal of Non-Crystalline Solids.*, 315, 107-113(2003).
15. S.O. Kasap , K. Koughia , M. Munzar, D. Tonchev, D. Saitou, T. Aoki," *Recent photoluminescence research on chalcogenide glasses for photonics applications*", *Journal of Non-Crystalline Solids.*, 353, 1364-1371(2007).
16. R. Tintu, V. P. N. Nampoori, P. Radhakrishnan, and Sheenu Thomas" *Nonlinear optical studies on nanocolloidal Ga-Sb-Ge-Se chalcogenide Glass*", *Journal Of Applied Physics.*, 108, 073525 (2010).
17. R. Tintu, V.P.N. Nampoori, P. Radhakrishnan, Sheenu Thomas" *Preparation and optical characterization of novel Ge-Se-Sb/PVA composite films for optical limiting application*", *J. Phys. D: Appl. Phys.*, 44, 025101(2011).
18. J. Troles, F. Smektala, G. Boudebs, A. Monteila, B. Bureau, J. Lucas,"*Optical limiting behaviour of chalcogenide glasses*", *Journal of Optoelectronics and Advanced Materials.*, 4, 729 - 735 (2002).
19. Ticha H and L. Tichy, " *Semiempirical relation between non-linear susceptibility (refractive index), linear refractive index and optical bandgap and its application to amorphous semiconductors*," *Journal of Optoelectronics and Advanced Materials.*, 4[2], 381 - 386 (2002).



Chapter 6

FABRICATION AND CHARACTERIZATION OF ERBIUM DOPED $\text{Ge}_{28}\text{Sb}_{12}\text{Se}_{60}$ ChG.

6.1. *Introduction*

6.2. *Experimental*

6.3. *Structural, thermal and optical characterization of bulk glasses*

6.4. *Optical characterization of erbium doped thin films*

6.5. *Conclusions*

6.6. *References*

This chapter reports the studies on bulk and thin films of erbium doped $\text{Ge}_{28}\text{Sb}_{12}\text{Se}_{60}$ glass. The refractive index (n), the optical band gap (E_g) and dielectric properties are analyzed from the transmission and reflection spectra on the basis of Wemple–Di Domenico (WDD) single effective oscillator model. Optical band gap obtained from WDD model is found to increase with increase in erbium concentration and it is in good agreement with the values obtained by Tauc’s extrapolation method. The observed results have been interpreted as due to rare earth impurities strongly affecting the network and structurally modifying these glasses.

6.1. Introduction

Chalcogenide glasses belong to an important class of photonic materials which assure importance due to their high refractive index, high transparency in the IR region, low phonon energies, large optical nonlinearities, ability to be directly patterned by exposure to near-band gap light, and ability to incorporate relatively high concentrations of rare-earth dopants with minimal clustering^{1,2}. Chalcogenide glasses doped with various rare earth (RE) ions are extensively studied as potential materials for fiber optic amplifiers operating at 1.3 μm and 1.5 μm telecom windows^{3,4}. The low phonon energy, good thermal stability, easy fiber fabrication and extended IR transmission had made chalcogenide glasses suitable host materials for RE ions. Chalcogenide glasses doped with rare earths are potential candidates for mid-infrared (IR) lasers for a variety of applications including environmental sensing, LIDAR and military counter-measures, powerful, coherent, robust and compact sources. Sulphide, selenide and telluride glasses have been shown to be chemically and mechanically durable, to possess wide glass-forming regions and to have extended infrared transparency windows. With high refractive index values and appropriate rare-earth (RE) solubility, chalcogenide glasses exhibit high spontaneous emission probabilities and consequently, large emission cross-sections of radiative electronic transitions of RE^{3+} ions. The low phonon energy of these materials 350 cm^{-1} (for sulphides) and 250 cm^{-1} (for selenides) limits the non-radiative multiphonon relaxation rates. Besides

excellent heat dissipation, the fiber geometry of ChG doped with rare earths offers the possibility of high pump intensity and good overlap of pump and laser modes, resulting in lower laser thresholds and increased laser efficiencies. Rare earths mainly doped in chalcogenide glasses are with Pr^{3+} , Tb^{3+} , Dy^{3+} , Ho^{3+} , Er^{3+} , and Tm^{3+} ions ⁵.

Photoluminescence studies in bulk and thin film samples reports the overlap of optical transitions involving absorption and emission bands due to discrete levels of RE ions with the conduction band and edge states of host materials⁶. The efficiency of luminescence is found to increase highly at mid IR wavelengths ⁷. Due to the high refractive index of these glasses they exhibit high optical non-linearity and could therefore be useful for all-optical switching (AOS) ⁸.

Even though a large number of studies on photoluminescence are reported on RE doped chalcogenide glasses, no studies on the influence of doping on the band gap and refractive index have been reported. Evaluation of refractive indices for chalcogenide thin film materials is indispensable for practical applications in integrated optical devices such as switches, filters and modulators where the refractive index of a material is a key parameter for device design⁸.

6.2. Experimental

The chalcogenide glass compositions studied were $\text{Ge}_{28}\text{Sb}_{12}\text{Se}_{60}$ doped with 0.1% Er, 0.2% Er and 0.3% Er. Bulk glassy materials were prepared by conventional melt quenching technique.

Materials (5N purity, Sigma Aldrich) were weighed (4 g for each batch) according to their atomic weight percentage and sealed in evacuated (at 10^{-5} mbar) quartz ampoules. The sealed ampoule was kept inside a rotating and rocking furnace where the temperature was increased up to 1050°C . After heating for 24 hours, the ampoules of molten materials were rapidly quenched in ice cooled water.

Films of bulk glasses were deposited on microscopic glass substrates using the vacuum evaporation technique (Hindhivac Model No. 12A4D). The thickness of the solid films has been monitored during depositions by using a thickness monitor (DTM-101). The thickness of the studied samples were 325nm.

6.3. Structural, thermal and optical characterization of bulk glass

6.3.2. Structural and thermal analysis

The XRD analyses of the doped and undoped samples were carried out to confirm the amorphous nature of the samples. X-ray diffraction data reveals the amorphous nature of the prepared specimens as shown in Figure 6.1 a and 6.1 b of 0.1 % Er doped and 0.3% erbium doped ChG. The XRD image of the undoped $\text{Ge}_{28}\text{Sb}_{12}\text{Se}_{60}$ glass is shown in Figure 4.3 in chapter 4.

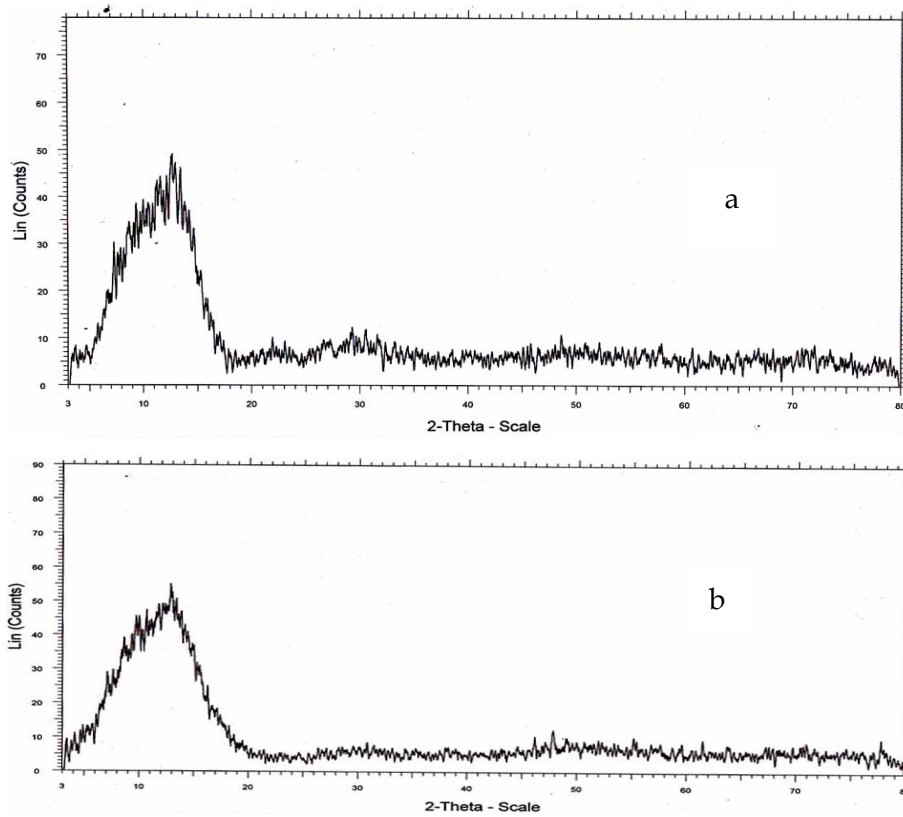


Figure 6.1: a) XRD pattern for 0.1% Erbium doped $\text{Ge}_{28}\text{Sb}_{12}\text{Se}_{60}$ glass b) 0.3% Erbium doped $\text{Ge}_{28}\text{Sb}_{12}\text{Se}_{60}$ glass.

In order to determine the characteristic temperatures of glasses ie, glass transition temperature (T_g), a differential scanning calorimeter was used under Ar atmosphere with a rate of $10^\circ\text{C}/\text{min}$. The DSC curve for $\text{Ge}_{28}\text{Sb}_{12}\text{Se}_{60}$ system doped with 0.1% and 0.3% erbium is shown in Figure 6.2. The T_g for $\text{Ge}_{28}\text{Sb}_{12}\text{Se}_{60}$ system is 274°C and 281°C , 287°C and 292°C for 0.1% Er, 0.2%Er, 0.3% Er doped $\text{Ge}_{28}\text{Sb}_{12}\text{Se}_{60}$ films respectively.

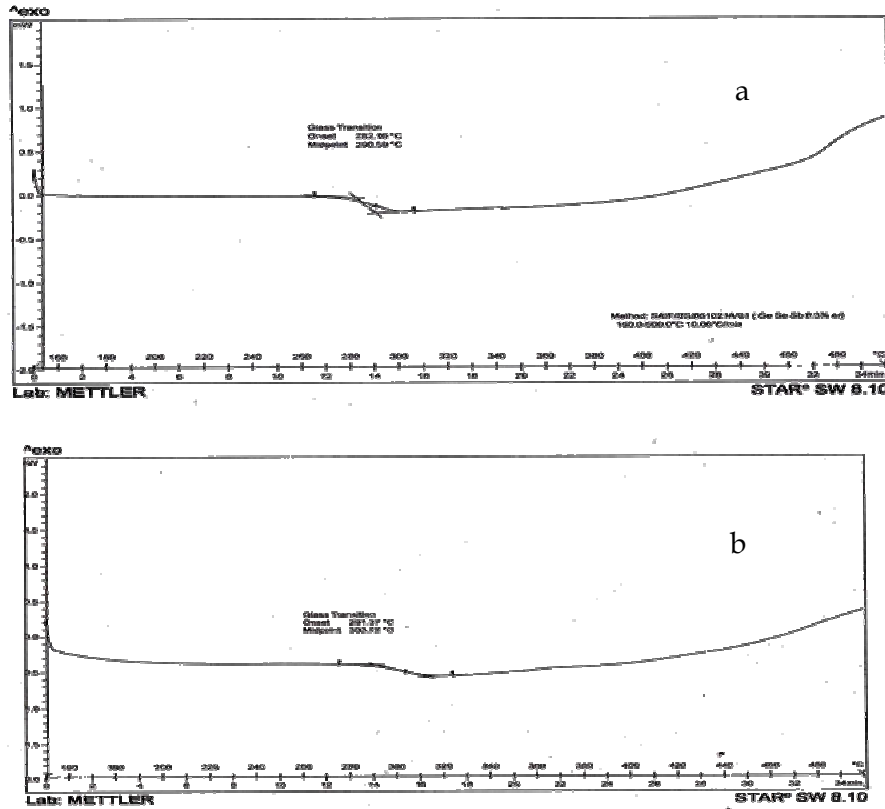


Figure.6.2: DSC curve for $\text{Ge}_{28}\text{Sb}_{12}\text{Se}_{60}$ system doped with a) 0.1% and b) 0.3% erbium

6.3.3. Absorption spectroscopy of erbium doped bulk glasses

Absorption spectra of erbium doped $\text{Ge}_{28}\text{Sb}_{12}\text{Se}_{60}$ bulk glasses is given in Figure 6.3. It is observed that an increase of erbium content in the system leads to a shift in absorption edge to lower wavelength side. Thus an increase in the optical band gap is observed by the addition of erbium to the glass. The band gap estimated from the plot of absorbance is 1.60 eV, 1.65 eV, 1.68 eV and 1.74 eV for un doped, 0.1%Er, 0.2%Er, 0.3%Er doped $\text{Ge}_{28}\text{Sb}_{12}\text{Se}_{60}$ glasses respectively.

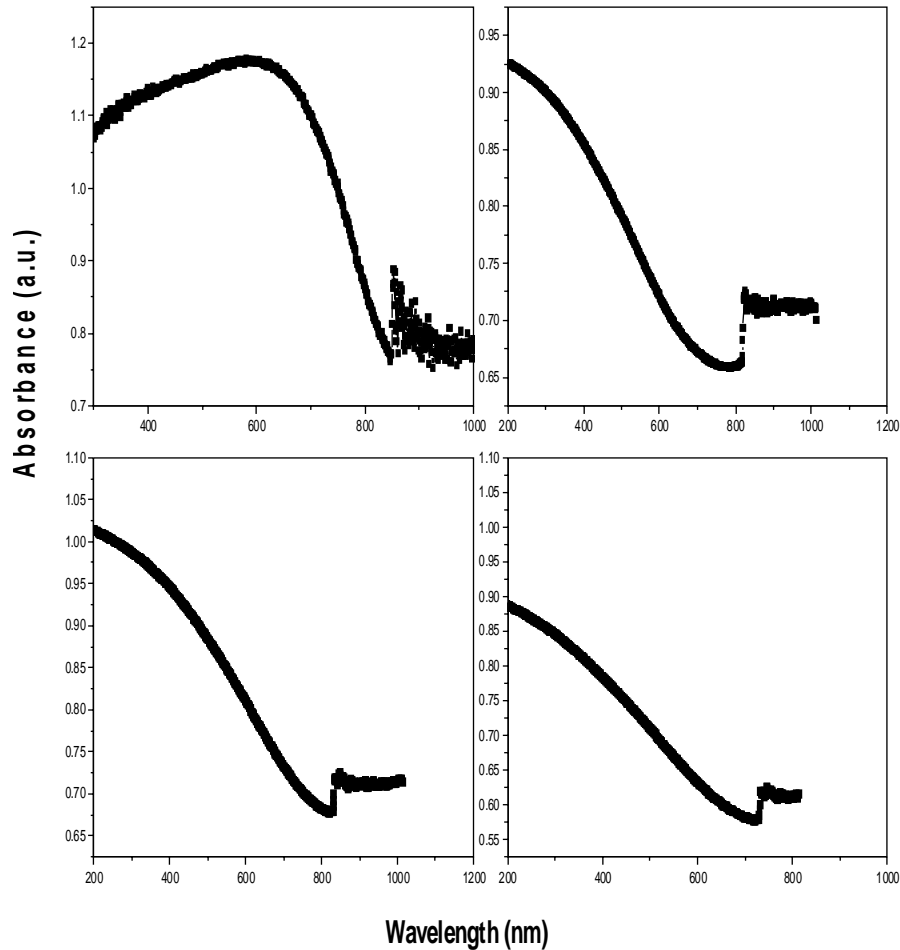


Figure 6.3: Plot of absorbance versus wavelength for bulk $\text{Ge}_{28}\text{Sb}_{12}\text{Se}_{60}$, 0.1%Er doped, 0.2% Er doped and 0.3 % Er doped glasses.

6.4. Optical characterization of erbium doped thin films

The amorphous nature of the thin films was confirmed by absence of sharp structural peaks in the X-ray diffraction patterns. The normal incidence transmittance and reflectance spectra in the

spectral range 250–2500 nm of films obtained by a double beam ultraviolet–visible–near infrared spectrophotometer (Jasco V 570) are presented in Figure 6.4.

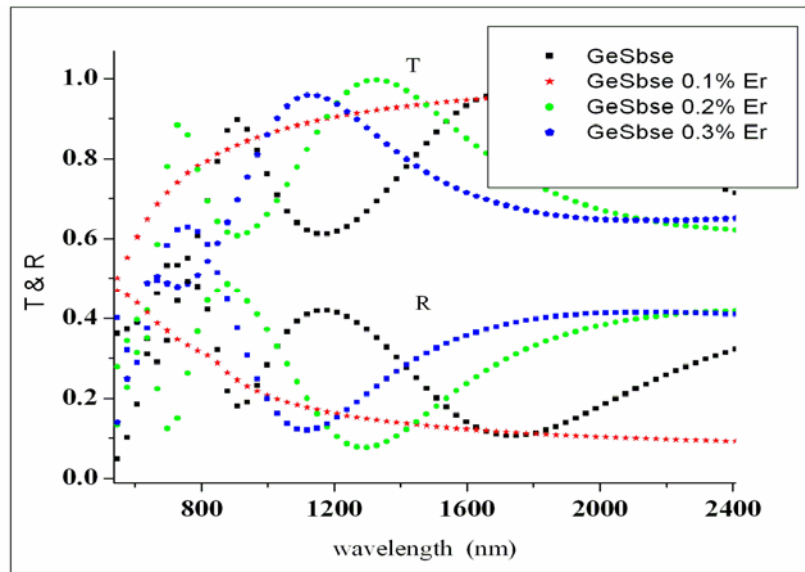


Figure 6.4: The transmittance and reflection spectra of $\text{Ge}_{28}\text{Sb}_{12}\text{Se}_{60}$ glasses with varying erbium concentrations.

The absorption coefficient (α) of these materials which strongly depends on optical transmission (T), reflection (R) and thickness of film (d) which was evaluated using the relation used to find the band gap of the films as discussed in section 2.2.4. From the linear plots of $(\alpha h\nu)^{1/2}$ against $(h\nu)$ for these samples, the optical energy gap has been determined from the intercepts of extrapolations to zero with the photon energy axis $(\alpha h\nu)^{1/2} \rightarrow 0$ (i.e. Tauc extrapolation)⁹. From the results obtained it is seen that an increase of erbium content in the system leads to an increase in the optical band gap (Table 6.1).

A number of theories are developed to understand network disorder of these glassy solids. Reports show that the existence of molecular clusters or domains in the glass structure plays a significant role in determining the absorption characteristics and refractive index of these materials¹⁰. Strong evidence of the presence of broken chemical order and structural heterogeneity of Ge containing chalcogenide glasses has also been reported¹¹. These unsaturated bonds along with some saturated bonds such as dative bonds, produced due to insufficient number of atoms in these solids, are responsible for the formation of localized states in the band gap^{12,13}. The increase in band gap in this system can be attributed to the impurity induced structural modifications which markedly manifest themselves in the absorption spectra.

The dependence of $\ln(\alpha)$ versus $h\nu$, as shown in Figure 6.5, is a straight line, from which the inverse of the slope, gives the width of the tails of the localized states at the band gap. The values of E_c obtained for the different compositions are listed in Table 6.1. The width of the tails of localized states in the band gap is found to decrease with the increase in erbium concentration. This again could be interpreted as due to the decrease in the degree of disorder as a result of impurity induced structural change^{14,15}. The decrease in disorder is manifested as an increase in E_g .

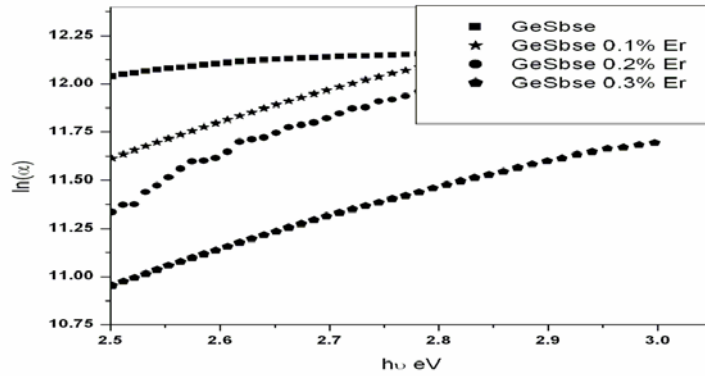


Figure 6.5: Plot of $\ln(\alpha)$ versus $h\nu$.

The extinction coefficient (k) and refractive index (n) are important parameters characterizing photonic materials. Values of n and k are calculated using the experimental data obtained for the samples under study using the relation $k = \alpha\lambda/4\pi$ where λ is the wavelength and α , the absorption coefficient.

The refractive index (n) tends to decrease with increasing wavelength exhibiting normal dispersion. The high refractive index values of these glasses are advantageous for strong optical confinement and enhance the optical intensities for nonlinear interactions. The knowledge of real part and imaginary part of the dielectric constant provide information about the loss factor¹⁶. The real part of the dielectric constant is associated with the term that shows how much it will slow down the speed of light in the material and the imaginary part shows how a dielectric absorbs energy from an electric field due to dipole motion. The dielectric constant (ϵ_r) and dielectric loss (ϵ_i) determined from refractive index and extinction coefficient and are given in Table 6. 1.

Table 6.1: Values of Band gap (E_g), the slope parameter of the Urbach region (E_e), the dielectric constant (ϵ_r), dielectric loss (ϵ_i), static refractive index (n_0), and the refractive index (n) (at 1.8 eV) for the films.

Composition	E_g (eV) Tauc Method	E_e (eV)	ϵ_r	ϵ_i	n_0	n (at1.8 eV)
$\text{Ge}_{28}\text{Sb}_{12}\text{Se}_{60}$	1.66	3.71	15.70	0.61	3.29	3.67
$\text{Ge}_{28}\text{Sb}_{12}\text{Se}_{60} + 0.1\% \text{Er}$	1.73	0.69	12.71	0.47	2.67	2.84
$\text{Ge}_{28}\text{Sb}_{12}\text{Se}_{60} + 0.2\% \text{Er}$	1.80	0.66	10.38	0.23	2.30	1.71
$\text{Ge}_{28}\text{Sb}_{12}\text{Se}_{60} + 0.3\% \text{Er}$	1.87	0.61	9.01	0.08	1.79	1.43

6.4.1. Dispersion analysis of the refractive index

The dispersion parameters are significant factors in optical communication and in designing devices for special applications. The spectral dependence of the refractive index, in the visible and near infrared regions, has been analyzed in terms of the Wemple-Di Domenico (WDD) single effective oscillator model ¹⁷.

According to this model the relation between the refractive index and the single oscillator strength can be described using the relation,

$$\left(n^2 - 1\right) = \left[\frac{E_d E_o}{E_o^2 - (h\nu)^2} \right] \quad 6.1$$

The dispersion energy (E_d) measures the average strength of interband optical transitions and is associated with the changes in the structural order of the material ie, it is related to the ionicity, anion valency and coordination number of the material and E_0 is the

effective oscillator energy. The increase in the dispersion energy value is usually associated with decrease in the band gap¹⁸.

Plotting $(n^2 - 1)^{-1}$ versus $(h\nu)^2$ as shown in Figure 6.6, yields a straight line for normal behavior. The observed positive deviation from linearity at longer wavelength is attributed to a negative contribution of the lattice vibrations to the refractive index¹⁸. The least-square fit of the linear parts of these plots allows us calculating the values of E_0 and E_d from the slope $(E_0 E_d)^{-1}$ and the intercept (E_0/E_d) , respectively.

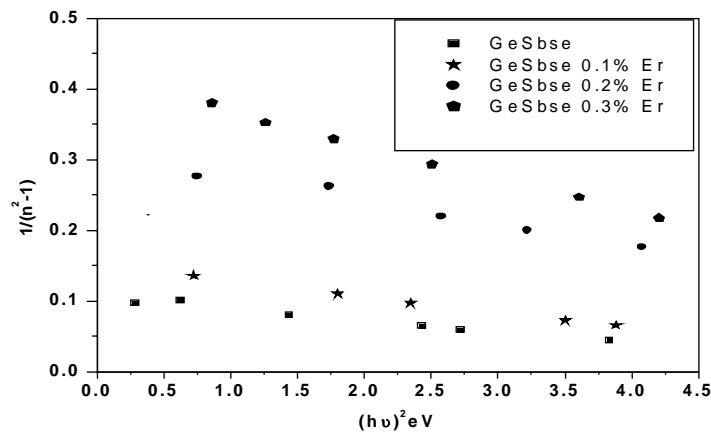


Figure 6.6: $(n^2 - 1)^{-1}$ versus $(h\nu)^2$ graph for doped and undoped thin films.

The static refractive index (n_0) has been calculated from WDD dispersion¹⁸ parameters E_0 and E_d using the formula,

$$n_o = \left(1 + \frac{E_d}{E_0}\right)^{1/2} \quad 6.2$$

The calculated value for static refractive index is tabulated in Table 6.1.

Simple empirical relation based on generalized Miller's rule can be used for the estimation of the non linear refractive index (n_2) and susceptibility ($\chi^{(3)}$). The non linear refractive index (n_2) and susceptibility ($\chi^{(3)}$) can be calculated by combining Miller's generalized rule¹⁹ and low-frequency linear refractive index estimated from Wemple-Di Domenico single effective oscillator model. The linear optical susceptibility in the case of chalcogenide glasses is given by relation: $\chi(1) = (n_2-1)/4\pi$. Using generalized Miller's rule we obtain

$$\chi^{(3)} = A(\chi^{(1)})^4 \quad 6.3$$

Estimated A value is 1.7×10^{-10} (for $\chi(3)$ in (esu)).

The n_2 can be calculated²⁰ from the relation,

$$n_2 = \frac{12 \pi \chi^{(3)}}{n_0} \quad 6.4$$

Values of dispersion energy (E_d), the single-oscillator energy or Wemple–Di Domenico gap (E_0), non linear susceptibility ($\chi(3)$) and non linear refractive index (n_2) are tabulated in Table 6.2. The high refractive index values of these glasses are advantageous for strong optical confinement and for nonlinear interactions.

Table 6.2: Calculated Values of dispersion energy (E_d), the single-oscillator energy or Wemple–Di Domenico gap (E_0), non linear susceptibility ($\chi^{(3)}$) and non linear refractive index (n_2).

Composition	E_d (eV)	E_0 (eV)	$\chi^{(3)}*10^{-13}$ (esu)	n_2*10^{-11} (esu)
$\text{Ge}_{28}\text{Sb}_{12}\text{Se}_{60}$	29.14	3.00	608.00	69.65
$\text{Ge}_{28}\text{Sb}_{12}\text{Se}_{60} + 0.1\% \text{Er}$	18.94	3.10	94.18	13.43
$\text{Ge}_{28}\text{Sb}_{12}\text{Se}_{60} + 0.2\% \text{Er}$	10.05	3.36	5.47	0.89
$\text{Ge}_{28}\text{Sb}_{12}\text{Se}_{60} + 0.3\% \text{Er}$	8.05	3.64	1.63	0.34

6.5. Conclusions

The transmission and reflection spectra of $\text{Ge}_{28}\text{Sb}_{12}\text{Se}_{60}$ thin film doped with different concentrations of erbium have been analyzed for the calculation of the optical parameters. It is found that these glasses are attractive candidates for applications requiring low transmission losses, as they are transparent to IR radiation. The optical band gap obtained by Tauc's extrapolation is in good agreement with the optical band gap by the Wemple–Di Domenico single oscillator model. The optical energy gap has been found to increase with increase in erbium content. The increase can be interpreted as due to the decrease of the width of the tails of localized states in the band gap. The refractive index (n) and extinction coefficient (k) tends to decrease with increasing wavelength exhibiting normal dispersion. Dispersion of refractive index has been studied using the WDD single oscillator model. The static refractive index decreases with increase of erbium concentration in the host glass. The oscillator energy, E_0 follows the empirical relation with the optical band gap. The high values of n_2 show they are interesting materials for non linear applications.

6.6. References

1. Victor K. Tikhomirov, "Photoinduced defects in undoped and rare-earth doped chalcogenide glasses: review", *Journal of Non-Crystalline Solids.*, 256&257, 328-336 (1999).
2. Angela B Seddon, Zhuoqi Tang, David Furniss, Slawomir Sujecki, and Trevor M Benson, "Progress in Progress in rare-earth-doped mid-infrared fiber lasers", *Optics Express.*, 18, 26704-26719 (2010).
3. Yu.S. Tver'yanovich and A. Tverjanovich, "Rare-earth doped chalcogenide glass", *Semiconductors and Semimetals.*, 80, 169-207(2004).
4. A. B Seddon, "Chalcogenide glasses: a review of their preparation, properties, and applications," *Journal of Non-Crystalline Solids.*, 184, 44-50 (1995).
5. J. S. Sanghera, L. B. Shaw, L. E. Busse, V. Q. Nguyen, P. C. Pureza, B. C. Cole, B. B. Harrison, I. D. Aggarwal, R. Mossadegh, F. Kung, D. Talley, D. Roselle, R. Miklos, "Development and infrared applications of chalcogenide glass optical fibers" , *Fiber Integrated Opt.*, 19 [3], 251 - 274 (2000).
6. N. Samson, T. Schweizer, D. W. Hewak, and R. I. Laming, " Properties of dysprosium doped GaLaS fiber amplifiers operating at $1.3 \mu m$," *Optics Letters.*, 22, 703-705 (1997).
7. Dan Hewak, "Properties Processing and applications of Glass and Rare earth -doped glasses for Optical fibers", INSPEC, The Institution of Electrical Engineers, London, United Kingdom (1998).
8. A. Zakery and S.R. Elliott, "Optical Nonlinearities in Chalcogenide Glasses and their Applications", Springer Series in Optical Sciences, Springer: Berlin (2007).
9. J. Tauc, "Absorption edge and internal electric fields in amorphous semiconductors," *Mater. Res. Bull.*, 5(8), 721-729 (1970).
10. S. Wemple, "Refractive-index behavior of amorphous semiconductors and glasses," *Phys. Rev. B.*, 7(8), 3767-3777 (1973).

11. Max Shurgalin, Vladimir N. Fuflyigin and Emilia Anderson, "The structural heterogeneity and optical properties in chalcogenide glass films " , J. Phys. D: Appl. Phys., 38, 4037-4047 (2005).
12. P. Boolchand, J. Grothaus, W.J Bresser and P. Surany, " Structure of GeSsub_2 glass: Spectroscopic evidence for broken chemical order" , Phy.Rev. B., 33, 5421-5434 (1986).
13. J.A Olley, "Structural disorder and the urbach edge", Solid State Communication., 13 [9], 1437-1440 (1973).
14. S.A.Kozyukhin, A. R Fairushin, E. N. Voronkov, "Amorphous Arsenic chalcogenide films modified using rare-earth complexes" , J. Optoelectron. Adv. Mater., 7(3), 1457 -1461 (2005).
15. Adler D, "Density of States in the Gap of Tetrahedrally Bonded Amorphous Semiconductors" , Phys. Rev. Lett., 41, 1755–1758 (1978).
16. P.Sharma and S. C.Katyal, "Optical study of $\text{Ge}_{10}\text{Se}_{90-x}\text{Te}_x$ glassy semiconductors" , Thin Solid Films., 515, 7966 (2007).
17. S. H. Wemple and M.DiDomenico, "Behavior of the Electronic Dielectric Constant in Covalent and Ionic Materials," Phys. Rev. B., 3, 1338-1351 (1971).
18. Y. A. El-Gendy, "Refractive index, oscillator parameters and optical band gap of e-beam evaporated $\text{Ga}_{10}\text{Ge}_{10}\text{Te}_{80}$ films" , J. Phys. D: Appl. Phys., 42, 115408 (2009).
19. Wang C, "Empirical Relation between the Linear and the Third-Order Nonlinear Optical Susceptibilities" , Phys. Rev. B., 2 [6] 2045-2048(1970).
20. H. Ticha and L.Tichy, "Semiempirical relation between non-linear susceptibility (refractive index), linear refractive index and optical bandgap and its application to amorphous semiconductors" , Journal of Optoelectronics and Advanced Materials., 4[2], 381 – 386 (2002).



Chapter 7

CHALCOGENIDE NANO COMPOSITES FOR ACTIVE AND PASSIVE PHOTONIC DEVICES

- 7.1. Section 1. Double-layered chalcogenide nano composites
 - 7.2. Section 2. Fabrication and characterization of nano colloid $Ga_5Sb_{10}Ge_{25}Se_{60}$ doped polymer optical fibers
 - 7.3. Conclusions
 - 7.4. References
-

This chapter presents the application of nano composites based on chalcogenide glass for active and passive photonic devices and it is divided into two sections. First sections deals with a new way of stacking nano composite films with nano sized thermally evaporated chalcogenide films. Different ways of stacking and the optical properties of single layers and double-layered stacked films are discussed. The photosensitivities of the double layered films are also studied using above band gap nano second pulsed laser. Fabrication and characterization of new nano colloid $Ga_5Sb_{10}Ge_{25}Se_{60}$ doped PMMA optical fibers are discussed in section 2. Preform technique is used to fabricate poly methyl methacrylate (PMMA) fibers incorporating nano colloid $Ga_5Sb_{10}Ge_{25}Se_{60}$ chalcogenide glass. The optical properties of the hybrid composite fibers are investigated by UV-VIS-NIR spectrophotometry and photoluminescence spectroscopy.

7.1. Section 1. Double-layered chalcogenide nano composites

7.1.1. Introduction

Stacked thin films of alternating dielectric layers have been used in optics for many decades for mirrors and filters¹⁻³. In recent days they are getting lot of importance because they can be designed to reflect combinations of incident wavelength, polarization, and angular range with nearly zero loss^{4,5}. The one-dimensional photonic bandgaps are created in the dielectric multilayers if optical constants and thicknesses of films meet the Bragg resonance condition. The curiosity in dielectric multilayers was improved again, when the omnidirectional bandgap was reported by Fink et al.⁶ in 1998 for the reflectors having the refractive index (n) difference of films higher than $\Delta n \geq 0.8$. The first successful fabrications of planar omnidirectional reflectors with bandgaps in the visible, near-infrared and middle-infrared ranges were reported on materials such as $\text{SiO}_2/\text{TiO}_2$, Si/SiO_2 or GaAlN/GaN ^{7,8}. These materials showed good optical properties and a high chemical, thermal, and mechanical stability.

S.H. Kim et al.⁹ have recently discovered that that appropriately designed stacks exhibit omnidirectional reflection (near unity reflectance for all incidence angles and polarization states) within one or more bands of wavelength. The omnidirectional total reflection from such quarter wave stacks (QWS) allows the designing of the reflectors that can reflect the light at any angles and polarizations. A common goal in current QWS

device design is then a maximization of a bandwidth of the omnidirectional bandgap by using materials having a high refractive index difference.

V. Balan et al.¹⁰ found that two multimode planar chalcogenide waveguides based upon $\text{Ge}_{29}\text{As}_{12}\text{Se}_{59}$ / $\text{Ge}_{21}\text{Sb}_{18}\text{Se}_{61}$ / $\text{Ge}_{29}\text{As}_{12}\text{Se}_{59}$ stacked layers can guide at 1.55 microns. They also showed that the discovered new rib waveguide can be applicable for spatial interferometry, which implies the use of components working in the far infrared for the detection and the spectroscopic study of extra solar planets and environmental metrology. Planar omnidirectional reflectors with fundamental stop bands centred at wavelength $\lambda=1.55 \mu\text{m}$ made-up from different chalcogenide glasses, e.g. $\text{GeS}_2/\text{Sb}_2\text{Se}_3$, have been reported^{11, 12}. Studies show that the key parameter for the successful preparation of omnidirectional reflecting coatings is the knowledge of thickness dependence of the refractive indices of the materials^{13,14}.

Possibilities of chalcogenide and polymer films as an alternative to dielectric materials have been developed recently¹⁴. The omnidirectional QWS devices can be fabricated as multilayers using thermal evaporation of high index chalcogenide glasses and the spin-coating of polymers which form a low index films. A combination of highly transparent chalcogenide and polymer films enables these QWS elements to cover the wavelength ranges reaching from the visible to the infrared spectral regions including telecommunication wavelengths¹⁵.

In order to fabricate the above mentioned mirrors and filters certain conditions have to be contented¹⁶. For example assume n_H , d_H , and n_L , d_L are the refractive index and thickness of the high and low index layers, respectively, $\Lambda=d_L+d_H$ is the period of the stack, and n_0 is the refractive index of the incident medium. The reality of an omnidirectional band requires that both $\delta n_0=n_L/n_0$ and $\delta n_1=n_H/n_L$ are relatively large. When these two parameters go over some minimum threshold, the Brewster line lies outside the acceptance angle for light rays incident on the mirror from the external medium, and there are finite ranges of wavelength for which no propagating modes be present inside the dielectric stack. A common design objective is to maximize the omnidirectional bandwidth, either because the application essentially requires broadband reflection or in order to unwind the fabrication tolerance for narrowband applications¹⁶⁻¹⁸.

An initial step for the fabrication of devices by stacking is the awareness of the optical parameters of the double layers and it is discussed in this section. By knowing the optical properties of the single layer and double layered films one can easily design the thickness and number of layers required for required application. The optical characterization of stacked layers of thermally evaporated $\text{Ga}_5\text{Sb}_{10}\text{Ge}_{25}\text{Se}_{60}$ (TE) and $\text{Ga}_5\text{Sb}_{10}\text{Ge}_{25}\text{Se}_{60}$ /PVA composite film were discussed. The photosensitivity of the stacked films were also studied.

7.1.2. Fabrication of stacked layers

Stacking was done mainly in two ways (1) the thermally evaporated $\text{Ga}_5\text{Sb}_{10}\text{Ge}_{25}\text{Se}_{60}$ film (TE) was coated above the spin coated $\text{Ga}_5\text{Sb}_{10}\text{Ge}_{25}\text{Se}_{60}$ composite film and (2) the composite film was coated on the thermally evaporated $\text{Ga}_5\text{Sb}_{10}\text{Ge}_{25}\text{Se}_{60}$ films. The composite films with two different grain size, C1 and C2 {C1 =1 ml nano colloid solution (0.67 mg $\text{Ga}_5\text{Sb}_{10}\text{Ge}_{25}\text{Se}_{60}$ dissolved in 1 ml butylamine) + 1 ml PVA) and C2=1 ml nano colloid solution (0.54 mg $\text{Ga}_5\text{Sb}_{10}\text{Ge}_{25}\text{Se}_{60}$ dissolved in 1ml butylamine) +1 ml PVA)} were also coated with thermally evaporated $\text{Ga}_5\text{Sb}_{10}\text{Ge}_{25}\text{Se}_{60}$ film. The thermally evaporation of the films were made from the bulk $\text{Ga}_5\text{Sb}_{10}\text{Ge}_{25}\text{Se}_{60}$ chalcogenide glass prepared by melt quenching method. The conditions used for the thermal evaporations were same for all thermally evaporated films. The evaporation was done at pressure of 2×10^{-5} m bar and at a rate of 10 Å/s. The composite films of $\text{Ga}_5\text{Sb}_{10}\text{Ge}_{25}\text{Se}_{60}$ /PVA were fabricated form the nano colloid $\text{Ga}_5\text{Sb}_{10}\text{Ge}_{25}\text{Se}_{60}$ chalcogenide glass and poly vinyl alcohol in the ratio 1:1. The evaporated thin films were having thickness of 520 nm. The composite films were having a thickness of 56 μm . Schematic representation of the Composite film coated above with TE film is shown in Figure 7.1.

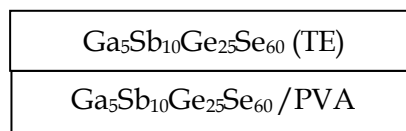


Figure 7.1: Schematic representation of stacked film.

7.1.3. Optical studies on double layered films

The transmission spectra of the investigated films are shown in Figure 7.2. Plot (a), (b), (c) and (d) in Figure 7.2 show the transmission spectra of thermally evaporated (TE) $\text{Ga}_5\text{Sb}_{10}\text{Ge}_{25}\text{Se}_{60}$ film, $\text{Ga}_5\text{Sb}_{10}\text{Ge}_{25}\text{Se}_{60}$ /PVA composite film, thermally evaporated $\text{Ga}_5\text{Sb}_{10}\text{Ge}_{25}\text{Se}_{60}$ film coated on the $\text{Ga}_5\text{Sb}_{10}\text{Ge}_{25}\text{Se}_{60}$ /PVA composite film and $\text{Ga}_5\text{Sb}_{10}\text{Ge}_{25}\text{Se}_{60}$ /PVA composite film coated on the thermally evaporated $\text{Ga}_5\text{Sb}_{10}\text{Ge}_{25}\text{Se}_{60}$ film respectively.

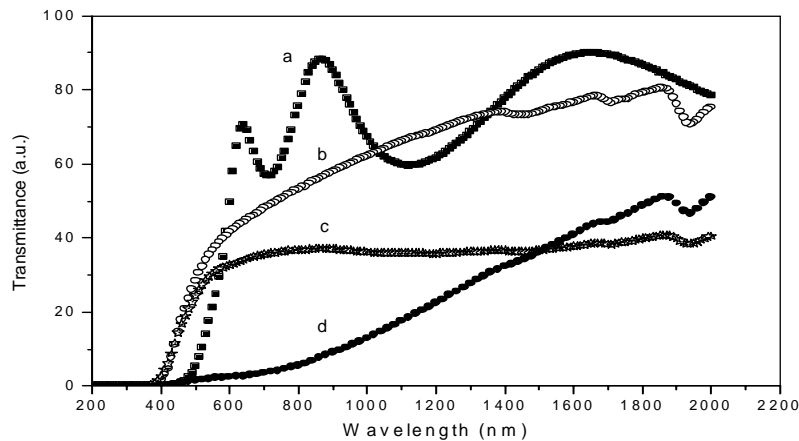


Figure 7.2: Transmission spectra of a) TE $\text{Ga}_5\text{Sb}_{10}\text{Ge}_{25}\text{Se}_{60}$ film, b) $\text{Ga}_5\text{Sb}_{10}\text{Ge}_{25}\text{Se}_{60}$ /PVA film, c) TE $\text{Ga}_5\text{Sb}_{10}\text{Ge}_{25}\text{Se}_{60}$ coated on $\text{Ga}_5\text{Sb}_{10}\text{Ge}_{25}\text{Se}_{60}$ /PVA film and d) $\text{Ga}_5\text{Sb}_{10}\text{Ge}_{25}\text{Se}_{60}$ /PVA coated on TE $\text{Ga}_5\text{Sb}_{10}\text{Ge}_{25}\text{Se}_{60}$ film.

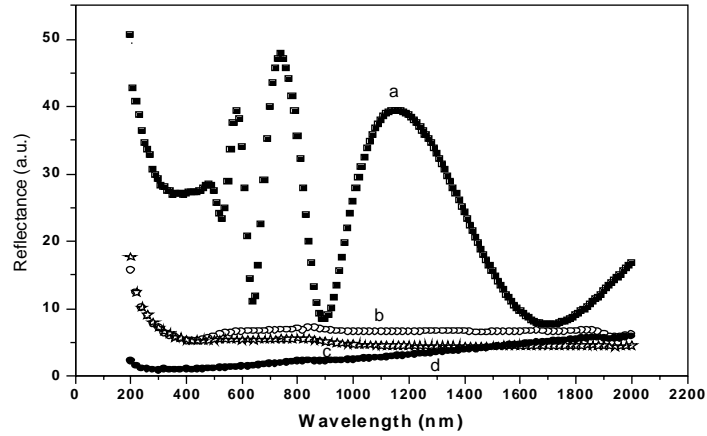


Figure 7.3: Reflectance spectra of TE Ga₅Sb₁₀Ge₂₅Se₆₀ film, b) Ga₅Sb₁₀Ge₂₅Se₆₀/PVA film, c) TE Ga₅Sb₁₀Ge₂₅Se₆₀ coated on Ga₅Sb₁₀Ge₂₅Se₆₀/PVA film and d) Ga₅Sb₁₀Ge₂₅Se₆₀/PVA coated on TE Ga₅Sb₁₀Ge₂₅Se₆₀ film.

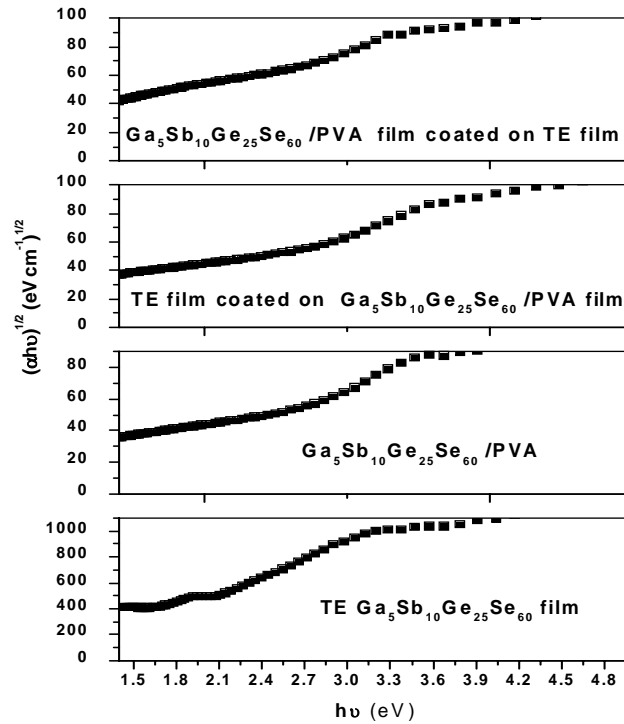


Figure 7.4: $(ah\nu)^{1/2}$ versus $h\nu$.

It is clear from the transmission spectra that $\text{Ga}_5\text{Sb}_{10}\text{Ge}_{25}\text{Se}_{60}/\text{PVA}$ coated on TE $\text{Ga}_5\text{Sb}_{10}\text{Ge}_{25}\text{Se}_{60}$ act as filter up to 700nm (labeled as d in Figure 7.2). Applications of variable wavelength stacked composite based chalcogenide films include IR filters used in portable miniaturized IR spectrometers, disposable chemical, and biological sensors. The reflectance spectra of the films are also shown in Figure 7.3. The optical parameters of the stacked films are studied using Manifer et al.¹⁹ and Swanepoel²⁰ method as discussed in section 2.2.4. The band gap of the films are found from the plot of $(\alpha h\nu)^{1/2}$ versus $(h\nu)$ as shown in Figure 7.4. The band gaps are found to be 1.65 eV, 2.10 eV, 1.96 eV and 1.61 eV for thermally evaporated (TE) $\text{Ga}_5\text{Sb}_{10}\text{Ge}_{25}\text{Se}_{60}$ film, $\text{Ga}_5\text{Sb}_{10}\text{Ge}_{25}\text{Se}_{60}/\text{PVA}$ composite film, TE $\text{Ga}_5\text{Sb}_{10}\text{Ge}_{25}\text{Se}_{60}$ film coated on $\text{Ga}_5\text{Sb}_{10}\text{Ge}_{25}\text{Se}_{60}/\text{PVA}$ composite film and $\text{Ga}_5\text{Sb}_{10}\text{Ge}_{25}\text{Se}_{60}/\text{PVA}$ coated on TE $\text{Ga}_5\text{Sb}_{10}\text{Ge}_{25}\text{Se}_{60}$ film respectively. Coating TE film above composite film remains as stacked one but when composite film was coated above on TE films some reaction took place and resulted in a film with highly concentration. The refractive index of the film are 2.50, 1.72, 1.55 and 1.38 for thermally evaporated (TE) $\text{Ga}_5\text{Sb}_{10}\text{Ge}_{25}\text{Se}_{60}$ film, $\text{Ga}_5\text{Sb}_{10}\text{Ge}_{25}\text{Se}_{60}/\text{PVA}$ composite film, TE $\text{Ga}_5\text{Sb}_{10}\text{Ge}_{25}\text{Se}_{60}$ film coated on $\text{Ga}_5\text{Sb}_{10}\text{Ge}_{25}\text{Se}_{60}/\text{PVA}$ composite film and $\text{Ga}_5\text{Sb}_{10}\text{Ge}_{25}\text{Se}_{60}/\text{PVA}$ coated on TE $\text{Ga}_5\text{Sb}_{10}\text{Ge}_{25}\text{Se}_{60}$ film respectively.

The TE films were coated on composite films ($\text{Ga}_5\text{Sb}_{10}\text{Ge}_{25}\text{Se}_{60}/\text{PVA}$ films prepared from nano colloid solutions) with two different grain size (C1 and C2). The thickness of the composite films and TE films were optimized so as to get the interference patterns

on the transmission spectra. The presence of the interference patterns makes the optical parameter calculation easy using the Swanepoels method as discussed in 2.2.4. The plot of the $(\alpha h\nu)^{1/2}$ versus $h\nu$ for composite films and stacked films are given in Figure 7.5. The composite films used for stacking are indicated as C1 and C2 and the stacked films as C1TE (composite film C1 stacked with TE film) and C2TE (composite film C2 stacked with TE film).

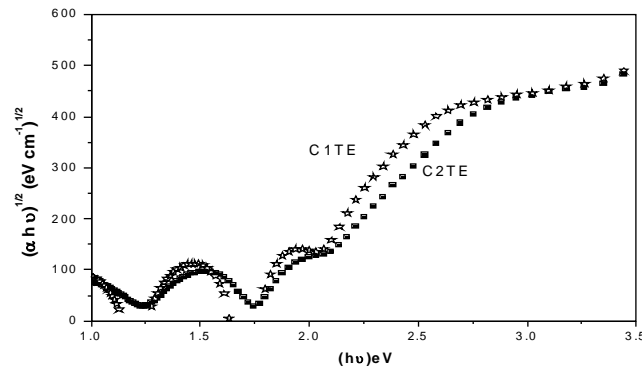


Figure 7.5: Plot of $(\alpha h\nu)^{1/2}$ versus $h\nu$ for C1TE and C2TE.

Table 7.1: Calculated values of bandgap (E_g), refractive index (n), extinction coefficient (k), dielectric constants (ϵ_r , ϵ_i), optical conductivity, third order non linear susceptibility (χ^3) and non linear refractive index (n_2).

Parameters	C1TE	C2TE
E_g (eV)	1.84	1.93
n	3.04	2.58
k	0.00001	0.005
ϵ_r (eV)	9.24	6.65
ϵ_i (eV)	6.08×10^{-5}	0.026
σ (s^{-1})	9.25×10^{-9}	3.9×10^{-4}
$\chi^3 \times 10^{-12}$ (esu)	15.4	6.51
$n_2 \times 10^{-11}$ (esu)	20.71	9.57

The optical parameters of the films are tabulated in Table 7.1. By stacking the TE film on composite films the band gap is found to be between the E_g of TE film and $\text{Ga}_5\text{Sb}_{10}\text{Ge}_{25}\text{Se}_{60}$ /PVA composite film. The refractive index has also increased with respect to the composite film. The change in band gap has led to the change in optical parameters like dielectric constants, extinction coefficient, nonlinear properties etc.

Understanding the knowledge of optical parameters (refractive index and extinction coefficient) of the single layers and double layers as discussed above are needed for the development of Quarter wave stacks, omnidirectional reflectors etc.²¹⁻²⁴.

➤ *Photosensitivity of stacked films*

An important property to be studied while fabricating devices using these films are the photoinduced changes of the refractive index. This can be used for enhancement of the optical contrast of both materials. Monomode channel or rib waveguides receive great importance in the field of spatial interferometry and in environmental metrology²⁵.

In order to study the photoinduced effects on the C1TE stacked films under excitation with nano second laser, the films were exposed with different Nd: YAG (532nm) laser powers. It is observed that above $6\mu\text{j}$ excitation, the $\text{Ga}_5\text{Sb}_{10}\text{Ge}_{25}\text{Se}_{60}$ film coated above the $\text{Ga}_5\text{Sb}_{10}\text{Ge}_{25}\text{Se}_{60}$ /PVA composite film gets damaged. The damage occurred to the film when exposed with $6\mu\text{j}$ nano second laser focused through a cylindrical lens is shown in Figure 7.6.

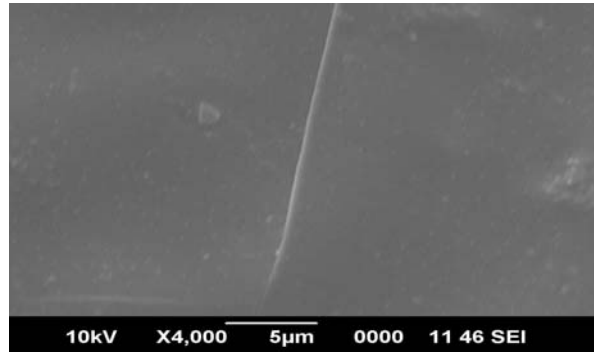


Figure 7.6: Laser damage occurred on stacked C1TE film.

The observed result show that exposure of $6\mu\text{j}$ laser can be used for patterning in photolithography and for making other photonic structures. In order to avoid the damage of the film we have studied the irradiation effect of the stacked film on exposure with $1\mu\text{j}$, $2\mu\text{j}$ and $4\mu\text{j}$ Nd: YAG laser for 30 minutes. The transmission spectra corresponding to the irradiated films are shown in Figure 7.7.

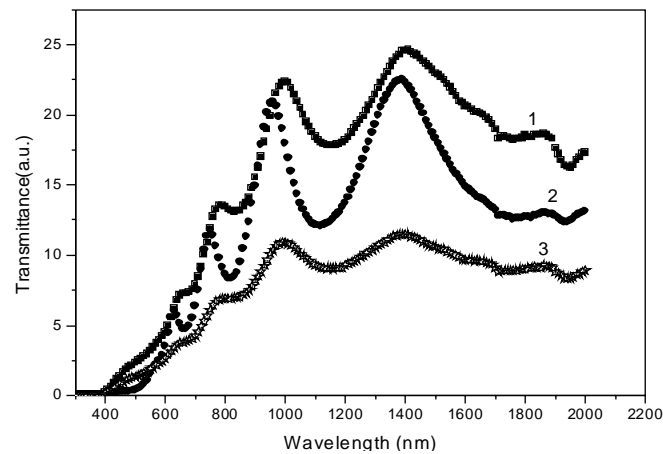


Figure 7.7: Transmission spectra of C1TE after exposure with $1\mu\text{j}$, $2\mu\text{j}$ and $4\mu\text{j}$ Nd: YAG laser for 30 minutes.

It is observed that the transmission edge gets shifted to the higher wavelength region on exposure. It shows that near band gap exposure results in photodarkening in the stacked films. The TE $\text{Ga}_5\text{Sb}_{10}\text{Ge}_{25}\text{Se}_{60}$ is found to be sensitive to above band gap and near band gap light²⁶. The photodarkening in the TE films are discussed in chapter 3. The band gap of the C1TE is 1.84 eV and irradiating it with above bandgap light (2.33 eV) results in the shift of band gap from 1.85 eV to 1.09 eV.

Photosensitivity of these films makes them promising materials for applications in optoelectronics and photonics. Studies show that the prepared stacked films act as a material for realization of holographic elements in waveguides, non linear all optical switching devices, Bragg gratings filters etc.

7.2. Section 2. Fabrication and characterization of nano colloid $\text{Ga}_5\text{Sb}_{10}\text{Ge}_{25}\text{Se}_{60}$ doped polymer optical fibers

7.2.1. Introduction

Now-a-days, in fiber technology the attention is paid in search of new tunable fibers like Photonic crystal fibers (PCF), microstructured polymer optical fibres (mPOF) doped with dyes and nano particles, dye and quantum dots doped polymer fibers²⁷⁻²⁹ etc. Photonic crystal fibers (PCF)²⁸, also known as microstructured optical fibers (MOF), can guide light by means of refractive index modulations created by the hole pattern surrounding the core^{28,29}. Such fibers have led to development of unique control over a range of

optical fiber properties including dispersion, numerical aperture and various nonlinear effects³⁰. MOF was fabricated first in silica and later on polymethylmethacrylate (PMMA)^{31,32}. The main advantage of microstructures in PMMA is the versatility of fabrication methods available to polymers, corresponding variety of microstructures and the relatively low processing temperatures employed. This low temperature processing allows the incorporation of both organic and inorganic materials, either through adding material to the monomer prior to polymerization or by solution doping at the preform stage³³. Such doping can further tailor mPOF properties beyond what is possible through the microstructure alone.

Polymethylmethacrylate (PMMA) is a transparent thermoplastic material used widely in the opto-electronic and photonics industries. The material most frequently used for polymer fibers is the thermoplastics PMMA better known as Plexiglass³⁴. The material was developed in 1928 was first brought to market in 1933 by Rohm and Haas Company³⁴. It has now become an alternative to silica-core optical fibers since they are comparatively cheaper and flexible. Another important practical limitation of using silica-core fibers is that they are very brittle when exposed and this imposes restrictions on sensor design such as limiting interaction length as well as precluding bending of fibers and applications involving moving fluids^{35,36}. Comparison of silica fiber and polymer fiber is tabulated in Table 7.2. Due to its good optical and thermal properties, it is often used in the manufacture of many devices like micro- and nano-devices including semiconductor

nanotube formation³⁷, nanoimprinting lithography³⁸, polymer optical fibers (POF)³⁹ and as a host matrix for electroluminescence devices⁴⁰.

Table 7.2: Comparison of silica and polymer optical fiber

	Silica fibre	Polymer fibre
Attenuation (dB/km)	0.2~3	10 ~ 100
Young's modulus (Gpa)	100	3
Breakdown strain (%)	1~2	5 ~ 10

Doping the polymer fibers with quantum dots (QD) have become an interesting area of research due to its unique optical properties that make them promising alternatives to traditional dyes in many luminescence based bioanalytical techniques. QD can grant a wide range of advantageous optical properties such as narrow emission spectra, non-linear properties, broad excitation spectra and an emission wavelength which can be readily 'tuned' by varying the characteristics and dimensions of the dots ^{41,42}.

Doping QD or other organic or inorganic materials in to mPOF allows the simultaneously tailoring of both the dopant embedded within the particles themselves and the microstructure in the fiber to achieve novel fiber properties beyond the reach of each modification option on its own. Organic dye doped polymers have been widely investigated as gain media in solid state dye lasers but organic dye has a disadvantage of photo-bleaching in which the dye loses its fluorescing properties by the combination of excitation light and oxidising agents. There arises the importance of nano-particle doped fibres for the manufacturing of proficient in-fibre single-photon

sources for quantum communication, magneto-optically active fibres for photonic devices such as isolators and switches and the doping of rare-earth organic complexes for amplification in polymer optical fibres⁴³⁻⁴⁵.

Considering the potential application of the QD doped PMMA fibers and the promising properties of chalcogenide glass, fabrication and characterization of nano colloid $\text{Ga}_5\text{Sb}_{10}\text{Ge}_{25}\text{Se}_{60}$ doped PMMA optical fibers are done and presented in the coming sections.

7.2.2. Fabrication of nano colloid doped polymer optical fibers

❖ Materials

$\text{Ga}_5\text{Sb}_{10}\text{Ge}_{25}\text{Se}_{60}$ nano colloid solutions were prepared from bulk $\text{Ga}_5\text{Sb}_{10}\text{Ge}_{25}\text{Se}_{60}$ chalcogenide glass. Glass solutions of three different concentrations $C_0=0.72$ mg/ml, $C_1=0.54$ mg/ml and $C_2=0.12$ mg/ml were obtained by the dissolution of bulk glass in n-butylamine solvent (Sigma-Aldrich, 99.9%). The dissolution was carried out inside a sealed glass container to prevent solvent evaporation. A magnetic stirrer is used to expedite the dissolution process. The studies on $\text{Ga}_5\text{Sb}_{10}\text{Ge}_{25}\text{Se}_{60}$ nano colloids used for the preparation of the preform are discussed in detail in chapter 3.

PMMA was chosen as the host as it has good optical quality and is compatible with most of the QD's and organic dyes used as dopants. Figure 7.8 shows the structure of monomer and its bonding to form polymer chains. PMMA comprises the molecular subunit, or

monomer as depicted in Figure 7.8. As the oxygen atoms within the PMMA monomer are electronegative, partial negative charge resides on them, whilst the resulting partial positive charge resides on the central carbon atom. The result of this partial charge separation is that a fiber made from PMMA will have a net negative charge at the surface of the fiber where the oxygen atoms within the PMMA monomer reside⁴⁶.

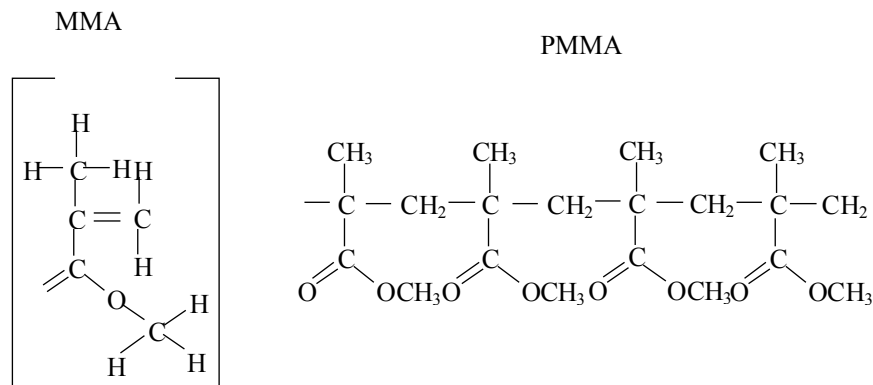


Figure 7.8: Molecular structure of PMMA.

Photodielectric effect can be observed for PMMA samples with excessive initiator or annealing near the glass transition temperature. PMMA is an organic compound forming long chains with typical molecule weights around 10^5 . The refractive index of PMMA is 1.49 and the glass transition temperature⁴⁶, T_g lies between 85 to 165°C. Each MMA monomer has a total of eight C-H bonds. The vibrations of this compound or more precisely its harmonic waves are a main cause for the absorptive losses encountered in PMMA polymer fibers.

In particular the harmonic waves at 627 nm (6th harmonic wave) and 736 nm (5th harmonic wave) fundamentally decide the level of attenuation within the application range of PMMA-POF. The wavelength-dependent attenuation curve of a PMMA-POF as in Figure 7.9 shows mainly three attenuation minima at wavelengths 520 nm, 570 nm and 650 nm which can be used for POF based communication systems^{46,47}. The greater part of the currently produced POF is based on polymethylmethacrylate (PMMA), a material that has been shown to be photoreactive. One of the disadvantage of PMMA fibers is that the transmission loss is not low, at a level above 80 per kilometer which is significantly higher than that of silica based optical fibers. This limits the application of polymer fibers in long length situations.

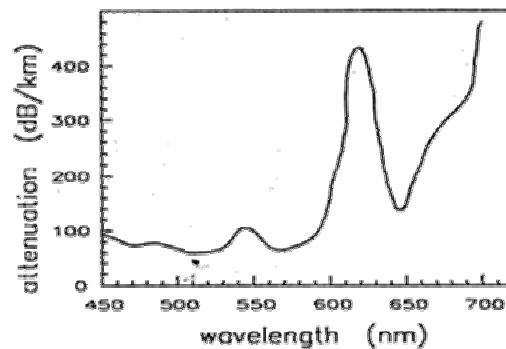


Figure 7.9: Plot of Attenuation of PMMA from 400nm to 700nm.

❖ Methods

Different methods exist for the fabrication of polymer optical fibers (POF) as discussed in chapter 2. Preform method was adopted in the present work for fabricating nano colloid doped POF. This method

involves two stages. In the first stage, a cylindrical preform of 1cm in diameter and 7 cm in length was fabricated and in the second stage, this preform was drawn in to fiber by the heat-drawing process.

The base material used for the fabrication of polymer preform is methylmethacrylate (MMA) monomer. The refractive index of pure methylmethacrylate is about 1.41 and it will increase up to 1.48 to 1.49 due to volume reduction during phase transition from liquid to solid⁴⁶. Present studies are concentrated primarily on only core fibers with air cladding, neglecting the scattering losses associated with it due to the absence of the cladding.

Commercially available MMA (Sd Fine) will contain inhibitors like hydroquinons which keeps MMA without polymerizing. Initially the inhibitors were removed by repeatedly washing the monomer with 5% NaOH solution followed by flushing with distilled water. The remaining water was removed by adding suitable drying agents like CaCl_2 . The monomer was then purified by distillation under reduced pressure. Distillation is a method of separating mixtures based on differences in their volatilities in a boiling liquid mixture. Distillation was done to purify the MMA from crude MMA.

Suitable initiators like benzoyl peroxide or azobisisobutyronitrile (AIBN) can be used to start the polymerization. Benzoyl peroxide was used for the present work since there is no gas such as nitrogen which gets released during polymerization as in the case of AIBN. This reduces the possibility of air bubble formation in the polymer preforms. Along with the initiator, n-butyl mercaptan was used as the chain transfer

agent to regulate and terminate the polymerization process. Addition of appropriate quantity of chain transfer agent and initiator controls the molecular weight of the polymer. The molecular weight regulation is an important factor that governs the drawability of the polymer preform.

An optimum molecular weight was fixed by adding benzoyl peroxide and mercaptan through numerous trial and error methods. The best preforms were obtained for MMA added and doped with (a) 40ml- MMA, 0.15 gm- benzoyl peroxide, 0.25 ml- mercaptan and C₀-10%, (b) 40 ml- MMA, 0.15 gm- benzoyl peroxide, 0.25 ml- mercaptan and C₁-10% and (c) 40 ml- MMA, 0.15 gm- benzoyl peroxide, 0.25 ml- mercaptan and C₂-10%. C₀, C₁, C₂ are Ga₅Sb₁₀Ge₂₅Se₆₀ nano colloid with 0.72 mg, 0.54 mg and 0.12 mg of Ga₅Sb₁₀Ge₂₅Se₆₀ dissolved in 1 ml n-butylamine respectively. The nano colloid solutions were added to the distilled MMA using a glass syringe. The resulting mixtures were stirred well so as to avoid aggregate formation. The MMA mixed with initiator, nano colloid and chain transfer agent was poured into a glass test tube of 1.7 cm diameter and 15 cm length. This was then kept in a constant temperature bath at 90°C for 2 weeks. The photograph of polymerized preform in test tube is shown in Figure 7.10. The test tube, 'a' is the preform of PMMA alone while b, c and d corresponds to the preforms doped with C₀, C₁, C₂ Ga₅Sb₁₀Ge₂₅Se₆₀ nano colloids respectively. The preforms were taken out of the test tube by breaking it. The prepared preform (C₁, C₂ doped PMMA) is now ready for drawing the fiber in a custom-made fiber drawing tower shown in Figure 7.11.

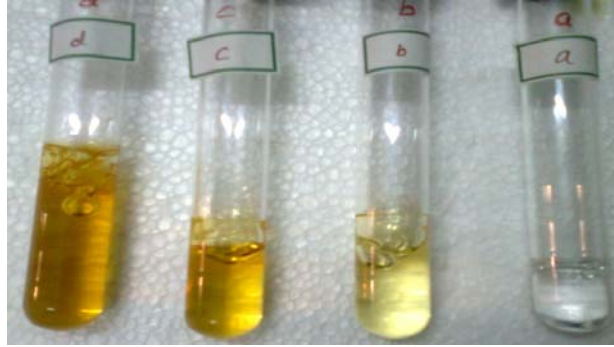


Figure 7.10: Photograph of preforms with different concentration of dopants.

By using a preform feeder, the preform is lowered into the furnace of the fiber drawing station and fiber is drawn at a temperature of 190°C (draw temperature optimized). The fiber diameter can be varied by adjusting the feed rate of the preform and the draw rate of the fiber. The draw rate was adjusted so that C_1 doped and C_2 doped fiber have a diameter of 500 μm .



Figure 7.11: Heat drawing furnace and the photograph of drawn C_1 doped fiber.

7.2.3. Optical characterization

The transmission and reflection spectra of the preforms of PMMA and nano colloid $\text{Ga}_5\text{Sb}_{10}\text{Ge}_{25}\text{Se}_{60}$ doped PMMA samples (as shown in Figure 7.10) were recorded using a spectrophotometer (JASCO UV/VIS/NIR V-570). The corresponding transmission and reflection spectra are shown in Figure 7.12 a and b respectively.

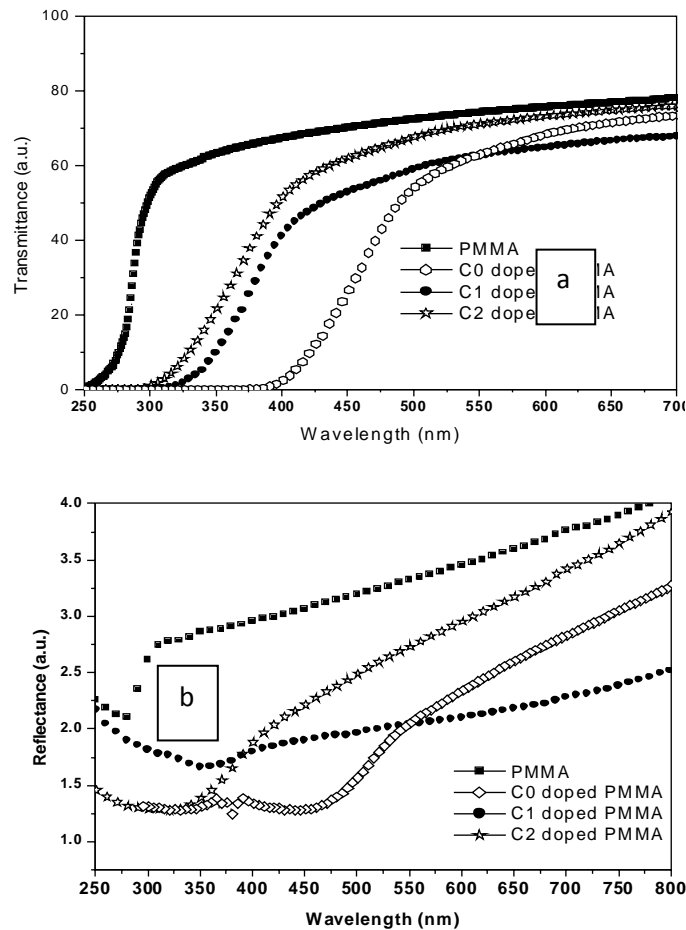


Figure 7.12: a) Transmission and b) reflection spectra of ChG nano colloid doped and undoped preforms.

It is clear from the transmission spectra that as the concentration of the chalcogenide glass in the PMMA decreases the transmission edge gets shifted to lower wavelength side resulting in an increase in band gap. The shift in the transmission edge can be made by altering the cluster size or the concentration of the nano colloid $\text{Ga}_5\text{Sb}_{10}\text{Ge}_{25}\text{Se}_{60}$ dopant in the monomer. Thus it is possible to tailor the absorption edge by varying the cluster size of the nano colloid ChG doped in PMMA fiber. This ability for tunability makes it promising for novel photonic applications.

7.2.4. Luminescence studies on $\text{Ga}_5\text{Sb}_{10}\text{Ge}_{25}\text{Se}_{60}$ nano colloid doped PMMA fiber

QD doped fibers can be used as fiber amplifiers. The QD doped fiber has many advantages, such as wide waveband, flat gain and low noise, which will possibly promote them to be a new fiber amplifier⁴⁸. The key parameters (such as bandwidth and gain) of such fibers are closely related with the doping concentration and fiber length. Therefore it is important to research the characteristics of light transmitted in the QD doped fiber before manufacturing a favourable fiber amplifiers. In the present work luminescence studies are carried out in $\text{Ga}_5\text{Sb}_{10}\text{Ge}_{25}\text{Se}_{60}$ nano colloid doped PMMA fiber under different experimental conditions by changing the doping concentration and fiber length.

7.2.4.1. Luminescence studies on excitation with 532nm (DPSS laser).

a) Transverse excitation

A schematic of the experimental set up for the luminescence studies on excitation with Diode pumped solid state laser (DPSS) is shown in Figure 7.13. The laser used is Micro DPSS laser model BWT-50 (B&W) at 532 nm. The fiber is mounted normally on a translation stage with respect to the incident beam. Pump beam is focused on the fiber using a convex lens of appropriate focal length. It should be noted that there is no absorption for nano colloid doped and undoped PMMA fiber at 532 nm.

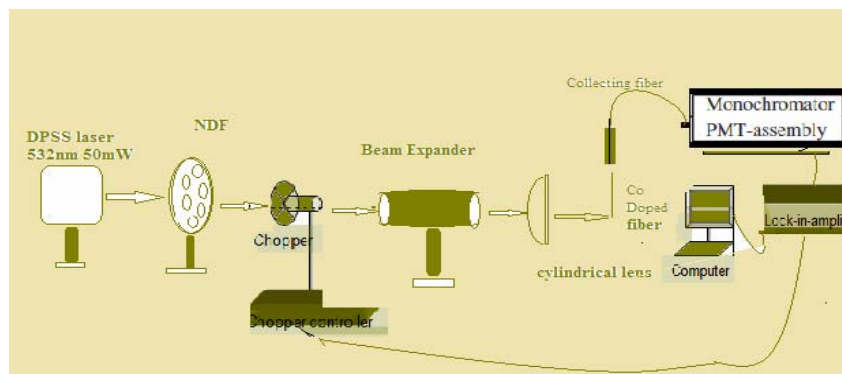


Figure 7.13: Experimental set up for the luminescence studies on excitation with Diode pumped solid state laser.

The luminescence from PMMA fiber and C_1 doped PMMA fiber is shown in Figure 7.14. The C_1 doped fiber shows a luminescence peak at 587 nm whereas it is absent in PMMA fiber. This clearly shows the effect of nano colloid ChG doped in the fiber.

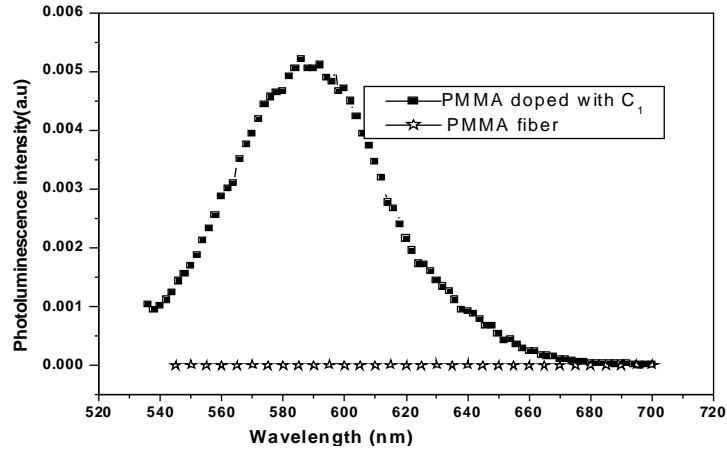


Figure 7.14: The luminescence from PMMA fiber and C₁ doped PMMA with length 8 cm on excitation with DPSS (532 nm).

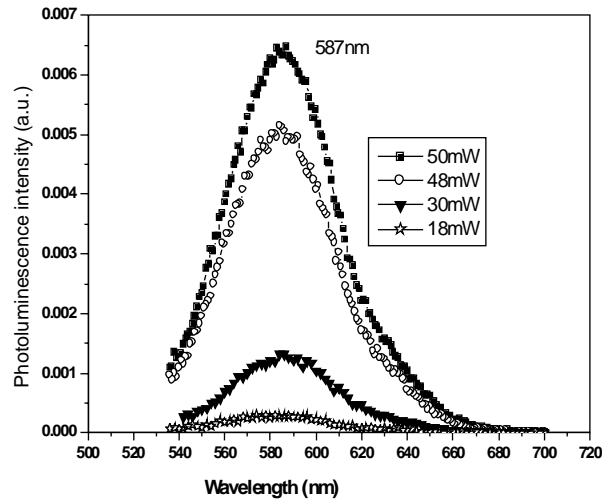


Figure 7.15: Luminous curve for C₁ doped PMMA fiber at different laser intensities.

The laser power dependent change in luminous intensity for the C₁ doped fiber (with length 8 cm) has been studied and the results obtained are presented in Figure 7.15. The laser power is changed

from 18 mW to 50 mW. It is observed that by increasing the laser power twice, the luminescence peak intensity has changed 7 times. In order to check the mode of absorption in the fiber the slope of the plot of log (luminescence intensity) versus log (laser power) is plotted as shown in Figure 7.16.

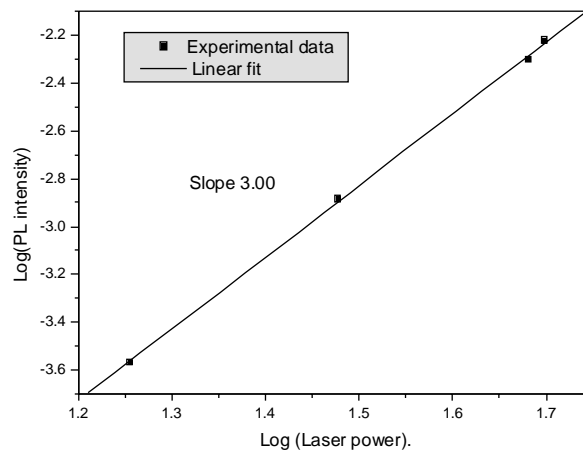


Figure 7.16: Log (luminescence intensity) versus log (laser power) for C_1 doped PMMA fiber having a length of 8 cm.

The log-log plot indicates the presence of three photon absorption⁴⁹ in the fiber. This can be due to the increase in effective interaction length compared to the nano colloid solution which shows two photon absorption on excitation with 532 nm. Two photon absorption induced fluorescence was reported by Sheeba et al.⁴⁶ in dye doped PMMA fibers.

The nano colloid $Ga_5Sb_{10}Ge_{25}Se_{60}$ shows a peak at 590nm and 645nm on excitation with the same laser source. The luminescence spectra of C_1 nano colloid and C_1 doped PMMA fiber are given in Figure 7.17.

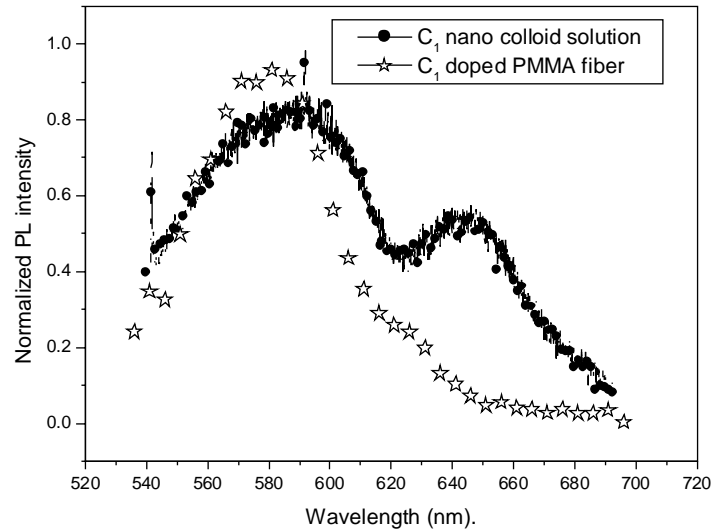


Figure 7.17: PL spectra of nano colloid ChG (C_1) and C_1 doped PMMA fiber. (C_1 -0.54 mg $Ga_5Sb_{10}Ge_{25}Se_{60}$ dissolved in 1ml n-butylamine).

Here a blue shift of around 8nm is observed in doped fiber compared to that of nano colloid C_1 solution. The full width at half maximum has also reduced in C_1 doped fiber. The observed results are in line with the results obtained for studies on CdSe/ZnS doped PMMA fiber by Helmut C. Y. Yu et al. ⁴⁸. The observed shift in peak fluorescence wavelengths in doped (QD or dye) fibers can be mainly due to two reasons ⁴⁸⁻⁵⁰. First one is due to the environment surrounding the photon source, being either QD or PMMA, shifts the electronic resonances. For QD's, the structure of its energy levels are highly dependent on their size and the surrounding dielectric as it changes the shape of the absorption lines and hence the emission characteristics. Second reason can be due to the process of emission and reabsorption dependent on the concentrations of the particles. That is, the change in nanoparticles

concentration would vary the strength of interaction between particles thus causing a shift in emission spectrum. The second reason is particularly reported for solutions, since solution doping leads to high concentration and the overlap of the emission and absorption bands of can result in a shifting of the maximum emission wavelength.

The luminescence from the C_1 doped fiber is also studied as a function of propagation distance through the fiber by translating the fiber horizontally across the laser source. Here the illuminating point on the fiber is varied by allowing different propagation distance. The luminescence spectra corresponding to different length is given in Figure 7.18.

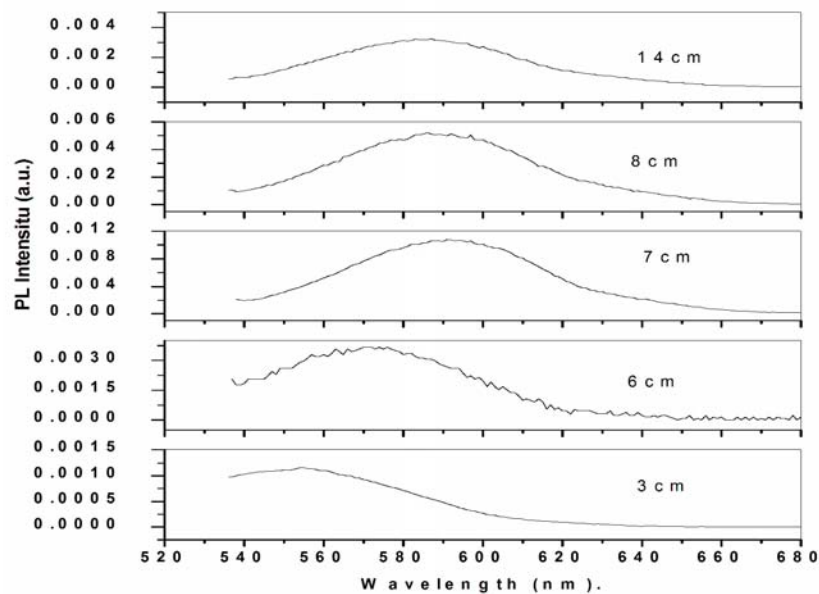


Figure 7.18: Luminescence curve for C_1 doped fiber with different propagation length.

It is clear from the plot that the luminescence intensity increases with length upto an optimum length and after this length the intensity decreases. It is observed that the optimum length for the luminescence peak and intensity is 7cm. There exist a clear red shift in the peak luminescence emission wavelength as the propagation distance is increased from 3 cm to 7cm. Red shift in the luminescence peak have been observed in dye doped PMMA fibers also. Similar results of red shift in the luminescence peak wavelength due to re-absorption of the emission from the QD doped in the fiber were also reported on CdSe/ZnS doped PMMA fibers⁴⁸. Studies on CdSe/ZnS doped in POF by Cheng Cheng and Xuefeng Peng⁵¹ reports the red shift is determined by both the doping concentration and the fiber length. The luminescence intensity from C₁ doped fiber on excitation with 48 mW DPSS laser increased from 14×10^{-4} (for 3 cm fiber length) to 100×10^{-4} (for 7 cm) and decreases thereafter to 30×10^{-4} . The observed increase in luminescence intensity up to a certain optimum fiber length and reduction thereafter is similar to the concentration quenching in the colloid nano particle solution or dye solutions. Assuming uniform dopant concentration along the fiber length, if ρ is the dopant concentration per unit length, the dopant concentration for fiber length l will be ρl or concentration proportional to l . Thus an increase in fiber length will be equivalent to an increase in concentration. The luminescence intensity dependence on interacting medium length can be schematically represented as in Figure 7.19.

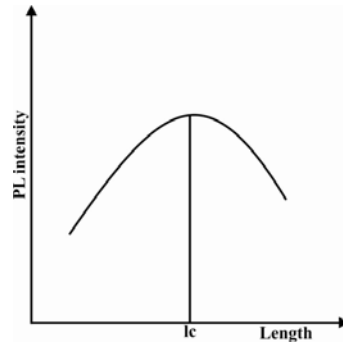


Figure 7.19: Schematic representation of dependence of luminescence intensity on fiber length. l_c is the optimum length at which luminescence intensity is maximum.

For 3 cm fiber length the concentration will not be sufficient to show concentration dependence on PL while as the length increases the concentration of the nano colloid that can interact with the radiation increases resulting in an increase in luminescence intensity and shift of luminescence peak towards the nano colloid solution. Red Shift in emission spectrum with change in fiber length can be due to the secondary absorption-emission effect in the doped fiber. The secondary absorption emission can be explained as follows, at a given wavelength, the PL emitted by one nano cluster may be absorbed by other neighbouring cluster before it is propagated out of the fiber. This is named as secondary absorption. The carrier excited by the exciting beam cannot freely transit to a high level, but only to a low level, generating the emission with the longer wavelength, compared with the absorption. Namely, the re-emission after the secondary absorption can only generate light with longer wavelength. The re-emitted photons and the original photons make the red shift. The observed tunability of luminescence peak

wavelength with fiber length elucidates the potentiality of the $\text{Ga}_5\text{Sb}_{10}\text{Ge}_{25}\text{Se}_{60}$ nano colloid doped POF as a length dependent wavelength tunable device.

b) *Excitation axially along the fiber*

The experimental set up used for studying the luminous behavior of the C_1 doped fiber is shown in Figure 7.20. Here the pump beam is allowed to propagate through the fiber and the output is collected using a fiber connected to monochromator PMT assembly.

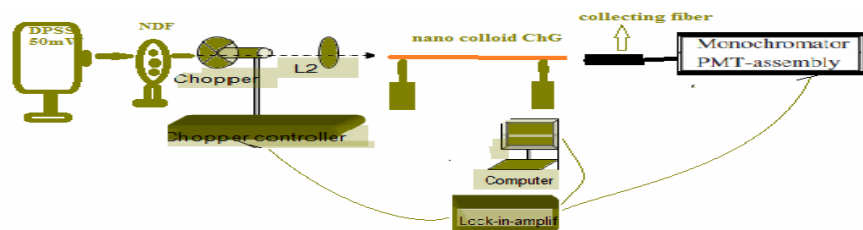


Figure 7.20: Experimental set up for luminescence study from fiber on excitation with DPSS axially.

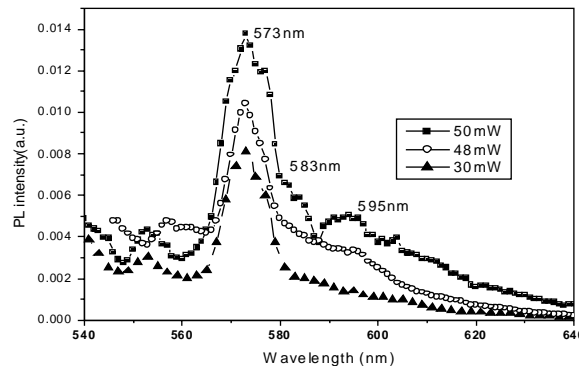


Figure 7.21: Luminescence spectra from C_1 doped PMMA fiber on excitation with 30 mW, 48 mW and 50 mW axially.

The luminescence spectra obtained on excitation with a DPSS laser (532 nm) axially to the C_1 doped fiber is shown in Figure 7.21.

Excitation with 50 mW results in luminescence peak at 573 nm and shoulders at 583 nm and 595 nm. The shoulder at 583 nm is absent on excitation at 48 mW and 30 mW. Luminescence at 573 nm is observed in 50 mW, 48 mW and 30 mW laser irradiation.

7.2.4.2. Luminescence from the fiber on excitation with white LED

The experimental set up used for the luminescence studies on chalcogenide glass nano colloid doped PMMA fiber is shown in Figure 7.22. The set up consist of a white LED connected to a 5V battery as the excitation source, a 10 cm lens and a chopper connected to the chopper controller. The chopped beam is again focused using a lens of focal length 2.5 cm to the fiber. The emission from the fiber is collected using a collecting fiber and given to the monochromator PMT assembly. The assembly is connected to a lock in amplifier interfaced to a computer. The output spectra for the doped and undoped fiber and the spectra of white LED used are given in Figure 7.23.

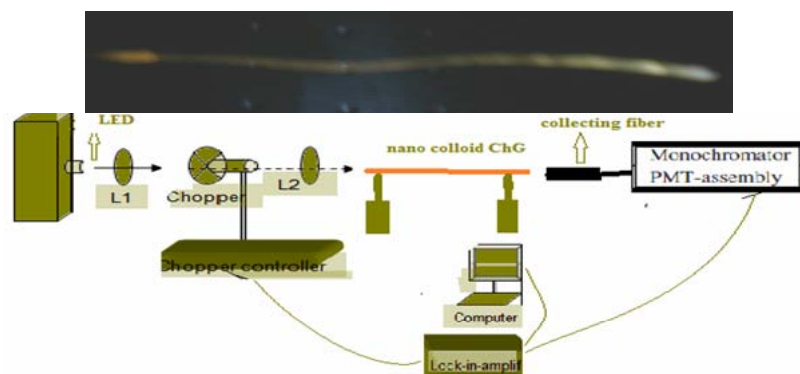


Figure 7.22: Set up used for luminescence studies on fiber using LED. Photograph of emission from the doped fiber is given in the top.

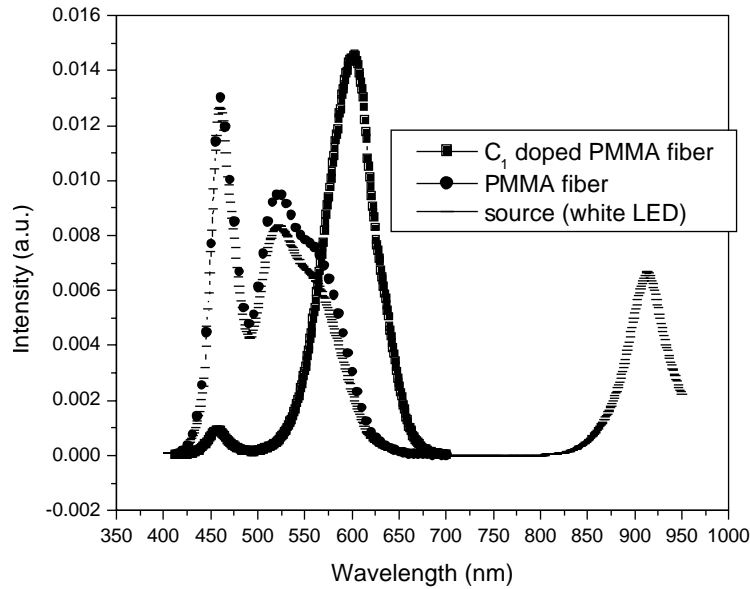


Figure 7.23: Luminescence spectra from the doped, undoped fiber and the spectra of excitation source.

The PMMA fiber guides the white light from the LED completely as the output spectrum from the LED and PMMA fiber is same. Doping effect is clear from the emission spectra. The nano colloid doped PMMA gives an output of orange light as shown in photograph. The peak at 600 nm corresponds to the luminescence from the nano colloid doped in the PMMA fiber.

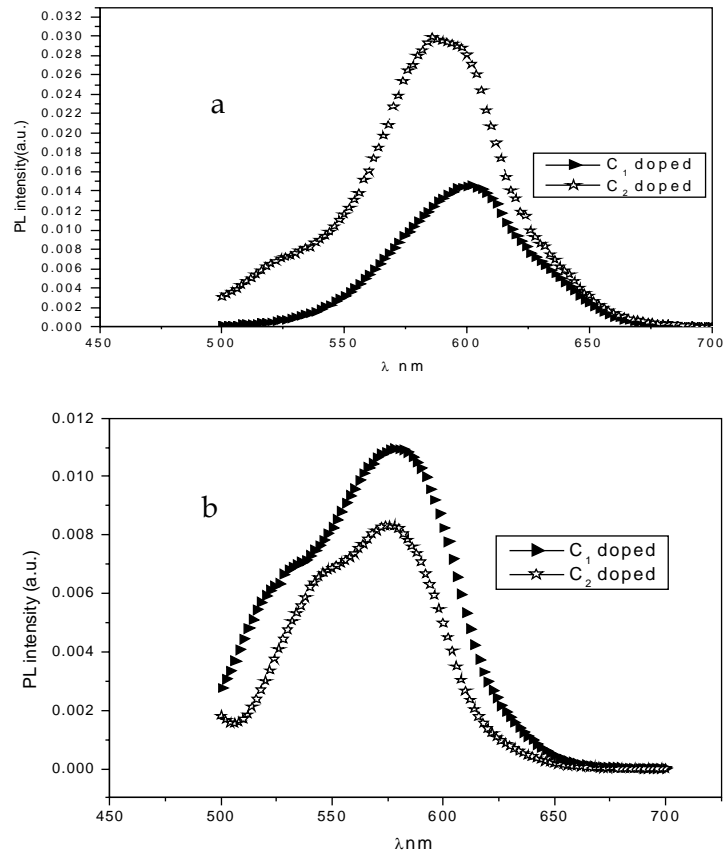


Figure 7.24: Luminescence from a) 14 cm and b) 3 cm C_1 and C_2 doped PMMA fiber.

Figure 7.24 depicts the luminescence from fiber with higher concentrated and lower concentrated nano colloid $Ga_5Sb_{10}Ge_{25}Se_{60}$ doped in PMMA. With increase in concentration of nano colloid ChG, there is a red shift in the PL peak from fiber having 14 cm. The luminescence studies carried out on the nano colloid $Ga_5Sb_{10}Ge_{25}Se_{60}$ solutions are presented in chapter 3. The nano colloid show cluster size dependent change in luminescence peak. The C_1 and C_2 solutions

show luminescence peak at 595 nm and 645 nm on excitation with nano second laser. The shift is less in fiber with length 3 cm. The luminescence intensity is higher for C_1 than C_2 at 3 cm and higher for C_2 than C_1 for fiber with length 14 cm. As the propagation distance increases we expect that the overall magnitude of the fluorescence intensity decreases in all the cases due to loss mechanisms such as absorption and scattering of the fluorescence emission. In the present case the luminescence intensity increases with increase in fiber length. For 3 cm length, concentration is not sufficient to show concentration dependence on PL while for 14 cm length we get sufficient concentration showing the redshift in PL. The redshift observed is due to the secondary-emission as discussed in 7.2.4.1.

7.3. Conclusions

Optical characterization of the double layered nano composite and thermally evaporated $Ga_5Sb_{10}Ge_{25}Se_{60}$ are done and the studies show that the flexible IR transmitting filters can be achieved by suitably stacking the films. The manufacturing process for the staked films is inexpensive and easy. Strong photoinduced effect under light irradiation with above bandgap have wide applications as inorganic photoresists with high resolution, for preparing different diffractive elements for integrated optics and telecommunication systems.

New chalcogenide nano colloid doped PMMA fiber was fabricated by the preform method. The optical studies showed that the size-tunable optical properties can be achieved in the polymer fibers by addition of nano colloids of $Ga_5Sb_{10}Ge_{25}Se_{60}$ chalcogenide glass. Propagation length dependent

luminescence studies show that there exist an optimum length at which the luminescence intensity is maximum. The fabricated fiber also exhibits tunability in luminescence peak with cluster size of the dopant.

7.4. References

1. P. Yeh, A. Yariv, and C.-S. Hong, "Electromagnetic propagation in periodic stratified media. II. Birefringence, phase matching, and x-ray lasers", *J. Opt. Soc. Am.*, 67, 423 (1977).
2. J. N. Winn, Y. Fink, S. Fan, and J. D. Joannopoulos, "Omnidirectional reflection from a one-dimensional photonic crystal", *Optics Letters.*, 23, 1573-1575 (1998).
3. J. D. Joannopoulos, R. Meade, and J. N. Winn, "Photonic Crystals: Molding the Flow of Light", Princeton U. Press, Princeton (1995).
4. D. N. Chigrin, A. V. Lavrinenko, D. A. Yarotsky, S. V. Gaponenko, "All-dielectric one-dimensional periodic structures for total omnidirectional reflection and partial spontaneous emission control", *J. Lightwave Technol.*, 17, 2018-2024 (1999).
5. J.-Q. Xi, M. Ojha, J. L. Plawsky, W. N. Gill, J. K. Kim, and E. F. Schubert, "Internal high-reflectivity omnidirectional reflectors", *Applied Physics Letters.*, 87, 031111-1-3 (2005).
6. Y. Fink, J. N. Winn, S. Fan, C. Chen, J. Michel, J. D. Joannopoulos, and E. L. Thomas, "A dielectric omnidirectional reflector", *Science.*, 282, 1679-1682 (1998).
7. K.M.Chen, A.W. Sparks, H.C. Luan, D.R. Lim, K. Wada and L.C.Kimerling, "SiO₂/TiO₂ Omnidirectional Reflector and Microcavity Resonator via the Sol-Gel Method", *Applied Physics Letters.*, 75, 3805-3807 (1999).
8. M. Deopura, C.K. Ullal, B. Temelkuran and Y.Fink, "Dielectric Omnidirectional Visible Reflector", *Optics Letters.*, 26, 1197-1199 (2001).
9. S. H. Kim and C.K.Hwangbo, "Design of Omnidirectional High Reflectors with Quarter-Wave Dielectric Stacks for Optical Telecommunication Bands," *Optics Letters.*, 23, 1573-1575 (1998).

10. V. Balan, C. Vigreux, A. Pradel, M. Ribes, "Waveguides Based Upon Chalcogenide Glasses", *Journal of Optoelectronics and Advanced Materials.*, 3, 367 - 372 (2001).
11. T. Kohoutek, T. Wagner, J. Orava, M. Krbal, Mir.Vlcek, J.Ilavsky, Mil. Vlcek and M. Frumar, "Multilayer Planar Structures Prepared from Chalcogenide Thin Films of As-Se and Ge-Se Systems and Polymer Thin Films using Thermal Evaporation and Spincoating Techniques", *J. Non-Cryst. Solids.*, 354, 529-532 (2008).
12. S. Chao, T.K. Wang and J.S. Chen, "Graphic method for numerical analysis of a periodically stratified thin-film omnidirectional reflector", *Applied Optics.*, 44, 3448-3453 (2005).
13. S. H. Kim, and C. K. Hwangbo, "Design of omnidirectional high reflectors with quarter-wave dielectric stacks for optical telecommunication bands", *Applied Optics.*, 41, 3187-3192 (2002).
14. R. G. DeCorby, H. T. Nguyen, P. K. Dwivedi, and T. J. Clement, "Planar omnidirectional reflectors in chalcogenide glass and polymer", *Opt. Express.*, 13, 6228-6233 (2005),
15. T. Kohoutek, J. Orava, M. Hrdlicka, T. Wagner, Vlcek Mil and M. Frumar, "Planar Quarter Wave Stacks Prepared from Chalcogenide Ge-Se and Polymer Polystyrene Thin Films", *J. Phys. Chem. Solids.*, 68, 2376-2380 (2007).
16. R. G. DeCorby, N. Ponnampalam, M. M. Pai, H. T. Nguyen, P. K. Dwivedi, T. J. Clement, C. J. Haugen, J.N. McMullin and S. O. Kasap, "High index contrast waveguides in chalcogenide glass and polymer", *IEEE J. Sel. Top. Quantum Electron.*, 11, 539-546 (2005).
17. T. J. Clement, N. Ponnampalam, H. T. Nguyen and R. G. DeCorby, "Improved omnidirectional reflectors in chalcogenide glass and polymer by using the silver doping technique", *Optics Express.*, 14, 1789 (2006).
18. W. Lin, G. P. Wang, and S. Zhang, "Design and fabrication of omnidirectional reflectors in the visible range", *J. Mod. Opt.*, 52, 1155-1160 (2005).
19. Manificier J C, Gasiot J and Filard P, *J. Phys. E: Sci. Instrum.*, 9, 1002 (1976).

20. R. Swanepoel, "Determination of the thickness and optical constants of amorphous silicon", *J. Phys. E.*, 16(12), 1214–1222 (1983).
21. R.G.DeCorby, N. Ponnampalam, H. T. Nguyen and T. J. Clement, "Robust and Flexible Free-Standing All-Dielectric Omnidirectional Reflectors", *Adv. Mater.*, 19, 193-196 (2007).
22. R Todorov, J Tasseva, Tz Babeva and K Petkov, "Multilayer As_2Se_3/GeS_2 quarter wave structures for photonic applications", *J. Phys. D: Appl. Phys.*, 43, 505103(2010) .
23. E. Bormashenko, S. Sutovsky, and R. Pogreb, "New oriented polymer /thermoplastic glass composites for IR optics", *Advanced Engineering Materials*, 2, 657–658 (2000).
24. J.Q. Xi, M. Ojha, J. L. Plawsky, W. N. Gill, J. K. Kim, and E. F. Schubert, "Internal high-reflectivity omnidirectional reflectors", *Appl. Phys. Lett.*, 87, 031111-1-3 (2005).
25. Edward Bormashenko, Roman Pogreb, Zosya Pogreb and Semion Sutovski, "Development of new near infrared filters based on the "sandwich" polymer-chalcogenide glass-polymer composites", *Optical engineering*, 40, 661 (2001).
26. R. Tintu, V.P.N. Nampoori, P. Radhakrishnan and Sheenu Thomas, "Photoinduced changes in optical properties of Ga-Sb-Ge-Se glasses", *Optics Communications*, 284, 222–225 (2011).
27. P. A. S. Jorge, M. Mayeh, R. Benrashid, P. Caldas, J. L. Santos, and F. Farahi, "Applications of quantum dots in optical fiber luminescent oxygen sensors", *Appl. Opt.*, 45(16), 3760–3767 (2006).
28. M. Van Eijkelenborg, M. Large, A. Argyros, J. Zagari, S. Manos, N. Issa, I. Bassett, S. Fleming, R. McPhedran, C. Martijn de Sterke and N. A. Nicorovici, "Microstructured polymer optical fibre", *Optics Express*, 9, 319-327 (2001).
29. P. St.J. Russell, "Photonic-crystal fibers," *J. Lightwave Technol.*, 24, 4729-4749(2006).
30. A. Argyros, M. A. van Eijkelenborg, S. D. Jackson, and R. P. Mildren, "Microstructured polymer fiber laser", *Optics Letters*, 29, 1882-1884 (2004).

31. J. Brandrup, E.H. Immergut, D.R. Bloch and E.A. Grulke, "*Polymer Handbook*", Volume 2, Wiley (2003).
32. L Eldada and L.W Shacklette, "*Advances in polymer integrated optics*, IEE.J. Select. Top. Quantum Electron., 6, 54 (2000).
33. C. Cheng, "*A multi-quantum-dot-doped fiber amplifier with characteristics of broadband, flat gain and low noise*", J. Lightw. Technol., 26, 1404-1410 (2008).
34. O. Ziemann, J. Krauser, P. E. Zamzow and W. Daum, "*POF Handbook*", Springer Berlin (2008).
35. Lee H.C, Akhtar M.S, Park J.G, Kim K.J, Lee S.K, O.B. Yang, "*Carbon nanotube (CNT)-polymethyl methacrylate (PMMA) composite electrolyte for solid-state dye sensitized solar cells*", J Nanoscience Nanotechnology., 10(5), 3502-7 (2010).
36. Stephen Y. Chou, Peter R. Krauss, and Preston J. Renstrom, "*Nanoimprint lithography*", J. Vac. Sci. Technol. B., 14(6), 4129-4131 (1996).
37. G. A Kumar, Vinoy Thomas, Gijo Thomas, N .V. Unnikrishnan and V. P. N. Nampoore "*Energy Transfer in Rh 6G: Rh B system in PMMA matrix under CW laser excitation*", J.Photochem. Photobiol A: Chemistry., 153,145-151(2002).
38. S. Gross, D. Camozzo, V. Di Noto, L. Armelao, and E. Tondello, "*PMMA: A key macromolecular component for dielectric low- κ hybrid inorganic-organic polymer films*", Eur. Polym. J., 43(3), 673-696 (2007).
39. J.C. Knight, T.A. Birks, P.St.J. Russell and D.M. Atkin, "*All-silica single-mode optical fiber with photonic crystal cladding*", Optics Letters., 21, 1547-1549(1996).
40. H. C. Y. Yu, C. Barbe, K. Finnie, F. Ladouceur, D. Ng and M. A. van Eijkelenborg, "*Fluorescence from nano-particle doped optical fibres*", Electron. Lett., 42, 620-621 (2006).
41. T.P. Mthethwa, M.J. Moloto, A. De Vries, K.P. "*Properties of electrospun CdS and CdSe filled polymethyl methacrylate (PMMA) nanofibres*", Matabola Materials Research Bulletin., 46, 569-575(2011).

42. H.C.Y. Yu, M.A. van Eijkelenborg, S.G. Leon-Saval, A. Argyros and G.W. Barton, "Enhanced magneto-optical effect in cobalt nanoparticle doped optical fiber", *Applied Optics.*, 47, 6497-6501(2008).
43. X. Yang and L. Wang "Silver nanocrystals modified microstructured polymer optical fibres for chemical and optical sensing", *Opt. Comm.*, 280, 368-373 (2007).
44. M. C. J. Large, S. Ponrathnam, A. Argyros, N. S. Pujari, and F. Cox, "Solution doping of microstructured polymer optical fibres", *Opt. Express.*, 12(9), 1966-1971 (2004).
45. M. C. J. Large, A. Argyros, F. Cox, M. A. van Eijkelenborg, S. Ponrathnam, N. S. Pujari, I. M. Bassett, R. Lwin, and G. W. Barton. "Microstructured polymer optical fibres: New opportunities and challenges," *Mol. Cryst. Liq. Cryst.*, 446, 219-231 (2006).
46. Sheeba M, "Fabrication and Characterization of Polymer Optical Fibers for Photonic Device Applications", PhD Thesis, CUSAT, Cochin (2008).
47. W Daum, J Krauser, P E Zamzow and O Ziemann, "POF-Polymer Optical Fibers for Data Communication", Springer, New York (2002).
48. H. C. Y. Yu, A. Argyros, G. Barton, M. A. van Eijkelenborg, C. Barbe, K. Finnie, L. Kong, F. Ladouceur, and S. McNiven, "Quantum dot and silica nanoparticle doped polymer optical fibers", *Optics Express.*, 15 (16), 9989-9994 (2007).
49. Jick H. Yee, "Three-Photon Absorption in Semiconductors", *Physical Review B.*, 5, 449-459 (1972).
50. Helmut C. Y. Yu, Alexander Argyros, Sergio G. Leon-Saval, Alex Fuerbach, Anatoly Efimov, and Geoff W. Barton, "Emission properties of quantum dots in polymer optical fibres", *Optics Express.*, 17, 21344 (2009).
51. Cheng Cheng and Xuefeng Peng, "Spectral Characteristics of a Quantum-Dot (CdSe/ZnS)-Doped Fiber in Low Concentrations", *Journal of Lightwave Technology.*, 27, 1362-1368 (2009).



Chapter 8

CONCLUSIONS AND FUTURE PROSPECTS

This chapter deals with the summary of the work reported in this thesis along with an outline of the future prospects. The overall goal of the thesis was to fabricate new chalcogenide glass based nano composites for device applications.

8.1. Conclusions

- $Ga_5Sb_{10}Ge_{25}Se_6$, $Ge_{28}Se_{60}Ga_5$ and $Ge_{28}Sb_{12}Se_{60}$ bulk glasses were prepared by melt quenching method. The prepared samples were found to be amorphous in nature by XRD analysis. The DSC analysis on the investigated samples show that they have having high glass transition temperature (above 200°C). Optical absorption studies on the samples show they are having high transparency in the IR region.
- Thin films of $Ga_5Sb_{10}Ge_{25}Se_6$, $Ge_{28}Se_{60}Ga_5$ and $Ge_{28}Sb_{12}Se_{60}$ were fabricated using thermal evaporation technique at a pressure of 2×10^{-5} mbar and at a rate of 10 Å/s. The prepared thin films were found to be homogeneous and amorphous in nature. The transmission spectra and reflection spectra of vacuum evaporated thin films taken at normal incidence have been analyzed for the calculation of various optical parameters. The films were found to have good transparency in the IR region. The refractive index and film thickness are calculated by using envelope method proposed by Swanepoel's method. The optical absorption in the given systems seems to be of non-direct type and the optical bandgap determined in the strong absorption region by Tauc's extrapolation method. The optical parameters of the thin films like width of the band tails, extinction coefficient, dielectric constants, optical conductivity, dispersive energy, oscillator energy, static refractive index, high frequency dielectric constants, third order non linear susceptibility and nonlinear refractive indices were calculated using dispersive analysis of the refractive index using WDD model and generalized Millers rule.

- Rare earth erbium doped $\text{Ge}_{28}\text{Sb}_{12}\text{Se}_{60}$ bulk and thin films were studied. The optical energy gap has been found to increase with increase in erbium content. The increase can be interpreted as due to the decrease of the width of the tails of localized states in the band gap.
- The photoinduced studies on $\text{Ga}_5\text{Sb}_{10}\text{Ge}_{25}\text{Se}_6$ and $\text{Ge}_{28}\text{Sb}_{12}\text{Se}_{60}$ thin films prepared by thermal evaporation show a red shift in absorption edge on irradiation with near and above band gap lasers. The observed red shift in absorption edge was due photodarkening mechanism in the films. The photodarkening found in the investigated samples depends on the exposure time, energy and power of the laser used. The photosensitivity in the films was studied by analyzing the transmission spectra and reflection spectra. The photosensitivity in the investigated films shows a dependence on the penetration depth of the laser beam. The shift in absorption edge was accompanied by a shift in other optical parameters like increase in width of the localized states, refractive index etc. The photodarkening can be attributed to the increase in the disorder due to creation of defect states. This darkening effect shows a saturation effect after a particular exposure period. The saturation can be due to the finite number of photo darkening sites which cannot be greater than the number of atoms in the glass. Studies show that a low power radiation was sufficient to provide a shift in the absorption edge and a change in the refractive index. This mechanism in $\text{Ga}_5\text{Sb}_{10}\text{Ge}_{25}\text{Se}_6$ and $\text{Ge}_{28}\text{Sb}_{12}\text{Se}_{60}$ thin films can be used to realize continuous wave laser written waveguide and for fabricating photosensitive optical components for various applications.

- Nano colloids of $Ga_5Sb_{10}Ge_{25}Se_6$, $Ge_{28}Se_{60}Ga_5$, $Ge_{28}Sb_{12}Se_{60}$ chalcogenide glasses were synthesized by dissolution in *n*-butylamine solvent. The formation of nano clusters in the solution was confirmed by the H^1 NMR and SEM along with EDAX analysis. The optical absorption studies show a blue shift in the absorption edge with decrease in cluster size (as the concentration of bulk chalcogenide glass decreases the cluster size decreases). The ordering and the defects also vary with the decrease in cluster size. This enables us to realize special requirements by engineering their concentration.
- Photoluminescence studies on $Ga_5Sb_{10}Ge_{25}Se_6$, $Ge_{28}Se_{60}Ga_5$ and $Ge_{28}Sb_{12}Se_{60}$ nano colloids shows a cluster size and excitation wavelength dependent change in emission spectra. The photoluminescence intensity of nano colloidal solutions of investigated chalcogenide glass change almost in proportion to changes to bandgap which in turn is related to the cluster size. Nano colloid solutions yield a strong two-photon induced luminescence signal. Two-photon induced luminescence was verified by a quadratic dependence of emission intensity on the excitation power. Owing to their advantageous size-tunable optical properties and good quantum efficiency, they are an important class of novel functional materials for bio imaging and other optoelectronic applications.
- Thermal diffusivity studies carried out on $Ga_5Sb_{10}Ge_{25}Se_6$ and $Ge_{28}Sb_{12}Se_{60}$ nano colloids using thermal lens technique show a decrease in thermal diffusivity value with an increase in concentration of chalcogenide glass in the solution. It was found from the linear absorption measurement that with decreasing concentration of ChG

(where by cluster size decreases), the E_g value increases. This can be attributed to the decrease in the number of defect states in the forbidden gap, which can offer minimum resistance to propagating thermal waves due to reduced scattering.

- Nonlinear optical response of nano colloid $Ga_5Sb_{10}Ge_{25}Se_6$, $Ge_{28}Se_{60}Ga_5$, $Ge_{28}Sb_{12}Se_{60}$ samples studied using nanosecond Nd:YAG (532nm) laser pulses shows that they are highly nonlinear exhibiting reverse saturable absorption. The observed nonlinear absorption has been explained through two photon absorption. The measured value of nonlinear absorption coefficient (β) for the samples decreases with decreasing cluster size and increasing input intensity. Increasing the concentration results in the enhancement of the cluster size which results in the reduction of the limiting threshold thereby enhancing the optical limiting performance.
- A low-cost, scalable method was used to fabricate optical grade composite thin films for nonlinear optical applications. The AFM and EDAX analysis done on the composite films confirms the presence chalcogenide nano clusters in the films. The transmission and reflection spectra of prepared $Ga_5Sb_{10}Ge_{25}Se_6/PVA$, $Ge_{28}Se_{60}Ga_5/PVA$, $Ge_{28}Sb_{12}Se_{60}/PVA$ composite films were investigated. Optical band gap of the thin films were calculated using Tauc's extrapolation method. The band gap of the nano composite thin films was found to be tunable depending on the grain size of the films. Nonlinear optical characterisation of the films studied by the z-scan technique show reverse saturable absorption, which makes it useful for optical limiting applications. The third-order optical susceptibility $\chi^{(3)}$

studies in the composite films with different grain size show that the non linear susceptibility is highly dependent on particle size and fluence of the laser beam used for studies. The studies show that the prepared nano composite films are promising candidates for optical limiters and for the development of nonlinear optical devices.

- Optical characterization of the double layered nano composite and thermally evaporated $Ga_5Sb_{10}Ge_{25}Se_{60}$ were done and the studies show that flexible thin composite IR transmitting filters can be achieved by suitably stacking the films. The manufacturing process for the stacked films is inexpensive and easy. Strong photoinduced effect under light irradiation with above bandgap have wide applications as inorganic photoresists with high resolution, for preparing different diffractive elements for integrated optics and telecommunication systems. Photonic bandgap structures were fabricated which shows a path way for making new waveguides.
- Chalcogenide nano colloids doped PMMA fibers were fabricated using preform method. The optical studies show that the size-tunable optical properties can be achieved in the polymer fibers by addition of nano colloids of $Ga_5Sb_{10}Ge_{25}Se_{60}$ chalcogenide glass. Propagation length dependent luminescence studies show that there exist an optimum length at which the luminescence intensity is maximum. The fabricated fiber also exhibits tunability in luminescence peak in accordance with the cluster size of the doped ChG nano colloid.

8.2. Scope for Future Work

Many opportunities exist for extending the research.

- ❖ In terms of glass science, the composition space examined in this study could be expanded to include sulfide, telluride, mixed-anion systems and nano particles like carbon nano rods, ZnO etc.
- ❖ The structural analysis of the glasses can be investigated using different methods to understand the bonding in the glasses. The physical properties of the glasses related to the molecular structure of the glass network can be studied since the physical properties influences the density of lone electron pairs, and the average coordination of bond strength of the various network units. Thus assessment of bond statistics and the associated bond energies and lone electron pair densities are predictive tool to estimate linear and nonlinear optical properties, glass transition temperatures and microhardness in the investigated glass systems.
- ❖ Despite different models presented so far, the context of photosensitivity in the chalcogenide glasses still lack a comprehensive microscopic model which could describe all the experimental observations. Thus the establishment of such a model to elucidate the physical origin of observed photoinduced phenomena in chalcogenide glass materials seems to be essential and can be investigated.

- ❖ Photosensitive processes of the films can be used to fabricate optical structures such as Bragg gratings, waveguides, and holographic devices.
- ❖ Thin films of the investigated samples in this thesis can be prepared by other methods like Pulsed laser deposition, chemical vapour deposition etc and can be compared.
- ❖ Prepared glasses can be used for the fabrication of spatially variable infrared photonic band gap filter by quarter wave stacking high refractive index contrast chalcogenide glasses that are thermally evaporated on a substrate consecutively. Applications of variable wavelength all-chalcogenide IR filters may potentially include portable miniaturized (IR), spectrometers, disposable chemical and biological sensors etc. It is also possible to fabricate hollow-core omnidirectional on-chip waveguide structures for photonic applications at near- and mid-IR wavelengths using the prepared chalcogenide glass by properly designing it for multilayer formation.
- ❖ Fabrication of on -chip optical interconnects and microcavity for multifunctional intergrated optics can be done on silver photodoped chalcogenide glasses. The etch resistivity exhibited by silver doped chalcogenide glass can be utilized for realizing strip waveguides.
- ❖ Radial polymer/chalcogenide multilayers form otherwise a perfect omnidirectional mirror, which guides light through the

hollow core of the transmission fibers. Polymer composites with different polymers can be studied. Micro ring resonators can be fabricated using chalcogenide glass/Polymer composites.

- ❖ Studies on nano colloid solution of chalcogenide glasses can be made by doping other metal/semiconductor nano particles. The synthesis of the nano colloid can be tried in different solvents. The dissolution mechanism and the resulting products of the investigated samples are not clear so the studies can be proceeded on that.
- ❖ The inverse opal chalcogenide photonic crystals could be achieved in nano colloid based chalcogenide opal films by conventional lithographic techniques.
- ❖ Combination of a photorefractive nano colloid chalcogenide glass cladding with a distributed Bragg reflectors grating on top of Quantum cascade lasers can be used for trace-gas detection in the mid-infrared where the spectroscopic “fingerprints” of most atmospheric trace gas are found.
- ❖ New chalcogenide nano colloid doped PMMA fiber can be used for writing grating.
- ❖ Microstructured PMMA fibers doped with nano colloid ChG can be tried which can lead to application-specific fibers with potential use in sensing, engineering, medicine, textiles and communications.

